THE PETROGENESIS OF OCEAN-FLOOR BASALTS: AN EXPERIMENTAL AND GEOCHEMICAL STUDY

by

Trevor John Falloon

B.Sc (Hons) (University of Canterbury)

Submitted in fulfilment of the requirements
for the degree of

Doctor of Philosophy

University of Tasmania
Hobart

August, 1987

STATEMENT

This thesis contains the results of research done in the Geology Department, University of Tasmania between 1983 and 1987. It consists of five articles which have been prepared for publication in the following international journals or scientific publications:

Part no.	Journal/Publication	Status
I	Mineralogy and Petrology	in press
II	Journal of Petrology	submitted
III	Australian Journal of Earth Sciences	in press
IV	Earth and Planetary Science Letters	published
V	Boninites and Related Rocks, A. J. Crawford (ed.), Allen and Unwin	submitted

All of the papers have co-authors as listed in the table of contents. Co-authors are either my supervisors for my Ph.D research or have provided analytical data. Contributions of co-authors are indicated in the acknowledgements.

This thesis contains no material which has been accepted or submitted for the award of any other degree or diploma in any university and to the best of my knowledge and belief contains no copy or paraphrase of material previously published or written by another person, except where due reference is made,

Trevor Falloon

Trevor J. Falloon
University of Tasmania
August, 1987.

STATEMENT

This thesis contains the results of research done in the Geology Department, University of Tasmania between 1983 and 1987. It consists of five articles which have been prepared for publication in the following international journals or scientific publications:

Part no.	Journal/Publication	Status
I	Mineralogy and Petrology	in press
II	Journal of Petrology	submitted
III	Australian Journal of Earth Sciences	in press
IV	Earth and Planetary Science Letters	published
V	Boninites and Related Rocks, A. J. Crawford (ed.), Allen and Unwin	submitted

All of the papers have co-authors as listed in the table of contents. Co-authors are either my supervisors for my Ph.D research or have provided analytical data. Contributions of co-authors are indicated in the acknowledgements.

This thesis contains no material which has been accepted or submitted for the award of any other degree or diploma in any university and to the best of my knowledge and belief contains no copy or paraphrase of material previously published or written by another person, except where due reference is made,

Trevor Falloon

Trevor J. Falloon
University of Tasmania
August, 1987.

THESIS CONTENTS

Section	Page
Statement	 i
List of tables	 vii
List of figures	 ix
Acknowledgements	xiii
Abstract	 xv

PART I : Anhydrous partial melting of MORB pyrolite and other peridotite compositions at 10kbar: implications for the origin of primitive MORB glasses
(T. J. Falloon and D. H. Green) 1

1.1	Introduction	1
1.2	Approach 1: High-pressure near-liquidus experiments on MORB	3
1.2.1	High-pressure near-liquidus studies on ALV527-1-1 and DSDP3-18-7-1	6
1.2.2	High-pressure near-liquidus experiments on ARP74-10-16	7
1.2.3	High-pressure near-liquidus experiments on 395A-8-1, 50cm and T-87	8
1.3	Approach 2: Direct melting studies of peridotite compositions	9
1.4	Natural peridotite suites as a constraint on suitable source compositions for MORB petrogenesis	11
1.5	Experimental approach and techniques	16
1.6	Experimental results	18
1.6.1	Attainment of equilibrium	18
1.6.2	Evaluation of the sandwich technique in peridotite melting studies	23
1.6.3	Fe Loss	28
1.7	Equilibrium glass compositions at 10kbar	32
1.7.1	The effect of analytical	32
1.7.2	Glass compositions from MORB pyrolite (MPY-87, MPY-90, MPY-90-40)	39

1.7.3 Glass compositions from Tinaquillo lherzolite (TQ-40) and Hawaiian pyrolite (HW-40) 41
1.7.4 Glass composition from KLB-1 42
1.7.5 Summary 42
1.8 Comparison with other 10kbar melting studies 44
1.8.1 Stolper (1980) 47
1.8.2 Elthon and Scarfe (1984) 47
1.8.3 Presnall et al. (1979) and Presnall and Hoover (1984) 48
1.8.4 Takahashi and Kushiro (1983) 49
1.8.5 Sen (1982) 50
1.8.6 Fujii and Scarfe (1985) 51
1.9 Are primitive MORB glasses primary magmas at 10kbar? 51
1.10 Conclusions 52

PART **II : Anhydrous partial melting of peridotite from 8 to 35kbars and the petrogenesis of MORB** (T. J. Falloon and D. H. Green) 55

2.1 Introduction 55
2.2 Experimental approach and technique 57
2.3 Experimental results 60
2.3.1 Attainment of equilibrium 60
2.4 Equilibrium glass compositions 65
2.4.1 MORB pyrolite 65
2.4.2 Tinaquillo lherzolite 68
2.5 Comparison with previous experimental studies 70
2.5.1 Jaqués and Green (1980) 70
2.5.2 Takahashi and Kushiro (1983) 72
2.5.3 Takahashi (1986) 72
2.5.4 Stolper (1980) 74
2.5.5 Elthon and Scarfe (1984) 74
2.5.6 Summary 76
2.6 Olivine fractionation calculations 76
2.6.1 Rationale 76
2.6.2 Constraints from the composition of primitive MORB glasses 80
2.6.2.1 Silica saturation 80
2.6.2.2 Al_2O_3 and CaO contents 82
2.6.2.3 SiO_2 contents 82

2.6.2.4 FeO and MgO contents 82
2.6.2.5 CaO/Al_2O_3 and CaO/Na_2O ratios 83
2.6.2.6 TiO_2, K_2O and Al_2O_3/TiO_2 and CaO/TiO_2 ratios 83
2.6.3 Results 84
2.6.4 Comparison with MORB picrite compositions 86
2.6.5 Comparison with compositions determined from trapped glass inclusions 88
2.7 Primary MORB magmas 93
2.8 Discussion 93
2.9 Case study in MORB petrogenesis: Famous-Narrowgate-Amar 96

PART III : **Dredged igneous rocks from the northern termination of the Tofua Magmatic Arc, Tonga and adjacent Lau Basin**
(T. J. Falloon, D. H. Green and A. J. Crawford) 102

3.1 Introduction 102
3.2 Geologic and tectonic setting 103
3.3 Dredge locations 103
3.4 Analytical techniques 107
3.5 Tofua Magmatic Arc 109
3.6 Station 15 112
3.6.1 Petrography 112
3.6.2 Geochemistry 112
3.6.3 Geochemical affinities 115
3.6.3.1 'Eua-Vavua' block basement sequence 115
3.6.3.2 Remnant arc, the Lau-Colville Ridge 115
3.6.3.3 Fiji 116
3.6.3.4 Early Lau Basin back-arc volcanism 116
3.7 Station 21 119
3.7.1 Petrography 119
3.7.2 Geochemistry 120
3.7.3 Geochemical affinities 120
3.8 Station 22 122
3.8.1 Petrography 122
3.8.2 Geochemistry and geochemical affinities 122
3.9 Station 23 123
3.9.1 Basaltic andesites 123
3.9.1.1 Petrography 123

3.9.1.2 Geochemistry and geochemical affinities 124
3.9.2 High-Mg lavas 124
3.9.2.1 Petrography 124
3.9.2.2 Geochemistry 124
3.10 Stations 24 and 25 127
3.10.1 Petrography 127
3.10.2 Geochemistry 128
3.11 Station 31 128
3.11.1 Petrography, geochemistry and geochemical affinities 128
3.12 Geochemical affinities of the high-Mg lavas 129
3.13 Summary 132

PART IV : **Glass inclusions in magnesian olivine phenocrysts from Tonga: evidence for highly refractory parental magmas in the Tongan Arc**
(T. J. Falloon and D. H. Green) 133

4.1 Introduction 133
4.2 Petrography 134
4.3 Composition of the glass inclusions 134
4.4 Chemical affinities of the calculated parental magma composition 137
4.5 Implications for calcic plagioclase in island-arc and mid-ocean ridge basalts 142

PART V : **Petrogenesis of high-mg lavas and associated island arc tholeiites from north Tonga**
(T. J. Falloon, D. H. Green and M. T. Mc Culloch) 147

5.1 Introduction 147
5.2 Petrography and mineral chemistry 148
5.2.1 Groundmass pyroxenes 148
5.2.2 Pyroxene phenocrysts 153
5.2.3 Plagioclase 155
5.2.4 Olivine and olivine glass inclusions 155
5.2.5 Cr-spinel 159
5.3 Discussion 162
5.4 Geochemistry 163

5.5 Petrogenesis 166
5.5.1 Depleted source component 168
5.5.2 Enriched source component 173
5.5.3 A two component mixing model 176
5.5.4 Origin of the enriched component in the two component mixing model 177
5.5.5 Evidence for a third enriched component 182

APPENDIX 1 : **Representative residual phase compositions from sandwich experiments on MORB pyrolite, Hawaiian pyrolite and Tinaquillo lherzolite** 184

APPENDIX 2 : **Primitive MORB glass data base** 188

APPENDIX 3 : **Geochemical analyses of dredged igneous rocks from the 1984 cruise of the 'Natsushima'** 193

A3.1 Major element geochemistry 193
A3.2 Trace element geochemistry 196
A3.3 REE geochemistry 198

APPENDIX 4 : **Mantle-derived magmas-roles of variable source peridotite and variable C-H-O fluid compositions**
(D. H. Green, T. J. Falloon and W. R. Taylor) .....
(back pocket)

References 199

LIST OF TABLES

Table		Page
1.	Composition of MORB glasses for which the high pressure phase relationships have been experimentally determined and the range in composition of primitive MORB glasses	4
2.	Compositions of peridotite and basalt compositions used in this study	10
3.	Comparison of peridotite starting compositions with natural peridotite suites on the basis of olivine control lines from (Fo_{91})	15
4.	10kbar peridotite-basalt sandwich experiments	19
5.	Compositions of equilibrium partial melts at 10kbar from MORB pyrolite (MPY-87)	20
6.	Compositions of equilibrium partial melts at 10kbar from various peridotite compositions	21
7.	Starting compositions used in partial melting experiments	58
8.	Experimental run details of 'sandwich' experiments on MORB pyrolite and Tinaquillo lherzolite compositions	61
9.	Equilibrium partial melt compositions from MORB pyrolite (MPY-87) and Tinaquillo lherzolite	62
10.	Equilibrium partial melt compositions from MORB pyrolite (MPY-90-40)	63
11.	Primitive MORB glass compositions	79
12.	Primary MORB compositions	85
13.	MORB picrite compositions	87
14.	Compositions of primitive MORB glass inclusions	90
15.	FAMOUS-Narrowgate-Amar lava series	99
16.	Summary of the volcano-tectonic cycle of the FAMOUS-Narrowgate-Amar area mid-Atlantic ridge and the composition of primary magmas	101
17.	Summary of dredge locations which recovered igneous material during the 1984 cruise of the 'Natsushima'	106
18.	Petrographic summary of dredged lavas from north Tonga	113
19.	Major, trace and REE geochemistry of basaltic andesites from station 15	114
20.	Major, trace and REE geochemistry of representative samples from station 21 and 22	121
21.	Major, trace and REE geochemistry of basaltic andesites from	

station 23, high-mg lavas from stations 23, 24 and 25, and pillow rind from station 31 ... 125
22. Olivine glass inclusion microprobe analyses ... 136
23. Refractory melts developed in oceanic tensional settings ... 138
24. Summary of the petrography and mineral chemistry of the dredged lavas from north Tonga ... 149
25. Representative electron microprobe analyses of groundmass pyroxenes from north Tonga lavas ... 150
26. Representative electron microprobe analyses of pyroxene phenocrysts and microphenocrysts in north Tonga lavas ... 154
27. Wholerock and groundmass major element chemistry of high-mg lavas basaltic andesites from north Tonga ... 156
28. Microprobe analyses of olivine glass inclusions and calculated parental magma compositions ... 157
29. Representative electron microprobe analyses of chromites from north Tonga lavas ... 160
30. Representative major, trace and REE geochemistry of dredged lavas from north Tonga and Lau Basin ... 164
31. Sr and Nd isotopes of representative dredged lavas from north Tonga and Lau Basin ... 165

LIST OF FIGURES

Figure		Page
1.	The compositions of primitive (Mg#$\geq$0.68) MORB glasses plotted in the CIPW molecular normative projection from plagioclase (Ab+An) onto the face olivine (Ol)-diopside (Di)-quartz (Qz) of the 'basalt tetrahedron'	5
2.	Major element oxides SiO_2, CaO, Na_2O, FeO^t, Al_2O_3 and TiO_2 versus MgO for peridotite compositions used in 10kbar melting experiments compared with natural peridotite suites	12-13
3.	Back scattered electron image photographs of run no.s T-2140, 2078 and 2140	22
4.	CIPW molecular normative projection from plagioclase (Ab+An) onto the face olivine (Ol)-diopside (Di)-quartz (Qz) of the 'basalt tetrahedron'	25
5.	Al_2O_3 versus CaO wt% of 10kbar experimental liquid compositions from various peridotite compositions	27
6.	$100Fe^{3+}/(Fe^{3+}+ Al^{3+}+ Cr^{3+})$ versus the $100Cr/(Cr + Al)$ ratio of spinels crystallizing in high pressure peridotite experiments in platinum and graphite capsules at pressures between 8 to 20kbars	30
7.	Equilibrium glass compositions from MORB pyrolite plotted in the CIPW molecular normative projection from diopside (Di) onto the base of the 'basalt tetrahedron'	33
8.	Equilibrium glass compositions from MORB pyrolite plotted in the CIPW molecular normative projection from plagioclase (Ab+An) onto the face olivine (Ol)-diopside (Di)-quartz (Qz) of the 'basalt tetrahedron'	34
9.	Equilibrium glass compositions from Hawaiian pyrolite, Tinaquillo lherzolite and spinel lherzolite KLB-1 plotted in the CIPW molecular normative projection from diopside (Di) onto the base of the 'basalt tetrahedron'	35
10.	Equilibrium liquid compositions from Hawaiian pyrolite, Tinaquillo lherzolite and spinel lherzolite KLB-1 plotted in the CIPW molecular normative projection from plagioclase (Ab+An) onto the face olivine (Ol)-diopside (Di)-quartz (Qz) of the 'basalt tetrahedron'	36
11.	CIPW molecular normative projection from plagioclase (Ab+An) onto the face olivine (Ol)-diopside (Di)-quartz (Qz) of the 'basalt tetrahedron' illustrating the effect of analytical uncertainity	38

12. Frequency histogram of SiO_2 contents of primitive MORB glasses ... 43
13. Glass compositions from various 10kbar melting studies plotted in the CIPW molecular normative basalt tetrahedron ... 45
14. Glass compositions from various 10kbar melting studies plotted in the CIPW molecular normative basalt tetrahedron ... 46
15. Back scattered electron image photograph for run no. T-1513 ... 64
16. Major element oxides SiO_2, Al_2O_3, CaO, Na_2O, TiO_2, FeO^t and MgO versus $100Mg/(Mg + Fe^t)$ for broad beam area scan analyses of the 'basalt' layer in run no. T-1501 ... 66
17. Equilibrium partial melt compositions from MORB pyrolite and Tinaquillo lherzolite plotted in the CIPW molecular normative basalt tetrahedron ... 67
18. Equilibrium partial melt compositions from MORB pyrolite and Tinaquillo lherzolite plotted in the CIPW molecular normative basalt tetrahedron ... 69
19. Cotectics defined by partial melt compositions from MORB pyrolite, Hawaiian pyrolite and Tinaquillo lherzolite at 5, 10, 15, 20 and 30kbars under anhydrous conditions in the CIPW molecular normative basalt tetrahedron ... 71
20. Equilibrium partial melt compositions from spinel lherzolite HK66 compared to cotectics defined by partial melt compositions from MORB pyrolite at 8, 10, 15, 20, 30 and 35kbars in the CIPW molecular normative basalt tetrahedron ... 73
21. Cotectics defined by partial melt compositions from MORB pyrolite at 10, 15, 20 and 30kbars compared to cotectics defined by spinel lherzolite KLB-1 at 10 and 30kbars as well as liquid compositions from Stolper (1980) and Elthon & Scarfe (1984) in the CIPW molecular normative basalt tetrahedron ... 75
22. Results of olivine fractionation calculations plotted in the CIPW molecular normative basalt tetrahedron ... 81
23. MORB picrite compositions compared with equilibrium partial melts from MORB pyrolite and primitive MORB glasses in the CIPW molecular normative basalt tetrahedron ... 89
24. The compositions of primitive MORB glass inclusions compared to equilibrium partial melt compositions from MORB pyrolite and primitive MORB glasses in the CIPW molecular normative basalt tetrahedron ... 92
25. Calculated primary MORB melt compositions from Takahashi et al. (1987) compared with equilibrium partial melt compositions from MORB pyrolite and primitive MORB glasses in the CIPW molecular

normative basalt tetrahedron ... 95
26. Primitive glass compositions from the FAMOUS-Narrowgate-Amar area of the mid-Atlantic ridge compared with equilibrium partial melt compositions from MORB pyrolite in the CIPW molecular normative basalt tetrahedron ... 97
27. Locality map southwest Pacific showing the relationship of the Tonga ridge and trench to other elements of the SW Pacific region ... 104
28. Locality map of the north Tonga ridge showing the location of the dredge stations which recovered igneous rock ... 105
29. Single channel seismic profile across the north Tonga ridge ... 108
30. FeO^t/MgO versus SiO_2 relationships of basaltic andesites and andesites from stations 15, 21 and 23 compared with those of the Tofua magmatic arc ... 110
31. REE patterns for dredged igneous rocks from the 1984 'Natsushima' cruise ... 111
32. Representative chondrite normalised element abundance patterns for the dredged igneous rocks and other related rocks ... 118
33. SiO_2 versus Mg# and TiO_2 versus Mg# for dredged rocks from station 21 and basaltic andesites from station 23 compared with rocks from the TM-arc ... 126
34. CaO versus MgO wt% for high-mg lavas from stations 23, 24 and 25 ... 131
35. glass inclusions in magnesian olivine phenocrysts ... 135
36. Crx100/(Cr + Al) and Mgx100/(Mg + Fe) variations in spinel inclusions in magnesian olivine phenocrysts from north Tonga ... 140
37. CIPW molecular normative projection from Di onto the base of the basalt tetrahedron ... 141
38. 100Ca/(Ca + Na) ratio of a bulk composition versus the most An-rich plagioclase capable of crystallizing under anhydrous conditions regardless of pressure and temperature ... 143
39. CaO/Na_2O versus MgO wt% for Tonga lavas from the Tonga islands and dredged lavas from the north Tonga arc ... 145
40. Representative compositions of pyroxenes from north Tonga lavas ... 151
41. SEM backscattered electron image photographs of small endiopside microphenocrysts ... 152
42. Plagioclase phenocryst and groundmass compositions in basaltic andesites from station 23, north Tonga ... 158

43. Compositional relationships in Cr-spinels from north Tonga ... 161
44. Representative chrondrite normalised abundance patterns for dredged north Tonga lavas ... 167
45. CIPW molecular normative projection from Di onto the base of the basalt tetrahedron ... 169
46. CaO/Al_2O_3 ratio of residue compositions from equilibrium batch partial melting of a MORB pyrolite composition at 10kbar versus Mg# (x100) of the residue ... 172
47. Ti/V versus Ti/Sc ratios of dredged north Tonga lavas ... 174
48. Nd versus Sr isotopic compositions of dredged north Tonga lavas ... 175
49. Chrondrite normalised abundance patterns of possible depleted and enriched endmember components ... 178
50. Nb ppm versus % enriched component ... 179
51. Pb isotopic composition of Tofua magmatic arc volcanics ... 181
52. Sr/La versus Ba/La ratios of north Tonga lavas ... 183

ACKNOWLEDGEMENTS

First I would like to thank my supervisors Professor David Green and Dr. Tony Crawford for initiating this project and for their support, enthusiasm, interest, encouragement and stimulation throughout.

Thanks are also extended to the many people who have helped me during this project especially:

- Wieslav Jablonski for his help with the electron microprobe and scanning electron microscope;
- Keith Harris for his help in the high-pressure laboratory;
- Phillip Robinson for his help with the analytical work in parts III to V;
- Simon Stevens for his help in making thin-sections and polishing probe mounts,
- Peter Cornish and Andrew Gillion for their help in the workshop at various times;
- June Pongratz for drafting diagrams in parts III and IV of this thesis;
- Dr. Malcolm Mc Culloch for providing the Nd and Sr isotope analyses presented in part V;
- to Drs. Ron Berry, Wayne Taylor and Graeme Wheller for their help with various computer programs used throughout the project;
- to the captain and crew of the 'Natsushima', chief scientists Drs. Keith Lewis and Elichi Honza and fellow shipboard scientists;
- to various correspondents who have provided material before publication; Drs. R. N. Thompson, Elichi Takahashi, Charles Langmuir, John Sinton, Bob Duncan and Tony Ewart;
- to various scientists for their helpful discussions, including Drs. Gehard Brey, Kurt Mengel, David Ellis, Elichi Takahashi, Steve Foley, Rick Varne, Lynton Jaques, Joe Stolz, Steve Weaver, Rod Sewell, George Jenner, Bob Duncan;
- many thanks to the graduate students (+ hangers-on) of this department for their hospitality, companionship, support and encouragement; Wayne Taylor, Graeme Wheller, Scott Kuehner, Steve Foley, Ai Yang, Bhakti Harahap, Yuenyong Panjasawatwong, Wyss Yim, Sutrisno, Rahmat Hermanto, Sjafra Dwipa, Salman, Vanessa Guthrie, Sharon Adrichem,, Ewan Reid, Kim Zhaw, Steve Eggins, Nick Odling, John Adam, Margaret Wallace, Malcolm Wallace, Garry Davidson, David Huston, Michael Seitz, Thanis Wongwanich and Richard Wedekind;

I also would like to extend my general thanks to all members of the Geology Department not already mentioned for their help and for providing a happy working environment.

Special thanks to Wayne Taylor for introducing me to bushwalking in Tasmania's wilderness areas on his many "man's walks" while Prof was out of town.

Thanks to my many flatmates at 22 Pottery Road and 19 Edith Avenue for putting up with a trumpet playing geology student: Douglas Findlay, Bernard Shaw, Jonathon Walker, Graham Hobbs, Bruce Morley, Bruce Levett, Charles Ling, John Robinson, Geoff Howells, Tim Kay, Steve Van Ommen, Robert Bryant, John Christian, Mark Aldridge.

Thanks to the many friends made through the University of Tasmania Squash Club, Glenorchy City Concert Brass and the Tasmanian Conservatorium Brass Ensemble.

Thanks also to the members of the Claremont Baptist Church, St. Peters Anglican Church Sandy Bay and St. Johns Presbyterian Church, Hobart for all their support and encouragement.

Thanks to Fay and Rudd Bussell for their hospitality and friendship.

Thanks to Tony, Jo-Anne, John and Andrew Herbert for their friendship and support.

Special thanks to my parents and family for their support and encouragement.

Lastly I wish to thank Wendy for her companionship, support, encouragement and enthusiasm during this study, and agreeing to marry me.

ABSTRACT

Parts I and II are an experimental study concerned with the current controversy regarding the evolved versus primary nature of primitive MORB glasses.

In part I equilibrium partial melt compositions under anhydrous conditions are presented on four peridotite compositions at 10kbar. The four peridotite compositions are: 'MORB pyrolite' ,'Hawaiian pyrolite', Tinaquillo lherzolite and the spinel lherzolite KLB-1. In part II equilibrium partial melt compositions are presented for MORB pyrolite from 8 to 35kbars and for Tinaquillo lherzolite at 15 to 20kbars. The equilibrium liquids were determined by 'sandwich' experiments. The results of the experiments are used to test a 10kbar melt model for the generation of primitive MORB glasses. The melt compositions from the four peridotites at 10kbar are significantly different from primitive MORB glasses in major element chemistry and plot away from the field of primitive MORB glasses in the CIPW molecular normative 'Basalt tetrahedron'. The results suggest primary MORB melts segregate from source diapirs at pressures of 8 to 25kbars in equilibrium with either lherzolite or harzburgite residues. MgO contents of primary MORB melts range from 10-17 wt% while primary melts >17 wt% MgO are of minor importance.

Parts III, IV and V consist of a petrographic, mineral chemical, geochemical and petrological study of dredged lavas from the North Tongan forearc recovered during the 1984 cruise of the research vessel 'Natsushima'.

In part III petrographic, wholerock major and trace element data is presented and the geochemical affinities of all the dredge suites discussed.

Part IV looks in detail at the chemistry of large (up to 0.2mm) glass inclusions contained in unusually magnesian olivine phenocrysts (Fo_{94}) within the high-mg lavas.

Part V is concerned with the petrogenesis of the high-mg lavas and associated island arc tholeiites from North Tonga. The mineral chemistry of phenocryst and groundmass phases combined with wholerock, glass and glass inclusion major element chemistry give unequivocal evidence of mixing of two or more distinct parental magmas. The major, trace and isotopic (Sr, Nd) geochemistry of the lavas can be explained by partial melting of refractory mantle peridotite (depleted after extraction of primary MORB picrite) at shallow depths (<10kb or higher pressures if water is present), which has been previously 'enriched' in silicate incompatible elements by two distinct components.

PART I

ANHYDROUS PARTIAL MELTING OF MORB PYROLITE AND OTHER PERIDOTITE COMPOSITIONS AT 10KBAR: IMPLICATIONS FOR THE ORIGIN OF PRIMITIVE MORB GLASSES.

1.1 INTRODUCTION

The nature, composition and depth of origin of primary magmas parental to Mid Ocean Ridge basalts (MORB) is at the present time a subject of controversy (Presnall & Hoover, 1984, 1986; Fujii & Scarfe, 1985; Elthon, 1986). Two differing models of MORB petrogenesis are currently proposed in the literature. The first model termed here the 10kbar[1] primary melt model states that the most primitive, in the sense of high $Mg/(Mg+Fe^{2+})$ ratio (Mg#), MORB glasses are close to or are in fact primary melts from the melting of upper mantle peridotite composition at relatively shallow depths, 30kms or 10kbar pressure being the most commonly proposed depth of origin (Bender et al., 1978; Fujii & Bougault, 1983; Fujii and Scarfe, 1985; Presnall et al., 1979; Presnall & Hoover, 1984; Green & Ringwood, 1967). The second model, termed here the picrite primary melt model, states that these more primitive MORB glasses are not primary but are fractionated compositions, derived by olivine extraction from more picritic parents. The latter are interpreted as primary melts of mantle peridotite at pressures ranging from 15-20 kbars (Green et al., 1979; Elthon & Scarfe, 1980, 1984; Stolper, 1980) or higher (30kbar) pressures (O'Hara, 1968).

The two models place differing emphasis on the type of primary magmas which are involved in MORB genesis. In the 10kbar primary melt model, picritic primary melts are considered to be of minor importance, primary melts being dominated by olivine tholeiite compositions similar to

1 In this paper the term '10kbar' is used in a general sense to mean approximately 10kbar, as some of the experiments discussed in this paper were conducted at pressures of 8, 9 and 10.5kbar.

the most primitive of MORB glasses. Similarly in the picrite primary melt model, picritic melts are the dominant primary melts, while the presence of primary olivine and quartz tholeiite melts is considered to be of minor importance.

Experimental petrologists have tested these two models by a combination of two methods, (1) near-liquidus studies of natural MORB glass compositions (Bender et al., 1978; Green et al., 1979; Fujii & Bougault, 1983; Fujii et al., 1978; Kushiro & Thompson, 1972) and (2) by the direct melting studies of peridotite compositions (Jaques & Green, 1980; Takahashi & Kushiro, 1983; Fujii & Scarfe, 1985; Presnall et al., 1979; Sen, 1982; Green et al., 1987). However despite these efforts disagreement exists, mainly due to differing interpretations of the results from the experimental studies. In this study the second approach has been adopted and melting experiments have been carried out on a MORB pyrolite[2] composition at 10kbar pressure using a basalt-peridotite sandwich technique. For comparison with MORB pyrolite, 10kbar experiments on Tinaquillo lherzolite, Hawaiian pyrolite (Jaques & Green, 1980) and spinel lherzolite KLB-1 (Takahashi, 1986) were also performed. The basalt in the 'sandwich' is one of the most primitive MORB glasses recovered from the Mid Atlantic ridge, DSDP3-18-7-1 (Frey et al., 1974). The liquidus phase relationships of this composition were studied by Green et al. (1979). By using the sandwich technique it is possible to obtain information regarding the nature of equilibrium partial melts from a suitable source composition for MORB at 10kbar. In this way we produce a direct testing of a 10kbar primary melt model for MORB petrogenesis. The results of the 10kbar melting experiments on the MORB pyrolite composition demonstrate that the majority of primitive MORB glasses are not primary melts at 10kbar, thus making the picrite primary melt our preferred model for MORB petrogenesis. Preliminary results of this study have been presented in Green et al. (1987) (Appendix 4). Before presenting the results of the 10kbar melting study, it is worthwhile briefly reviewing the results and implications of high pressure near-liquidus experiments on MORB compositions.

2 "MORB pyrolite" is the name applied to a model source peridotite composition based on combining liquid (mid ocean ridge basalt) with residual peridotite (Green et al., 1979).

1.2 APPROACH 1: HIGH PRESSURE NEAR-LIQUIDUS EXPERIMENTS ON MORB

Although the rationale behind this approach is relatively straightforward, the interpretation of the experimental results has been the cause of controversy (Fujii & Bougault, 1983; Wyllie et al., 1981). The rationale is as follows: if primitive MORB glasses are primary magmas then we expect to find at some pressure and temperature multiple saturation at or near the liquidus in the phases olivine, clinopyroxene and orthopyroxene or olivine and orthopyroxene suggesting equilibrium with an lherzolite or harzburgite residue respectively. In evaluating the importance of multiple saturation at or near liquidus temperatures, the glass in equilibrium with olivine, orthopyroxene ± clinopyroxene must be very close to the original bulk composition of the glass.

MORB populations are geochemically diverse and show clear evidence of the compositional effects of low pressure crystal fractionation (Bryan & Dick, 1982; Bryan et al., 1976; Walker et al., 1979; Thompson, 1987). In this study primitive MORB glasses are defined solely on the basis of the $Mg/(Mg + Fe^{2+})$ ratio(Mg#), where Fe^{2+} is calculated using a $Fe^{2+}/(Fe^{3+}+ Fe^{2+})$ ratio which has been set equal to 0.9. This value is appropriate for the reduced oxygen fugacity present in MORB source regions (Christie et al., 1986; Green et al., 1987). MORB glasses with $Mg\# \geq 0.68$ are defined as primitive, as they are consistent with equilibrium with a mantle olivine of $Mg\# \geq 0.87$ and are thus potential primary magmas from upper mantle peridotite. For the purposes of this study a data set of over 80 primitive MORB glasses were collected from the literature (Appendix 2). The maximum and minimum values for major element oxides, molecular normative mineralogy and selected major oxide ratios are presented in Table 1. All the worlds oceans are represented in the data set, however the glasses are dominated by those from the FAMOUS area of the Mid-Atlantic Ridge. Data sources for the glasses are given in the caption to Fig.1. Glass compositions have been chosen instead of whole rock data as glass compositions represent liquid compositions, and do not suffer from the effects of crystal accumulation (Bryan, 1983; Staudigel & Bryan, 1981) and alteration (Melson et al., 1977; Morrison & Thompson, 1983). In Fig.1 the primitive MORB glasses are projected on to the face olivine(Ol)-diopside(Di)-quartz(Qz) of the 'Basalt tetrahedron' from plagioclase(An+Ab). This projection shows that the primitive MORB glasses have a significant range of silica-saturation from slightly nepheline normative to quartz normative compositions. This is an important observation which must be explained by any model on MORB petrogenesis (Thompson, 1987).

Table 1

Compositions of MORB Glasses for which the high pressure phase relationships have been experimentally determined and the range in composition of primitive MORB Glasses

	1	2	3	4	5	6
SiO_2	48.20	49.47	49.70	50.00	49.68	48.20 - 51.64
TiO_2	0.73	0.82	0.72	1.64	1.55	0.50 - 1.30
Al_2O_3	16.30	15.23	16.40	15.00	15.49	15.50 - 17.62
FeO^t	8.92	8.15	7.90	11.20	9.08	7.30 - 9.40
MgO	10.70	10.66	10.10	8.40	9.17	8.10 - 10.70
CaO	12.00	12.21	13.10	10.60	10.61	11.23 - 13.57
Na_2O	1.95	1.94	2.00	2.70	2.88	1.42 - 2.71
K_2O	0.09	0.16	-	-	-	0.01 - 0.32
P_2O_5	-	0.10	-	-	-	0.03 - 0.14
MnO	0.25	0.14	0.12	0.22	0.18	0.09 - 0.25
Cr_2O_3	0.05	-	0.07	-	-	0.01 - 0.13
Total	99.19	98.88	100.12	99.89	98.75	
Mg#	0.70	0.72	0.72	0.60	0.66	0.68 - 0.73
CIPW norm (molecular)						
Qz	-	-	-	-	-	<8.39
Ne	-	-	-	-	-	<1.00
Ab	14.51	14.76	15.04	20.47	21.77	10.53 - 20.79
An	29.39	27.44	29.95	24.02	24.44	24.92 - 34.04
Di	19.95	23.34	24.50	20.41	19.90	18.76 - 29.45
Hy	9.32	15.97	11.63	15.54	10.78	<24.96
Ol	22.78	13.93	15.34	12.27	16.53	<28.33
CaO/Al_2O_3	0.78	0.80	0.79	0.71	0.68	0.67 - 0.88
CaO/Na_2O	6.15	6.29	6.55	3.92	3.68	4.58 - 9.49
CaO/TiO_2	16.44	14.90	18.19	6.50	6.84	9.32 - 25.60
Al_2O_3/TiO_2	22.33	18.57	22.77	9.14	9.99	12.00 - 33.80

(1) primitive MORB glass ALV527-1-1 from the FAMOUS area of the Mid-Atlantic Ridge (Bender et al., 1978).

(2) primitive MORB glass ARP74-10-16 from the FAMOUS area of the Mid-Atlantic Ridge (Fujii & Bougault, 1983).

(3) primitive MORB glass DSDP3-18-7-1 from the South Atlantic (Frey et al., 1974; Green et al., 1979).

(4) aphyric glassy olivine tholeiite, sample Leg45-395A-8-1-9 from the Mid-Atlantic Ridge (Fujii & Kushiro, 1977).

(5) olivine tholeiite, sample T-87 from the Mid-Atlantic Ridge (Kushiro & Thompson, 1972; Kushiro, 1973).

(6) Minimum and maximum values for over 80 primitive MORB glasses (data sources, see caption to Fig.1).

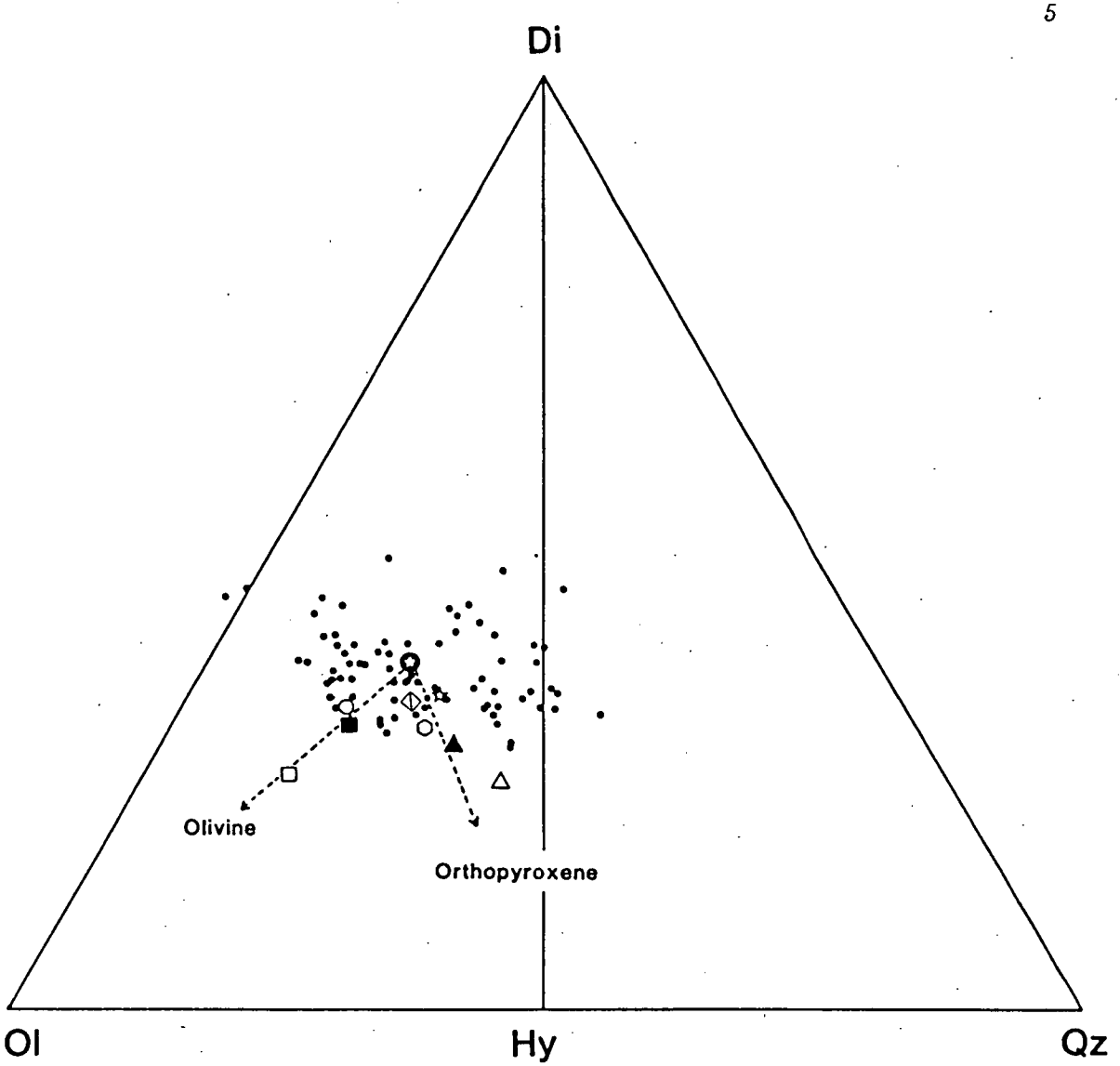

Figure 1.

The compositions of primitive (Mg#≥0.68) MORB glasses plotted in the CIPW molecular normative projection from plagioclase(Ab+An) onto the face olivine(Ol)-diopside(Di)-quartz(Qz) of the 'basalt tetrahedron',

(✪) primitive MORB glass DSDP3-18-7-1 (Frey et al., 1974; Green et al., 1979),

(○) primitive MORB glass ALV527-1-1 (Bender et al., 1978),

(☆) primitive MORB glass ARP74-10-16 (Fujii & Bougault, 1983; Fujii & Scarfe, 1985),

(◇) olivine tholeiite T-87 (Kushiro & Thompson, 1972; Kushiro, 1973),

(⬡) aphyric glassy olivine tholeiite, sample Leg45-395A-8-1-9 (Fujii & Kushiro, 1977; Fujii et al., 1978),

(■) mix D (DSDP3-18-7-1 + 9 wt% olivine), Green et al. (1979),

(□) mix E (DSDP3-18-7-1 + 17 wt% olivine), Green et al. (1979),

(▲) glass in equilibrium with calcic clinopyroxene, run T25, 1300°C, 12kbar (Green et al., 1979),

(△) glass in equilibrium with orthopyroxene, run T16, 1360°C, 12kbar (Green et al., 1979),

(●) primitive MORB glasses (Natland et al., 1984; Melson et al., 1977; Melson et al., 1976; Frey et al., 1973; Frey et al., 1974; Green et al., 1979; O'Donnell & Presnall, 1980; Melson & O'Hearn, 1979; Scarfe & Smith, 1977; Shipboard.S.P., 1977; Hekinian et al., 1976; Langmuir et al., 1977; Bender et al., 1978; Fujii & Bougault, 1983; Basaltic Volcanism Study Project, 1981; Shibata et al., 1979; Barker et al., 1983; Melson, 1973; Stakes et al., 1984; Sigurdsson, 1981; Bryan, 1979a; Bryan & Moore, 1977; Bryan et al., 1981).

---> olivine or orthopyroxene addition lines,

Also listed in Table 1 and plotted on Fig.1 are the compositions of MORB glasses which have had their high-pressure near liquidus phase relationships determined. Three of the MORBs, DSDP3-18-7-1, ALV527-1-1 and ARP74-10-16 have high Mg# and conform to our definition of primitive MORB glasses. However two of the MORBs, 395A-8-1-9 and T-87 have significantly lower CaO, Mg# and higher FeO than the three above mentioned primitive MORB glasses and are not considered primitive according to our criteria. In the following sections the results of the high-pressure near liquidus experiments are evaluated to determine whether or not primitive MORB glasses are saturated in orthopyroxene near their liquidii at 10kbars pressure.

1.2.1 High-pressure near-liquidus experiments on ALV527-1-1 and DSDP3-18-7-1

Both ALV527-1-1 (studied by Bender et al., 1978) and DSDP3-18-7-1 (Green et al., 1979) have very similar phase relationships. Both have olivine alone on the liquidus until approximately 12kb when clinopyroxene replaces olivine as the liquidus phase. Both compositions fail to show multiple saturation at any pressure with the assemblage olivine + orthopyroxene ± clinopyroxene. An orthopyroxene reported in a run at 15kbar on ALV527-1-1 (Bender et al., 1978) is now considered to be an aberrant result (Fujii & Bougault, 1983; Elthon & Scarfe, 1984).

Green et al. (1979) added orthopyroxene to DSDP3-18-7-1 at 12kbar to test how close to orthopyroxene saturation DSDP3-18-7-1 was. Green et al. (1979) found that between 5 to 9 wt% orthopyroxene had to be added to DSDP3-18-7-1, significantly changing the bulk composition, before orthopyroxene appeared on the liquidus. This is illustrated in Fig.1 where the glass compositions from runs T25 and T16 (Green et al., 1979) are plotted. The bulk composition of run T25 is equal to DSDP3-18-7-1 plus 5 wt% orthopyroxene whereas the bulk composition of T16 contained 9 wt% orthopyroxene. At 12kbar, 1300°C, T25 had calcic clinopyroxene only on the liquidus, whereas T16 at 1360°C had orthopyroxene only on the liquidus. The composition of T16 plots well below the field of primitive MORBs in Fig.1 indicating that primitive MORB glasses are far from orthopyroxene saturation and are not primary magmas but have suffered a prior history of olivine fractionation. On the basis of this result Green et al. (1979) added olivine to DSDP3-18-7-1 to evaluate whether at a higher pressure and temperature an olivine-enriched magma could be saturated in olivine and orthopyroxene ± clinopyroxene and parental to DSDP3-18-7-1 by extraction of

olivine alone at lower pressures. Two compositions were prepared, which are also plotted in Fig.1, mix D consisted of DSDP3-18-7-1 + 9 wt% olivine and mix E consisted of DSDP3-18-7-1 + 17 wt% olivine. Mix E was found to be multiply saturated in olivine and orthopyroxene at 20kbar, 1430°C, thus this composition is a possible primary MORB magma in equilibrium with a harzburgite residue.

Fujii & Bougault (1983) discussed the validity of the orthopyroxene addition experiments of Green et al. (1979); because the topology of the orthopyroxene-olivine phase boundary is unknown or uncertain, permissible topologies could be constructed in which a large amount of added orthopyroxene would be required before orthopyroxene saturation is reached even though the composition of DSDP3-18-7-1 is close to the olivine-orthopyroxene cotectic (see for example Fig.3.3.14, Basaltic Volcanism Study Project, 1981). Thus the orthopyroxene addition experiments of Green et al. (1979) did not fully evaluate the 'closeness' to multiple saturation of DSDP3-18-7-1 nor directly determined the composition of liquids, close to DSDP3-18-7-1, which were olivine + orthopyroxene ± clinopyroxene saturated at 10kbar. However the sandwich technique used in this experimental study by its very nature will 'force' the composition of DSDP3-18-7-1 to equilibrate with a peridotite mineralogy. The resulting equilibrium glass composition can then be compared with the bulk composition of DSDP3-18-7-1. It will be shown that liquids in equilibrium with olivine + orthopyroxene ± clinopyroxene at 10kbar, as determined by the sandwich technique in this study, are substantially different from DSDP3-18-7-1 confirming the conclusion of Green et al. (1979) based on the orthopyroxene addition experiments.

1.2.2 High-pressure near-liquidus experiments on ARP74-10-16

The experimental results on ARP74-10-16 (Fujii & Bougault, 1983) however differ from the previous two studies as multiple saturation in olivine + clinopyroxene + orthopyroxene occurred at 10kbar. The appearance of orthopyroxene could be explained by the fact that ARP74-10-16 has a higher normative Hy content than DSDP3-18-7-1 or ALV527-1-1 (Table 1), plotting further towards the Qz apex in Fig.1 from DSDP3-18-7-1 and ALV527-1-1. On the basis of their experiments Fujii & Bougault (1983) claim that ARP74-10-16 is a possible primary magma of spinel or plagioclase lherzolite at 10kbar, thus giving support to a 10kbar primary melt model. However the run data presented by Fujii & Bougault (1983) (their Table 3) shows that the multiple saturation occurred between 25 to 50°C below the liquidus, at

10kbar. If ARP74-10-16 was a primary magma multiple saturation would be expected ~5-10°C below the liquidus. Fujii & Bougault (1983) fail to provide electron microprobe (EMP) analyses of the glass composition in equilibrium with olivine + orthopyroxene + clinopyroxene at 10kbar, making it impossible to evaluate whether or not their conclusions concerning ARP74-10-16 are valid or not. If the orthopyroxene did in fact crystallize ~ 50°C below the liquidus at 10kbar, then it is likely that the charge was highly crystalline making it impossible to obtain unmodified glass compositions, hence explaining the lack of this critical data in Fujii & Bougault (1983).

1.2.3 High-pressure near-liquidus experiments on 395A-8-1,50cm and T-87

The experimental results on the two more Fe-rich MORBs 395A-8-1,50cm (Fujii et al., 1978) and T-87 (Kushiro & Thompson, 1972) showed that they were saturated in orthopyroxene approximately 20°C below the liquidus at approximately 8kbar for 395A-8-1,50cm and approximately 10°C below the liquidus at 7.5kbar for T-87. For these two magmas to be considered primary magmas then we must envisage a mantle source peridotite with olivine $\leq Fo_{86}$. The possibility of more Fe-rich mantle peridotite sources for MORBs has been suggested by Wilkinson (1982). The liquid in equilibrium with orthopyroxene published by Kushiro (1973) has a Mg# of 0.57 and would only be in equilibrium with a mantle olivine of Fo_{82} which differs considerably from previous estimates of mantle peridotite for MORB, which have an olivine of $Fo_{90\pm2}$ (Green, 1970, 71; Frey et al., 1985; Nickel & Green, 1984; Jaques & Green, 1980). Thus if we accept arguments in favour of a mantle olivine of $Fo_{90\pm2}$ then the two Fe-rich MORBs must be regarded as fractionated compositions, a possibility recognized by Kushiro & Thompson (1972). The Ni contents of these two compositions are appreciably lower than commonly inferred for primitive magmas (Allegre et al., 1977; Sato, 1977), supporting the conclusion that T-87 and 395A-8-1,50cm are fractionated compositions, which have reached orthopyroxene saturation at some lower pressure from that of their parental compositions.

In summary the first approach has not been all that successful in demonstrating the primary nature of primitive MORB. However when interpreted correctly the results from the primitive MORBs ALV527-1-1, DSDP3-18-7-1 and ARP74-10-16 suggest that these and MORB of similar composition are not multiply saturated at 10kbar, near their liquidii. The multiple saturation in ARP74-10-16 occurs well below its liquidus

temperature. The three primitive MORB compositions fall within the middle of the MORB cluster in Fig.1, compositions which plot towards the nepheline and quartz normative sides so far have not been studied. The rest of this paper will now address the second approach, that of direct melting studies of peridotite compositions.

1.3 APPROACH 2: DIRECT MELTING EXPERIMENTS ON PERIDOTITE COMPOSITIONS

The second approach which experimental petrologists have used in the investigation of MORB petrogenesis is the direct melting of upper mantle peridotite. The rationale of this approach is again straightforward: if primitive MORB glasses are primary magmas at 10kbar then it should be possible to produce similar compositions as equilibrium partial melts from suitable source compositions at 10kbar. Choosing a suitable starting composition however is of critical importance as numerous studies have shown that liquid compositions are not invariant but are affected by the bulk compositions of the starting material (Jaques & Green, 1980; Takahashi & Kushiro, 1983; Fujii & Scarfe, 1985). The peridotite starting compositions used in this study are listed in Table 2. The main composition used is a MORB pyrolite composition calculated by Green et al. (1979) based on combining 24 wt% of the picrite composition (mix E, Green et al., 1979) which was in equilibrium with olivine and orthopyroxene at 20kb, 1430°C with a harzburgite residue. The choice of 'harzburgite' residue in the calculation of 'MORB' pyrolite composition requires some comment as Fujii & Scarfe (1985) criticize the Green et al. (1979) calculation of the model source on the basis that most ultramafic rocks dredged from the ocean floor are not harzburgite but lherzolite. However Dick & Fisher (1984) calculate an average composition for dredged ultramafic rocks (lherzolites) from the Indian-Antarctic ridge which is remarkably similar to the residual 'harzburgite' of Green et al. (1979) (see Fig.2). Reconciliation of the apparently different interpretations lies in recognizing that the orthopyroxene in residual harzburgite at 15-20kbar, 1400-1450°C contains >5 wt% Al_2O_3 and >2.5 wt% CaO. Residual harzburgite of this character will recrystallize at lower temperatures to spinel lherzolite.

The other compositions used are Tinaquillo lherzolite minus 40 wt% olivine, Hawaiian pyrolite minus 40 wt% olivine and the spinel lherzolite KLB-1 (powder kindly supplied by E.Takahashi). The melting relations of Tinaquillo and Hawaiian pyrolite have been studied previously by Jaques & Green (1980) and that of KLB-1 has been studied by Takahashi (1986). Three different MORB pyrolite compositions were used in the experiments

TABLE 2

Compositions of peridotites and basalt compositions used in this study

	1	2	3	4	5	6	7	8	9
SiO_2	44.32	44.74	47.15	47.50	47.90	44.48	49.70	49.03	49.76
TiO_2	0.16	0.17	0.28	0.13	1.18	0.16	0.72	0.30	3.20
Al_2O_3	4.33	4.37	7.28	5.35	5.91	3.59	16.40	14.35	14.28
FeO^t	9.82	7.55	7.27	7.51	8.81	8.10	7.90	9.00	8.96
MnO	0.10	0.11	0.12	0.18	0.13	0.12	0.12	-	-
MgO	36.84	38.57	30.57	32.80	28.80	39.22	10.10	13.63	10.48
CaO	3.34	3.38	5.63	4.97	5.14	3.44	13.10	12.40	9.14
Na_2O	0.39	0.40	0.66	0.30	0.95	0.30	2.00	1.15	3.27
K_2O	0.00	0.00	0.00	0.03	0.22	0.02	0.00	-	0.76
P_2O_5	0.00	0.00	0.00	0.02	0.06	0.03	0.00	-	-
Cr_2O_3	0.44	0.45	0.75	0.75	0.72	0.31	0.07	-	-
NiO	0.25	0.26	0.29	0.43	0.13	0.25	0.03	-	-
Total	99.99	100.00	100.00	99.97	99.95	100.02	100.14	99.86	99.85
Mg#	0.87	0.90	0.88	0.89	0.85	0.90	0.69	0.73	0.67
CIPW norm (molecular)									
Ab	2.14	2.17	3.97	1.79	5.81	1.62	15.09	8.45	23.34
An	6.16	6.12	11.33	8.73	7.64	5.10	30.07	27.82	17.53
Di	3.98	4.01	7.39	7.54	9.47	5.04	24.56	22.53	18.53
Hy	13.20	12.49	22.22	27.97	25.46	12.18	12.10	20.82	3.56
Ol	72.52	73.47	52.56	51.69	45.88	74.37	14.69	18.10	23.22
CaO/Al_2O_3	0.77	0.77	0.77	0.93	0.87	0.96	0.79	0.86	0.64
CaO/Na_2O	8.56	8.45	8.53	16.56	5.41	11.46	6.55	10.78	2.79
CaO/TiO_2	20.87	19.88	20.11	38.23	4.35	21.50	18.19	41.33	2.86
Al_2O_3/TiO_2	27.06	25.70	26.00	41.15	5.01	22.44	22.77	47.83	4.46

(1) MORB pyrolite composition MPY-87.

(2) MORB pyrolite composition MPY-90.

(3) MORB pyrolite MPY-90 minus 40% olivine ($Mg_{91.6}Fe_{8.1}Ni_{0.2}Mn_{0.1}$), MPY-90-40.

(4) Tinaquillo lherzolite minus 40% olivine ($Mg_{91.9}Fe_{8.0}Mn_{0.1}$), TQ-40.

(5) Hawaiian pyrolite minus 40% olivine ($Mg_{91.6}Fe_{8.1}Ni_{0.2}Mn_{0.1}$), HW-40.

(6) Spinel lherzolite KLB-1 (Takahashi, 1986).

(7) Primitive MORB glass DSDP3-18-7-1 (Green et al., 1979).

(8) Jaques & Green (1980) calculated melt composition from Tinaquillo at 10kbar, 1300°C. Composition given is the mix composition as determined by broad beam electron microprobe analysis.

(9) Jaques & Green (1980) calculated melt composition from Hawaiian pyrolite at 10kbar, 1250°C. Composition given is the mix composition as determined by broad beam electron microprobe analysis.

t=total iron as FeO, Mg#=MG/(Mg + Fe^t), (-) below detection limit.

designated MPY-87, MPY-90 and MPY-90-40. MPY-90 is the MORB pyrolite originally calculated by Green et al. (1979), MPY-90-40 is MPY-90 minus 40 wt% olivine and MPY-87 is a result of recalculating MPY-90 to a lower Mg# to produce a more Fe-rich pyrolite composition. The more Fe-rich composition is biassed towards yielding MORB olivine tholeiites as primary melts since most primitive olivine tholeiites have Mg# between 0.68-0.70 and if they are primary melts require residual peridotite with olivine $\geq Fo_{87}$ $(K_D)^{Ol/Liq}_{Fe/Mg}=0.32$). Olivine contains only Mg, Fe and Ni in solid solution and the effect of extracting 40 wt% olivine from the model source composition cannot affect phase relations or phase compositions in any way except in Mg, Fe, or Ni concentration, as long as olivine is a residual phase. Put another way, the effect of extracting 40 wt% olivine of Fo_{91} composition will only be to lessen the buffering role of olivine in Mg# and Ni content -thus liquids and residues for pyrolite-40 wt% olivine will change a little more rapidly than for pyrolite in Mg# and Ni content with increasing degree of melting. The net result of olivine subtraction is to increase the modal abundance of pyroxene, spinel and melt at the expense of olivine and to slightly underestimate the Mg# of liquids and residues in equilibrium with residual olivine of $<Fo_{91}$ (i.e. low degrees of melting) and to slightly over estimate the Mg# of liquids and residues in equilibrium with olivine of $>Fo_{91}$. In the following section the suitability of these starting compositions for studies of MORB petrogenesis is discussed with reference to natural peridotite suites.

1.4 NATURAL PERIDOTITE SUITES AS A CONSTRAINT ON SUITABLE SOURCE COMPOSITIONS FOR MORB PETROGENESIS

An important constraint on the choice of a suitable source composition is the variability in natural peridotite compositions of upper mantle origin. Two peridotite suites which are representative of moderate pressure upper mantle peridotite samples have therefore been chosen to illustrate their chemical coherence and relevance in defining upper mantle source compositions. The peridotite suites are the Ronda high temperature peridotite intrusion (Frey et al., 1985) and spinel lherzolite inclusions from Lake Bullenmerri, Victoria (Nickel & Green, 1984). Both suites have suitable major, trace element characteristics for the production of MORB (Frey et al., 1985; Nickel & Green, 1984).

Both the peridotite suites give well-defined linear major element trends when plotted against MgO (Fig.2). These linear oxide trends are interpreted as being produced by batch partial melting combined with the

Figure 2.

Major element oxides SiO_2, CaO, Na_2O, FeOt, Al_2O_3 and TiO_2 versus MgO for peridotite compositions used in 10kbar melting experiments compared with natural peridotite suites,

(●) peridotite compositions from the Ronda high temperature peridotite intrusion (Frey et al., 1985). R717 is the most 'fertile' composition from the Ronda suite,

(○) peridotite xenolith compositions from Lake Bullenmerri, Victoria, (Nickel & Green, 1984). BME-15 is the most 'fertile' peridotite composition from Lake Bullenmerri,

(△) estimated primitive undepleted mantle composition (Maaloe & Aoki, 1977),

(□) estimate of mantle composition (Jagoutz et al., 1979),

(⬡) average of 50 representative plagioclase-free spinel harzburgites and lherzolites from the ocean ridges and fracture zones (Dick & Fisher, 1984),

(⬢) residue composition based on the extraction of a 24% partial melt of a MORB picrite (DSDP3-18-7-1 + 17 wt% olivine) from MORB pyrolite (Green et al., 1979),

(▲) peridotite compositions used in 10kbar melting studies, each composition is individually marked as follows: HAW, Hawaiian pyrolite (Jaques & Green, 1980); HW-40, Hawaiian pyrolite minus 40 wt% olivine (Jaques & Green, 1980); TQ, Tinaquillo lherzolite (Jaques & Green, 1980); TQ-40 Tinaquillo lherzolite minus 40 wt% olivine (Jaques & Green, 1980); 77PAII-1, plagioclase and spinel lherzolite from Pali vent no.2, Oahu (Sen, 1982); HK66, spinel lherzolite from Salt Lake Crater, Hawaii (Takahashi & Kushiro, 1983); PMM-1, PMM-2, PMM-4, spinel lherzolite compositions studied by Fujii & Scarfe (1985); KLB-1, spinel lherzolite inclusion from the Kilbourne Hole Crater, New Mexico (Takahashi, 1986); MPY-87, MPY-90, MPY-90-40, MORB pyrolite starting compositions used in this study,

(☆) olivine ($Fo_{91.6}$) composition,

———— olivine control lines from olivine ($Fo_{91.6}$),

—·—·—·— regression line for 83 oceanic spinel lherzolite xenoliths (Maaloe & Aoki, 1977),

– – – – – – – regression line for ocean-floor peridotites (Shibata & Thompson, 1986).

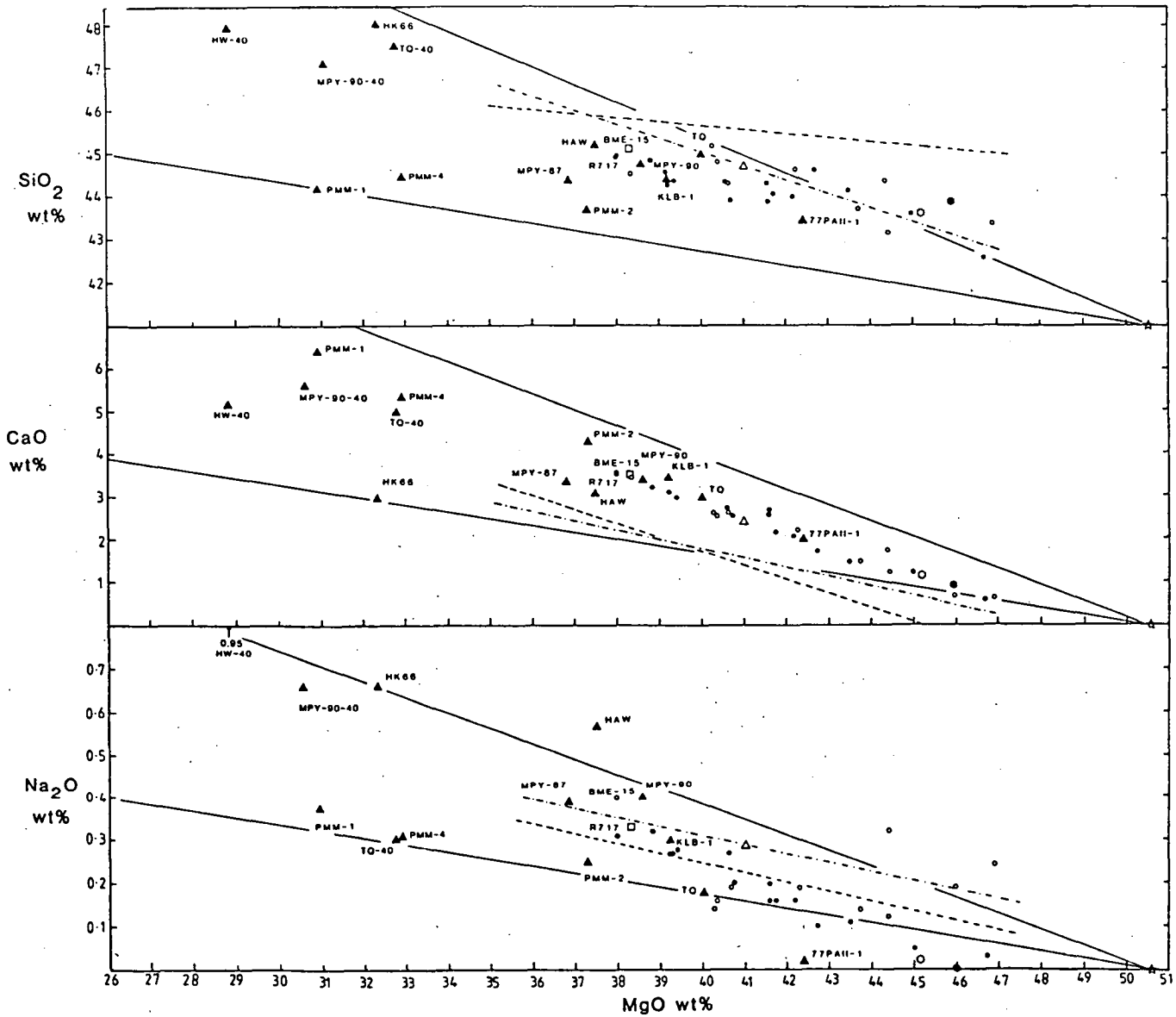
SiO2 wt%
CaO wt%
Na2O wt%
MgO wt%
HW-40
HK66
TO-40
MPY-90-40
PMM-1
PMM-4
PMM-2
HAW
BME-15
R717
MPY-87
MPY-90
KLB-1
77PAII-1
TO
0.95

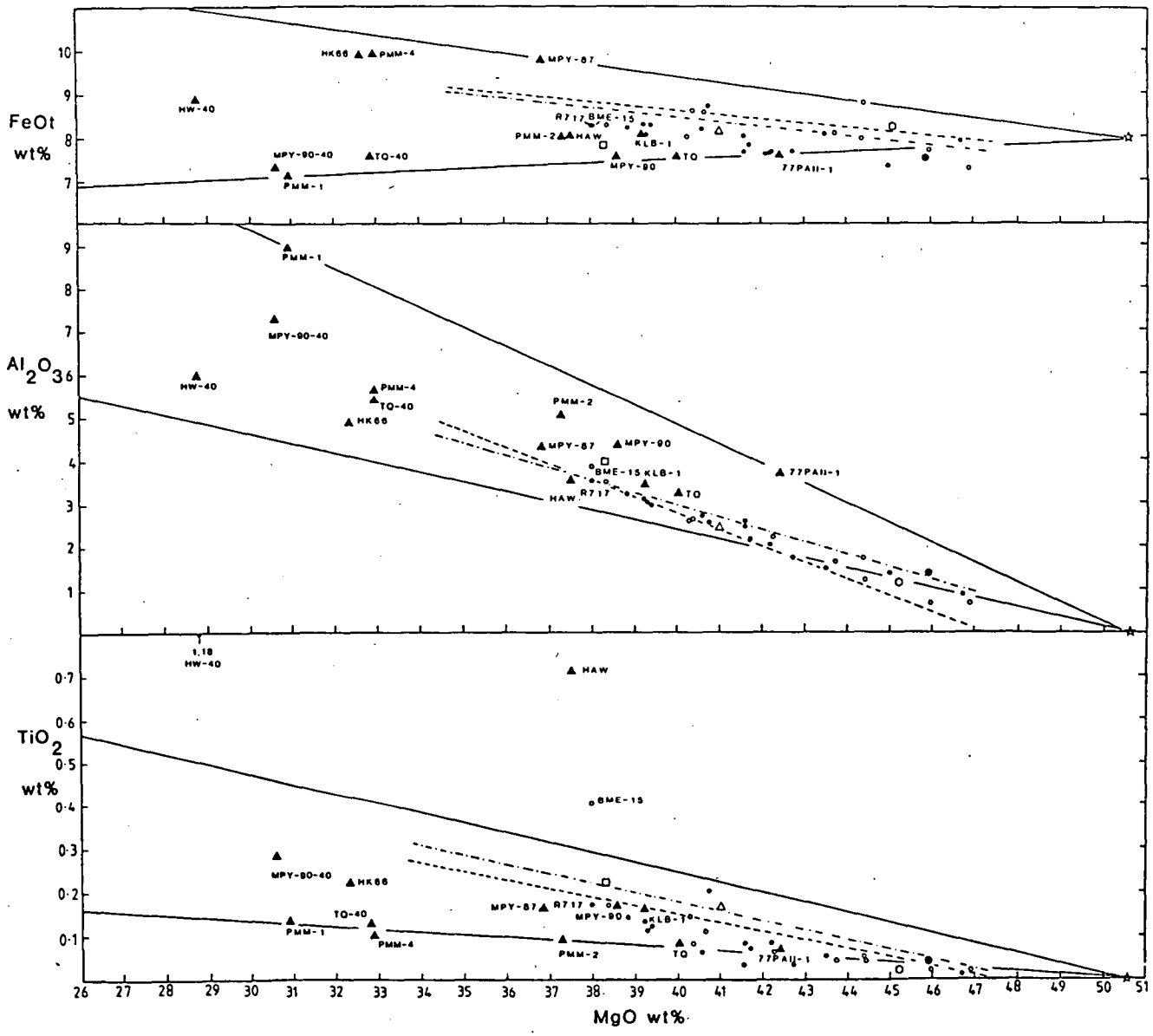
FeOt wt%
HK66
PMM-4
MPY-87
HW-40
R717
BME-15
PMM-2
HAW
KLB-1
MPY-90-40
TQ-40
MPY-90
TQ
77PAII-1
PMM-1
Al2O3 wt%
MPY-90-40
PMM-4
TQ-40
HK66
PMM-2
MPY-87
MPY-90
BME-15
KLB-1
R717
TQ
HAW
77PAII-1
1.18
HW-40
TiO2 wt%
BME-15
MPY-90-40
HK66
MPY-87
R717
MPY-90
KLB-1
TQ-40
PMM-1
PMM-4
PMM-2
TQ
77PAII-1
MgO wt%

incomplete extraction of a partial melt of picritic composition (Frey et al., 1985; Nickel & Green, 1984). These picritic melts, which relate the more fertile to the more depleted peridotite compositions are suitable parental magmas to MORB (Frey et al., 1985; Nickel & Green, 1984).

These linear oxide trends include at their residual or refractory MgO-rich end, the average of 50 representative plagioclase-free spinel harzburgite and lherzolites dredged from oceanic ridges and fracture zones (Dick & Fisher, 1984) and the very similar residue composition calculated by Green et al. (1979) for extraction of 24 wt% partial melt of MORB picrite (DSDP3-18-7-1 + 17 wt% olivine) from MORB pyrolite composition. The trends also include less refractory primitive mantle composition estimates based on spinel lherzolite suites by Maaloe & Aoki (1977) and Jagoutz et al. (1979).

For comparison the regression line for 83 oceanic lherzolite xenoliths from Maaloe & Aoki (1977) and the regression line for ocean-floor peridotites from Shibata & Thompson (1986) are plotted in Fig.2. Both regression lines plot within the peridotite array defined by Ronda and Bullenmerri for most oxides. However the regression line of Shibata & Thompson (1986) plots at significantly higher SiO_2 contents and lower CaO contents than the Ronda and Bullenmerri suites. The data set used by Shibata & Thompson (1986) is of serpentinized peridotite and the process of serpentinization is not always isochemical but may increase the SiO_2/MgO ratios and leach CaO.

Based on the above linear oxide trends displayed by the Ronda and Bullenmerri suites, suitable starting compositions for melting experiments relevant to MORB should lie within or close to the trends defined by the two peridotite suites. In Fig.2 a number of peridotite compositions used in melting experiments, such as PMM-1 (Fujii & Scarfe, 1985) and HK66 (Takahashi & Kushiro, 1983) plot well away from the peridotite array. However these compositions plot in a similar position to the minus 40 wt% olivine compositions of Tinaquillo lherzolite, Hawaiian and MORB pyrolite (TQ-40,HW-40,MPY-90-40 respectively Fig.2). Thus the suitability of peridotite starting compositions used in melting experiments must be evaluated on the basis of whether they plot in or near the peridotite array, or whether they would plot in or near the array if olivine was added to them until they plot within the natural peridotite array. For the purposes of this comparison olivine control lines were drawn from an olivine composition of $Fo_{91.6}$. Table 3 summaries the results of this

Table 3

Comparison of peridotite starting compositions with natural peridotite suites on the basis of olivine control lines from (Fo_{91})

	SiO_2	CaO	Na_2O	FeO	Al_2O_3	TiO_2
TQ (TQ-40)	OK	OK	LO	OK	OK	OK
HW (HW-40)	OK	LO	HI	OK	OK	HI
MPY-87	LO	OK	OK	HI	OK	OK
MPY-90 (MPY-90-40)	OK	OK	OK	OK	OK	OK
HK66	HI	LO	HI	HI	OK	OK
KLB-1	OK	OK	OK	OK	OK	OK
77PAII-1	OK	OK	LO	OK	OK	OK
PMM-1	LO	HI	OK	OK	HI	OK
PMM-2	LO	HI	OK	OK	HI	OK
PMM-4	LO	OK	OK	HI	OK	OK

The terms OK, LO, HI are used to indicate the relative position of the above peridotite compositions to the natural peridotite array in Fig.2. OK indicates the composition falls near or close to the natural array, HI indicates it falls above and LO indicates it plots below the natural array, see text for a more complete explanation.

analysis for all the peridotite starting compositions used in 10kbar melting studies. From Table 3 it can be seen that the compositions KLB-1, Tinaquillo and MORB pyrolite are the most suitable starting materials for MORB petrogenesis. Compositions such as those used by Fujii & Scarfe (1985) (PMM-1,-2 and -4) are not suitable as they have significantly lower SiO_2 and slightly higher Al_2O_3 and CaO contents than the natural peridotite array. Hawaiian pyrolite is clearly unsuitable as a MORB source in TiO_2 and Na_2O content but not in other major oxides.

1.5 EXPERIMENTAL APPROACH AND TECHNIQUES

The experimental determination of equilibrium partial melts of peridotite compositions in the past has been fraught with difficulties. The direct EMP analyses of glass in the charge does not give correct glass compositions due to quench modification of the glasses (Green, 1973). However if the glass is sufficiently abundant, as is the case in higher degrees of partial melting, then reasonably accurate glass compositions can be obtained. Jaques & Green (1979, 1980) avoided the quench problem by analysis of all the residual crystalline phases, combined with modal analysis of the charge, thus enabling the calculation of the equilibrium partial melt by mass balance. This approach suffers from uncertainties in the modal analysis and in the composition of the residual phases where Fe-loss has occurred in the experiments. Reversal work on the Jaques & Green (1980) calculated equilibrium liquids has shown many of them to be too olivine rich, the equilibrium liquids lying at more silica-saturated compositions (Falloon et al., 1987). Another successful approach has been the 'sandwich' technique where a basalt is placed in between peridotite and allowed to equilibrate with the peridotite and its partial melt at a desired pressure and temperature. This provides a large area of glass to be analysed at the end of the run (Stolper, 1980; Takahashi & Kushiro, 1983; Fujii & Scarfe, 1985; Thompson, 1984). The character of the resultant partial melts however is very much dependent on the character of the basalt used in the sandwich and the resulting bulk composition of the mixture. As will be discussed later, the resultant liquids from sandwich experiments thus far bear little or no relationship to the composition of the peridotite used in the sandwich but to some undefined peridotite composition. In this study we have used the MORB glass DSDP3-18-7-1 (Green et al., 1979; Frey et al., 1974) as the basalt in the 'sandwich' between layers of MORB pyrolite and because there is a close compositional link between DSDP3-18-7-1 and the calculated MORB pyrolite composition of Green et al. (1979) the resultant equilibrium melts are an internally consistent

and coherent evaluation of the ability of the MORB pyrolite composition to yield MORB basaltic or picritic primary magmas. In the 'sandwich' experiments on Hawaiian pyrolite and Tinaquillo lherzolite, the basaltic layers were glasses of the compositions calculated by Jaques & Green (1980) for the appropriate P, T conditions.

All the starting mixes used (Table 2) except KLB-1 were made up from sintered oxides, crushed in acetone and fired at 1000°C. Fayalite was then added to the mixes before refiring in a silica evacuated tube at 1000°C. The mixes were then stored in an oven at 110°C. The DSDP3-18-7-1 mix was the same as that used by Green et al. (1979). The KLB-1 mix consists of powdered natural peridotite. The mixes were then loaded into graphite capsules and sealed in an outer platinum capsule. Two sizes of graphite capsule were used; in the large bore graphite capsule, a layer of DSDP3-18-7-1 mix was loaded between layers of MORB pyrolite. In the small bore graphite capsules only two layers were used the basalt layer forming the bottom layer (DSDSP3-18-7-1 or Jaques & Green, 1980 calculated liquids in the case of Tinaquillo lherzolite and Hawaiian pyrolite). The wt% basalt in each bulk composition is given in Table 4.

All experiments were carried out in a high pressure piston cylinder apparatus at the University of Tasmania, a piston-in technique with a pressure correction of minus 10% nominal piston pressure was used. A 0.5 inch diameter, talc-pyrex assembly was used with a graphite heater. A pure alumina thermocouple sheath was used, with sintered alumina components surrounding the capsule. The thermocouple sheath enters the assembly through a mullite sleeve. The bottom spacer is fired pyrophyllite (mullite and silica).

Both $Pt/Pt_{90}Rh_{10}$ and $W_{75}Re_{25}/W_{97}Re_3$ thermocouples were used in the course of the experimental study. Significant thermocouple drift was experienced on long runs when using the $Pt/Pt_{90}Rh_{10}$ thermocouple. Calculated drift rates at constant power input were approximately -2°C/hour at 1300°C increasing approximately to -5°C/hour at temperatures greater than 1500°C. Thermocouple drift using $Pt/Pt_{90}Rh_{10}$ thermocouples have been reported by other workers (Boyd et al., 1964; Mao & Bell, 1971; Mao et al., 1971; Presnall et al., 1973). As the composition of olivine above the solidus is sensitive to temperature (Jaques & Green, 1980; Roedder & Emslie, 1970), in those runs which had experienced thermocouple drift, the temperature of the run was determined by comparing the equilibrium olivine composition with olivine compositions produced in experiments using

$W_{75}Re_{25}/W_{97}Re_3$ thermocouples. The $W_{75}Re_{25}/W_{97}Re_3$ thermocouples were controlled by a Kent P96M controller, temperatures being accurate to $\pm$ 1°C. Temperatures listed in Table 4 are in agreement with the experiments of Takahashi (1986) on KLB-1 which is similar in composition to the MORB pyrolite composition studied.

At the end of the run the sample was removed from the graphite capsule and sectioned longitudinally for microprobe analysis. All analyses were done on a JEOL JX 50A electron microprobe-scanning electron microscope, at the University of Tasmania, fitted with an energy dispersive EDAX analytical system (operating conditions 15kv, $7x10^{-10}$A), calibration was on pure Cu. Back scattered electron photographs were taken of all run products to check on the compositional uniformity of all the phases (Phillips 505 SEM, operating conditions 20kv, spot size 100 ηm).

1.6 EXPERIMENTAL RESULTS

Details of the experimental runs are given in Table 4. The compositions of equilibrium partial melts produced in the experiments are given in Tables 5 and 6. The compositions of the partial melts are compared with primitive MORB glasses in Figs.7, 8, 9 and 10. Representative residual phase compositions are given in Appendix 1.

1.6.1 Attainment of Equilibrium

In most runs the liquid layer was quenched as a coherent glass layer (100-300μm) between or on top of the peridotite layer(s) which consist of crystals and glass (Fig.3a). In some runs close to the solidus (T-1511 and T-2078) abundant clinopyroxene crystallization occurred within the glass layer and the glass composition was obtained by analysing large pools of glass (50-70μm) within the charge (Fig.3b).

Due to the nature of the sandwich technique modal homogeneity is not produced during the experiment, and although the melt phase is distributed throughout the charge, being in contact with all grain boundaries, the melt is concentrated in one layer. Due to the presence of this glass layer crystal growth is enhanced resulting in much larger and more abundant clinopyroxene and orthopyroxene crystals near the glass/peridotite (now crystals + glass) contact. All phases near or in the glass layer were found to be compositionally uniform from core to rim even for short run times. Clinopyroxene is commonly attached to orthopyroxene (Fig.3c) or forms large

Table 4

10kbar peridotite-basalt sandwich experiments

Run no.	T(°C)	Time(hrs)	Capsule type	Peridotite Composition	Basalt wt%	Phases present
T-1511	1310	24.0	A	MPY-87	5.5	Ol + Opx + Cpx + Sp + m + L
T-1472	1350	3.0	A	MPY-87	9.5	Ol + Opx + Cpx + Sp + L
T-2123	1350	30.0	B	MPY-87	18.0	Ol + Opx + Cpx + Sp + L
T-1493	1350	3.0	A	MPY-87	10.4	Ol + Opx + Cpx + m + L
T-1478	1400	3.5	A	MPY-87	10.3	Ol + Opx + Cpx + m + L
T-2140	1400	32.0	B	MPY-87	23.0	Ol + Opx + Cpx + Sp + L
T-1464	1420	1.5	A	MPY-87	12.0	Ol + Opx + m + L
T-1480	1420	2.0	A	MPY-87	10.2	Ol + Opx + m + L
T-1461	1420	24.0	A	MPY-87	14.0	Ol + Opx + m + L
T-2113	1375	18.0	B	TQ-40	23.5	Ol + Opx + Cpx + Sp + L
T-2117	1325	25.0	B	HW-40	24.0	Ol + Opx + Cpx + L
T-2133	1350	25.0	B	KLB-1	23.0	Ol + Opx + Cpx + Sp + L
T-2121	1230	24.0	B	MPY-90-40	30.0	Ol + Opx + Cpx + Pl + Sp + L
T-2078	1300	25.0	B	MPY-90-40	17.6	Ol + Opx + Cpx + Sp + L
T-2138	1350	24.0	B	MPY-90-40	27.0	Ol + Opx + Cpx + Sp + L
T-2136	1350	24.0	B	MPY-90	24.0	Ol + Opx + Cpx + Sp + L

Ol olivine, Opx orthopyroxene, Cpx clinopyroxene, Sp aluminous spinel, m metallic globule (Fe,Ni), Pl plagioclase, L liquid (Glass), Q quench crystals.

A and B stand for large and small bore graphite capsules respectively

Table 5

Compositions of equilibrium partial melts at 10kbar from MORB pyrolite (MPY-87)

	1	2	3	4	5	6	7	8	9	10
SiO_2	50.90	50.20	50.36	50.37	50.54	50.78	50.07	50.04	50.38	0.17
TiO_2	0.81	0.65	0.77	0.65	0.60	0.67	0.53	0.57	0.55	0.05
Al_2O_3	19.16	17.21	17.05	17.11	15.94	15.42	14.87	14.61	14.25	0.12
FeO	6.82	7.68	7.51	7.54	7.61	7.79	8.15	8.40	8.15	0.13
MgO	8.52	10.50	10.37	10.41	11.34	11.12	13.46	13.57	13.58	0.17
CaO	10.48	11.60	11.53	11.74	11.96	12.10	11.26	11.11	11.74	0.09
Na_2O	3.31	2.18	2.18	2.17	1.89	1.83	1.55	1.53	1.57	0.06
Cr_2O_3	-	-	0.24	-	0.26	0.27	0.24	0.26	0.36	0.04
Total	100.00	100.02	100.01	99.99	100.14	99.98	100.09	100.09	99.86	
Mg#	0.69	0.71	0.71	0.71	0.73	0.72	0.75	0.74	0.75	
CIPW norm (molecular)										
Ab	25.22	16.52	16.63	16.52	14.31	13.98	11.48	11.32	11.67	
An	31.77	31.40	31.22	31.32	29.54	28.83	27.73	27.21	26.37	
Di	12.37	17.20	17.39	18.05	20.52	22.27	18.53	18.24	19.32	
Hy	9.01	17.79	20.14	18.42	22.12	24.74	25.22	26.28	27.60	
Ol	18.10	13.92	10.75	12.56	10.11	6.49	14.04	13.58	11.59	
CaO/Al_2O_3	0.55	0.67	0.67	0.68	0.75	0.78	0.76	0.76	0.78	
CaO/Na_2O	3.16	5.32	5.28	5.41	6.33	6.61	7.26	7.26	7.08	
CaO/TiO_2	12.94	17.85	14.97	18.06	19.93	18.06	21.24	19.49	20.22	
Al_2O_3/TiO_2	23.65	26.47	22.14	26.32	26.56	23.01	28.06	25.63	25.91	

(1) run no.T-1511, (2) run no.T-1472, (3) run no.T-2123, (4) run no.T-1493, (5) run no.T-1478, (6) run no.T-2140, (7) run no.T-1464, (8) run no.T-1480, (9) run no.T-1461.

(10) average σ values for the glass analyses.

Mg#=Mg/(Mg + Fe^t), t= total iron as FeO, (-) below detection limit, MnO values all below detection limit, for run details please refer to Table 4.

Table 6

Compositions of equilibrium partial melts at 10kbar from various peridotite compositions

	1	2	3	4	5	6	7	8	9
SiO_2	50.47	50.78	50.27	50.55	49.88	50.73	50.69	51.32	50.48
TiO_2	0.42	3.34	0.68	0.96	0.81	0.73	0.70	0.61	0.87
Al_2O_3	15.29	15.45	17.31	17.71	18.99	17.68	16.81	16.11	15.33
FeO	7.41	7.78	6.94	7.77	6.92	6.67	6.53	4.89	8.36
MgO	12.05	8.57	10.75	9.31	9.40	10.19	11.14	12.42	10.72
CaO	12.83	9.56	11.95	11.06	11.11	11.71	12.04	12.66	11.84
Na_2O	1.15	3.47	2.03	2.63	2.84	2.19	1.97	1.58	1.88
K_2O	-	0.71	-	-	-	-	-	-	0.17
Cr_2O_3	0.32	0.22	-	-	-	-	-	0.34	nd
MnO	-	-	-	-	-	-	-	-	0.15
P_2O_5	-	-	-	-	-	-	-	-	0.09
Total	99.94	100.08	99.93	99.99	99.95	99.90	99.88	99.93	99.80
Mg#	0.74	0.66	0.73	0.68	0.71	0.73	0.75	0.82	0.69
CIPW norm (molecular)									
Ab	8.84	25.55	15.45	20.11	21.39	16.83	14.99	12.10	14.39
An	31.30	20.09	32.32	31.11	32.79	32.90	31.39	31.45	28.05
Di	23.19	18.82	17.94	15.63	13.47	16.85	21.85	28.04	21.21
Hy	30.87	7.09	19.29	16.53	8.25	21.28	21.85	28.04	23.52
Ol	2.80	13.89	11.86	8.27	20.61	8.57	9.00	3.14	8.01
CaO/Al_2O_3	0.84	0.62	0.69	0.62	0.58	0.66	0.72	0.78	0.77
CaO/Na_2O	11.16	2.75	5.89	4.20	3.91	5.35	6.11	8.01	6.29
CaO/TiO_2	30.55	2.86	17.57	11.52	3.91	16.04	17.20	20.75	13.61
Al_2O_3/TiO_2	36.40	4.62	25.45	18.45	23.44	24.22	24.00	26.41	17.62

(1) TQ-40, run no.T-2113, (2) HW-40, run no.T-2117, (3) KLB-1, run no.T-2133, (4) MPY-90-40, run no.T-2121, (5) MPY-90-40, run no.T-2078, (6) MPY-90-40, run no.T-2138, (7) MPY-90, run no.T-2136, (8) MPY-90-40, run no.T-2098 (this run has suffered Fe loss), (9) P_2, most primitive olivine basalt from FAMOUS (Le Roex et al., 1981), t=total iron as FeO, Mg#=Mg/(Mg + Fe^t), for run details please refer to Table 4, (-) below detection limit, nd not determined.

Figure 3a.

Back scattered electron image photograph of run no.T-2140. Lightest gray is glass, light grey is clinopyroxene and dark grey is olivine and orthopyroxene. Scale bar is 100um.

Figure 3b.

Back scattered electron image photograph of run no.T-2078. Lightest gray is glass, light grey is clinopyroxene, dark grey is olivine and orthopyroxnene. Scale bar is 100um.

Figure 3c.

Back scattered electron image photograph of run no.T-2140. lightest grey is glass, light grey is clinopyroxene and dark grey is olivine and orthopyroxene, euhedral bright crystal is spinel. Scale bar is 100um.

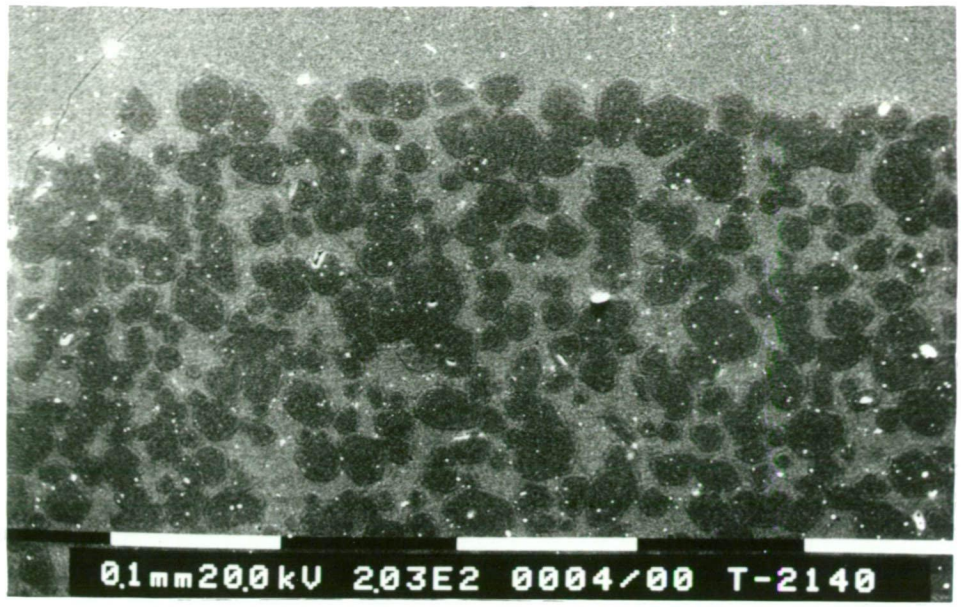
0.1mm20.0kV 2.03E2 0004/00 T-2140

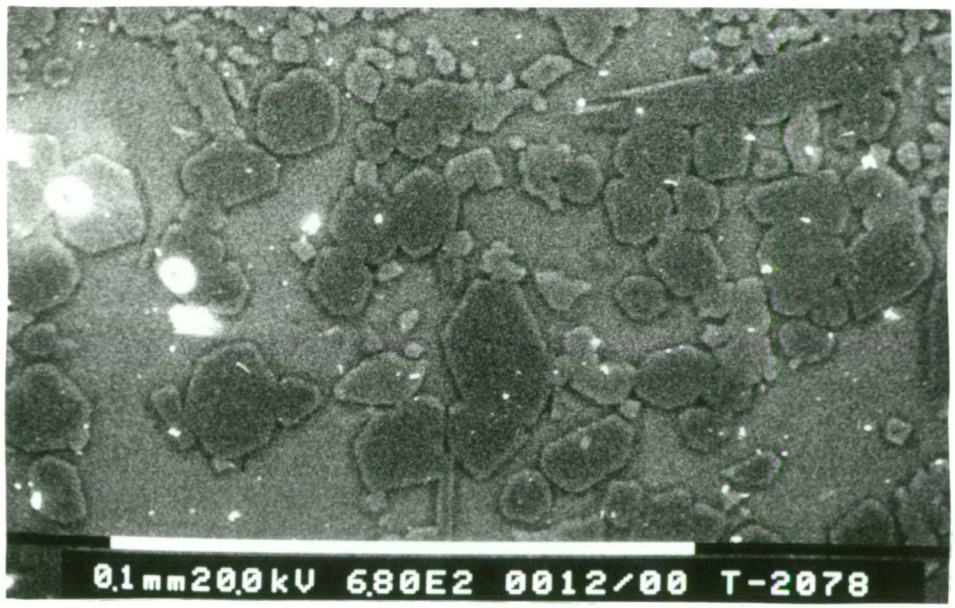
0.1mm20.0kV 6.80E2 0012/00 T-2078

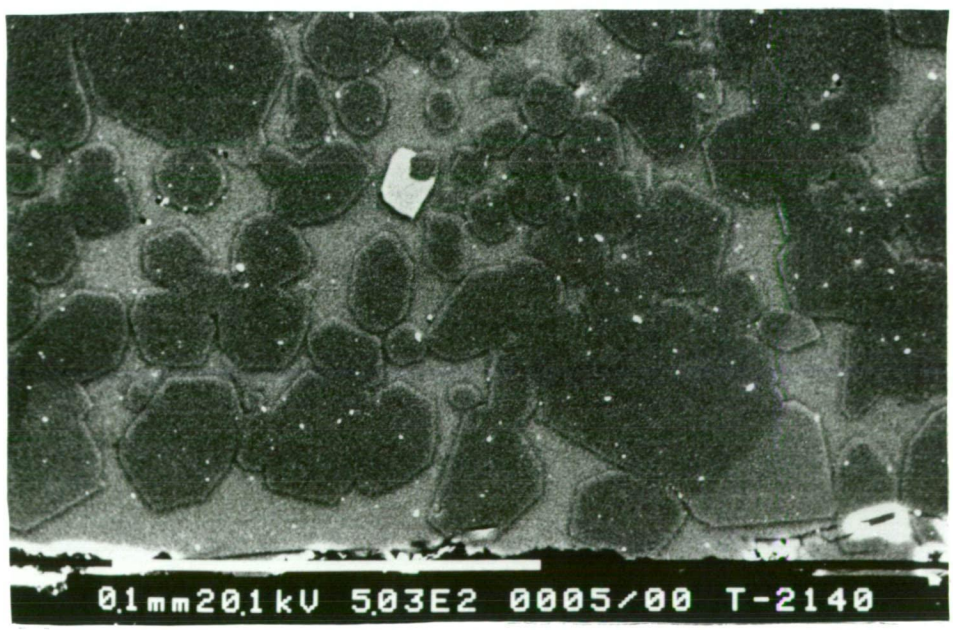
0.1mm20.1kV 5.03E2 0005/00 T-2140

poikilitic grains enclosing smaller olivine crystals. In run T-2121 plagioclase occurred as large crystals projecting into the glass layer, as well as smaller interstitial grains throughout the MORB pyrolite end of the charge. The plagioclase was compositionally uniform from core to rim as well as compositionally uniform throughout the charge (An_{67-69}). However phases away from the glass layer were not compositionally uniform from core to rim. Rim compositions were identical to the cores and rims of phases close to the glass layer, while cores were of a different composition. In general the cores of olivines were less magnesian than the rims, the rim composition being in equilibrium with glass on the basis of a $(Kd)^{Ol/Liq}_{Fe/Mg}$ equal to 0.32 (Takahashi & Kushiro, 1983). Cores of pyroxenes away from the glass layer have lower CaO, Al_2O_3 and slightly lower Mg# than the equilibrium rim compositions. As a result of this zoning in crystals removed from the glass layer, bulk equilibrium was not achieved during the length of even the longest runs (30hrs), however local equilibrium was achieved between the glass composition and residual crystals near the glass layer and rims of crystals away from the glass layer. Equilibrium is also confirmed by comparing the glass compositions in short runs (3hrs) to compositions in long run times (>20hrs), differences are all within analytical uncertainty. Using the sintered oxide mix as a starting material as opposed to a powdered natural peridotite enables equilibrium to be obtained relatively rapidly. The single experiment performed on KLB-1 (T-2133) resulted in large unreacted cores in the pyroxenes, although compositionally uniform crystals of pyroxene occurred near the glass layer. Previous workers have shown that longer run times (>72 hrs, Fujii & Scarfe, 1985) still do not eliminate these relict cores. Excessively long run times also run the risk of Fe-loss, as will be discussed later.

1.6.2 Evaluation of the Sandwich Technique in Peridotite melting studies

The results from this study and the studies of Takahashi & Kushiro (1983) and Fujii & Scarfe (1985) allow us to evaluate the use of the sandwich technique in obtaining equilibrium partial melts. One of the important unknown factors in using the sandwich technique for determining equilibrium liquid compositions is the effect of changing the bulk composition of the peridotite by adding a basaltic component. The results of this study and those of Takahashi & Kushiro (1983) and Fujii & Scarfe (1985) allow us to make the following observations.

(1) Changing the modal proportion of basalt to a peridotite composition does not affect the liquid compositions along a olivine + orthopyroxene +

clinopyroxene + liquid cotectic so long as the amount of added basalt mix does not exceed ~40wt% and provided none of the residual phases are eliminated. For example experiments T-1472 and T-2123 produced similar equilibrium liquid compositions despite having different modal proportions of DSDP3-18-7-1 (9.5 and 18 wt% respectively). Experiments by Fujii & Scarfe (1985) showed slight compositional differences in liquid composition with differing proportions of basalt added. These differences (mainly in Mg#, CaO, Na_2O and K_2O content of the glasses) can be readily explained by Fe-loss, as will discussed in another part of this paper.

(2) In general using different basalt compositions with the same peridotite host or vice-versa produces differences in the equilibrium liquid composition. For some of the experiments using HK66 and PMM-4 differences in the equilibrium liquids were not observed when different basalt compositions were used. This can be explained by the very fertile nature of HK66 and PMM-4, both being enriched in 'melt' components, they were able to 'swamp' differences in most basalt compositions which were used in the sandwich experiments of Takahashi & Kushiro (1983) and Fujii & Scarfe (1985).

Although varying the modal proportions of the added basalt component has little effect on the liquid composition along a olivine + orthopyroxene + clinopyroxene + liquid cotectic, the presence of an added basaltic component does affect the stability of pyroxene, especially orthopyroxene. This illustrated with reference to the glass compositions from runs T-1424,1447,1434 and 1437 which were all in equilibrium with olivine only (not reported in Table 4). In Fig.4 the glass composition from these runs are plotted in the CIPW molecular normative projection from plagioclase(An+Ab). Bulk compositions for the sandwich experiments, which lie on a tie line between DSDP3-18-7-1 and MPY-87, have been plotted in Fig.4. Also plotted are the olivine + orthopyroxene + clinopyroxene + spinel + liquid and olivine + orthopyroxene + liquid cotectics determined for MORB pyrolite in this study. As can be seen from Fig.4 none of the liquids in equilibrium with olivine fall on a olivine control line through MPY-87, instead they fall on olivine control lines through the respective bulk composition for each sandwich experiment. The liquid compositions represent simple mixtures between DSDP3-18-7-1 and a melt in equilibrium with olivine lying on a olivine control line through MPY-87. The position on the olivine control line through MPY-87 is determined by drawing a line from DSDP3-18-7-1 through the respective liquid composition onto the olivine control line through MPY-87 (Fig.4). At each of these intersections

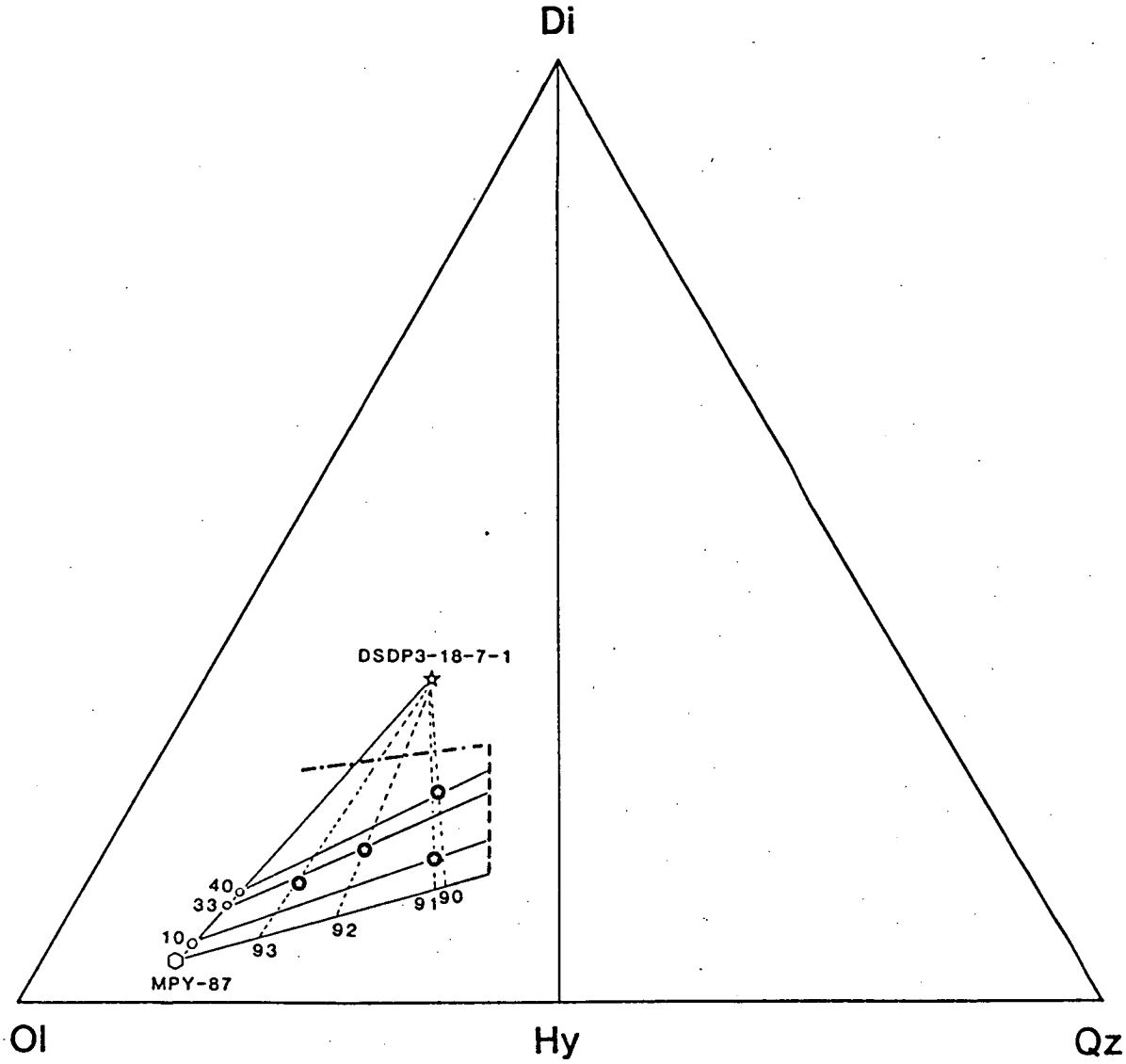

Figure 4.

CIPW molecular normative projection from plagioclase(Ab+An) onto the face olivine(Ol)-diopside(Di)-quartz(Qz) of the 'basalt tetrahedron',
90, 91, 92, 93 represent equilibrium olivine compositions (Fo mole%) along an olivine + Liquid cotectic for MPY-87,
10, 33, 40 represent percent DSDP3-18-7-1 in the bulk composition of the sandwich experiments,
(✪) experimental glass compositions in equilibrium with olivine only from 10kbar sandwich experiments on MORB pyrolite (DSDP3-18-7-1 plus MPY-87)
—·—·—· represents the locus of liquid compositions in equilibrium with olivine + orthopyroxene + clinopyroxene + spinel from 10kbar experiments on MORB pyrolite,
– – – – – represents locus of liquid compositions in equilibrium with olivine and orthopyroxene from 10kbar experiments on MORB pyrolite,
——— represents locus of liquids compositions in equilibrium with olivine only from 10kbar experiments on MORB pyrolite,
-------- represents a mixing line between DSDP3-18-7-1 and a liquid composition lying on the olivine + liquid cotectic for MPY-87. Mixing lines pass through the experimentally determined glass compositions.

the equilibrium olivine composition (Fo mol%) observed in the experiment is given indicating temperature is increasing from right to left in Fig.4. The effect of increasing the proportion of DSDP3-18-7-1 in the sandwich is to rotate the olivine control lines upwards towards DSDP3-18-7-1. The result of this is to shrink the above-solidus stability fields of orthopyroxene initially, then followed by clinopyroxene, until eventually only olivine is left, which is the liquidus phase of DSDP3-18-7-1 at 10kbar (Green et al., 1979). Therefore the sandwich technique is limited in that it will not permit access to liquids formed at high degrees of melting of the peridotite composition i.e. compositions in equilibrium with olivine + orthopyroxene near the point at which orthopyroxene is eliminated are not accessible. The liquids near this composition should be determinable by direct melting studies on the peridotite composition alone, provided quenching problems can be evaluated and dismissed.

Another problem with the sandwich technique is related to the definition and constancy of the peridotite whose melting behaviour is being studied. The equilibrated composition will be determined by the composition of the added basalt and an (unknown) component of the enclosing peridotite, determined by its grainsize and the extent of reaction with the liquid. This is unfortunate as one of the aims of experimental partial melting studies is to characterize the range of liquid compositions which can be produced from a particular bulk composition at a particular pressure, in this case 10kbar. This problem is illustrated by reference to Fig.5b, where the Al_2O_3 vs CaO contents of equilibrium partial melts in sandwich experiments at 10kbar from PMM-1, HK66 and MPY-87 are compared with the CaO/Al_2O_3 ratios of the peridotite used in the sandwich experiment. Also plotted in Fig.5a are the 10kbar experiments from Jaques & Green (1980) and Sen (1982). In Fig.5a, 5b the line drawn from the origin through the peridotite bulk compositions defines the CaO/Al_2O_3 ratio of the bulk composition. Liquid compositions in equilibrium with olivine only fall on these lines as residual olivine contains negligible CaO and Al_2O_3. The olivine control line bounds the range of CaO/Al_2O_3 ratios of equilibrium liquids which can be produced from a particular bulk composition. The change in the CaO/Al_2O_3 ratio with partial melting is shown by the liquids from Hawaiian pyrolite and Tinaquillo lherzolite. At low degrees of partial melting with important residual clinopyroxene the Al_2O_3 content of the melt is high relative to CaO, consequently the CaO/Al_2O_3 ratio is low. With increasing degree of melting partial melting the Al_2O_3 content of the melt falls as the CaO content increases, causing the CaO/Al_2O_3 ratio of the melt to increase. At the point of disappearance of clinopyroxene as a residual

Figure 5.

Al_2O_3 versus CaO wt% of 10kbar experimental liquid compositions from various peridotite compositions,
Striaght lines through the respective peridotite compositions are olivine control lines of constant CaO/Al_2O_3 ratio. Bulk compositions of sandwich experiments lie on lines joining '✪' to '☆'.

A. 77PAII-1 (Sen, 1982), HW and TQ (Jaques & Green, 1980) abbreviations as for Fig.2,
   (+) glass compositions from HW (Jaques & Green, 1980; and this study),
   (△) glass compositions from TQ (Jaques & Green, 1980; and this study),
   (◇) glass compositions from 77PAII-1 (Sen, 1982).

B. Sandwich experiments on MPY-87, HK66 (Takahashi & Kushiro, 1983) and PMM-1 (Fujii & Scarfe, 1985),
   (□) glass compositions from MPY-87 (see Table 5),
   (×) glass compositions from HK66 (Takahashi & Kushiro, 1983),
   (●) glass compositions from PMM-1 (Fujii & Scarfe, 1985),
   (☆) basalt compositions used in the sandwich experiments. DSDP3-18 (this study), L45 (Takahashi & Kushiro, 1983) and B-1 (Fujii & Scarfe, 1985),

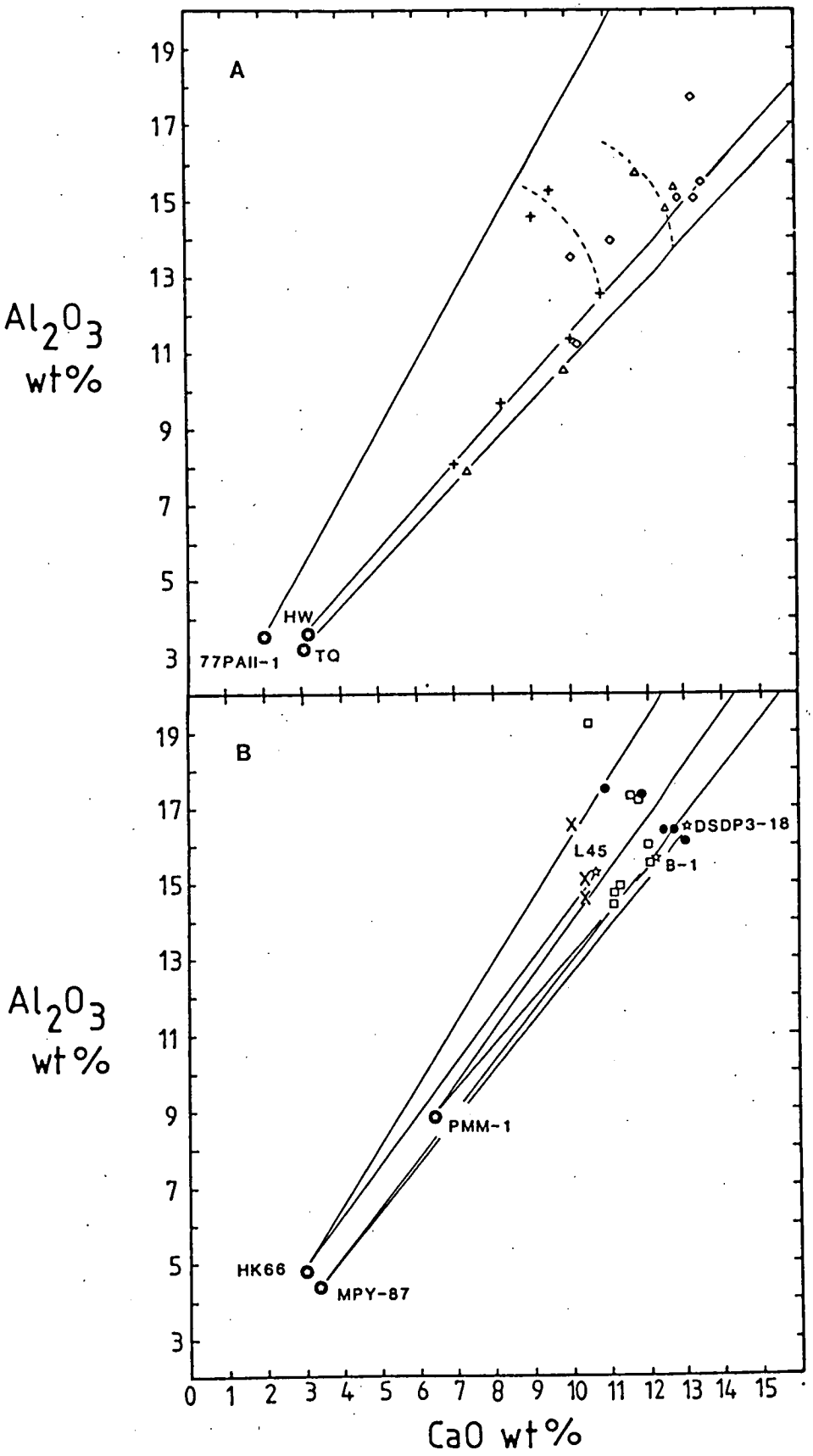
A
B
Al_2O_3 wt%
Al_2O_3 wt%
CaO wt%
77PAII-1
HW
TQ
L45
DSDP3-18
B-1
PMM-1
HK66
MPY-87
19
17
15
13
11
9
7
5
3
0 1 2 3 4 5 6 7 8 9 10 11 12 13 14 15

phase the CaO/Al_2O_3 ratio of the melt is slightly less or equal to the CaO/Al_2O_3 of the bulk composition. Orthopyroxene has little affect on the CaO/Al_2O_3 ratio of the melt so that with increasing degree of partial melting liquids fall close to and then along the olivine control line.

In Fig.5b the sandwich experiments on MPY-87, HK66 and PMM-1 are presented. Bulk compositions lie on a tie line between the peridotite host and the basalt composition added. In the case of the MPY-87 and DSDP3-18-7-1 experiments all the 10kbar equilibrium liquids fall above the olivine control lines drawn through the bulk composition of the experiment and MPY-87, indicating that these liquids are closely related to the MORB pyrolite composition. However in the case of HK66 and PMM-1 equilibrium liquid compositions cross over the olivine control lines through their respective host peridotite and bulk compositions indicating that the liquid compositions from HK66 and PMM-1 are not related to the bulk compositions HK66 and PMM-1 respectively.

The liquids from 77PAII-1 Sen (1982) illustrate a different problem, in that the liquids determined by Sen (1982) plot well away from the olivine control line through 77PAII-1 in Fig.5a. Sen (1982) determined the liquids from 77PAII-1 by direct EMP analysis of glass pools, and it seems likely that the liquid compositions have been modified by either quench growth or proximity to large residual crystals which have depleted the liquids in Al_2O_3. Other inconsistencies, such as in the erratic behaviour of Na_2O and CaO contents with increasing partial melting, point to quench modification of Sen (1982) liquids.

1.6.3 Fe-loss

The problem of Fe-loss to noble metal containers is a major problem to be addressed in experimental petrology (Merrill & Wyllie, 1973; Green, 1976; Stern & Wyllie, 1975; O'Hara & Humphreys, 1977; Jaques & Green, 1979; Nehru & Wyllie, 1975; Thompson, 1984). The extent of iron loss is dependent on the temperature of the run and run duration. The effect of iron loss is to increase the silica saturation of the equilibrium liquid composition, due to the expansion of the olivine and orthopyroxene phase fields at the expense of clinopyroxene. This expansion also results in more calcic liquid compositions and the stabilization of calcic pyroxene in the residue (Jaques & Green, 1979). Fe-loss also increases the overall oxygen fugacity in the charge, which is reflected in an increase of the mole ratio $FeO_{1.5}/FeO$ in the melt with time (Takahashi, 1980). Some of the possible

chemical reactions causing an increase in fO_2 in the charge are listed below;

$$Fe_2SiO_4\ \text{olivine} \longrightarrow SiO_2\ \text{melt} + 2(Fe/Pt)_{\text{solid solution}} + O_2 \qquad (1)$$

$$Pt + 3FeO_{\text{melt}} \longrightarrow (Fe/Pt)_{\text{solid solution}} + Fe_2O_3\ \text{melt} \qquad (2)$$

etc.

The effect of increasing fO_2 during a run in which Fe-loss is occurring is to stabilize chromian spinel (Cr-spinel) to very high degrees of partial melting, as was the case with the experiments performed by Jaques & Green (1980) where Cr-spinel was still present even after the elimination of all other phases except olivine. The higher fO_2 occurring in Pt capsules due to iron-loss, compared to experiments performed in graphite is reflected in the trivalent cation ratio $100Fe^{3+}/(Fe^{3+} + Al^{3+} + Cr^{3+})$ (FE#).

In Fig.6 the FE# vs the $100Cr^{3+}/(Cr^{3+} + Al^{3+})$ (CR#) of spinels crystallizing in graphite from the experiments of Takahashi & Kushiro (1983), Takahashi (1986) and this study are compared with spinel crystallizing in Pt capsules in the experiments of Jaques & Green (1980). Spinels crystallizing in graphite capsules can be distinguished from spinels from Pt capsules due to their lower FE# and CR#. The lower CR# reflects the reducing conditions of the graphite capsule. At 10kbar the fO_2 of a graphite container lies in the wustite stability field between the IW and MW buffers (Kushiro & Thompson, 1972) and should lie between GCO and GW on the graphite saturation surface (Taylor, 1985; Taylor & Green, 1987). These reduced conditions cause the reduction of Cr^{3+} to Cr^{2+}, which is reflected in detectable Cr^{2+} contents in olivines at higher temperatures, when spinel is no longer present. (Murck & Campbell, 1986; Barnes, 1986).

During the course of this experimental study Fe-loss occurred in some experiments (not reported in Table 4) due to leakage of melt through the porous nature of the graphite container. The graphite in this case was of inferior density and quality than that used in the experiments presented in Table 4. This resulted in melt being able to make contact with the outer Pt capsule. The glass composition for one such experiment T-2098 is reported in Table 6. The glass composition compared with equilibrium partial melts from MORB pyrolite, has higher SiO_2, CaO and lower Na_2O contents and has a much higher Mg#. These features are a result of equilibrium being shifted by Fe-loss away from an olivine + orthopyroxene + clinopyroxene + spinel + liquid assemblage to an orthopyroxene + clinopyroxene + liquid assemblage.

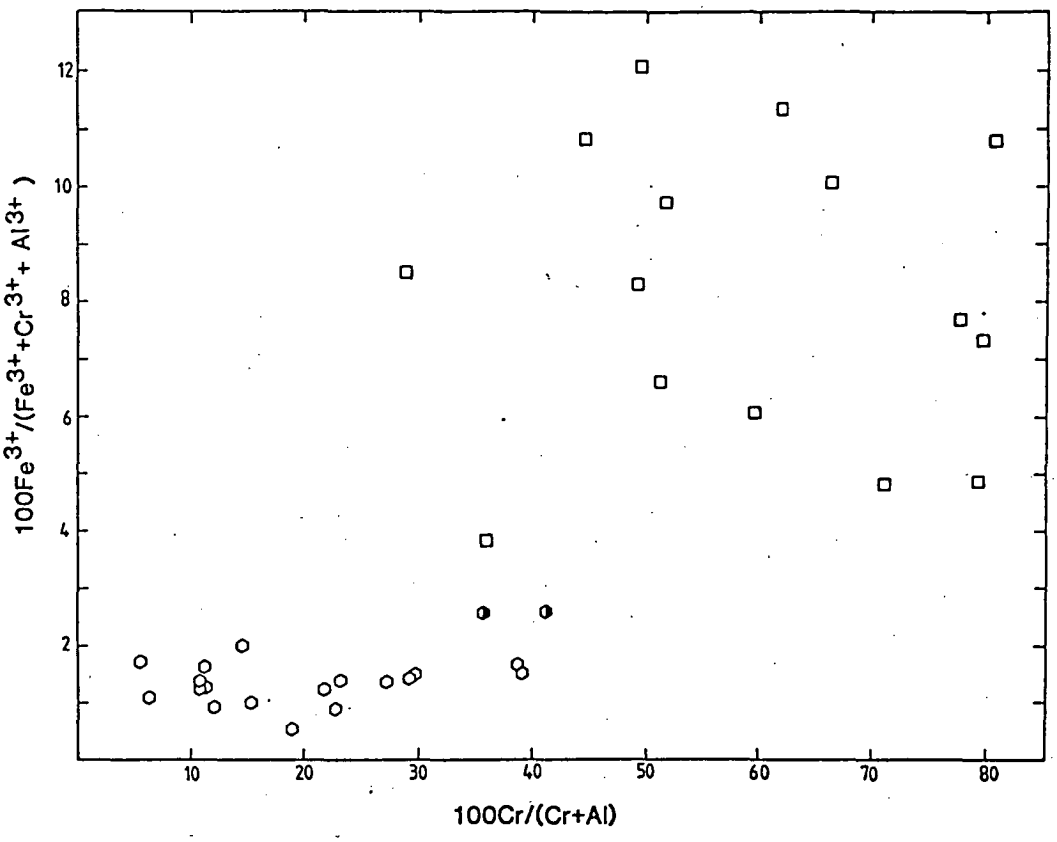

Figure 6.

$100Fe^{3+}/(Fe^{3+} + Al^{3+} + Cr^{3+})$ versus the 100Cr/(Cr + Al) ratio of spinels crystallizing in high pressure peridotite experiments in platinum and graphite capsules at pressures between 8 to 20kbars,

(⬡) spinels crystallizing in graphite from 8-20kbar (Takahashi & Kushiro, 1983; Takahashi, 1986; Falloon unpublished data),

(□) spinels crystallizing in platinum from experiments of Jaques & Green (1980) between 10-15kbar (Jaques, 1980),

(◑) spinels crystallizing in graphite, where some iron loss has occurred during the run (Falloon, unpublished data),

The important features of Fe-loss in noble metal containers can be summarized below:

(1) Fe-loss stabilizes a more Fe^{3+} and Cr^{3+} rich spinel, due to an increase of fO_2.

(2) Liquid compositions become more silica-saturated, and have higher CaO contents, due to the expansion of the Mg-rich olivine and orthopyroxene fields at the expense of calcic pyroxene.

(3) Mg# of the liquid becomes very high due to loss of Fe to Pt, which is also reflected in magnesian residual phase compositions.

The above features of Fe-loss appear to be present in the experiments of Fujii & Scarfe (1985). Fujii & Scarfe (1985) conducted melting experiments on peridotite compositions PMM-1 and PMM-2 between the temperatures of 1250°C and 1310°C, within this temperature interval the Mg# of the equilibrium glasses changed from 0.69 for PMM-1 and 0.72 for PMM-2 to 0.78 and 0.80 respectively. Based on the equilibrium $(Kd)^{ol/liq}_{Fe/Mg}$ of 0.32 in graphite determined by Takahashi & Kushiro (1983) at 10kbar the change in the Mg# of the glasses represents a change in the olivine composition from Fo_{87} to Fo_{92} in the case of PMM-1 and from $Fo_{88.8}$ to Fo_{93} in the case of PMM-2. This change in olivine composition is too large to be explained simply by an increase in temperature of only 60°C. The large range and high Mg# of the glasses from Fujii & Scarfe (1985) can be attributed to iron loss occurring over the long run times used, iron loss being more evident in the high temperature runs than the lower temperature runs. The presence of Fe-loss in the higher temperature runs of Fujii & Scarfe (1985) explains many of the unique features of their experiments. Firstly the very high CaO contents of the higher temperature liquids compared to MORB pyrolite glass compositions can be explained by the contraction of the calcic pyroxene field. Secondly the more chromium rich spinels relative to spinels in graphite experiments reported by Fujii & Scarfe (1985) can be explained by an increase in fO_2 due to Fe-loss. However complete spinel compositions were not reported by Fujii & Scarfe (1985) and it is not possible to ascertain if spinel is significantly different from spinels crystallizing in graphite. Thirdly the decrease in iron contents of the glasses from 7.77 to 6.52 wt% for PMM-1 and from 7.25 to 6.03 wt% for PMM-2 is the opposite of that expected with increasing degree of partial melting. FeO contents should gradually increase towards the FeO content of the bulk

composition during batch partial melting. The falling FeO contents can be explained by Fe-loss to the Pt container.

1.7 EQUILIBRIUM GLASS COMPOSITIONS AT 10KBAR

In order to portray the chemical relationships between the composition of the equilibrium partial melts compositions of MORB pyrolite at 10kbar and primitive MORB glasses a graphical projection based on the molecular CIPW norm is used in Fig.7 and 8. The normative minerals are assigned to the four end members of a tetrahedron (Green, 1970). The tetrahedron is based on the 'Basalt tetrahedron' of Yoder & Tilley (1962). To illustrate the three-dimensional relationships within the tetrahedron , two subprojections onto the face of the tetrahedron will be used. The first is a projection from diopside (Di) onto the base of the tetrahedron Jadeite plus Ca-tschermak's molecule (Jd+CaTs)-quartz(Qz)-olivine(Ol) as in Fig.7. The second is a projection from plagioclase (An+Ab) onto the the face olivine(Ol)-diopside(Di)-quartz(Qz) as in Fig. 8. The subprojection from plagioclase is very similar to the projection used by Walker et al. (1979) and Grove et al. (1982). The projection scheme of Elthon (1983) gives a result different from Walker et al. (1979) but is very similar to a subprojection from Jd+CaTs onto the face olivine(Ol)-diopside(Di)-quartz(Qz) in our projection scheme.

In the subprojection from diopside (Figs.7,9) equilibrium melt compositions from MPY-87, MPY-90, MPY90-40, HW-40, TQ-40 and KLB-1 all plot within the primitive MORB glass field, indicating the possibility that primitive MORB glasses are indeed primary melts at 10kbar. However when viewed from the plagioclase(An+Ab) projection (Fig.8 and 10), except for the glasses from HW-40, all the 10kbar equilibrium liquids plot below the spectrum of primitive MORB glasses indicating that primitive MORB glasses are not primary magmas. In a companion study to that reported here (PARTII), it is demonstrated that the MORB glasses are derivative compositions lying on olivine control lines from more picritic primary magmas segregating from peridotite at pressures greater than 10kbar. Due to the importance of this conclusion, the effect of analytical uncertainty in the plagioclase(An+Ab) projection must be evaluated.

1.7.1 The effect of analytical uncertainty

Presnall et al. (1979) and Presnall & Hoover (1984, 1986) have suggested that analytical uncertainty plays a major effect in diagrams such

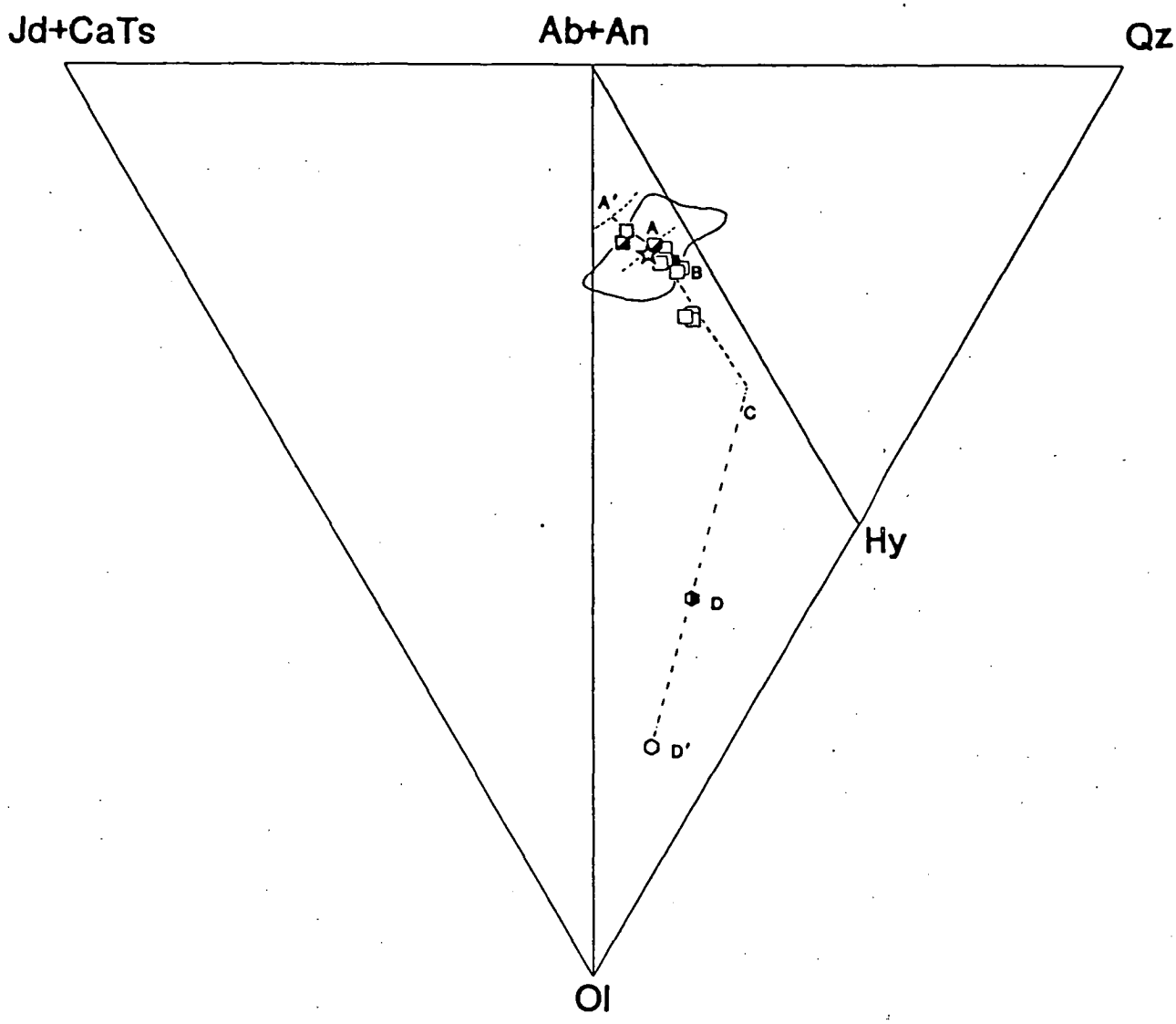

Figure 7.

Equilibrium glass compositions from MORB pyrolite plotted in the CIPW molecular normative projection from diopside(Di) onto the base of the 'basalt tetrahedron' jadeite plus calcium tschermak's molecule(Jd + CaTs)-quartz(Qz)-olivine(Ol), letters A, A', B, C, D, D' are referred to in the text,

(⬡) MORB pyrolite (MPY-87, MPY-90),
(◑) MORB pyrolite minus 40 wt% olivine (MPY-90-40),
(□) glass compositions from MPY-87 (Table 5),
(◪) glass compositions from MPY-90-40 (Table 6),
(■) glass compositions from MPY-90 (Table 6),
(☆) composition of primitive MORB glass DSDP3-18-7-1 enclosed by the field of primitive MORB glasses (references see caption to Fig.1)
—·—·— locus of liquids in equilibrium with olivine
– – – – – locus of liquids in equilibrium with olivine + orthopyroxene
———— locus of liquids in equilibrium with olivine + clinopyroxene + orthopyroxene + spinel

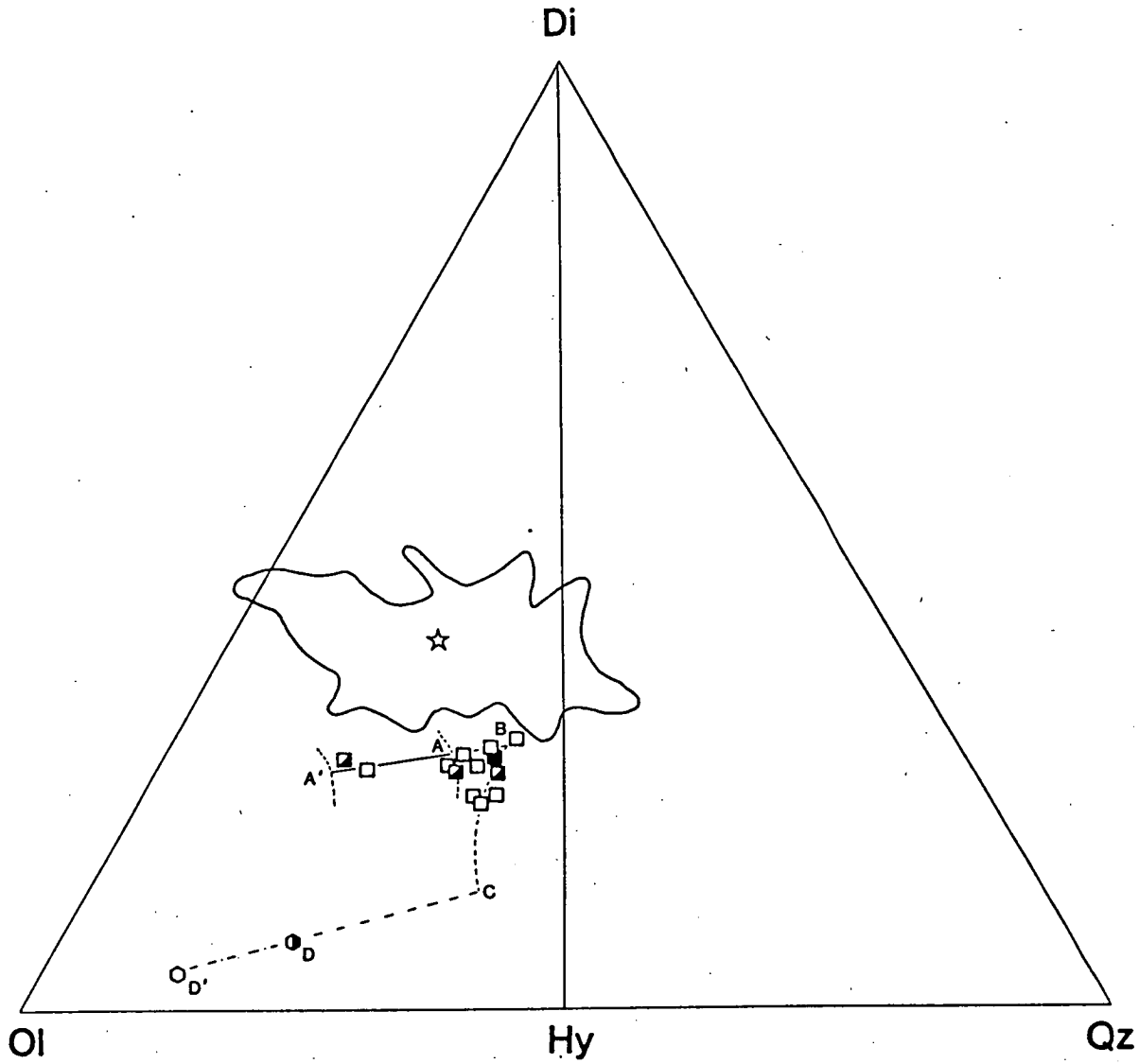

Figure 8.

Equlibrium glass compositions from MORB pyrolite plotted in the CIPW molecular normative projection from plagioclase(Ab + An) onto the face olivine(Ol)-diopside(Di)-quartz(Qz) of the 'basalt tetrahedron'. Symbols and cotectics as for Fig.7.

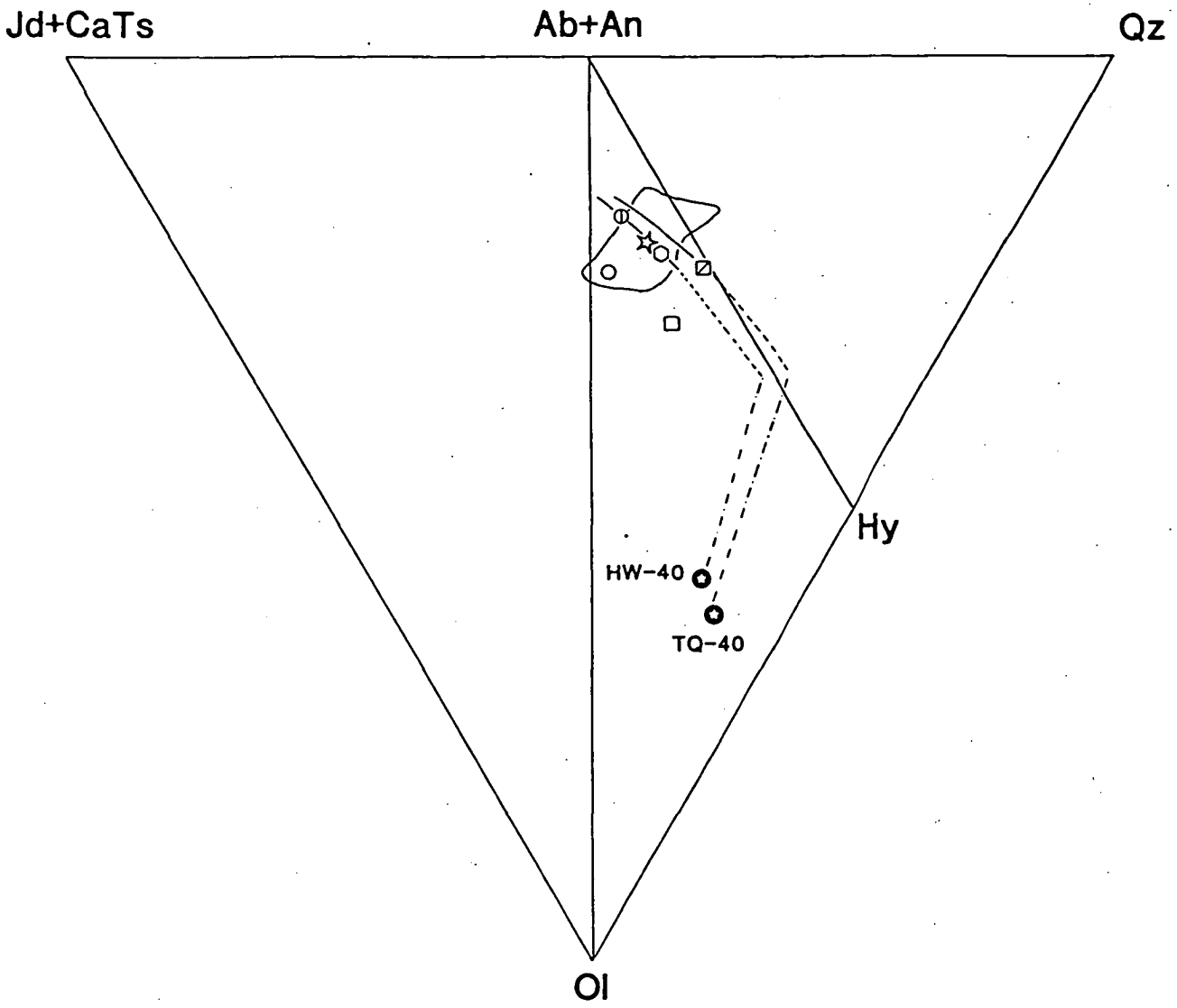

Figure 9.

Equilibrium glass compositions from Hawaiian pyrolite, Tinaquillo lherzolite and spinel lherzolite KLB-1 plotted in the CIPW molecular normative projection from diopside(Di) onto the base of the 'basalt tetrahedron' jadeite plus calcium tschermak's molecule(Jd + CaTs)-quartz(Qz)-olivine(Ol), cotectics as for Fig.7,

(○) calculated Jaques & Green (1980) 10kbar liquid composition from Hawaiian pyrolite (Table 2),

(□) calculated Jaques & Green (1980) 10kbar liquid composition from Tinaquillo lherzolite (Table 2),

(⬡) equilibrium glass composition from KLB-1 (Table 6),

(▨) equilibrium glass composition from Tinaquillo lherzolite (Table 6),

(⦶) equilibrium glass composition from Hawaiian pyrolite (Table 6),

(☆) primitive MORB glass DSDP3-18-7-1 enclosed by the field of primitive MORB glasses (references see caption to Fig.1).

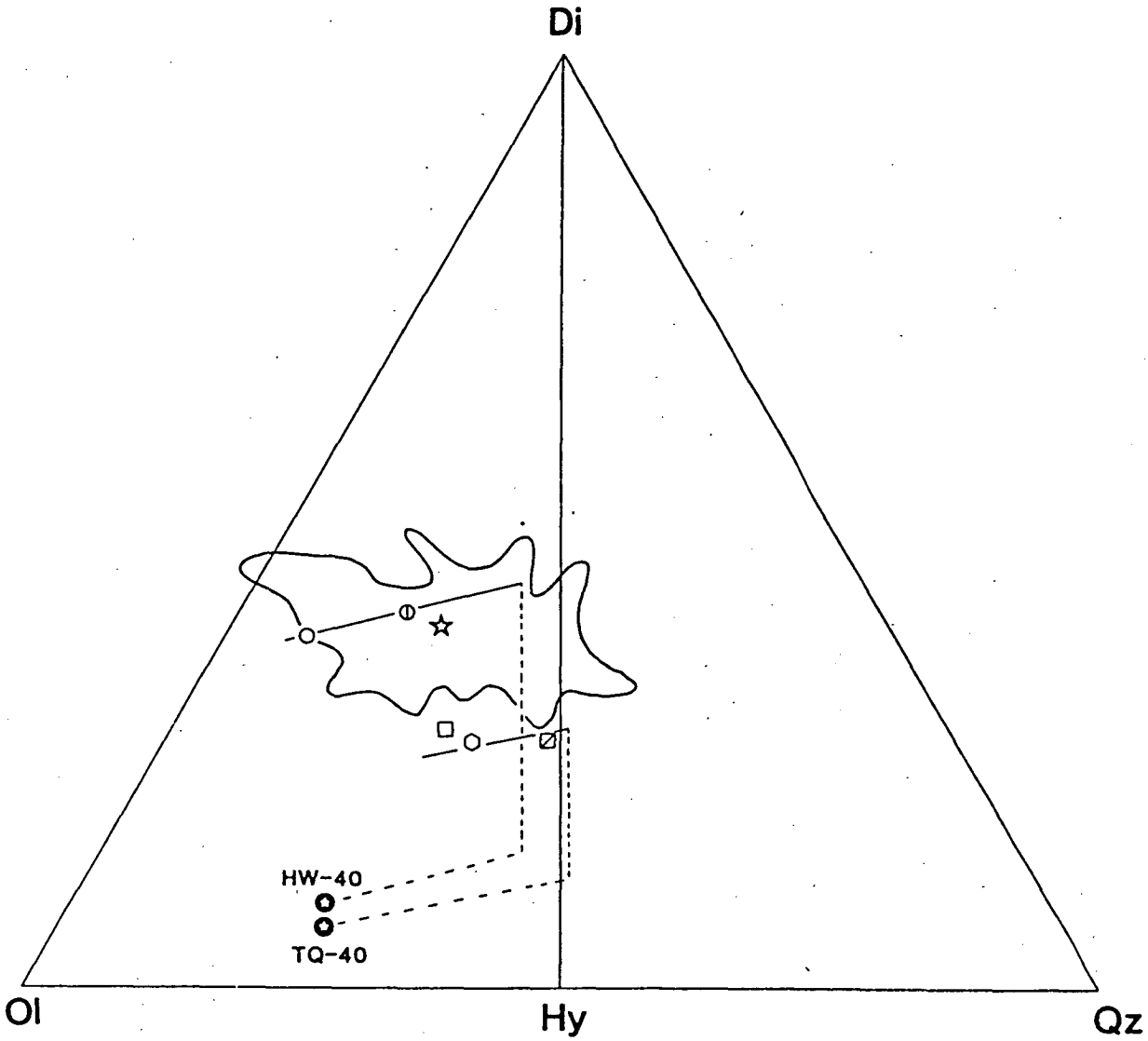

Figure 10.

Equilibrium liquid compositions from Hawaiian pyrolite, Tinaquillo lherzolite and spinel lherzolite KLB-1 plotted in the CIPW molecular normative projection from plagioclase(Ab + An) onto the face olivine(Ol)-diopside(Di)-quartz(Qz) of the 'basalt tetrahedron', symbols as for Fig.9 and cotectics as for Fig.7.

as in Fig.1, 8 and 10. It is therefore necessary to investigate the effect of analytical uncertainty as the conclusions of this study depend partly on the observation that the 10kbar partial melts from MORB pyrolite plot below the primitive MORB glasses in Fig.8.

In Fig.11a we plot all the glass EMP broad area scans for run T-1478. The composition given in Table 5 is the average of these 10 area scans. The area scans show a restricted range in the projection but none of the scans fall within the MORB field. The spread of points is also significantly less than the 'ellipse of uncertainty' calculated by Presnall & Hoover (1984). The spread of points is elongate towards and away from the quartz apex as small uncertainties in SiO_2, Na_2O, Al_2O_3, CaO, MgO and FeO all contribute to uncertainties in normative Hy. To demonstrate the effect of these uncertainties for each individual oxide in Fig.11b we have shown the effect of a 2σ +ve and -ve error respectively for each major oxide. The 2σ values are taken from Table 5 and are based on over 100 microprobe analyses on the University of Tasmania's probe. The 2σ values compare well with similar values for the microprobe at the Smithonsian Institution and the Massachusetts Institute of Technology reported in Presnall & Hoover (1984). The resultant spread of points is again much less than the 'ellipse of uncertainty' of Presnall & Hoover (1984) both for +ve and -ve errors and all the points fall below the MORB glass field. However it is possible to calculate a worst possible case of analytical error based on the 2σ values. This worst possible case is plotted as a star in Fig.11a, b and c, and is the result of -ve errors on SiO_2, TiO_2 and Al_2O_3 and +ve errors on MgO, CaO and Na_2O. The probability of such an analysis is very small and such an analysis is highly unlikely to appear in any reasonable or practical number of broad beam area scan analyses. Even in the worst possible case the glass analysis still plots below the MORB glasses. The composition of the glass is also unlike any MORB glass with too much SiO_2 and MgO and low Al_2O_3 and TiO_2 compared to MORB glasses plotting with low normative Di. These low normative Di glasses (when seen in the An+Ab projection) could be moved to lower normative Di contents overlapping with the 10kbar cotectic defined by the equilibrium partial melts, yet the probability of this occurring is very small and the composition of these MORBs would be unlike the equilibrium 10kbar liquids. In summary therefore, the positions of the 10kb cotectics relative to the MORB glasses in Fig.8 and 10 can be used to draw petrogenetic conclusions about the primary nature of MORB glasses in full cognizance of analytical uncertainty. Similar conclusions regarding the value of diagrams such as the CIPW molecular norm projection to give petrogenetic information have been reached by Grove & Bryan (1983), Stolper

Figure 11.

CIPW molecular normative projection from plagioclase(Ab + An) onto the face olivine(Ol)-diopside(Di)-quartz(Qz) of the 'basalt tetrahedron' illustrating the effect of analytical uncertainity. Thick dark line encloses the field of primitive MORB glasses (see Fig.1) in A, B and C. Thin lined ellipse is the 'ellipse of uncertainity' from Presnall & Hoover (1984). (✪) 'worst possible case' of analytical error (see text for explanation),

A. (○) inidividual broad beam glass analyses from run T-1478,

B. (□) average glass analysis for run T-1478,

(●) numbered 1 to 8 represent the effect of a 2σ -ve error due to analytical uncertainity based on the σ values given in Table 5 on the average glass scan for T-1478, 1=SiO_2, 2=TiO_2, 3= Al_2O_3, 4=FeO, 5= MgO, 6= CaO, 7=Na_2O and 8= 2σ -ve error on all major oxides,

C. (●) numbered 1 to 8 represent the effect of a 2σ +ve error due to analytical uncertainity. Numbers and symbols same as for Fig.11b.

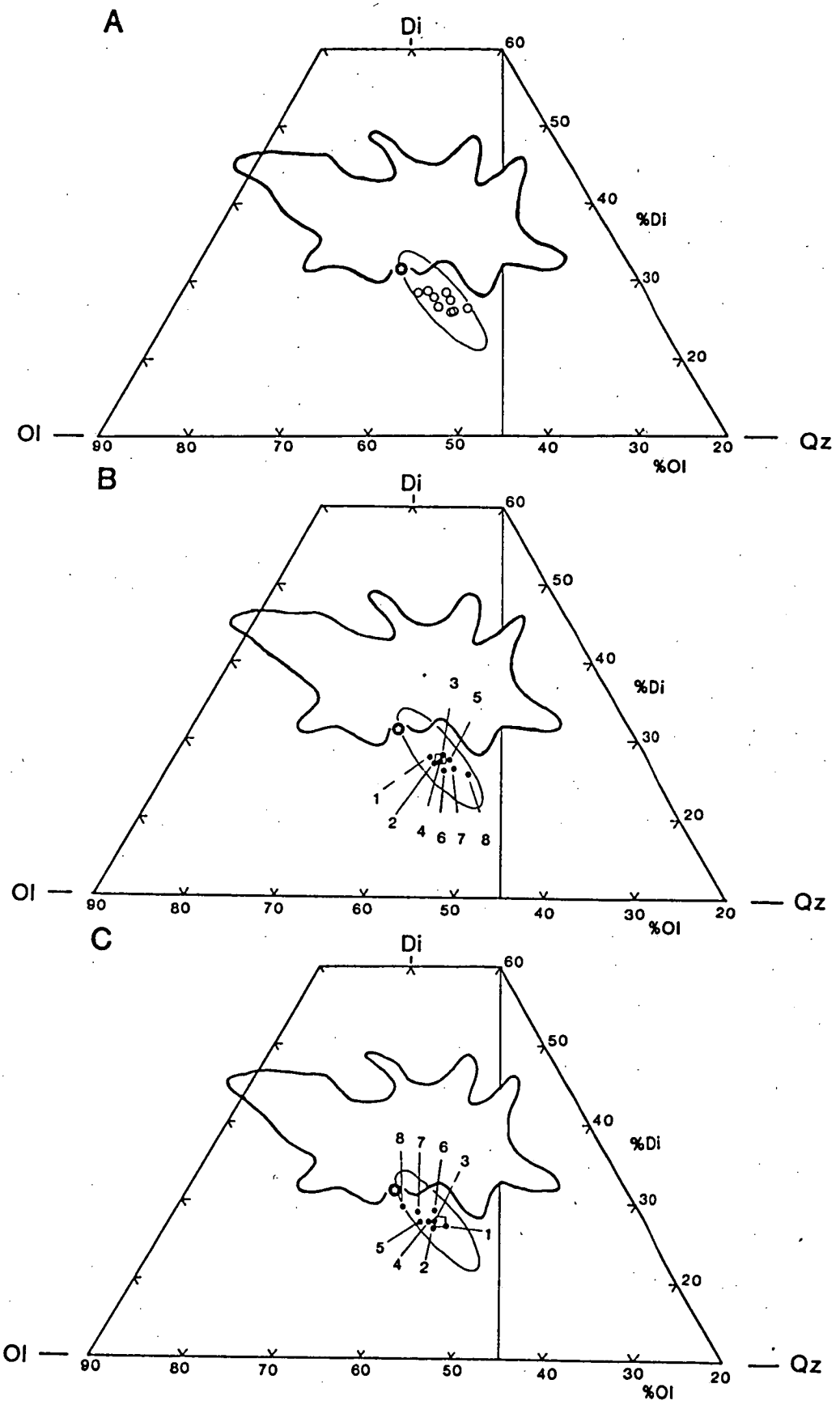
A
Di
60
50
40
%Di
30
20
Ol
90
80
70
60
50
40
30
20
%Ol
Qz
B
Di
60
50
40
%Di
30
20
3
5
1
2
4
6
7
8
Ol
90
80
70
60
50
40
30
20
%Ol
Qz
C
Di
60
50
40
%Di
30
20
8
7
6
3
1
5
4
2
Ol
90
80
70
60
50
40
30
20
%Ol
Qz

(1980), Christie & Sinton (1986), Grove & Kinzler (1986), Elthon (1986) and Thompson (1987).

1.7.2 Glass compositions from MORB pyrolite (MPY-87, MPY-90, MPY-90-40)

The equilibrium liquid compositions from MORB pyrolite are presented in Table 5 and are compared to primitive MORB glasses in Figs.7 and 8. The liquid compositions define the following equilibrium phase boundaries;

(1) A six phase point (olivine + orthopyroxene + clinopyroxene + spinel + plagioclase + liquid) defined by run no. T-2121.

(2) A olivine + orthopyroxene + clinopyroxene + spinel + liquid cotectic, defined by run nos. T-1511, 1472, 2123, 1493, 1478, 2140, 2078, 2138 and 2136.

(3) A olivine + orthopyroxene + liquid cotectic defined by runs T-1464, 1480 and 1461.

The course of melting of MORB pyrolite is described with reference to letters A, A', B, C, D and D' in Figs.7,8. Melting begins at A which represents a six-phase cotectic. The liquid composition represented by T-2121 is high in Al_2O_3, TiO_2 and Na_2O but low in CaO compared to primitive MORB glasses. The plagioclase composition at the six-phase cotectic is An_{68-69}. The six-phase cotectic is not invariant but moves towards A', where plagioclase is eliminated from the residue. The movement is a consequence of plagioclase melting, which enriches the liquid in Al_2O_3 and Na_2O. Na_2O depolymerizes the melt structure expanding the olivine phase volume (Kushiro, 1975). This expansion of the olivine phase volume can be seen best in the projection from Di (Fig.7). After plagioclase is eliminated continual melting moves liquid compositions from A' to B, along an olivine + orthopyroxene + clinopyroxene + spinel + liquid cotectic. A large variation in liquid composition is possible along this cotectic due to the solid solution behaviour of olivine, pyroxenes and spinel. At B clinopyroxene is eliminated from the residue. Spinel also is eliminated as a consequence of the low fO_2 within the graphite capsules. Between B and C liquid compositions move along an olivine + orthopyroxene + liquid cotectic. At some point between B and C, depending on bulk composition, orthopyroxene is eliminated from the residue, and the liquids thereafter lie on an olivine control line through the bulk composition. At C orthopyroxene is eliminated from bulk compositions consisting of MORB

pyrolite without any added DSDP3-18-7-1. Important observations from Fig.7 and 8 are;

(1) The 10kbar equilibrium liquids from MORB pyrolite plot below primitive MORB glasses and plot well below the composition of DSDP3-18-7-1.

(2) The 10kbar equilibrium liquids from MORB pyrolite only span the middle range of the primitive MORB glass spectrum in terms of silica saturation. The range in silica saturation of the 10kbar liquids is limited due to the plagioclase phase volume which stops liquids from crossing over to the Ne-normative side of the tetrahedron, and the elimination of clinopyroxene stops liquids crossing to the quartz normative side of the diagram.

The equilibrium liquids at low degrees of partial melting (<9wt%, determined from least-squares mass balance calculations) in equilibrium with olivine + clinopyroxene + orthopyroxene + spinel ± plagioclase are distinct from primitive MORB glasses in their high Na_2O and Al_2O_3 contents and low FeO, MgO and CaO contents. Equilibrium liquids at higher degrees of partial melting differ significantly from primitive MORB glasses in having lower TiO_2, Al_2O_3, CaO and Na_2O contents and have higher MgO contents.

Important characteristics of the primitive MORB glasses are their high CaO and Al_2O_3 contents and relatively high CaO/Al_2O_3 ratios compared with most other basalt series. This characteristic conflicts with the equilibrium partial melts from MORB pyrolite at 10kbar, as high Al_2O_3 contents do not correlate with high CaO contents. At low degrees of partial melting Al_2O_3 contents are high but CaO contents are low, consequently CaO/Al_2O_3 ratios are low (<0.55). As the percent partial melting increases, CaO contents increase as Al_2O_3 contents decrease raising the CaO/Al_2O_3 ratio. A maximum CaO content is reached at the point at which clinopyroxene is eliminated as a residual phase and the CaO/Al_2O_3 ratio now approaches that of the source. So although high CaO and Al_2O_3 contents can be produced by partial melting it is the combination of both high CaO and Al_2O_3 contents in MORB that is distinctive and difficult to achieve by partial melting alone at 10kbar.

In terms of CIPW molecular normative mineralogy, the equilibrium liquids have significantly higher normative Hy than most primitive MORB glasses, which is one of the main causes for the glasses plotting below the primitive MORB in Fig.7. The high Hy contents of the equilibrium liquids is partly a result of the high SiO_2 contents compared to most primitive MORB

glasses. In Fig.12 the frequency distribution of SiO_2 contents of primitive MORB glasses is presented. Primitive MORB glasses appear to have a bimodal distribution with a maximum between 49.3 to 50.2 and another smaller maximum between 51 and 51.3 wt% SiO_2. Primitive MORB glasses with higher SiO_2 contents than the 10kbar liquids from MORB pyrolite have low olivine normative contents or are quartz normative and they plot to the right of the 10kbar cotectic in Fig.7. These distinctive MORB glasses are therefore possible primary melts at pressures of less than 10kbar. This possibility will be discussed later. Although primitive MORB glasses plot above the 10kbar cotectic in Fig.8, there are some primitive MORB compositions that do fall on the 10kbar cotectic, an example is given in Table 6 (no. 9) which is the average primitive olivine basalt composition P_2 from the FAMOUS area of the Mid-Atlantic ridge (Le Roex et al., 1981). The composition of P_2 is identical to the liquid composition T-1478 (Table 5) except for a slight difference in FeO and MgO contents. Although P_2 is not a glass composition but an average of three sparsely phyric to aphyric olivine basalt compositions it should still be close to a liquid composition. This result suggests that some MORB parental magmas are 10kbar primary melts in equilibrium with a lherzolite residue. However the overwhelming majority of primitive MORB compositions represented by the glass compositions in Figs. 1, 7 and 8 are not primary melts at 10kbar. Le Roex et al. (1981) demonstrated that the composition of P_2 was not a suitable parental composition to the majority of olivine basalts from FAMOUS. In a companion paper (PARTII) primitive olivine basalts from FAMOUS are shown to be near or close (<10 wt% olivine fractionation) to primary melts segregating from pressures of between 10 to 18 kbars leaving a lherzolitic residue.

1.7.3 Glass compositions from Tinaquillo lherzolite (TQ-40) and Hawaiian pyrolite (HW-40)

The results of the two 10kbar experiments on TQ-40 and HW-40 are part of a more comprehensive study from 0-30kb on these two compositions reported in Falloon et al. (1987). Due to the uncertainties involved in the modal analyses of experimental charges in order to calculate equilibrium liquids at 10kbar, the calculated liquids of Jaques & Green (1980) were reversed by use of the sandwich technique. The results of the sandwich experiments demonstrate a significant shift in the olivine + orthopyroxene + clinopyroxene + liquid cotectics for Tinaquillo lherzolite and Hawaiian pyrolite to more silica saturated compositions (Falloon et al., 1987). This shift is seen more clearly in the projection from Di (Fig.9). Compared with

calculated 10kbar liquids from Tinaquillo, the glass composition of T-2113 (Table 6) has higher SiO_2, Al_2O_3 and CaO. Compared with primitive MORB glasses the composition of run T-2113 plots below the primitive MORB glasses spectrum in Fig.12 and plots to the right of 10kbar liquids from MORB pyrolite, which is expected for a more depleted source composition. T-2113 has higher CaO/Al_2O_3 and CaO/Na_2O ratios than most primitive MORB glasses as a result of lower Al_2O_3 and Na_2O contents. T-2113 also has significantly lower TiO_2 and higher MgO contents than primitive MORB glasses.

Compared to calculated liquids from HW-40 the 10kbar reversal run T-2117 (Table 6) has significantly higher SiO_2 and Al_2O_3 contents and lower FeO and MgO contents. It is significant that the composition of run T-2117 plots within the primitive MORB glass spectrum in Fig.10 indicating it is possible to have peridotite sources which produce melts which define olivine + orthopyroxene + clinopyroxene + spinel + liquid cotectics at high normative Di contents in the projection from plagioclase (An+Ab). However such peridotite compositions differ in Na_2O, TiO_2, K_2O contents from typical oceanic upper mantle represented by the Ronda and Bullenmerri peridotite suites (Fig.2) and the melt compositions are unlike primitive MORB glasses. In the case of HW-40, melt compositions at 10kbar are lower in Al_2O_3 and CaO than primitive MORB glasses and are enriched in Na_2O, K_2O and TiO_2.

1.7.4 Glass compositions from KLB-1

The one experiment performed using KLB-1 as the peridotite in the sandwich with DSDP3-18-7-1 produced a liquid composition very similar to the liquid compositions from MORB pyrolite. The composition of run T-2133 (Table 6) plots in a similar position to liquid compositions from MORB pyrolite, below primitive MORB glasses in Fig.10. This result is not unexpected due to the very close similarities between MORB pyrolite and KLB-1.

1.7.5 Summary

The results of the 10kbar melting study on MORB pyrolite, Hawaiian pyrolite, Tinaquillo lherzolite and the spinel peridotite KLB-1 demonstrate that equilibrium liquids are sufficiently different from primitive MORB glasses to warrant the conclusion that primitive MORB glasses are not primary magmas at 10kbar. All the 10kbar liquids except those from Hawaiian pyrolite define olivine + orthopyroxene + clinopyroxene + spinel + liquid

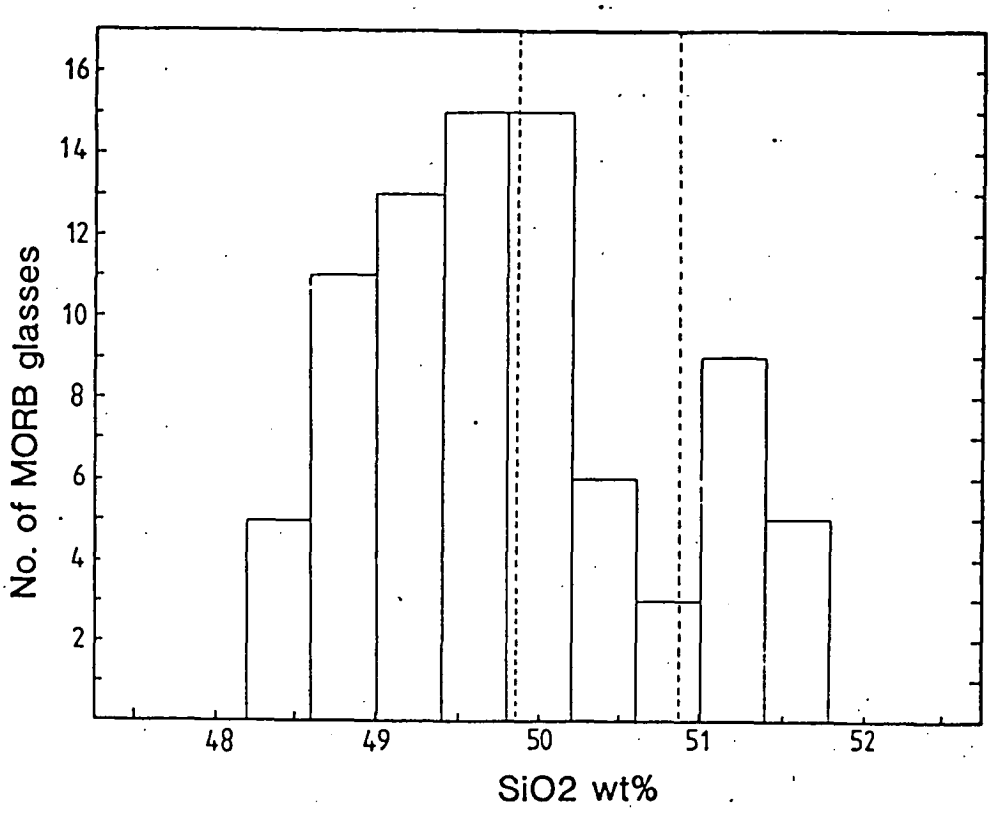

Figure 12.

Frequency histogram of SiO_2 contents of primitive MORB glasses (references see caption to Fig.1). Dashed lines delineate the range of SiO_2 contents for equilibrium liquid compositions from this study.

cotectics which plot below primitive MORB glasses in Figs.8 and 10. The following section will attempt to integrate these new results with previous 10kbar melting studies relevant to MORB petrogenesis.

1.8 COMPARISON WITH OTHER 10KBAR MELTING STUDIES

Equilibrium liquid compositions from previous 10kbar melting studies are plotted in the basalt tetrahedron (Figs.13 and 14) where they are compared with the spectrum of primitive MORB glasses and equilibrium partial melt compositions from MORB pyrolite at 10kbar. In the projection from Di (Fig 13) not all the liquid compositions at 10kbar define the same olivine + orthopyroxene + clinopyroxene + liquid or olivine + orthopyroxene + liquid cotectics. This could be due to differences in bulk compositions used or to differences in pressure calibration between different laboratories using the piston-cylinder apparatus. With regards to differences in pressure calibration PARTII and Falloon et al. (1987) demonstrate that for three different peridotite compositions MORB pyrolite, Hawaiian pyrolite and Tinaquillo lherzolite equilibrium partial melt compositions overlie each other in the projection from Di, and define the same olivine + clinopyroxene + orthopyroxene + liquid and olivine + orthopyroxene + liquid cotectics at 5, 10, 15, 20 and 30kbars. Cotectics moving systematically with pressure towards the olivine apex parallel to the Ol-Jd + CaTs join. The position of these cotectics is also consistent with 30, 20, 15 and 5 kbar cotectics from HK66 (Takahashi & Kushiro, 1983) and 10 and 30kbar cotectics from KLB-1 (Takahashi, 1986; this study). These results provide an internally consistent set of data, upon which other melting studies can be compared and evaluated. The position of cotectics at pressures higher and lower than 10kbar demonstrate that the position of the 10kbar cotectics from MORB pyrolite are correctly located. Because different peridotite compositions (Hawaiian pyrolite, MORB pyrolite, Tinaquillo lherzolite, HK66 spinel lherzolite, KLB-1 spinel lherzolite) define similar cotectics at 30, 20, 15 and 5 kbars, differences in bulk composition are not considered likely in explaining differences in the position of cotectics at 10kbar in the projection from Di. The most likely explanation is differences in pressure calibration of the piston cylinder apparatus between pressures of 8 to 12 kbars. Previous experimental studies are discussed on an individual basis below.

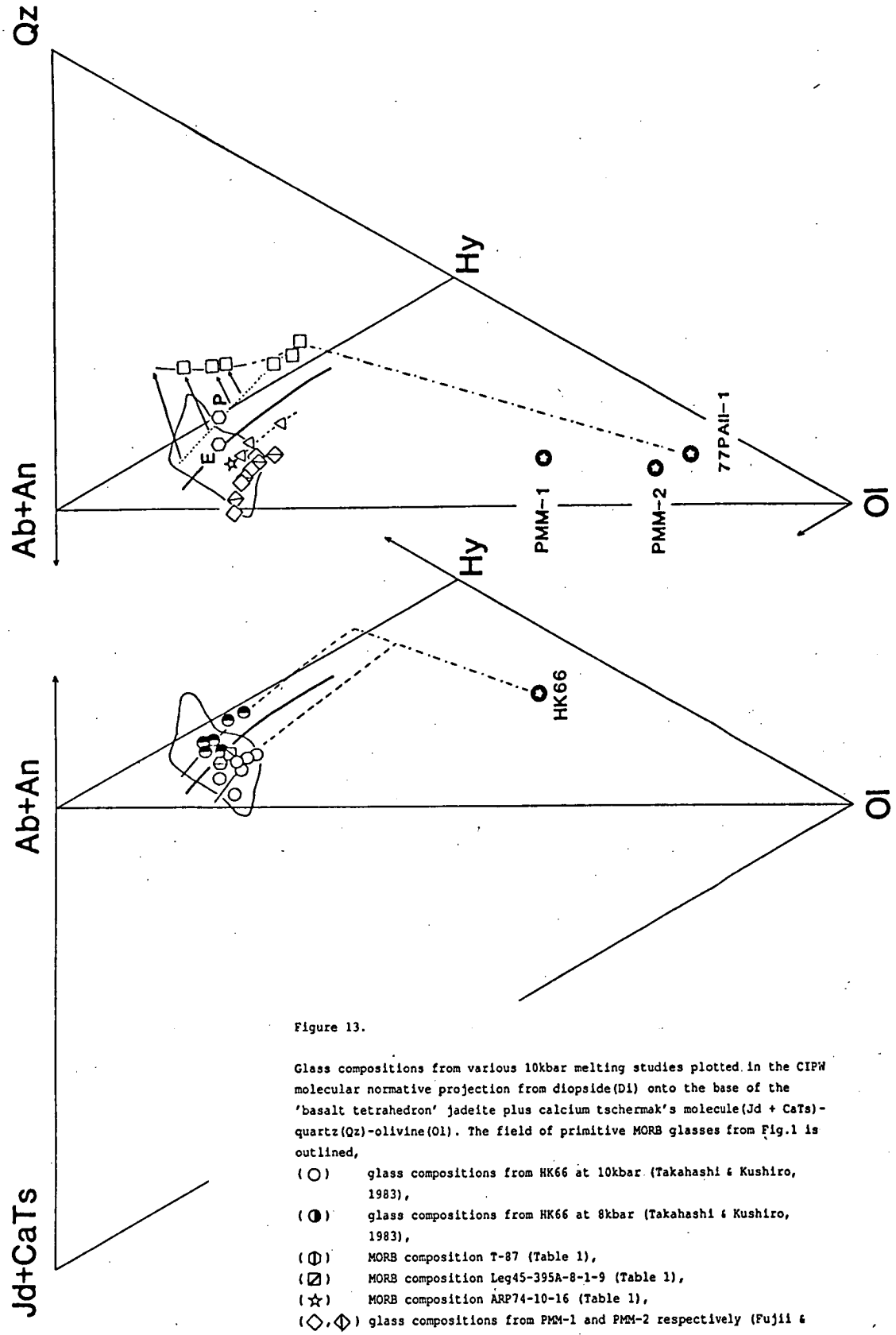

Figure 13.

Glass compositions from various 10kbar melting studies plotted in the CIPW molecular normative projection from diopside(Di) onto the base of the 'basalt tetrahedron' jadeite plus calcium tschermak's molecule(Jd + CaTs)-quartz(Qz)-olivine(Ol). The field of primitive MORB glasses from Fig.1 is outlined,

(○) glass compositions from HK66 at 10kbar (Takahashi & Kushiro, 1983),

(◑) glass compositions from HK66 at 8kbar (Takahashi & Kushiro, 1983),

(⌀) MORB composition T-87 (Table 1),

(▨) MORB composition Leg45-395A-8-1-9 (Table 1),

(☆) MORB composition ARP74-10-16 (Table 1),

(◇,◈) glass compositions from PMM-1 and PMM-2 respectively (Fujii & Scarfe, 1985),

(□) glass compositions from 77PAII-1 (Sen, 1982),

(△) glass compositions from Stolper (1980),

(○ P) six phase invariant point in the system CaO-MgO-Al_2O_3-SiO_2 (Presnall et al., 1979),

(○ E) six phase pseudoinvariant point in the complex system from Elthon & Scarfe (1984),

——— solid line represents the 10kbar cotectic from MORB pyrolite,

/.../.../... dotted line represents a possible cotectic for liquids in equilibrium with olivine + orthopyroxene + clinopyroxene at 9kbar from 77PAII-1, arrows show the effect of quench modification on equilibrium liquid compositions.

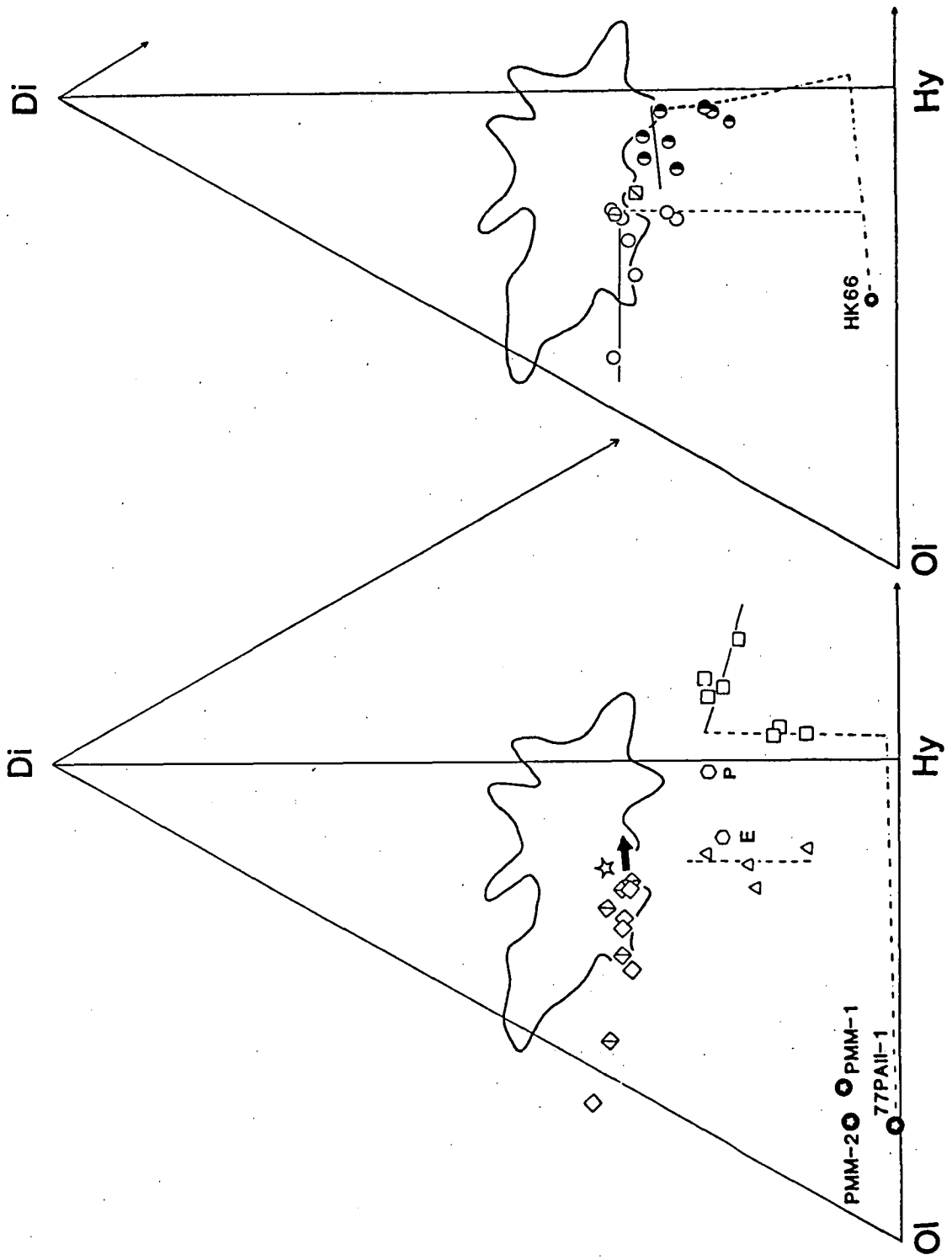

Figure 14.

Glass compositions from various 10kbar melting studies plotted in the CIPW molecular normative projection from plagioclase(Ab + An) onto the face diopside(Di)-olivine(Ol)-quartz(Qz) of the 'basalt tetrahedron', symbols as for Fig.13, cotectics as for Fig.7,

➡ arrow shows expected trend of liquid compositions with progressive Fe-loss at higher temperatures.

1.8.1 Stolper (1980)

In the experiments of Stolper (1980) a primitive MORB glass ALV519-4-1 was equilibrated with olivine and orthopyroxene in a sandwich type experiment. The aim of the study was to establish the nature of liquids in equilibrium with orthopyroxene at 10kbar. The liquids in equilibrium with olivine + orthopyroxene at 10kbar from Stolper (1980) are plotted in Figs.13 and 14. The liquid compositions define an olivine + orthopyroxene + liquid cotectic almost identical to that from MORB pyrolite, the liquid compositions of Stolper (1980) being very similar to the glass compositions of runs T-1464, 1461 and 1480. However the cotectic defined by 10kbar liquids from Stolper (1980) plots slightly away from the MORB pyrolite olivine + orthopyroxene + liquid cotectic towards the olivine apex in Figs. 13 and 14. The liquid compositions from Stolper (1980) being more consistent with a 12kbar olivine + orthopyroxene + liquid cotectic. The results of this experimental study are however still in agreement with the conclusion of Stolper (1980), that primitive MORB glasses do not lie close to orthopyroxene saturation at 10kbar and therefore are not primary melts. The only differences between the study of Stolper (1980) and this study are;

(1) Stolper (1980) bulk compositions are undefined.

(2) The olivine + orthopyroxene + clinopyroxene + liquid cotectic is projected as a point in the phase diagram presented by Stolper (1980) whereas in reality it projects as a line.

(3) Stolper (1980) 10kbar liquids are more consistent with a 12kbar olivine + orthopyroxene + liquid cotectic.

1.8.2 Elthon and Scarfe (1984)

Elthon & Scarfe (1984) studied the high pressure phase relationships of a high-MgO picrite NT-23 from the Tortuga ophiolite complex, in southern Chile. As a result of this study Elthon & Scarfe (1984) established the composition of a liquid in equilibrium with olivine + orthopyroxene + clinopyroxene + plagioclase + spinel at 10kbar (run 333, Table 3, Elthon & Scarfe, 1984). This liquid composition plots very close to run T-2121 from MORB pyrolite and is similar in major element chemistry, having similar high Al_2O_3 relative to CaO contents. However the composition has a low Mg# of 0.63, in equilibrium with Fo_{83} olivine. The liquid composition

therefore can not be regarded as equivalent to a mantle melt from peridotite of $Fo_{90\pm2}$. The liquid composition is substantially different from primitive MORB glasses at 10kbar. The results of this study are in agreement with the conclusion of Elthon & Scarfe (1984) that MORB glasses with >9.5 wt% MgO are not primary magmas, but are derived from more picritic parents.

1.8.3 Presnall et al. (1979) and Presnall and Hoover (1984)

Presnall et al. (1979) based on the results of their experimental study in the simple system $CaO-MgO-Al_2O_3-SiO_2$ (CMAS) presented a model for the generation of Mid-Ocean ridge tholeiites. In the system CMAS the solidus curve for a simplified plagioclase and spinel lherzolite was found to have a cusp at 9kbar, where the transition from plagioclase to spinel lherzolite intersects the solidus forming an invariant point. In the model of Presnall et al. (1979) magma generation is caused by the intersection of a mantle geotherm at the 9kb cusp, and the composition of the near-solidus liquid produced at the 9kb cusp models the composition of primitive MORB glasses. The composition of the 9kb invariant point in the system CMAS is plotted in Figs.13 and 14. The 9kbar liquid composition plots close to but outside the field of primitive MORB glasses in Figs.13 and 14. Presnall et al. (1979) predicted that in the complex system, the 9kbar point would move towards the primitive MORB glass spectrum due to the addition of components such as Na_2O, TiO_2 etc. The results of this experimental study have confirmed the predicted shift except for two important points;

(1) The six-phase point in the complex system represented by T-2121 does indeed fall in the middle of the primitive MORB glass spectrum in the projection from Di in Fig.7, but in the projection from plagioclase(An+Ab) (Fig.8) falls below the primitive MORB glasses.

(2) In the model of Presnall et al. (1979) the composition of the liquids at the cusp are broadly similar to primitive MORB glasses although Figs. 13 and 14 illustrate important differences. However in the complex system the composition in equilibrium with olivine + orthopyroxene + clinopyroxene + spinel + plagioclase is substantially different from primitive MORB glasses, as are liquids lying along a olivine + orthopyroxene + clinopyroxene + spinel + liquid cotectic. The results of this study do not support the model of Presnall et al. (1979).

More recently Presnall & Hoover (1984) recognizing the fact that there is indeed a range of silica saturation amongst primitive MORB glasses, and as a single pressure of origin is inadequate to explain this feature, proposed that primary MORBs are generated from pressures of between 7 and 11kbar, based on the results from simple systems (CMAS and SCAMN, N= Na_2O). However in the complex system based on the equilibrium liquids from MORB pyrolite at 8kbar (PARTII), Tinaquillo lherzolite and Hawaiian pyrolite at 5kbar (Falloon et al., 1987; Jaques & Green, 1980), peridotite partial melts have SiO_2 contents of between 50 to 55 wt%. These compositions are substantially more SiO_2-rich than most primitive MORB glasses.

1.8.4 Takahashi and Kushiro (1983)

In Figs.13 and 14 the 10kbar and 8kbar partial melt compositions from HK66 are plotted. The partial melts define olivine + orthopyroxene + clinopyroxene + liquid and an olivine + orthopyroxene + liquid cotectics. The 10kbar and 8kbar liquids from HK66 have much higher FeOt, Na_2O and TiO_2 contents and lower CaO contents when compared to liquids from MORB pyrolite and are unlike any primitive MORB glass. In the projection from Di (Fig.13), the 10kbar cotectic from HK66 is displaced towards the olivine apex and its position is more consistent with a cotectic lying somewhere between 12 and 15kbars. The 10kbar liquids from HK66 in Figs. 13 and 14 plot in a similar position to 12-15kbar partial melts from Hawaiian pyrolite, Tinaquillo lherzolite, and MORB pyrolite. The 10kbar partial melts from HK66 also plot very close to 15kbar partial melts from HK66 in the projection from Di and overlie 15kbar partial melts in the projection from plagioclase(Ab+An). The 8kbar partial melts from HK66 plot close to the 10kbar cotectic from MORB pyrolite in the projection from Di and overlie 10kbar partial melts from MORB pyrolite in the projection from plagioclase(An+Ab) (Fig.14) and are therefore more likely to represent 10kbar partial melts than the reported 10kbar compositions from Takahashi & Kushiro (1983).

The partial melts from HK66 at 8 and 10kbar, although unlike primitive MORB glasses, are very similar in composition to the more Fe-rich MORB T-87 and 395A-8-1-9 which were studied by Kushiro & Thompson (1972) and Fujii et al. (1978) respectively. These two MORB compositions are also plotted in Fig.14. Some of the partial melt compositions from HK66 are identical to the composition T-87 studied by Kushiro & Thompson (1972), leading to the possible conclusion that T-87 and similar Fe-rich MORBs are

primary magmas from a Fe-rich mantle having an olivine of less than Fo_{86}. In this study only MORB glasses with Mg#$\geq$0.68 are considered as candidates for primary magmas. Because of this, only mantle source compositions with olivine compositions of $\geq Fo_{87}$ are suitable for the production of primitive MORB glasses. The range of mantle compositions applicable to the generation of such magnesian MORB are represented by the Ronda and Bullenmerri peridotite suites. However if more Fe-rich mantle is involved in MORB petrogenesis then MORB glasses with Mg#$\leq$0.68 must be considered as potential candidates for primary magmas. Although ocean islands such as Hawaii may require more Fe-rich mantle than MORB (Langmuir & Hanson, 1980; Wilkinson, 1985) evidence for such Fe-rich mantle sources, such as HK66 is lacking in the MORB setting. The investigation of whether more Fe-rich MORBs could be primary magmas is beyond the scope of this paper. However a recent study by Takahashi et al. (1987), using olivine-liquid relationships for MnO, NiO, CoO, MgO and FeO suggests mantle sources as Fe-rich as Fo_{85-87} are involved in MORB petrogenesis. If we accept that MORB source mantle has a composition similar to the MORB pyrolite composition studied, then the Fe-rich MORBs such as T-87 and 395A-8-1-9 can not be regarded as primary magmas, but are fractionation products from a more picritic parent.

1.8.5 Sen (1982)

Sen (1982) studied the melting relationships of a depleted plagioclase and spinel lherzolite 77PAII-1. Unfortunately Sen (1982) determined liquid compositions by direct EMP analysis of glass pools. The erratic behaviour of Na_2O and CaO, as well as the anomalous CaO/Al_2O_3 ratios of the liquid compositions compared to the CaO/Al_2O_3 ratio of 77PAII-1 (see Fig.5b) indicate that the liquids presented by Sen (1982) have suffered some degree of quench modification. Further evidence for the effects of quench modification of Sen's (1982) liquid compositions is seen in the projection from Di (Fig.13). Partial melt compositions define a olivine + orthopyroxene + clinopyroxene + liquid cotectic which is displaced towards the quartz apex, when compared with the 10kbar cotectic from MORB pyrolite. The displacement is larger for the lower temperature compositions, where the effects of quench modification will be most evident. Arrows in Fig. 13 indicate the displacement of equilibrium liquids from a predicted 9kbar cotectic by quench modification to the actual published compositions of Sen (1982).

The liquids from 77PAII-1 have value in establishing the character of melt compositions from depleted compositions at shallow depths. The nature

of such melts from depleted peridotite sources has implications for assessing the role of that second-stage melting processes play in MORB petrogenesis (Duncan & Green, 1987). The glass compositions relative to primitive MORB glasses have high SiO_2 and CaO contents and low TiO_2 and Na_2O contents. The melt compositions are similar in character to those from Tinaquillo lherzolite, which is also a depleted peridotite composition relative to MORB pyrolite.

1.8.6 Fujii and Scarfe (1985)

In Figs. 13 and 14 the glass compositions from equilibrium melting of PMM-1 and PMM-2 are presented (Table 6, Fujii & Scarfe 1985). The liquid compositions define a olivine + orthopyroxene + clinopyroxene + spinel + liquid cotectic at higher normative Di and higher normative Ol in Fig.14 and 13 respectively, than MORB pyrolite. As previously discussed the higher temperature liquid compositions from Fujii & Scarfe (1985) show evidence of Fe-loss, the arrow in Fig. 13 indicates the direction liquid compositions will lie at even higher temperatures than those run by Fujii & Scarfe (1985). As Fe-loss progresses, equilibrium moves away from the olivine apex towards more quartz normative, diopside rich liquids, eventually olivine disappears leaving the liquid in equilibrium with Mg-rich calcic pyroxene ± Mg-rich orthopyroxene. The position of lower temperature liquid compositions, which show no evidence of Fe-loss, define a olivine + orthopyroxene + clinopyroxene + spinel + liquid cotectic plotting in a similar position to the 10kbar cotectic from HK66. As with the HK66 cotectic, the cotectic defined by PMM-1 and PMM-2 is more consistent with a 12-15kbar cotectic. The low temperature liquid compositions from PMM-1 and PMM-2 are unlike primitive MORB glasses, due to their high Al_2O_3, Na_2O and low CaO contents, and low CaO/Na_2O and CaO/Al_2O_3 ratios. Higher temperature liquids have suffered Fe-loss resulting in more CaO-rich liquid compositions, with very high Mg# and low FeO contents. These liquids therefore are not suitable compositions to debate the primary versus evolved character of primitive MORB glasses.

1.9 ARE PRIMITIVE MORB GLASSES PRIMARY MAGMAS AT 10KBAR?

Based on the results of the 10kbar melting study on MORB pyrolite, Tinaquillo lherzolite, Hawaiian pyrolite and KLB-1, primitive MORB glasses with $Mg\# \geq 0.68$ are not primary magmas at 10kbar, nor do most of them lie on olivine control lines from 10kbar olivine + orthopyroxene + clinopyroxene + spinel + liquid cotectics. However primitive MORB glasses with

SiO_2 contents greater than 50 wt% can either be derived from picritic parents or alternatively are primary magmas at depths less than 10kbar. The SiO_2 rich primitive MORB glasses, which are characterized by low olivine normative contents or are quartz normative, have several compositional characteristics that distinguish them from most other primitive MORB glasses. Compared to most other primitive MORB glasses, these SiO_2 rich glasses have higher CaO contents, lower Na_2O and TiO_2 contents and have higher CaO/Al_2O_3 and CaO/Na_2O ratios. They show geochemical affinities to proposed second-stage melts in the oceanic setting (Duncan & Green, 1987; PARTIV).

Second-stage melts result from the remelting of a depleted peridotite diapir at shallow depths (<30km) the diapir having lost a first stage melt fraction at some greater depth. Proposed second stage melt compositions include the upper pillow lavas of the Troodos ophiolite, Cyprus (Cameron, 1985; Duncan & Green, 1987), basalt glass compositions from the Lau back arc basin (Hawkins & Melchior, 1985) and glass inclusions in magnesian olivine (Fo_{94}) phenocrysts from the North Tonga forearc (PARTIV). Although such compositions have so far not been identified amongst MORB suites, they are necessary to explain the existence of calcic plagioclase megacrysts found within MORB (Fisk, 1984; Donaldson & Brown, 1977; Autio & Rhodes, 1984; Stakes et al., 1984; Price et al., 1986). The failure to locate magma batches retaining such refractory compositions may be due to processes such as magma mixing of small volume second-stage melts with dominant and subjacent stage-one picrites (Duncan & Green, 1980).

The 10kbar melts from Tinaquillo lherzolite and 77PAII-1 are similar to those expected of second-stage melts. However in Fig.10 and 14 the primitive MORB glasses with low normative olivine or with normative quartz, plot at higher normative Di contents than liquid compositions from Tinaquillo lherzolite and 77PAII-1. This suggests that these distinctive primitive MORB glass compositions have undergone some degree of olivine fractionation. These glass compositions do not appear to be primary melts but the characteristics of these distinctive primitive MORB glasses demands a source composition more depleted than MORB pyrolite.

1.10 CONCLUSIONS

(1) Primitive MORB glasses with Mg#$\geq$0.68 encompass a large range of silica saturation in CIPW molecular normative projections (Ne to Qz normative) in the 'basalt tetrahedron'.

(2) Previous high pressure liquidus studies on some of these primitive MORB glasses have failed to conclusively demonstrate multiple saturation in olivine + orthopyroxene ± clinopyroxene at any pressure.

(3) Equilibrium partial melts at 10kbar from MORB pyrolite, Hawaiian pyrolite, Tinaquillo lherzolite and the spinel lherzolite KLB-1 form a relatively self consistent data set. The liquid compositions from these four peridotite compositions are all distinctly different from primitive MORB glasses and except for liquid compositions from Hawaiian pyrolite plot below primitive MORB glasses in the projection from plagioclase(An+Ab) in the molecular CIPW normative 'basalt tetrahedron'. This leads to the preferred interpretation that primitive MORB glasses are not primary melts but are fractionated compositions lying on olivine control lines from more picritic parents.

(4) Many bulk compositions used previously in melting studies relevant to MORB petrogenesis, when compared with natural peridotite suites representative of oceanic upper mantle, such as the Ronda peridotite and Lake Bullenmerri lherzolite nodules, are found to have distinct compositional differences from the natural suites and are inappropriate for use in 10kbar melting studies.

(5) Silica contents of primitive MORB glasses show a slight bimodal distribution with most primitive MORB glasses having SiO_2 contents <50 wt%, and a small, but significant number, having SiO_2 contents greater than 51 wt%. These more silica rich glasses have characteristics similar to those expected of second-stage melting of depleted mantle peridotite.

(6) Some previous 10kbar melting studies are shown to have used inappropriate bulk compositions, and have suffered from problems such as quench modification of glasses and Fe-loss.

(7) The experiments of Takahashi & Kushiro (1983) produced liquid compositions unlike primitive MORB glasses but very similar to more Fe-rich MORB. If Fe-rich mantle is involved in the petrogenesis of MORB then such magmas are possible primary melts at low pressures.

(8) The composition of a liquid in equilibrium with olivine + orthopyroxene + clinopyroxene + spinel + plagioclase is unlike primitive MORB glasses at 10kbar. The model of Presnall et al. (1979) involving melting at a 9kbar 'cusp' can not explain the range in composition of primitive MORB glasses.

(9) At pressures between 7-11 kbars liquid compositions from peridotite in the complex system, as opposed to the simple systems (Presnall & Hoover, 1984, 1986), will be too silica rich compared to most primitive MORB glasses. Higher pressures and consequently more MgO-rich parents are required.

PART II

ANHYDROUS PARTIAL MELTING OF PERIDOTITE FROM 8 TO 35KBARS AND THE PETROGENESIS OF MORB

2.1 INTRODUCTION

The nature, composition and depth of origin of primary magmas parental to mid ocean ridge basalts (MORB) is at the present time a subject of controversy (Presnall & Hoover, 1984, 1986; Fujii & Scarfe, 1985; Elthon & Scarfe, 1984; Elthon 1986; Fujii & Bougault, 1983; PART I; Green et al., 1987; Wilkinson, 1982; Thompson, 1987; Basaltic Volcanism Study Project, 1981). A commonly held model is that the more primitive[1] MORB glasses recovered from the ocean floors are close to are or are primary magmas, generated by partial melting of upper mantle peridotite at depths of approximately 30kms (10kbar). This is attributed to a cusp in the peridotite solidus at ~30kms. A second competing model states that the more primitive MORB glasses are not primary magmas but fractionated compositions lying on olivine control lines from more picritic parents which are themselves primary magmas at pressures of 15-25kbars or 30kbars. The former model has been tested by numerous experimental studies via a two-pronged approach of high pressure near liquidus studies of primitive MORB glasses combined with direct partial melting studies of peridotite compositions. The results and interpretations of these experimental studies are the cause of the controversy regarding the primary or nonprimary nature of primitive MORB glasses. High-pressure near liquidus studies of primitive MORB glasses (Bender et al., 1978; Green et al., 1979; Fujii & Scarfe, 1985) have not been successful in demonstrating multiple saturation in olivine + orthopyroxene ± clinopyroxene near the liquidus at any pressure, as expected for possible equilibrium with lherzolite or harzburgite

[1] as measured by higher values of Mg# ($Mg/(Mg + Fe^{2+})$), calculated assuming $Fe^{2+}/(Fe^{2+} + Fe^{3+}) = 0.9$.

residues (see PART I for a more complete discussion). Green et al. (1979) considered the failure of the primitive MORB glass DSDP3-18-7-1 to crystallize orthopyroxene near the liquidus at any pressure, to be evidence for the non-primary nature of primitive MORB glasses. They demonstrated that a more olivine enriched parental composition (DSDP3-18-7-1 + 17wt% olivine) is a possible primary magma at 20kbar in equilibrium with a harzburgite residue.

In the second approach of direct melting studies of peridotite compositions the majority of studies have demonstrated that liquid compositions produced from suitable source compositions are unlike primitive MORB glasses at 10kbar (Stolper, 1980; Elthon & Scarfe, 1984; Fujii & Scarfe, 1985; Takahashi & Kushiro, 1983; Takahashi, 1986; Sen, 1982; PART I; Jaques & Green, 1980). Specifically PART I demonstrated that 10kbar partial melts from four peridotite compositions, Hawaiian and MORB pyrolite, Tinaquillo lherzolite and spinel lherzolite KLB-1, were unlike primitive (Mg#$\geq$0.68) MORB glasses. PART I also discusses previous melting studies highlighting the problems of Fe-loss to noble metal containers, quench modification of primary equilibrium glass compositions and the use of inappropriate bulk compositions as a cause of differences in interpretation over the nature of primary MORB magmas.

The results of PART I leaves a picrite primary magma as the only alternative. However a picrite primary magma is considered unacceptable by many workers for the following reasons;

(1) If a picrite melt model requires extensive olivine fractionation to produce primitive MORB glasses, then based on Ni partitioning data (Hart & Davis, 1978; Sato, 1977), Ni should be depleted to much lower levels than observed in primitive MORB glasses.

(2) Absence of primitive MORB glasses of picritic compositions.

(3) Absence of abundant cumulate rocks of dunitic composition from dredge hauls of oceanic ridges and fracture zones. Most commonly, ultramafic rocks consist of lherzolite and gabbroic material.

(4) The failure to date of any experimentally produced picrite composition to yield MORB like compositions when subjected to olivine fractionation calculations.

(5) For many workers, the consistent observation of olivine tholeiites and quartz tholeiites over the sampled areas of the entire 66,000 km ridge system is compelling evidence that these and not the rare or absent picrite lavas, must be primary magmas.

In this PART we present the results of a partial melting study on a MORB pyrolite composition, suitable for the production of primary MORB magmas, from pressures of 8 to 35kbars and from a slightly more depleted composition, Tinaquillo lherzolite, at pressures of 15 and 20kbars. The partial melts were determined using a peridotite-basalt 'sandwich' technique. In experiments using MORB pyrolite the primitive MORB glass DSDP3-18-7-1 (Table 7, no.4) was used as the basalt in the sandwich, in the case of Tinaquillo lherzolite a calculated liquid from Jaques & Green (1980) was used (Table 7, no.5).

The results of the melting study are used to determine the range in composition, and depth of origin of possible picritic primary magmas parental to primitive MORB glasses and eventually more typical MORB compositions. The results of this study demonstrate that highly MgO-rich (>17 wt%) picrites are only one end member of a spectrum of primary magmas which range to more basaltic primary magmas of 10-11 wt% MgO.

2.2 EXPERIMENTAL APPROACH AND TECHNIQUE

The MORB pyrolite composition chosen for study is that calculated by Green et al. (1979), based on combining 24 wt% of the picrite composition (DSDP3-18-7-1 + 17wt% olivine, mix E, Green et al., 1979) which was experimentally demonstrated to be in equilibrium with olivine and orthopyroxene at 20kbar, 1430°C, indicating possible equilibrium with a harzburgite residue. Two pyrolite compositions were used (Table 7, no.1 and 2 respectively) designated MPY-87 and MPY-90-40. MPY-90-40 is the MORB pyrolite composition of Green et al. (1979) minus 40 wt% olivine ($Fo_{91.6}$) and MPY-87 is a result of recalculating the MORB pyrolite composition from a Mg# of 90 to 87 to produce a more Fe-rich pyrolite composition (cf. Wilkinson, 1982). The Tinaquillo lherzolite composition studied (TQ-40, Table 7, no.3) has also been modified by subtraction of 40 wt% olivine. All three compositions were studied at 10kbars in PART I. The subtraction of olivine from the lherzolite compositions will not affect phase relations or phase compositions except in Mg, Fe and Ni concentration so long as olivine is a residual phase. The purpose of subtracting olivine is to increase the modal abundance of pyroxene, spinel and melt present in the experimental runs.

Table 7

Starting compositions used in partial melting experiments

	1	2	3	4	5
SiO_2	44.32	47.15	47.50	49.70	49.16
TiO_2	0.16	0.28	0.13	0.72	0.52
Al_2O_3	4.33	7.28	5.35	16.40	14.32
FeO	9.82	7.27	7.51	7.90	11.06
MnO	0.10	0.12	0.18	0.12	-
MgO	36.84	30.57	32.80	10.10	14.49
CaO	3.34	5.63	4.97	13.10	10.80
Na_2O	0.39	0.66	0.30	2.00	1.37
K_2O	0.00	0.00	0.03	0.00	-
P_2O_5	0.00	0.00	0.02	0.00	-
Cr_2O_3	0.44	0.75	0.75	0.07	-
NiO	0.25	0.29	0.43	0.03	-
Total	99.99	100.00	99.97	100.14	99.72
Mg#	0.87	0.88	0.89	0.69	0.70
CIPW norm (molecular)					
Ab	2.14	3.97	1.79	15.09	9.70
An	6.16	11.33	8.73	30.07	25.97
Di	3.98	7.39	7.54	24.56	16.29
Hy	13.20	22.22	27.97	12.10	13.66
Ol	72.52	52.56	51.69	14.69	31.26
CaO/Al_2O_3	0.77	0.77	0.93	0.79	0.75
CaO/Na_2O	8.56	8.53	16.56	6.55	7.88
CaO/TiO_2	20.87	20.11	38.23	18.19	20.77
Al_2O_3/TiO_2	27.06	26.00	41.15	22.77	27.54

(1) MORB pyrolite composition MPY-87.

(2) MORB pyrolite composition MPY-90-40 (MPY-90 minus 40 wt%. olivine $Mg_{91.6}Fe_{8.1}Ni_{0.2}Mn_{0.1}$).

(3) TQ-40 (Tinaquillo lherzolite minus 40 wt% olivine $Mg_{91.9}Fe_{8.0}Mn_{0.1}$).

4) Primitive MORB glass DSDP3-18-7-1 (Green et al., 1979).

5) Jaques & Green (1980) calculated melt composition from Tinaquillo lherzolite, 15kbar, 1350°C. Composition given is the mix composition as determined by broad beam electron microprobe analysis.

Mg# calculated on basis of total iron as FeO. CIPW norm calculated on basis of $Fe^{2+}/(Fe^{2+}+ Fe^{3+})=0.9$, (-) below detection limit.

Both Tinaquillo lherzolite and MORB pyrolite compositions are suitable source compositions for generating primary MORB magmas by partial melting based on a comparison with natural peridotite suites (Frey et al., 1985; Nickel & Green, 1984; PART I). The aim of this study is to test the ability of these two compositions to produce primary picritic or basaltic MORB magmas i.e. a detailed matching of observed equilibrium melts with natural MORB.

The basalt-peridotite 'sandwich' technique has been used successfully in a number of previous studies to determine equilibrium partial melt compositions (Stolper, 1980; Takahashi & Kushiro, 1983; Fujii & Scarfe, 1985; PART I). Potential problems associated with the 'sandwich' technique have been discussed and evaluated in PART I. In the 'sandwich' technique a layer of basalt is placed in between layers of peridotite and allowed to equilibrate with the peridotite and its partial melt at a desired pressure and temperature. This provides a large area of glass to be analysed at the end of the run and avoids the problem of quench modification of primary liquids.

All the starting mixes used (Table 7) were made up by sintering high purity oxides, crushed in acetone and fired at 1000°C. Fayalite was then added to the mixes before refiring in a silica evacuated tube at 1000°C. The mixes were stored in an oven at 110°C. The mixes were loaded into graphite capsules and sealed in an outer platinum capsule. In some experiments an outer platinum capsule was not used; no differences were observed between liquid compositions run in unsealed or sealed capsules. Two sizes of graphite capsules were used; in the large bore graphite capsule, a layer of DSDP3-18-7-1 mix was loaded between layers of MORB pyrolite. In the small bore graphite capsules only two layers were used:the basalt layer forming the bottom layer (DSDP3-18-7-1 or Jaques & Green, 1980 calculated liquid in the case of Tinaquillo lherzolite).

All experiments were carried out in a high pressure piston cylinder apparatus at the University of Tasmania, using a piston-in technique with a pressure correction of minus 10% nominal piston pressure. A 0.5 inch diameter, talc-pyrex assembly was used with a graphite heater. A pure alumina thermocouple sheath was used, with sintered alumina components surrounding the capsule. The thermocouple sheath enters the assembly through a mullite sleeve. The bottom spacer is fired pyrophyllite (mullite and silica).

Both $Pt/Pt_{90}Rh_{10}$ and $W_{75}Re_{25}/W_{97}Re_3$ thermocouples were used in the course of the experimental study. Thermocouple drift was experienced on long runs when using the $Pt/Pt_{90}Rh_{10}$ thermocouple (see also PART I). The $W_{75}Re_{25}/W_{97}Re_3$ thermocouples were controlled by a Kent P96M controller, temperatures being accurate to $\pm$ 1°C.

At the end of the run the sample was removed from the graphite capsule and sectioned longitudinally for microprobe analysis. All analyses were done at the University of Tasmania on a JEOL JX 50A electron microprobe-scanning electron microscope, fitted with an energy dispersive EDAX analytical system (operating conditions 15kv, $7x10^{-10}$A), calibration was on pure Cu. Back scattered electron photographs were taken of all run products to check on the compositional uniformity of all the phases (Phillips 505 SEM, operating conditions 20kv, spot size 100 ηm).

2.3 EXPERIMENTAL RESULTS

Details of the experimental runs are given in Table 8. The compositions of equilibrium partial melts produced in the experiments are given in Tables 9 and 10. The compositions of the partial melts are plotted in the CIPW molecular normative basalt tetrahedron in Fig.17 and 18 and compared with primitive MORB glasses. Representative residual phase compositions are given in Appendix 1.

2.3.1 Attainment of equilibrium

In runs at 8, 12, 15 and 18kbar the basalt layer was quenched as a coherent glass layer (100-300μm) between or on top of the peridotite layer(s) which consist of crystals and glass. In runs close to the solidus abundant clinopyroxene crystallization occurred within the glass layer, in these cases the glass composition was obtained by analysing large pools of glass (50-70μm).

In runs at higher pressure (20, 25, 30 and 35kbar) the basalt layer quenched to clinopyroxene and glass (Fig.15), the quench clinopyroxene becoming coarser with pressure. In these cases equilibrium partial melt compositions were determined by large broad beam area scans of the quench pyroxene and glass. In cases where the resulting broad beam area scan analyses were all uniform in composition, the liquid compositions were determined by averaging the area scans. In cases where a range in composition of the area scans was obtained, the area scans were observed to

Table 8

Experimental run details of 'sandwich' experiments on MORB pyrolite and Tinaquillo lherzolite compositions

Run no.	P (Kbars)	T (°C)	Time (hrs)	Capsule type	Capsule	Peridotite	wt % basalt	Phases present
T-1516	8	1350	24	B	Pt/C	MPY-87	4.7	Ol + Cpx + Opx + L
T-1512	8	1400	24	B	Pt/C	MPY-87	6.25	Ol + Opx + L
T-1479	12	1450	12	B	Pt/C	MPY-87	9.5	Ol + Opx + L
T-1994	12	1375	6.5	B	C	MPY-90-40	9.9	Ol + Opx + Cpx + L
T-2189	12	1400	21	A	Pt/C	MPY-90-40	20	Ol + Opx + L
T-1989	15	1360	6.5	B	C	MPY-90-40	11.1	Ol + Opx + Cpx + Sp + L
T-1999	15	1420	3	B	C	MPY-90-40	14.1	Ol + Opx + Cpx + L
T-2192	15	1450	20	A	Pt/C	MPY-90-40	24	Ol + Opx + L
T-2056	15	1450	24	A	Pt/C	TQ-40	23	Ol + Opx + L
T-2029	18	1370	26	A	C	MPY-90-40	6.25	Ol + Opx + Cpx + Sp + L
T-2031	18	1450	42.5	A	C	MPY-90-40	10.39	Ol + Opx + Cpx + Sp + L
T-2069	20	1500	24	A	Pt/C	TQ-40	26	Ol + Opx + L
T-1515	20	1420	24	B	Pt/C	MPY-87	5	Ol + Opx + Cpx + Sp + L
T-1501	20	1430	24	B	Pt/C	MPY-87	10	Ol + Opx + Cpx + Sp + L
T-1513	20	1450	1.2	B	Pt/C	MPY-87	10	Ol + Opx + Cpx + Sp + L
T-1499	20	1475	1.0	B	Pt/C	MPY-87	9.4	Ol + Opx + L
T-2207	20	1500	16	A	Pt/C	MPY-87	12	Ol + Opx + L
T-2086	25	1550	24	A	Pt/C	MPY-90-40	21	Ol + Opx + Cpx + L
T-2065	30	1600	23	A	Pt/C	MPY-90-40	16	Ol + Opx + Cpx + L
T-2075	30	1620	6	A	Pt/C	MPY-90-40	23	Ol + Opx + L
T-2087	35	1600	24.5	A	Pt/C	MPY-90-40	9	Ol + Opx + Cpx + Ga + L

A and B refer to small and large bore graphite capsules respectively.
Pt = platinum, C = graphite, Ol = olivine, Opx = orthopyroxene, Cpx = clinopyroxene, Sp = spinel, Ga = garnet, L = liquid (glass).

Table 9

Equilibrium partial melt compositions from MORB pyrolite (MPY-87) and Tinaquillo lherzolite

	MPY-87								Tinaquillo	
	1	2	3	4	5	6	7	8	9	10
Pressure (kbars)	8	8	12	20	20	20	20	20	15	20
SiO_2	51.09	52.63	49.64	47.03	46.94	47.52	47.39	48.75	48.97	47.52
TiO_2	0.65	0.58	0.59	1.00	0.70	0.73	0.60	0.53	0.42	0.52
Al_2O_3	16.26	14.50	14.34	16.62	15.44	14.39	14.26	11.97	13.77	12.96
FeO	7.32	7.39	8.58	9.67	9.83	9.62	9.44	9.71	6.87	8.29
MgO	10.25	11.68	13.83	12.99	14.24	14.51	15.46	17.67	15.52	17.17
CaO	12.16	11.14	11.10	9.93	10.53	10.98	10.94	9.56	12.98	12.09
Na_2O	1.91	1.66	1.65	2.63	2.30	1.84	1.60	1.36	1.07	1.03
K_2O	-	-	-	0.12	-	-	-	-	-	-
Cr_2O_3	0.35	0.41	0.59	-	0.20	0.38	0.28	0.53	0.36	0.39
Total	99.99	99.99	100.32	99.99	100.18	99.97	99.97	100.08	99.96	99.97
Mg#	0.71	0.74	0.74	0.71	0.72	0.73	0.74	0.78	0.80	0.79
CIPW norm (molecular)										
Qz	0.00	7.65	0.00	0.00	0.00	0.00	0.00	0.00	0.00	0.00
Ne	0.00	0.00	0.00	1.81	1.06	0.00	0.00	0.00	0.00	0.00
Ab	14.84	12.08	12.04	16.37	14.66	12.84	11.10	9.47	7.66	7.09
An	31.00	26.05	25.79	25.56	24.23	24.11	24.53	20.60	26.13	23.58
Di	21.24	18.78	18.19	12.37	15.56	18.24	17.43	16.18	25.21	22.43
Hy	26.63	32.04	21.45	0.00	0.00	6.97	8.86	22.20	16.85	11.74
Ol	2.55	0.00	18.29	39.23	40.90	33.88	34.66	28.66	21.40	31.99
CaO/Al_2O_3	0.75	0.76	0.77	0.60	0.68	0.76	0.77	0.79	0.94	0.93
CaO/Na_2O	6.36	6.71	6.73	3.77	4.58	5.97	6.84	7.03	12.13	11.74
CaO/TiO_2	18.71	19.21	18.81	9.93	15.04	15.04	18.23	18.04	30.90	23.25
Al_2O_3/TiO_2	25.01	25.00	24.30	16.62	22.06	19.71	23.77	22.58	32.78	24.92
PM %	27.0	30.0	28.0	12.0	17.0	24.0	28.0	36.0	17.0	17.0
Residue	L	H	H	L	L	L	H	H	H	H
Temp (°C)	1350	1400	1450	1420	1430	1450	1475	1500	1450	1500

L = lherzolite residue, H =harzburgite residue.
Mg# calculated on the basis of total iron as FeO, CIPW norm calculated on the basis of $Fe^{2+}/(Fe^{2+}+Fe^{3+})=0.9$, (-) below detection limit, MnO contents all below detection limit.

Table 10

Equilibrium partial melt compositions from MORB pyrolite (MPY-90-40)

	1	2	3	4	5	6	7	8	9	10	11
Pressure (kbars)	12	12	15	15	15	18	18	25	30	30	35
SiO_2	49.86	50.09	50.50	49.11	49.19	47.78	47.88	46.86	46.72	46.99	45.83
TiO_2	0.69	0.59	0.82	0.69	0.59	1.52	0.66	0.66	0.55	0.50	1.08
Al_2O_3	17.18	15.00	18.00	15.88	14.58	17.31	15.16	13.73	12.71	12.21	11.70
FeO	6.74	7.13	7.00	7.38	7.36	9.03	8.12	8.06	8.40	8.09	9.04
MgO	11.13	13.04	10.00	12.97	14.42	10.89	14.58	17.75	19.31	20.23	19.99
CaO	11.96	12.14	9.60	11.69	11.79	9.45	11.64	10.92	10.60	10.12	10.66
Na_2O	2.06	1.63	3.50	1.87	1.67	3.66	1.56	1.60	1.19	1.31	1.36
K_2O	-	-	-	-	-	0.14	-	-	-	-	-
Cr_2O_3	0.34	0.35	0.82	0.37	0.38	-	0.36	0.38	0.51	0.52	0.42
Total	99.96	99.97	100.24	99.96	99.98	99.78	99.96	99.96	99.99	99.97	100.08
Mg#	0.75	0.77	0.72	0.76	0.78	0.68	0.77	0.79	0.80	0.82	0.80
CIPW norm (molecular)											
Ne	0.00	0.00	0.00	0.00	0.00	5.86	0.00	0.00	0.00	0.00	0.00
Ab	15.50	12.09	26.02	13.63	11.99	19.58	11.04	10.71	7.90	8.61	8.78
An	31.55	27.78	27.67	28.38	25.82	23.54	27.11	22.57	21.71	20.09	18.57
Di	18.19	21.99	11.78	18.73	20.95	12.77	18.44	17.81	17.20	16.67	19.46
Hy	16.40	21.06	5.64	13.96	14.71	0.00	10.78	3.32	8.64	8.40	0.97
Ol	14.70	13.71	25.40	21.63	23.19	32.17	29.05	42.20	41.23	43.12	48.25
CaO/Al_2O_3	0.69	0.81	0.53	0.74	0.81	0.54	0.77	0.79	0.83	0.83	0.91
CaO/Na_2O	5.80	7.45	2.74	6.25	7.06	2.58	7.46	6.82	8.90	7.70	7.84
CaO/TiO_2	17.73	20.57	11.71	16.94	19.98	6.22	17.64	16.54	19.27	20.24	9.87
Al_2O_3/TiO_2	24.90	25.42	21.95	23.01	24.71	11.39	22.97	20.80	23.19	24.42	10.83
PM %	23.0	30.0	5.0	25.0	28.0	10.0	22.0	27.0	33.0	37.0	15.0
Residue	L	H	L	L	H	L	L	L	L	H	GL
Temp (^oC)	1375	1400	1360	1420	1450	1370	1450	1550	1600	1620	1600

L -lherzolite residue, H -harzburgite residue, GL -garnet lherzolite residue.
Mg# calculated on the basis of total iron as FeO, CIPW norm calculated on basis of $Fe^{2+}/(Fe^{2+}+Fe^{3+})=0.9$, (-) below detection limit, MnO contents all below detection limit.

Figure 15.

Back scattered electron image photograph for run no. T-1513. Light grey is quench clinopyroxene plus quenched modified glass, dark grey is primary clinopyroxene. Scale bar is 100um.

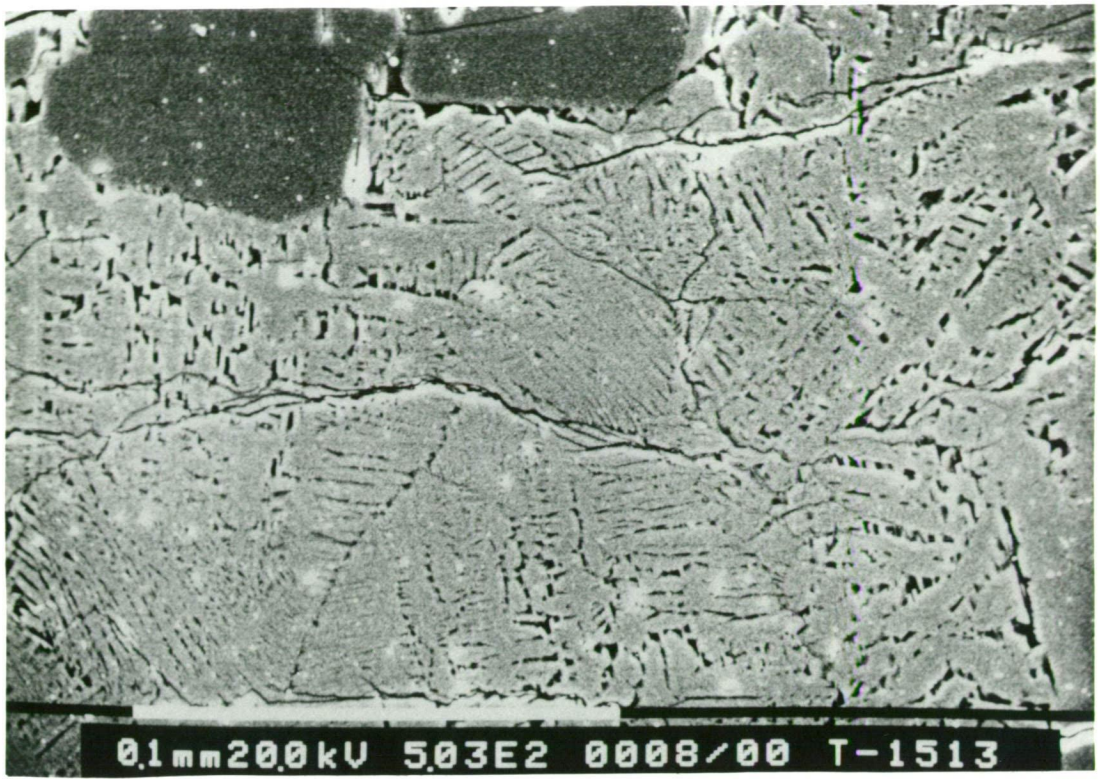
0.1mm20.0kV 5.03E2 0008/00 T-1513

display good linear relationships when major oxides were plotted against Mg# (Fig.16). This linear relationship is due to different proportions of pyroxene and quench modified glass in the area scans. The liquid compositions were determined by first calculating the equilibrium Mg# of the liquid in equilibrium with the olivine composition in the run based on the $(Kd)^{ol/liq}_{Fe/Mg}$ determined by Takahashi & Kushiro (1983) for graphite capsules and secondly reading off the major element composition of the liquid from the major oxide versus Mg# plots. An example is given for run T-1501 in Fig.16.

Due to the nature of the sandwich technique modal homogeneity is not produced during the experiment, and although the melt phase is distributed throughout the charge, being in contact with all grain boundaries, the melt is concentrated in one layer. Due to the presence of this glass layer crystal growth is enhanced resulting in much larger and more abundant clinopyroxene and orthopyroxene crystals near the glass/peridotite (now crystals + glass) contact. All phases near or in the glass layer were found to be compositionally uniform from core to rim even for short run times. However phases away from the glass layer were not compositionally uniform from core to rim. Rim compositions were identical to the cores and rims of phases close to the glass layer, while cores were of a different composition. As a result of this zoning in crystals removed from the glass layer, bulk equilibrium was not achieved during the length of even the longest runs, however local equilibrium was achieved between the glass composition and residual crystals near the glass layer and rims of crystals away from the glass layer. Equilibrium is also confirmed by comparing the glass compositions in short runs to compositions in long runs, differences are all within analytical uncertainity (see also PART I).

2.4 EQUILIBRIUM GLASS COMPOSITIONS

2.4.1 MORB pyrolite

In the projection from Di (Fig.17) onto the base of the basalt tetrahedron, liquid compositions from MORB pyrolite define olivine + orthopyroxene + clinopyroxene + liquid and olivine + orthopyroxene + liquid cotectics from 8 to 35kbars. The cotectics moving systematically with pressure towards the olivine apex. The movement of the cotectics with pressure is a consequence of the contraction of the olivine phase volume as predicted by O'Hara (1965). As pressure increases, for a given degree of partial melting, SiO_2 contents fall and melts become more FeO and MgO rich.

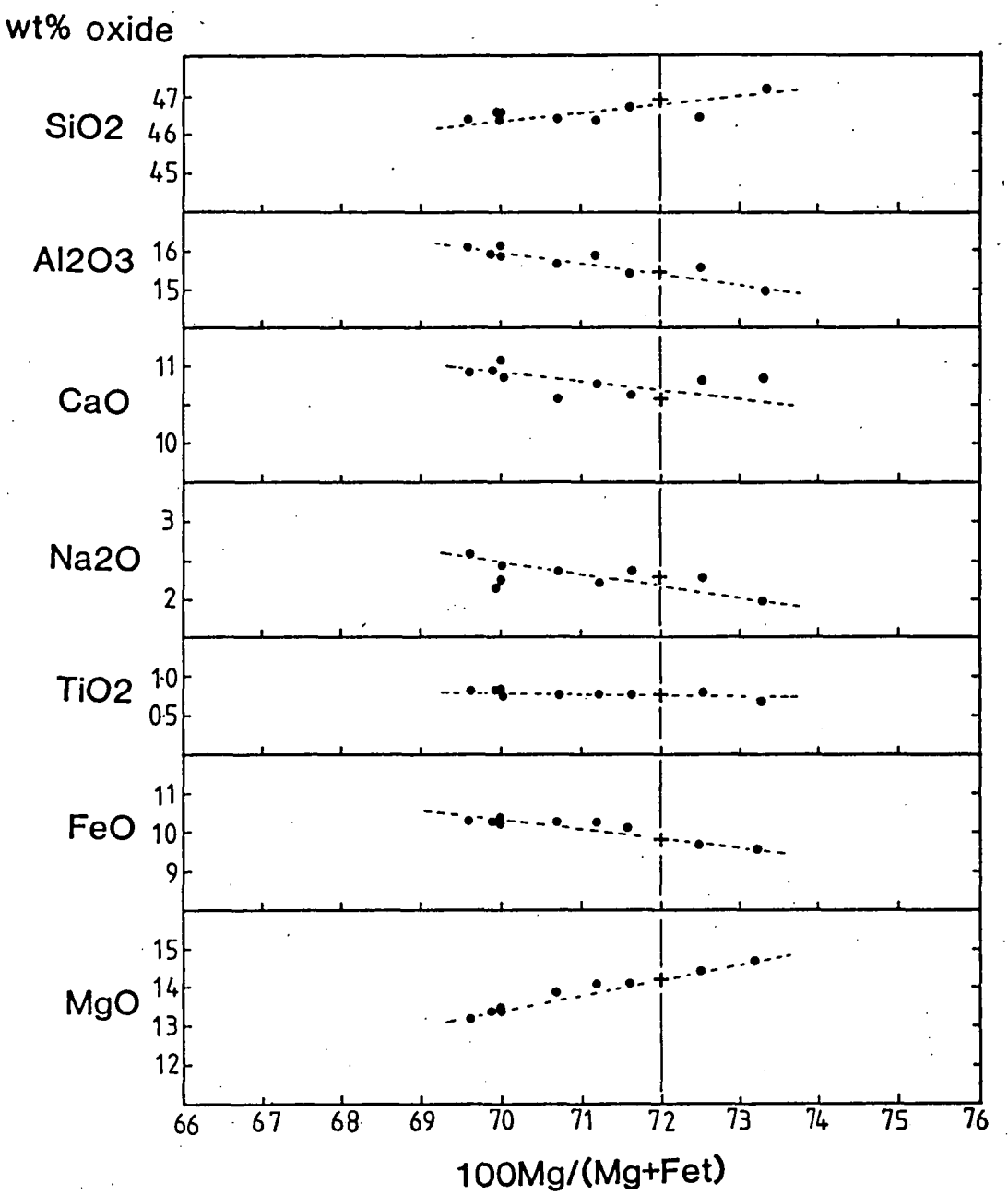

Figure 16.

Major element oxides SiO_2, Al_2O_3, CaO, Na_2O, TiO_2, FeO^t and MgO versus $100Mg/(Mg + Fe^t)$ for broad beam area scan analyses of the 'basalt' layer in run no. T-1501,
thin line indicates the equilibrium $100Mg/(Mg + Fe^t)$ ratio of a liquid composition in equilibrium with the olivine composition of the charge, based on the relationship of Takahashi & Kushiro (1983),
(●) individual broad beam area scans,
(+) calculated equilibrium partial melt composition.

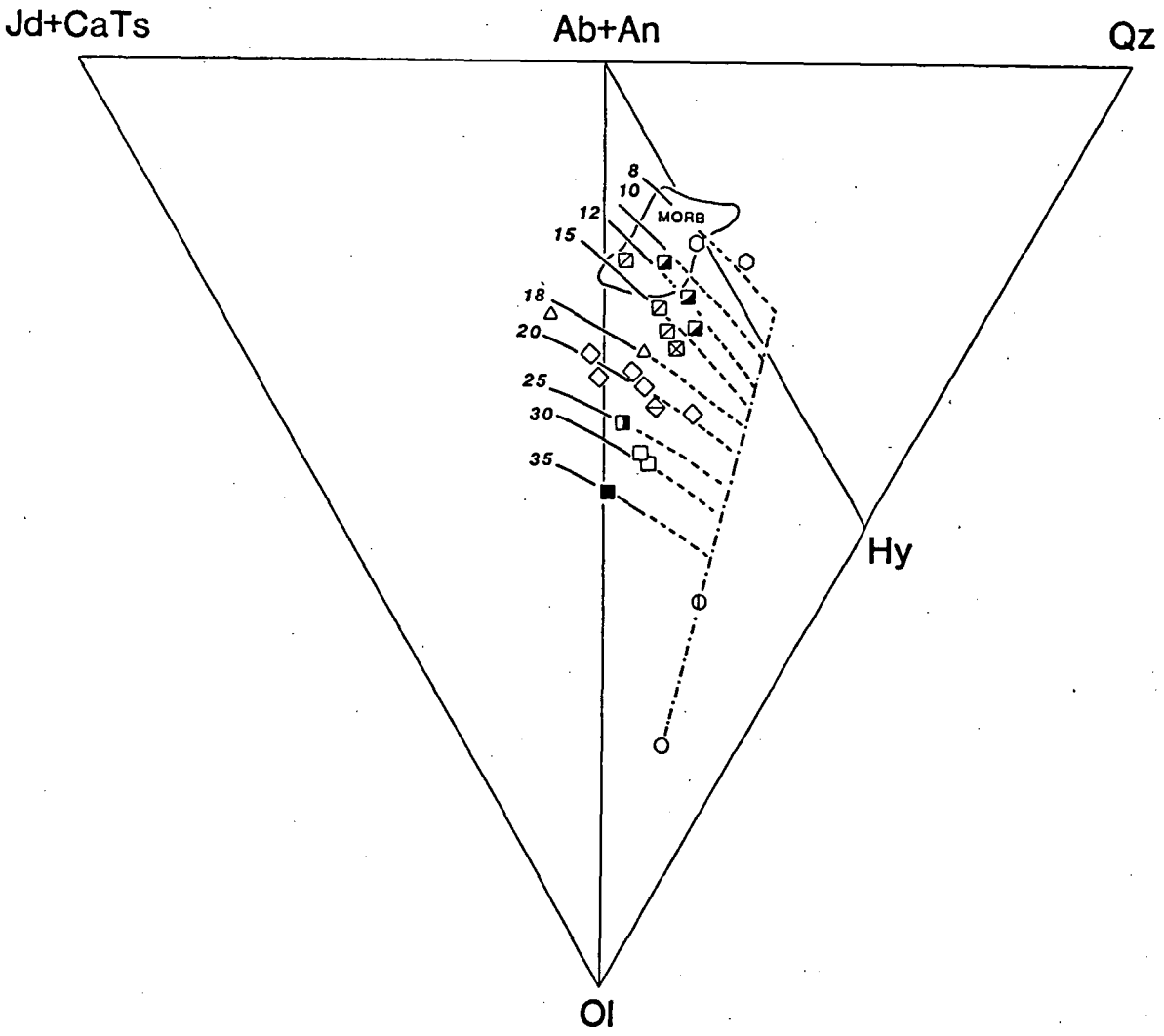

Figure 17.

Equilibrium partial melt compositions from MORB pyrolite and Tinquillo lherzolite plotted in the CIPW molecular normative basalt tetrahedron, projected from diopside (Di) onto the base jadeite plus calcium tschermak's molecular (Jd + CaTs)-quartz (Qz)- olivine (Ol), 10kbar cotectic from PART I. MORB encloses field of primitive MORB glasses, references see caption to Fig.22.

(○) MORB pyrolite (MPY-87),

(⊕) MORB pyrolite minus 40 wt% olivine (MPY-90-40),

The following symbols represent partial melt compositions at the indicated pressures (kbars):

(○) 8, (◪) 12, (▨) 15, (⊠ , Tinaquillo) 15, (△) 18, (◈ ,Tinaquillo) 20, (◇) 20, (◨) 25, (□) 30, (■) 35,

—·—·—·— locus of liquids in equilibrium with olivine.

– – – – – locus of liquids in equilibrium with olivine + orthopyroxene.

———— locus of liquids in equilibrium with olivine + orthopyroxene + clinopyroxene ± spinel.

Al_2O_3 contents of equilibrium liquids, for a given degree of partial melting, decrease due to the increasing Al_2O_3 contents of residual pyroxenes with pressure. This results in CaO/Al_2O_3 ratios greater than the bulk CaO/Al_2O_3 ratio of MORB pyrolite. Residual clinopyroxene becomes less calcic with increasing temperature at higher pressure, due to the narrrowing of the pyroxene solvus, such that the CaO contents of liquids at the point of elimination of clinopyroxene become less calcic with increasing pressure.

The systematic movement of olivine + orthopyroxene + clinopyroxene + liquid and olivine + orthopyroxene + liquid cotectics towards the olivine apex with pressure is less obvious in the projection from plagioclase (Ab+An) (Fig.18) as the cotectics tend to be projected one on top of each other as a consequence of the three-dimensional relationships within the basalt tetrahedron. As the cotectics all form a slight angle to the join Jd + CaTs-Qz of the basalt tetrahedron (Fig.17), when a projection from plagioclase (Ab + An) is taken, the cotectics plot one on top of the other. This emphasizes the importance of looking at least two different projections to establish the three-dimensional relationships between different compositions. In the projection from Di, primitive MORB glasses overly ~5 to ~16 kbar cotectics, however in the projection from plagioclase (Ab+An) primitive MORB glasses plot above these cotectics. Although this indicates that primitive MORB glasses are not primary magmas, some of the glasses characterized by low normative Di in the projection from plagioclase (Ab+An) plot close to the cotectics indicating that possibly only small to moderate amounts of olivine fractionation is required to move equilibrium partial melt compositions into the field of primitive MORB glasses. This possibility will be discussed in another section of this PART.

2.4.2 Tinaquillo lherzolite

Equilibrium partial melts from sandwich experiments on Tinaquillo lherzolite at 15 and 20kbar are also plotted in Figs.17 and 18. The 15 and 20kbar liquids are consistent with the 15 and 20kbar cotectics determined for MORB pyrolite. Although the 15 and 20kbar cotectics for Tinaquillo lherzolite and MORB pyrolite overlie each other in Fig.17, liquid compositions are distinctly different. The liquid compositions from Tinaquillo lherzolite compared to MORB pyrolite have higher CaO contents, lower Al_2O_3, Na_2O and TiO_2 contents, and have higher CaO/Al_2O_3 and CaO/Na_2O ratios.

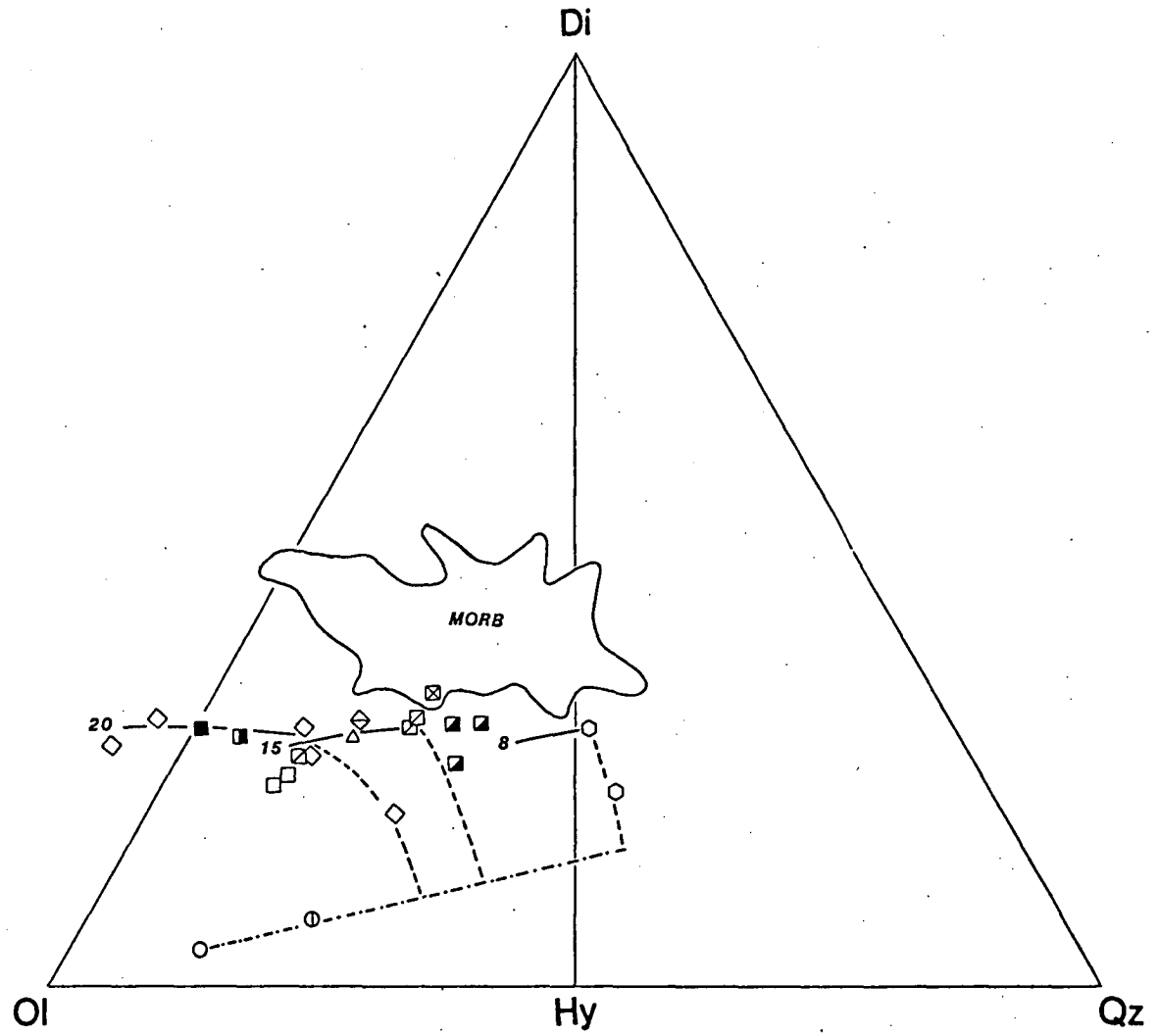

Figure 18.

Equilibrium partial melt compositions from MORB pyrolite and Tinaquillo lherzolite plotted in the CIPW molecular normative basalt tetrahedron, projected from plagioclase (Ab + An) onto the face diopside (Di)-olivine (Ol)-quartz (Qz). Symbols and cotectic lines as for Fig.17.

2.5 COMPARISON WITH PREVIOUS EXPERIMENTAL STUDIES

In this section equilibrium partial melt compositions from MORB pyrolite are compared with liquid compositions produced in previous high pressure experimental studies of peridotite melting and other relevant experimental studies on MORB petrogenesis. For this comparison, the projection from Di in the basalt tetrahedron is used as the movement of olivine + orthopyroxene ± clinopyroxene + liquid cotectics with pressure is well defined. The aim of this section is to emphasize the consistency in projected position of olivine + orthopyroxene ± clinopyroxene + liquid cotectics and the movement of these cotectics with pressure despite differences in peridotite bulk compositions in the projection from Di. Although equilibrium partial melts reflect the respective bulk compositions, cotectics at a particular pressure will overly or plot close to one another in the basalt tetrahedron when projected from Di (Fig.19) for a range of different peridotite bulk compositions. A detailed comparison of equilibrium partial melt compositions at 10kbar is reported in PART I.

2.5.1 Jaques & Green (1980)

Jaques & Green (1980) calculated equilibrium partial melts from Tinaquillo lherzolite and Hawaiian pyrolite at 2, 5, 10 and 15kbars. Equilibrium partial melt compositions were determined by chemical analysis of all residual phases combined with complete modal analysis of the charge, taking into account the effect of Fe-loss. Liquid compositions were calculated by mass balance. Falloon et al. (1987) have extended the study of Jaques & Green (1980) to 20 and 30kbars, using the approach of Jaques & Green (1980) combined with 'sandwich' reversal experiments using a calculated liquid composition as the basalt in the 'sandwich'. The results of the reversal experiments demonstrate that most calculated liquid compositions of Jaques & Green (1980) are too olivine normative, the equilibrium liquids being more silica saturated than calculated by Jaques & Green (1980) (Falloon et al., 1987).

In Fig.19 equilibrium liquid cotectics from MORB pyrolite, Hawaiian pyrolite and Tinaquillo lherzolite are plotted. Despite three different peridotite compositions and correspondingly different equilibrium liquid compositions, liquid compositions can be used to define a single 'average' cotectic in the projection from Di (Fig.19) for pressures from 5 to 30kbars. In the projection from plagioclase (Ab + An) however equilibrium

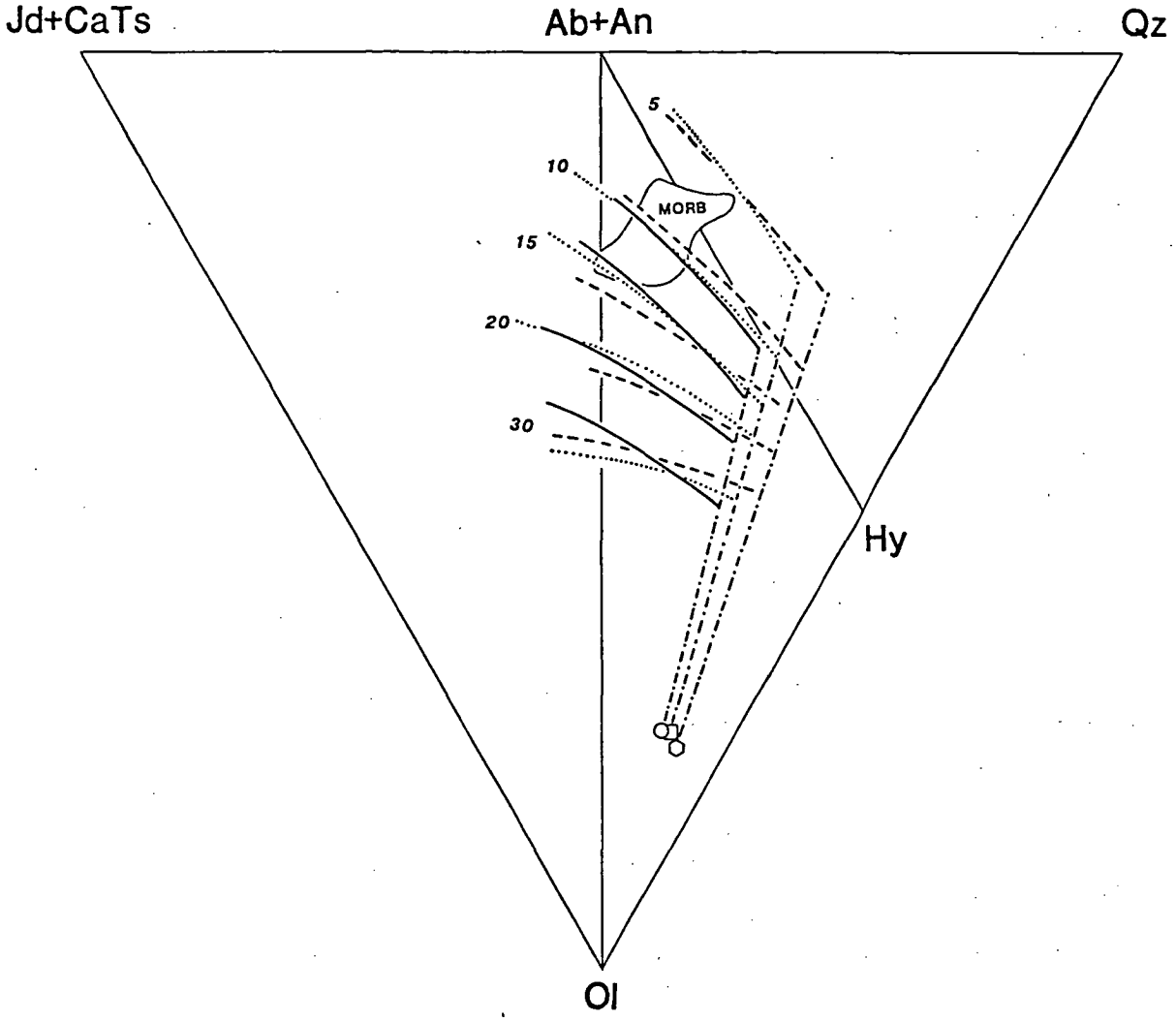

Figure 19.

Cotectics defined by partial melt compositions from MORB pyrolite (this study and PART I), Hawaiian pyrolite and Tinaquillo lherzolite (Jaques & Green, 1980; Falloon et al., 1987) at 5, 10, 15, 20 and 30kbars under anhydrous conditions as seen in the projection from diopside (Di) onto the base of the CIPW molecular normative basalt tetrahedron jadeite plus calcium tschermak's molecule (Jd + CaTs)-quartz (Qz)-olivine (Ol). MORB field as for Fig.17.

(○) MORB pyrolite.

(□) Hawaiian pyrolite.

(⬡) Tinaquillo lherzolite.

—·—·—·— locus of liquids in equilibrium with olivine only.

———— locus of liquids in equilibrium with olivine + orthopyroxene ± clinopyroxene ± spinel for MORB pyrolite.

..... locus of liquids in equilibrium with olivine + orthopyroxene ± clinopyroxene ± spinel for Hawaiian pyrolite.

– – – – – – locus of liquids in equilibrium with olivine + orthopyroxene ± clinopyroxene ± spinel for Tinaquillo lherzolite.

liquids do not define a unique 'average' cotectic , as Hawaiian pyrolite liquids define a olivine + orthopyroxene + clinopyroxene + liquid cotectic at significantly higher normative Di contents than MORB pyrolite and Tinaquillo lherzolite. The results of this study and that of Falloon et al. (1987) and PART I provide an internally consistent data set for peridotite melting from 5 to 35kbars. The cotectics from MORB pyrolite will be used as a point of reference when discussing the following experimental studies.

2.5.2 Takahashi & Kushiro (1983)

Takahashi & Kushiro (1983) determined equilibrium partial melts in equilibrium with olivine + orthopyroxene ± clinopyroxene + liquid by the 'sandwich' technique using the fertile, Fe-rich spinel lherzolite HK66 and a diverse range of basalt compositions (MORB tholeiite, alkali basalt, boninite, picrite). Equilibrium liquid compositions from HK66 are plotted in Fig.20. Equilibrium liquids define olivine + orthopyroxene + clinopyroxene + liquid and olivine + orthopyroxene + liquid cotectics at 5, 8, 10, 15, 20, 25, 30 and 35kbars. There is a problem with 25kbar liquid compositions from HK66 which plot with the 20kbar liquids in the projection from Di. The cotectics from HK66 overlie liquid compositions for MORB pyrolite, Hawaiian pyrolite and Tinaquillo lherzolite at 5, 15, 20, 30 and 35kbars. This result strongly suggests these cotectics at these pressures are correctly located in the projection from Di. The only inconsistencies are the 8 and 10kbar cotectics from HK66 which, particularly at the lower temperature ends, overlie 10 and 12kbar cotectics respectively from the other three peridotite compositions. In view of the internal consistency of liquid compositions between MORB, Hawaiian pyrolite, and Tinaquillo lherzolite and the liquid cotectics at 5, 15, 20, 30 and 35kbars from HK66, the regular spacing and movement of cotectics with pressure towards the Ol-Jd + CaTs join in the Di projection, all suggest that the 8 and 10kbar cotectics from HK66 are possibly incorrectly located in the Di projection. This could be due to possible small differences in pressure calibration with the piston-cylinder apparatus.

2.5.3 Takahashi (1986)

Takahashi (1986) published partial melt compositions from spinel lherzolite KLB-1 from 10 to 140kbars. Most liquid compositions reported by Takahashi (1986) are in equilibrium with olivine only, except for liquids at 10 and 30kbar. The 30kbar liquid from KLB-1 published by Takahashi (1986) and the 10kbar liquid from KLB-1 determined in PART I overlie and are

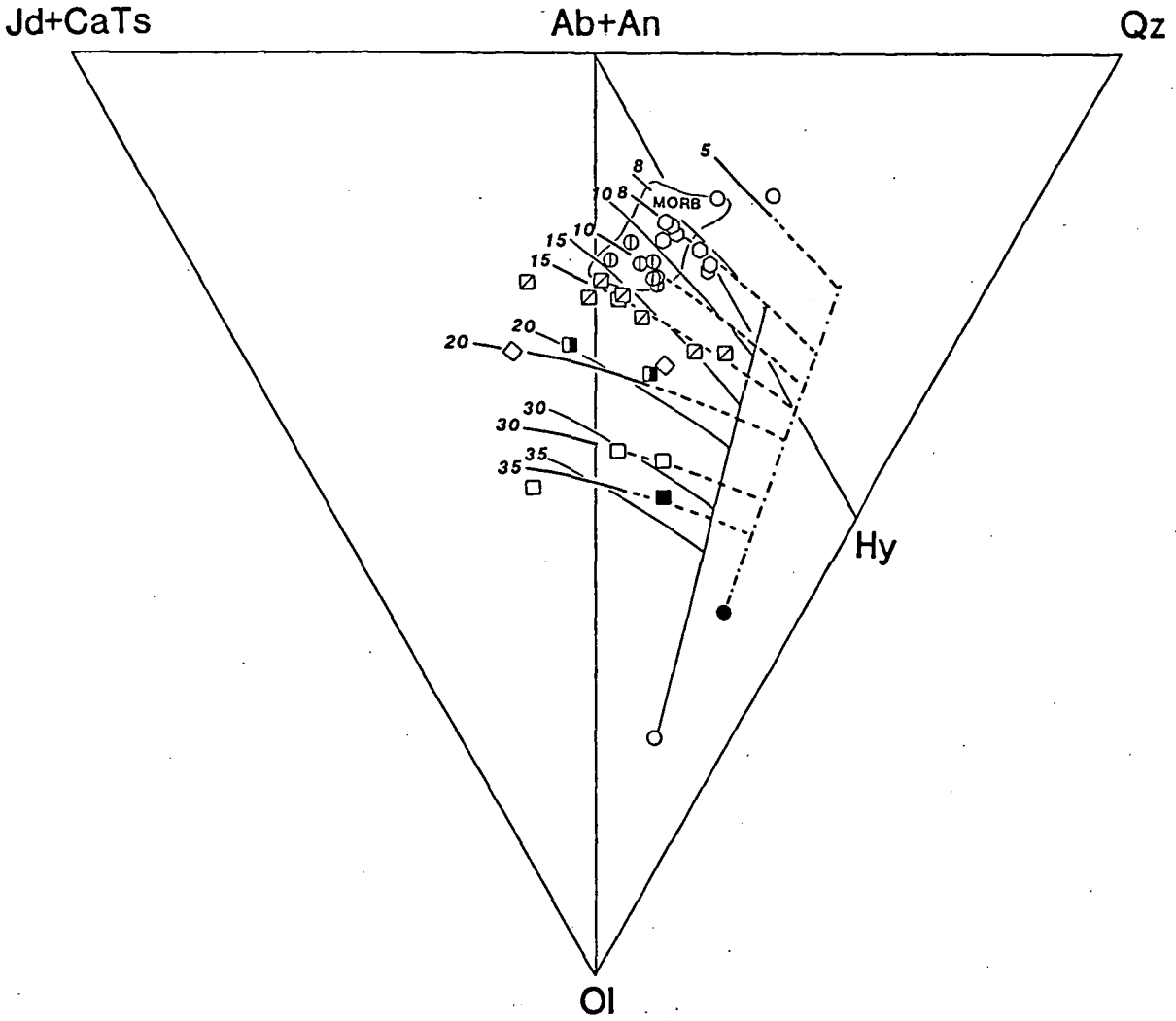

Figure 20

Equilibrium partial melt compositions from spinel lherzolite HK66 (Takahashi & Kushiro, 1983) compared to cotectics defined by partial melt compositions from MORB pyrolite at 8, 10, 15, 20, 30 and 35kbars in the projection from Di onto the base of the CIPW molecular normative basalt tetrahedron jadeite plus calcium tschermak's molecule (Jd + CaTs)-quartz(Qz)-olivine (Ol). MORB field as for Fig.17.

The following symbols represent partial melt compositions at different pressures (kbars) from HK66.

(○) 5, (⬡) 8, (◑) 10, (▨) 15, (◇) 20, (◨) 25, (□) 30, (■) 35.

(○) MORB pyrolite.

(●) spinel lherzolite HK66.

———— cotectics (olivine + liquid, olivine + orthopyroxene + liquid, olivine + orthopyroxene + clinopyroxene ± spinel + liquid) from MORB pyrolite.

—·—·— locus of liquids in equilibrium with olivine.

– – – – – locus of liquids in equilibrium with olivine + orthopyroxene.

———— locus of liquids in equilibrium with olivine + orthopyroxene + clinopyroxene ± spinel.

therefore consistent with similar cotectics from MORB pyrolite, Hawaiian pyrolite, Tinaquillo lherzolite and spinel lherzolite HK66 (at 30kbars only) (Fig.21).

2.5.4 Stolper (1980)

Stolper (1980) determined liquid compositions in equilibrium with olivine + orthopyroxene at 10, 15 and 20kbars by equilibrating a MORB glass composition with harzburgite in a 'sandwich' type experiment. The 15 and 20kbar liquids are compared with cotectics from MORB pyrolite in Fig.21, 10kbar liquids from Stolper (1980) are discussed in PART I. The 15kbar liquids from Stolper (1980) plot closer to the 18kbar cotectic from MORB pyrolite rather than the 15kbar cotectic. Similarly the 20kbar liquid plots closer to the 25kbar cotectic of MORB pyrolite. These differences are unlikely to be due to differences in bulk composition but may be due to systematic differences in pressure calibration using the piston-clyinder apparatus between the two different laboratories.

2.5.5 Elthon & Scarfe (1984)

Elthon and Scarfe (1984) studied the high pressure liquidus phase relations of a high-MgO picrite dyke composition NT-23 and determined the composition of liquids in equilibrium with olivine + orthopyroxene + clinopyroxene + garnet + liquid at 25kbar, olivine + orthopyroxene + clinopyroxene + liquid at 20 and 15kbar and olivine + orthopyroxene + clinopyroxene + plagioclase + spinel + liquid at 10kbar. These liquid compositions are plotted in Fig.21. The liquid compositions except for the 10kbar liquid are not consistent with any of the cotectics from MORB pyrolite. The 15, 20 and 25kbar liquid compositions from Elthon & Scarfe (1984) plot close to a 12, 15-17 and 18-20 kbar cotectic respectively from MORB pyrolite. The bulk composition of NT-23 plots close to a 20kbar olivine + orthopyroxene + liquid cotectic from MORB pyrolite in Fig.21 suggesting that NT-23 is a possible primary magma in equilibrium with a harzburgite residue. However Elthon & Scarfe (1984) report that NT-23 is multiply saturated at 25kbar with olivine + orthopyroxene + clinopyroxene + garnet, a result which is inconsistent with the compositions derived by partial melting of MORB pyrolite. A liquid in equilibrium with garnet at 20 or 25kbar is expected to lie in the Ne-normative side of the basalt tetrahedron. This conflict is attributed to misidentification of primary phases by Elthon & Scarfe (1984) in run no.164 (Elthon & Scarfe, 1984). In run no.164, primary olivine and orthopyroxene were large enough to be

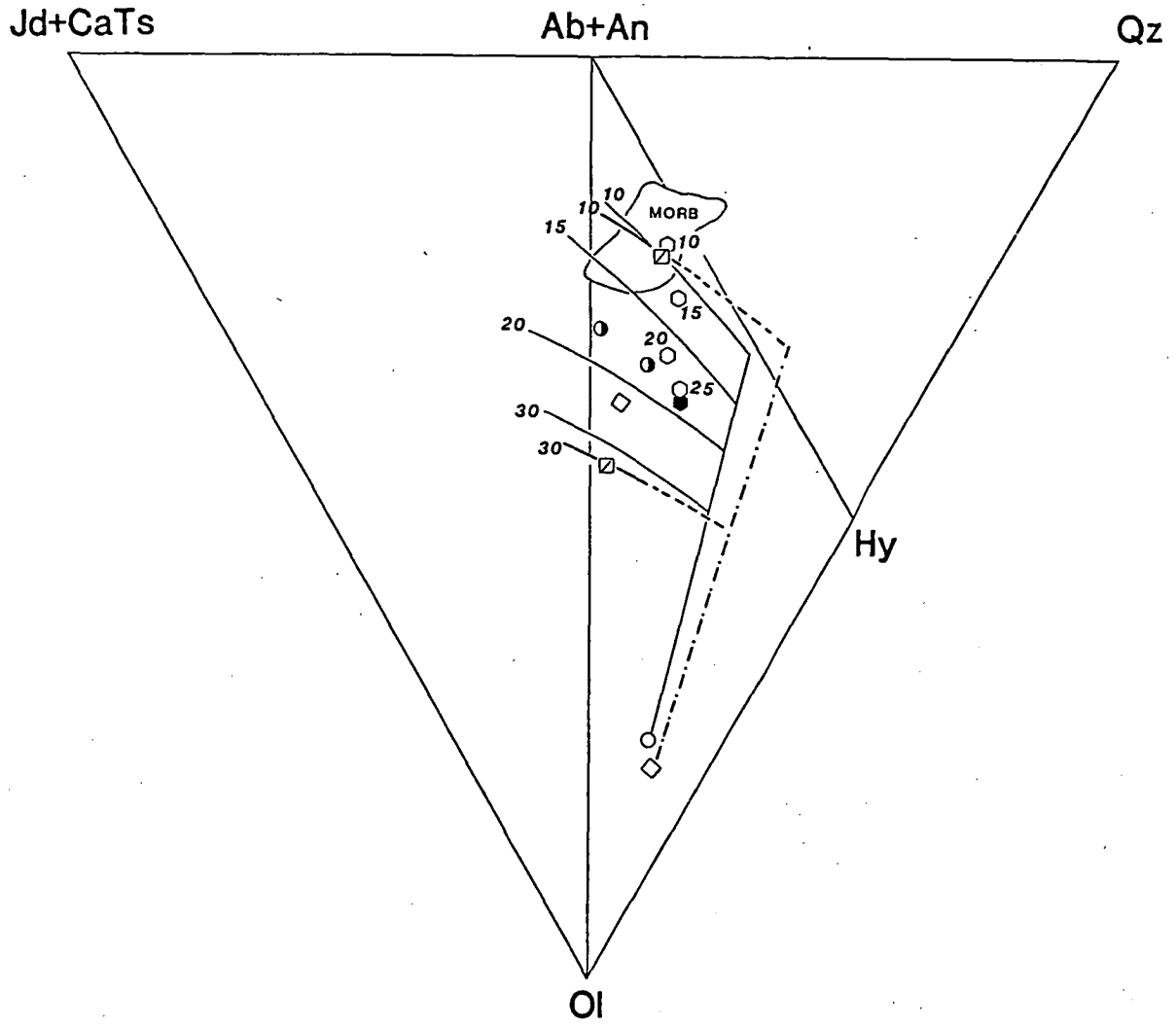

Figure 21.

Cotectics defined by partial melt compositions from MORB pyrolite (this study and PART I) at 10, 15, 20 and 30kbars compared to cotectics defined by spinel lherzolite KLB-1 at 10 and 30kbars (Takahashi, 1986; PART I) as well as liquid compositions from Stolper (1980) and Elthon and Scarfe (1984) in the projection from diopside (Di) onto the base of the CIPW molecular normative basalt tetrahedron jadeite plus calcium tschermak's molecule (Jd + CaTs)-quartz (Qz)-olivine (Ol). Cotectics as for Fig.20. MORB field as for Fig.17.

(○) MORB pyrolite.

(◇) spinel lherzolite KLB-1.

(▨) partial melt compositions from KLB-1 (Takahashi, 1986; PART I).

(◑ , ◇) melt compositions in equilibrium with olivine + orthopyroxene at 15 and 20kbar respectively from Stolper (1980).

(●) bulk composition of NT-23 (Elthon & Scarfe, 1984).

(⬡) are the pseudoinvariant points at 10, 15, 20 and 25kbar from Elthon & Scarfe (1984).

easily analyzed (Elthon & Scarfe, 1984). However 'primary' clinopyroxene and garnet was apparently so small that glass-overlap was a potential problem. The low Mg# of the clinopyroxene (0.85) and garnet (0.76) compared to the primary olivine and orthopyroxene (0.90 and 0.89 respectively) suggests the clinopyroxene and garnet are quench phases. All phases should be large enough to analyse in a charge if primary. The result of run no.164 suggests multiple saturation in olivine and orthopyroxene only, consistent with results from MORB pyrolite, however the reported pressure of 25kbar is too high, 20kbars being more consistent.

2.5.6 Summary

The results of partial melting experiments on MORB pyrolite, Tinaquillo lherzolite, Hawaiian pyrolite (Falloon et al., 1987; PART I; Jaques & Green, 1980), spinel lherzolite HK66 (Takahashi & Kushiro, 1983) and spinel lherzolite KLB-1 (Takahashi, 1986; PART I) provide an internally consistent set of data enabling the establishment of a melting grid in the projection from Di. This melting grid can be used to establish for any primitive magma composition a possible depth of magma segregation when projected from Di in the basalt tetrahedron. The melting grid also provides information on the possible residual phases and likely degree of partial melting of a primitive magma composition. In the following section the melting grid established for MORB pyrolite from 8 to 35kbars is used in conjunction with olivine fractionation calculations to establish a possible range of primary liquids parental to primitive MORB glasses, as well as the depth of magma segregation, degree of partial melting and how much olivine fractionation has occurred.

2.6 OLIVINE FRACTIONATION CALCULATIONS

2.6.1 Rationale

The rationale for the these calculations is to test whether a simple model of equilibrium batch partial melting of a MORB pyrolite source, primary magma segregation, followed by olivine crystal fractionation can produce the range in composition of primitive MORB glasses, and to determine the range in pressures, temperatures and degree of partial melting that is required. The assumption that olivine fractionation only has occurred since primary magma segregation is supported by experimental studies of primitive MORB glasses, which have only olivine on their liquidus at 1atm (Green et al., 1979; Bender et al., 1978; Fujii &

Bougault, 1983). Other workers have suggested that high pressure crystal fractionation of clinopyroxene ± orthopyroxene is also an important process (Elthon & Scarfe, 1984; Stolper, 1980; Fujii & Bougault, 1983; Elthon et al., 1982; Elthon, 1986; Bence et al., 1979). Evidence for this high pressure crystal fractionation include;

(1) diopsidic clinopyroxene megacrysts rich in Cr (>1wt%, Cr_2O_3) (Donaldson & Brown, 1977; Thompson 1980; Stakes et al., 1984).

(2) The 'clinopyroxene paradox' (Francis, 1986), where successful crystal-fractionation models require crystallizing assemblages dominated by clinopyroxene to explain the observed variation in major element geochemistry despite the absence or rarity of clinopyroxene as a phenocryst phase. The 'paradox' is explained by high-pressure clinopyroxene fractionation, with subsequent dissolution of high-pressure clinopyroxene at lower pressure (O'Donnell & Presnall, 1980; Fujii & Bougault, 1983; Bryan, 1983).

(3) Cumulate rocks exposed in ophiolite sections, which include magnesian clinopyroxenes and orthopyroxenes (Elthon et al., 1982; Elthon & Casey, 1985).

Concerning the first two points, experimental work by Grove & Bryan (1983) can reproduce the range in clinopyroxene composition observed in MORB at 1atm. The presence of more magnesian (#Mg>0.90) clinopyroxene as well as calcic plagioclase megacrysts in MORB can be explained by contributions from refractory second-stage melts (Duncan & Green, 1980, 1987) in magma mixing processes in sub-axial magma chambers. They are not the result of high pressure crystal fractionation processes. Francis (1986) and Bryan et al. (1981) have suggested that the 'clinopyroxene paradox' is the result of an array of parental picritic parents, fractionating olivine and arriving at different points along the 1atm olivine + plagioclase + clinopyroxene + liquid cotectic between the limiting cases of equilibrium and fractional crystallization. Francis (1986) proposes that the existence of the 'clinopyroxene paradox' in MORB glasses is evidence of the picritic nature of parental magmas for MORB, emphasizing the importance of olivine fractionation from picritic parents.

Concerning the third point, it is now doubtful whether most ophiolites represent major ocean basin crust, but rather dismembered pieces of island arc, forearc, and back-arc crust (Leitch, 1984). Thus inferences

about processes at major mid ocean ridges from ophiolite cumulate sequences could be misleading. For example submarine lavas from the North Tonga forearc contain abundant magnesian orthopyroxene> clinopyroxene phenocrysts (PART III), lavas from the island of Mere Lava, Vanuatu arc contain abundant magnesian clinopyroxene (Barsdell,in prep). Both areas, if incorporated into an ophiolite terrain would show the presence of magnesian clinopyroxene or orthopyroxene in cumulate sequences. Cumulate sequences from a major mid ocean ridge basin would be expected to be dominated by olivine + plagioclase + clinopyroxene, as is the case for the Macquarie Island ophiolite (Griffin & Varne, 1980).

Before presenting the results of olivine fractionation calculations there are several constraints which can be imposed on potential primary magma compositions. These constraints are the major element composition of MORB glasses, and constraints derived from olivine control lines in the CIPW molecular normative basalt tetrahedron. Olivine control lines within the basalt terahedron form two important constraints on potential primary magma compositions:

(1) A potential peridotite source composition can only produce equilibrium partial melts to the left of an olivine control line passing through the bulk composition in the projection from Di (Green et al., 1987) and above the olivine control line in the projection from plagioclase (An + Ab) in Fig.18.

(2) potential primary/parental magmas to primitive MORB glasses must lie within olivine control lines bounding the range in silica saturation of primitive MORB glasses.

An important criteria for a MORB composition to be considered a primary magma is a Mg# (calculated with $Fe^{2+}/Fe^{2+}+ Fe^{3+}$ equal to 0.9) appropriate to be in equilibrium with a mantle olivine composition of $Fo_{90\pm3}$ (Green, 1971). Using this criteria a data base of over 80 MORB glasses with Mg#$\geq$ 0.68 was obtained from the literature (Appendix 2). Glass compositions were chosen as they represent liquid compositions and do not suffer from the effects of crystal accumulation and alteration (Melson et al., 1977). The primitive MORB glasses display a significant range in major element and CIPW normative geochemistry, which is summarized in Table 11. This range in chemistry is a complex function of depth of magma segregation, source composition, degree of partial melting and extent of olivine fractionation. In conjunction with peridotite melting studies

Table 11

Primitive MORB glass compositions

	1	2	3	4	5	min - max
SiO_2	48.20	49.70	49.07	51.36	49.56	48.20 - 51.64
TiO_2	0.51	0.72	0.74	0.78	0.67	0.50 - 1.30
Al_2O_3	17.00	16.40	16.44	15.03	15.90	15.50 - 17.62
FeO	8.51	7.90	8.86	7.86	8.29	7.30 - 9.40
MnO	0.16	0.12	0.16	0.10	0.17	0.09 - 0.25
MgO	10.10	10.10	10.15	9.01	9.19	8.10 - 10.70
CaO	12.70	13.10	11.65	12.38	13.57	11.23 - 13.57
Na_2O	2.34	2.00	2.13	2.04	2.15	2.40 - 2.38
K_2O	0.04	0.01	0.07	0.10	0.07	0.01 - 0.32
P_2O_5	nd	nd	nd	nd	nd	0.03 - 0.14
Cr_2O_3	nd	0.07	0.03	0.11	nd	0.01 - 0.13
Total	99.56	100.12	99.30	98.77	99.57	
Mg#	0.70	0.72	0.69	0.69	0.69	0.68 - 0.73
CIPW norm (molecular)						
Qz	0.00	0.00	0.00	2.24	0.00	< 8.39
Ne	0.51	0.00	0.00	0.00	0.00	< 1.00
Ab	16.66	15.04	16.08	15.90	16.27	10.53 - 20.79
An	29.24	29.95	29.51	27.41	28.27	24.92 - 34.04
Di	22.27	24.50	19.09	25.92	28.49	18.76 - 29.45
Hy	0.00	11.63	13.24	24.16	6.79	< 24.96
Ol	28.33	15.34	18.08	0.00	16.53	< 28.33
CaO/Al_2O_3	0.74	0.79	0.71	0.82	0.85	0.67 - 0.88
CaO/Na_2O	5.42	6.55	5.47	6.07	6.31	4.58 - 9.49
CaO/TiO_2	24.90	18.19	15.74	15.87	20.25	9.32 - 25.60
Al_2O_3/TiO_2	33.33	22.77	22.22	19.27	23.73	12.00 - 33.80

(1) ARP74-14-31 (Bryan, 1979a).
(2) DSDP3-18-7-1 (Green et al., 1979).
(3) ALV519-4-1 (Bryan & Moore, 1977).
(4) ALV526-1-1B (Bryan & Moore, 1977).
(5) 332B 36-3 (Shipboard S. P., 1977).

Mg# and CIPW norm calculated on the basis of $Fe^{2+}/(Fe^{2+}+ Fe^{3+})=0.9$, nd not determined, Min and Max indicate the range in composition of primitive MORB glasses (Mg#$\geq$0.68), data sources see caption to Fig.22.

several important constraints based on the primitive MORB glass compositions have been selected, they are discussed separately below.

2.6.2 Constraints from the composition of primitive MORB glasses

2.6.2.1 Silica saturation

In terms of molecular normative mineralogy (Fig.22) primitive MORB glasses range from ne-normative to quartz normative compositions. The primitive MORB glasses also display a significant range in normative diopside in the projection from plagioclase (Ab+An). Differing degrees of silica-saturation can be explained by differing degrees of partial melting, primary magmas produced by high degrees of partial melting will upon olivine fractionation move derivative compositions towards the qz-normative side of the diagram in Fig.22. Primary magmas produced by low degrees of partial melting will on olivine fractionation move derivative liquids towards the ne-normative side of the diagram. At 10kbar equilibrium liquid compositions from MORB pyrolite (PART I) could not explain the range of silica saturation of primitive MORB glasses. At low degrees of partial melting the presence of the plagioclase phase volume acts as a barrier to low melting fraction liquids crossing over towards the ne-normative side of the diagram, while the elimination of clinopyroxene as a residual phase acted as a barrier to liquids crossing over to the quartz normative side of the diagram (PART I). Qz-normative glasses must either be low-pressure primary melts (<10kbar) or derived by olivine fractionation from picritic liquids at higher pressures than 10kbar. In this case the picritic parents would be produced by relatively high degrees of partial melting, sufficient to eliminate clinopyroxene from the residue. Ne-normative glasses must be derived from parental magmas which are primary melts greater than 10kbar, the primary melts having a alkali picritic character, produced by smaller degrees of partial melting than parental magmas to hy-normative or qz-normative glasses. The degree of silica-saturation in the primitive MORB glasses is therefore broadly related to the degree of partial melting, Ne-normative and low Hy normative glasses are derived by lower degrees of partial melting than qz-normative and low ol-normative glasses which are derived by higher degrees of partial melting.

The range in normative Di contents displayed in Fig.22 could be explained simply by differing degrees of olivine fractionation, glasses with higher normative Di in Fig.22 having undergone more olivine fractionation than low olivine normative glasses. However in detail there

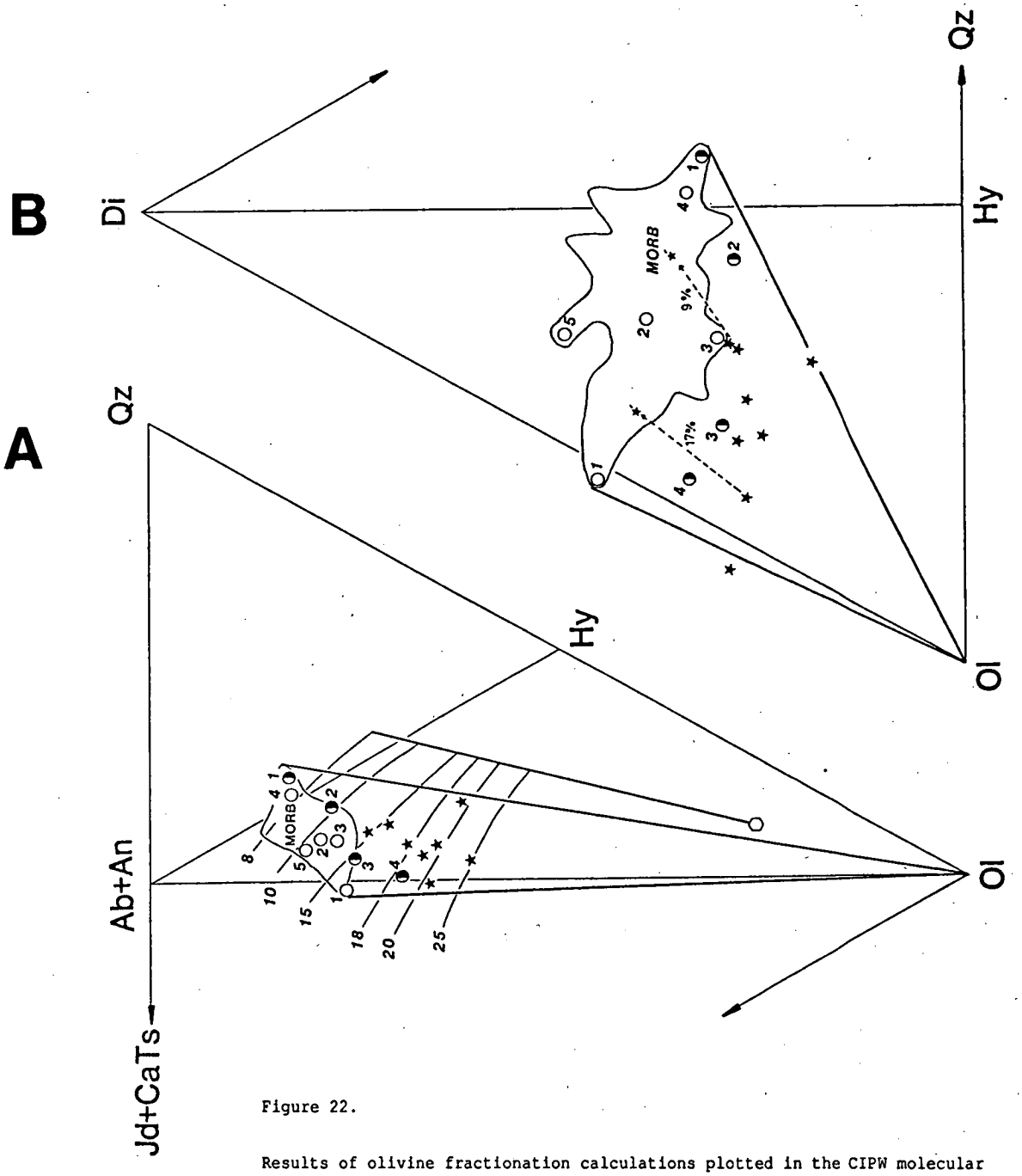

Figure 22.

Results of olivine fractionation calculations plotted in the CIPW molecular normative basalt tetrahedron projected from Di onto the base jadeite plus calcium tschermak's molecule (Jd + CaTs)-quartz (Qz)-olivine (Ol) in A, and onto the face diopside (Di)-quartz (Qz)-olivine (Ol) from plagioclase (Ab + An) in B. MORB encloses field for primitive MORB glasses (Natland et al., 1984; Melson et al., 1977; Melson et al., 1976; Frey et al., 1973; Frey et al., 1974; Green et al., 1979; O'Donnell & Presnall, 1980; Melson & O'Hearn, 1979; Scarfe & Smith, 1977; Shipboard S. P., 1977; Hekinian et al., 1976; Langmuir et al., 1977; Bender et al., 1978; Fujii & Bougault, 1983; Basaltic Volcanism Study Project, 1981; Shibata et al., 1979; Barker et al., 1983; Melson, 1973; Stakes et al., 1984; Sigurdsson, 1981; Bryan, 1979a; Bryan & Moore, 1977; Bryan et al., 1981).

(★) equilibrium partial melts from MORB pyrolite which produced successful matches with primitive MORB glasses upon olivine fractionation. Examples of some successful fractionation paths (-------→) and wt% olivine removed are also presented, (★′) derivative liquid composition.

(○) numbered 1 to 5 are primitive MORB glass compositions from Table 11.

(◑) numbered 1 to 4 are primary MORB compositions from Table 12.

(⬡) MORB pyrolite.

——— olivine control lines.

——— cotectics from MORB pyrolite at 8, 10, 15, 18, 20 and 25kbars.

is no simple relationship between low and high normative diopside glasses. This is probably a consequence of the superposition of olivine fractionation paths from multiple primary liquids in Fig.22. Olivine fractionation paths from a range of primary melts at different pressures and degrees of partial melting are superimposed in this diagram. However in general high Di-normative glasses such as DSDP3-18-7-1 (Table 7) have undergone higher degrees of olivine fractionation than low Di normative glasses.

2.6.2.2 Al_2O_3 and CaO contents

An important characteristic of primitive MORB glasses are their combined high CaO and Al_2O_3 contents (11.23-13.57 wt% and 15.5-17.62 wt% respectively, Table 11) compared to evolved MORB and primitive basalts of other tectonic regimes. Partial melting of peridotite at low pressures is unable to produce high CaO and Al_2O_3 contents (PART I). At low degrees of partial melting liquid compositions are characterized by high Al_2O_3 and low CaO contents and vice versa at higher degrees of partial melting. As olivine fractionation will increase both CaO and Al_2O_3 in derivative liquids from picritic parents, the Al_2O_3 and CaO content of primitive MORB glasses can act as a constraint on how much olivine fractionation has occurred.

2.6.2.3 SiO_2 contents

The SiO_2 contents of primitive MORB glasses range between 48.20 to 51.64 wt%. As SiO_2 content along a olivine + orthopyroxene + clinopyroxene + liquid cotectic is primarily a function of pressure, and assuming the SiO_2 content of primitive MORB glasses is a primary feature, then a pressure range of between 20 to 8kbar is required to explain the SiO_2 content of primitive MORB glasses. However in reality the SiO_2 content of primitive MORB glasses is a function of both depth of primary melt segregation, degree of partial melting and olivine fractionation.

2.6.2.4 FeO and MgO contents

FeO and MgO contents of primitive MORB glasses are a complex function of depth of primary magma segregation, bulk composition and degree of partial melting. For a given bulk composition FeO contents in partial melts will increase with pressure. At low pressures FeO contents of initial partial melts will be low relative to the FeO content of the bulk

composition and FeO contents will increase with degree of partial melting. At high pressures FeO contents of low melt fraction liquids will be higher or equal to the FeO content of the bulk composition , thus FeO contents will remain relatively constant or decrease with increasing partial melting. The FeO contents of primitive MORB glasses vary from 7.3 to 9.4 wt% and assuming that the glasses are primary melts then the FeO contents indicate depths of magma segregation of between 15-20kbar based on a bulk composition with 7.5 wt% FeO. The calculation of the CIPW normative molecular norm 'masks' FeO and MgO variation, causing compositions of differing FeO and MgO contents to plot in the same position within the basalt tetrahedron. Because FeO contents are sensitive to the bulk composition, the Fe/Mg ratio of equilibrium partial melts from MORB pyrolite can be varied to match the FeO contents of primitive MORB glasses.

2.6.2.5 CaO/Al_2O_3 and CaO/Na_2O ratios

Partial melting studies including this present work demonstrate that CaO/Al_2O_3 and CaO/Na_2O ratios vary systematically with degree of partial melting along a olivine + orthopyroxene + clinopyroxene + liquid cotectic. CaO/Al_2O_3 and CaO/Na_2O ratios both increase with increasing degree of partial melting until clinopyroxene is eliminated from the residue, CaO/Al_2O_3 and CaO/Na_2O ratios remaining relatively constant thereafter. CaO/Na_2O and CaO/Al_2O_3 ratios of primitive MORB glasses can therefore be used as a constraint on the degree of partial melting.

2.6.2.6 TiO_2, K_2O and Al_2O_3/TiO_2 and CaO/TiO_2 ratios

Because K_2O and TiO_2 can be regarded as relatively incompatible during partial melting they can also be used as an indicator of the degree of partial melting (Thompson et al., 1984). Ratios such as Al_2O_3/TiO_2 and CaO/TiO_2 vary systematically with partial melting along a olivine + orthopyroxene + clinopyroxene + liquid cotectic (Sun & Nesbitt, 1978; Sun et al., 1979). Because TiO_2, K_2O contents, Al_2O_3/TiO_2 and CaO/TiO_2 ratios of partial melts are so source dependent they are not considered a significant constraint in this study, TiO_2 and K_2O contents can be increased or decreased in a peridotite bulk composition without affecting phase relations significantly. High Al_2O_3/TiO_2 and CaO/TiO_2 ratios and low TiO_2 contents could be produced by high degrees of partial melting of a relatively fertile source or a low degree of partial melting of a relatively depleted source. Broadly speaking high Al_2O_3/TiO_2, CaO/TiO_2, low TiO_2 and K_2O indicate relatively depleted sources.

2.6.3 Results

All the equilibrium partial melt compositions from MORB pyrolite were subjected to simple incremental olivine fractionation calculations using increments of 0.1 wt% olivine. At each step the equilibrium olivine was determined using a $(Kd)^{ol/liq}_{Fe/Mg}$ =0.3, with total Fe calculated as FeO. Several equilibrium partial melts from MORB pyrolite produced successful matches between calculated daughter liquids and primitive MORB glasses as indicated in Fig.22. Partial melt compositions from pressures above 25kbar did not produce successful matches, as calculated derivative liquids become too Al_2O_3 and CaO rich when compared to primitive MORB glasses of similar Mg#. Partial melt compositions at less than 15kbar did not produce good matches for most primitive MORB glass compositions as calculated liquid compositions become too aluminous compared to primitive MORB glasses at a similar Mg#. Partial melts from MPY-87 at 20kbar produced successful matches, but FeO contents of calculated derivative liquids were too high compared to most primitive MORB glasses at a similar Mg#. Because the CIPW molecular norm calculation 'masks', Fe/Mg variation, it is possible to recalculate the Fe/Mg ratio of the partial melts, without changing its molecular norm. Closer matches were obtained in this way with the primitive MORB glasses.

Olivine subtraction calculations performed on the equilibrium melt compositions suggest that the majority of primitive MORB glasses can be produced from between 11-25wt% olivine fractionation, from primary magmas segregating from a MORB source diapirs at pressures of between 25 to 15kbars, with between 17-30 wt% partial melting of the MORB pyrolite composition, leaving lherzolite and harzburgite residues. The harzburgite residues would recrystallize to lherzolite during subsolidus recrystallization at lower pressures, because of high CaO and Al_2O_3 in residual orthopyroxene.

Although olivine fractionation is required to explain the composition of most MORB glasses, some primitive MORB glasses have major element compositions compatible with them being near primary melts. Four examples are given in Table 12 and plotted in Fig.22. T3-71D 159-10C1 (Table 12, no.4) is from the mid-Atlantic ridge at 29° 47'N (Keays & Scott, 1976). In Fig.8 T3-71D 159-10C1 plots close to the 20kbar olivine + orthopyroxene + clinopyroxene + liquid cotectic defined by equilibrium partial melts from MPY-87, and is similar in major element chemistry. CH21 D20-29 is a primitive MORB glass reported in the Basaltic Volcanism Study Project

Table 12

Primary MORB compositions

	1	2	3	4
SiO_2	51.33	50.48	48.26	47.28
TiO_2	0.61	0.87	0.89	0.97
Al_2O_3	15.60	15.33	16.80	14.48
FeO	7.86	8.36	9.32	10.98
MnO	nd	0.15	0.17	0.19
MgO	8.97	10.72	10.48	12.52
CaO	13.48	11.84	11.23	10.78
Na_2O	1.42	1.88	2.40	2.38
K_2O	0.05	0.17	0.03	0.04
P_2O_5	0.03	0.09	0.06	0.09
Total	99.35	99.80	99.64	99.71
Mg#	0.69	0.72	0.69	0.69
CIPW norm (molecular)				
Qz	8.39	0.00	0.00	0.00
Ab	10.53	14.39	17.65	16.98
An	29.79	28.05	28.66	22.74
Di	25.31	21.21	16.66	19.31
Hy	22.73	23.52	6.16	1.84
Ol	0.00	8.01	26.70	34.73
CaO/Al_2O_3	0.86	0.77	0.67	0.74
CaO/Na_2O	9.49	6.29	4.68	4.53
CaO/TiO_2	22.09	13.61	12.61	11.11
Al_2O_3/TiO_2	25.57	17.62	18.87	14.93

(1) primitive MORB glass 212 (Melson et al., 1976).

(2) P_2, most primitive olivine basalt from FAMOUS (Le Roex et al., 1981).

(3) primitive MORB glass CH21-D20-29 (Basaltic Volcanism Study Project, 1981).

(4) primitive MORB glass T3-71D 159-10C1 (Keays & Scott, 1976).

Mg# and CIPW norm calculated on basis of $Fe^{2+}/(Fe^{2+}+ Fe^{3+})=0.9$, nd not determined.

(1981), this composition plots close to the 15kbar olivine + orthopyroxene + clinopyroxene + liquid cotectic of MPY-90-40 and again is similar in major element chemistry to the 15kbar partial melts from MPY-90-40. P_2 is the average primitive olivine basalt composition of Le Roex et al. (1981) for the olivine basalts from the FAMOUS area. This composition plots on a olivine + orthopyroxene + clinopyroxene + liquid cotectic at 10kbar and is very close in composition to the 10kbar partial melt compositions reported in PART I. Primitive MORB glass 212 from Melson et al. (1977) is quartz normative and plots very close to a 8kbar olivine + orthopyroxene + clinopyroxene + liquid cotectic from MORB pyrolite. MORB glass 212 however plots at higher normative Di than the 8kbar cotectic in Fig.22 and has significantly higher CaO content and higher CaO/Al_2O_3 and CaO/Na_2O ratios than the 8kbar liquids from MORB pyrolite. The glass 212 however is similar in composition to 10kbar liquid compositions from the more depleted lherzolite composition Tinaquillo lherzolite (PART I). Thus 212 could be a near primary liquid composition derived by minor olivine fractionation from a 10-8kbar olivine + orthopyroxene + clinopyroxene + liquid cotectic from a more depleted peridotite than MORB pyrolite.

2.6.4 Comparison with MORB picrite compositions

A common objection to a picrite model for MORB petrogenesis is the lack of picrite especially picrite glass compositions amongst MORB dredge or borehole collections. However due to the efficiency of olivine fractionation, picrite primary compositions will be unlikely to survive unmodified. Experimental work by Stolper & Walker (1980) and Sparks et al. (1980) demonstrate that picritic melts would necessarily be denser than common evolved MORB, and would be trapped at the base of magma chambers where they would fractionate olivine and other phases to produce more common evolved MORB compositions. Although olivine phenocryst-rich MORBs have been documented from MORB settings, most workers have not considered whole-rock compositions as representative of liquid compositions but as olivine accumulates. However by using the most magnesian olivine present in a picrite suite and using an appropriate olivine -liquid Kd, the FeO and MgO contents of the equilibrium liquid can be obtained (Basaltic Volcanism Study Project, 1981; Irvine, 1977; Francis, 1985, 1986). In most cases the equilibrium liquid is of picrite composition. So even though picritic compositions are rare, the presence of magnesian olivine phenocrysts and megacrysts implies the existence of such liquids. In Table 13 are listed picrite compositions from the MORB setting, all of which are in equilibrium with the most magnesian olivine in the respective rock or suite. Most are

Table 13

MORB picrite compositions

	1	2	3	4	5	6	7	8	9	10	11
SiO_2	46.87	46.95	47.09	47.70	47.60	48.78	46.90	48.19	47.78	48.33	48.30
TiO_2	0.79	0.77	0.75	0.63	0.58	0.63	1.13	0.83	0.86	0.74	0.60
Al_2O_3	16.51	16.59	16.84	13.72	13.80	15.77	12.60	14.12	14.50	11.35	13.70
FeO	10.47	9.65	9.69	9.45	9.37	7.96	10.16	9.22	9.07	10.19	7.90
MnO	0.17	0.16	0.17	0.16	0.18	0.15	0.18	0.14	0.14	0.17	0.12
MgO	12.05	11.60	11.29	15.80	14.80	12.32	16.40	15.32	13.27	17.70	16.90
CaO	11.07	11.16	11.29	10.14	10.70	12.61	10.30	10.19	10.64	9.57	10.90
Na_2O	2.13	2.15	2.19	2.07	1.84	1.55	2.00	1.41	2.19	1.34	1.65
K_2O	0.06	0.04	0.02	0.12	0.10	0.09	0.20	0.02	0.06	0.11	0.01
P_2O_5	0.04	0.05	0.04	0.04	0.05	0.05	0.00	0.14	0.13	0.06	0.06
Cr_2O_3	nd	nd	nd	0.13	nd	nd	nd	nd	nd	0.25	nd
NiO	nd	nd	nd	nd	nd	nd	nd	nd	nd	0.09	nd
LOI	nd	0.32	0.45	nd	nd	nd	nd	0.41	0.26	nd	nd
Total	100.16	99.44	99.82	99.96	99.02	99.91	99.87	99.90	98.90	99.90	99.94
Mg#	0.67	0.68	0.67	0.75	0.74	0.74	0.74	0.75	0.72	0.76	0.79
CIPW norm (molecular)											
Ne	0.00	0.00	0.00	0.00	0.00	0.00	0.38	0.00	0.00	0.00	0.00
Ab	15.05	14.52	14.25	14.11	12.93	11.40	12.95	9.20	14.78	9.23	11.36
An	27.81	26.72	26.14	21.11	22.79	29.35	18.43	23.37	22.22	18.89	22.97
Di	15.23	14.70	14.27	16.90	18.52	21.66	19.52	12.72	16.82	17.22	18.51
Hy	0.92	2.69	1.49	3.68	7.47	13.48	0.00	20.13	6.76	19.90	10.10
Ol	36.95	31.25	31.22	40.41	34.82	20.61	43.47	21.89	29.56	30.42	34.16
CaO/Al_2O_3	0.67	0.67	0.67	0.73	0.77	0.79	0.82	0.72	0.73	0.84	0.79
CaO/Na_2O	5.20	5.20	5.15	4.89	5.81	8.13	5.15	7.23	4.86	7.14	6.61
CaO/TiO_2	14.01	14.49	15.05	16.09	18.45	20.01	9.11	12.27	12.37	12.93	18.16
Al_2O_3/TiO_2	20.89	21.54	22.45	21.77	23.79	25.03	11.15	17.01	16.86	15.34	22.38

(1) TR123 4D-5 (Schilling et al., 1983).
(2) TR123 4D-7 (Schilling et al., 1983).
(3) TR123 4D-9 (Schilling et al., 1983).
(4) calculated primitive liquid (Irvine, 1977).
(5) calculated parental magma composition (Ramsay et al., 1984).
(6) calculated parental magma composition P_1 (Le Roex et al., 1981).
(7) SO12 88-1 (Eissen et al., 1981).
(8) SD-7A (Schrader et al., 1979).
(9) SD-7B (Schrader et al., 1979).
(10) calculated parental composition (Beets et al., 1982).
(11) primary MORB picrite DSDP3-18-7-1 + 17wt% olivine (Green et al., 1979).

CIPW norm calculated on the basis of $Fe^{2+}/(Fe^{2+}+Fe^{3+})$-0.9.
Mg# calculated on the basis of total iron as FeO, nd not determined.

actual whole rock compositions the rest are calculated compositions based on olivine addition or subtraction calculations. The picrite compositions in Table 13 are plotted in the CIPW molecular normative basalt tetrahedron in Fig.23a, b. The picrite compositions in terms of silica saturation fall within olivine control lines drawn from the extremities of the MORB glass field. Significantly the picrite compositions can explain the entire range of silica-saturation displayed by primitive MORB glasses via olivine fractionation. One picrite composition lies outside the control lines to the MORB field in Fig.23, SD-7A (Table 13, no.8) from the East Pacific Rise (Schrader et al., 1979).

Using the melting grid of equilibrium melt compositions from MORB pyrolite and assuming the picrite compositions are close to or are primary MORB magmas, the picrite compositions in Table 13 represent magma segregation at pressures between 15 to 25kbar, in equilibrium with spinel lherzolite and harzburgite residues. In no case is garnet a residual phase. The range of depth of magma segregation is similar to that inferred from analysis of equilibrium liquids from MORB pyrolite.

Another common objection to picrite primary melts is the Ni content of primitive MORB glasses which should be lower than observed if the primitive MORB glasses are derived by olivine fractionation from picrite primary melts. This objection is based on experimentally determined olivine-liquid partition coefficients for Ni in synthetic systems (Sato, 1977; Hart & Davis, 1978). This objection is overcome if partition coefficients from experimental studies on natural basalts are used (Arndt, 1977; Bickle et al., 1977; Clarke & O'Hara, 1979; Elton & Ridley, 1979; Budahn, 1986) and if a more appropriate crystallization equation is chosen e.g. equilibrium crystallization (Budahn, 1986).

2.6.5 Comparison with compositions determined from trapped glass inclusions

The presence of trapped glass inclusions in early crystallizing phases olivine, spinel and plagioclase phenocrysts in MORB, offers an opportunity to see through the effects of magma mixing, and crystal fractionation, helping to identify parental and primitive magma compositions. The only problem with this approach is to see through the effects of post-entrapment interaction between the host mineral and the glass inclusion. In Table 14 are listed compositions of trapped glass inclusions where the effects of post-entrapment processes have been

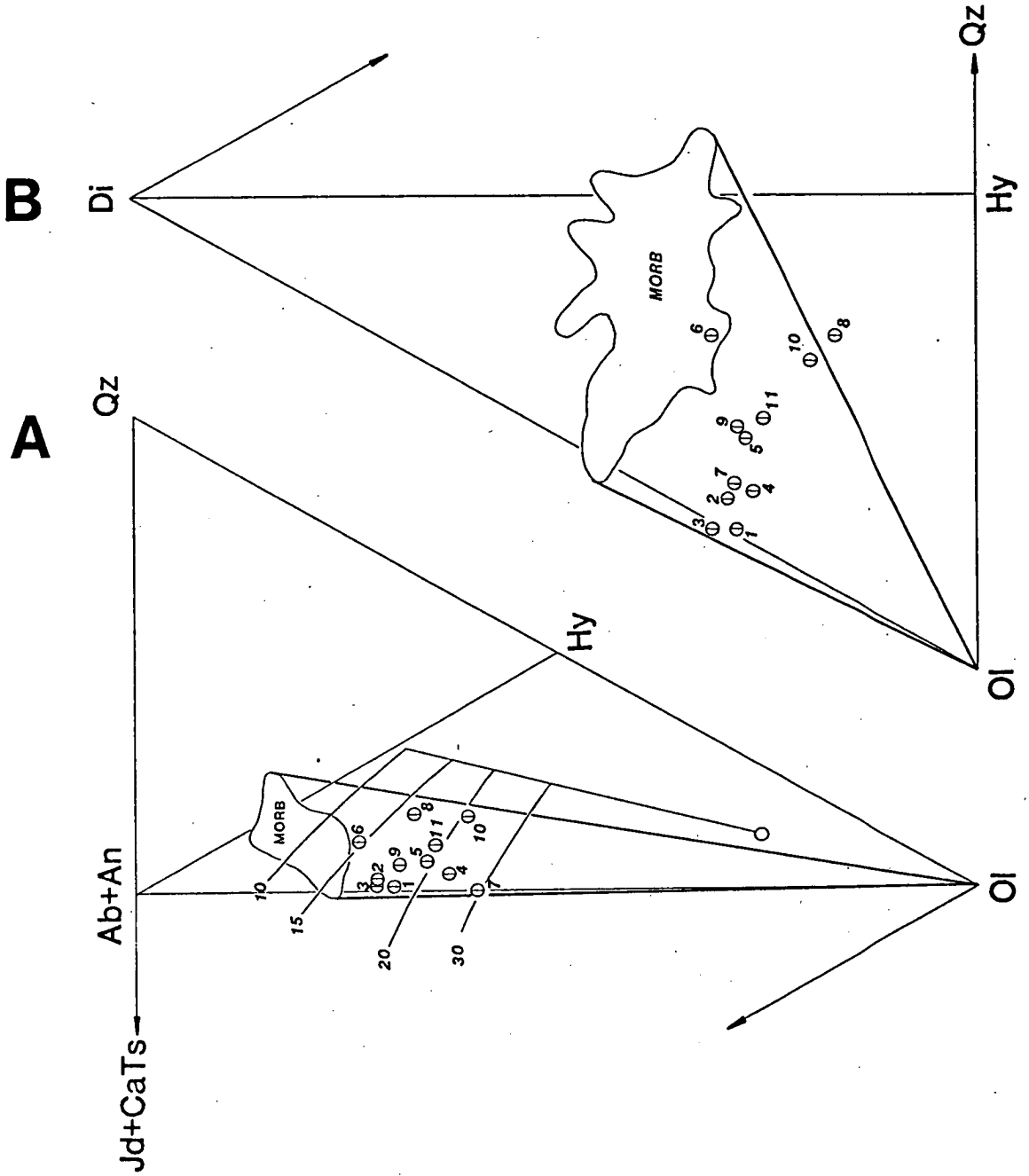

Figure 23.

MORB picrite compositions compared with equilibrium partial melts from MORB pyrolite and primitive MORB glasses in the CIPW molecular normative basalt tetrahedron projected from Di onto the base jadeite plus calcium tschermak's molecule (Jd + CaTs)-quartz (Qz)-olivine (Ol) in A, and projected from plagioclase (Ab + An) onto the face diopside (Di)-quartz (Qz)-olivine (Ol) in B. Lines and cotectics as for Fig.22.

(○) MORB pyrolite.

(⊕) numbered 1 to 11 are MORB picrite compositions from Table 13.

Table 14

Compositions of primitive MORB glass inclusions.

	1	2	3	4	5	6	7	8
SiO_2	50.57	49.38	50.30	49.61	49.58	50.26	49.41	49.32
TiO_2	0.54	0.64	1.20	0.86	0.65	0.61	0.54	0.24
Al_2O_3	15.39	15.71	14.50	14.28	14.43	14.21	14.37	13.96
FeO	7.88	7.84	8.80	9.39	8.19	6.82	8.06	7.91
MnO	0.16	nd	0.16	0.13	nd	0.10	0.18	0.16
MgO	10.41	12.04	10.10	10.00	11.64	11.89	13.70	14.20
CaO	12.83	12.68	12.10	11.89	12.89	13.46	10.90	11.03
Na_2O	1.44	1.44	2.50	2.21	1.70	1.42	2.55	2.31
K_2O	0.03	0.08	0.05	0.07	0.03	0.07	0.03	0.03
P_2O_5	nd	nd	nd	nd	0.04	nd	nd	nd
Cr_2O_3	nd	nd	nd	0.06	nd	nd	0.09	nd
Total	99.25	99.81	99.71	98.50	99.15	98.84	99.83	99.16
Mg#	0.72	0.75	0.69	0.68	0.74	0.77	0.77	0.78
CIPW norm (molecular)								
Ab	11.31	10.77	18.66	16.85	12.77	10.84	17.96	16.41
An	31.01	30.14	23.44	24.49	26.50	27.39	21.72	21.87
Di	24.68	22.28	26.46	25.60	26.81	29.42	20.72	21.43
Hy	29.18	18.87	10.78	14.75	16.21	21.83	3.72	6.17
Ol	0.70	14.43	15.52	13.77	14.34	7.09	32.90	32.10
CaO/Al_2O_3	0.83	0.81	0.83	0.83	0.89	0.94	0.75	0.79
CaO/Na_2O	8.91	8.80	4.84	5.38	7.58	9.47	4.27	4.77
CaO/TiO_2	23.76	19.81	10.08	13.82	19.83	22.06	20.18	45.96
Al_2O_3/TiO_2	28.50	24.55	12.08	16.60	22.20	23.29	26.61	58.16

(1) Melt inclusion in Cr-spinel phenocryst (Le Roex et al., 1981).
(2) Melt inclusion in Cr-spinel phenocryst (Le Roex et al., 1981).
(3) Melt inclusion in olivine phenocryst (Fujii & Fujioka, 1978).
(4) Melt inclusion in plagioclase phenocryst (Dungan & Rhodes, 1978).
(5) Melt inclusion in olivine phenocryst (Dungan & Rhodes, 1978).
(6) Average melt inclusion in Cr-spinel (Donaldson & Brown, 1978).
(7) Melt inclusion in plagioclase phenocryst (Price et al., 1986).
(8) Melt inclusion in plagioclase phenocryst (Price et al., 1986).

Mg# and CIPW norm calculated on the basis of $Fe^{2+}/(Fe^{3+}+ Fe^{2+}) = 0.9$, nd not determined.

minimal or have been taken into account. The inclusion compositions are compared with primitive MORB glasses in the projection from Di and plagioclase (An+Ab) in Fig.24a, b. The glass inclusion compositions are all primitive, with high Mg# (0.68-0.78). In the projection from Di most of the inclusions plot within or close to the primitive MORB glass compositions (Fig.24a). However glass inclusions from calcic plagioclase phenocrysts from the southwest Indian ridge (Price et al., 1986) plot away from the primitive MORB glasses due to their high MgO contents (13.70-14.20 wt%). In the projection from plagioclase (An+Ab), glass inclusions can be separated into two groups, which are discussed separately below:

(1) glass inclusions plotting with primitive MORB glasses. Glass inclusions reported by Dungan & Rhodes (1978), Donaldson & Brown (1977) and Fujii & Fujioka (1978) plot within the primitive MORB glass spectrum. However the composition of the inclusions is unlike any primitive MORB glass in low Al_2O_3 contents (14.21-14.50 wt%) and high CaO/Al_2O_3 ratios (0.83-0.94). The difference between the primitive glass compositions and MORB compositions is evidence for processes of magma mixing occurring amongst MORB suites (Dungan & Rhodes, 1978). The glass inclusions although not primary melt compositions are very similar in composition to equilibrium partial melts from the relatively depleted Tinaquillo lherzolite composition. The glass composition identified by Donaldson & Brown (1977) could be derived from a 15kbar olivine + orthopyroxene + clinopyroxene + liquid cotectic from Tinaquillo with minor olivine fractionation.

(2) glass inclusions plotting below primitive MORB glasses. These glass inclusions are possible primary melt compositions. Glass inclusions in Cr-spinel phenocrysts from the FAMOUS area (Le Roex et al., 1981) plot in a similar position to 8 (no.1 Table 14) and 12kbar (no.2 Table 14) olivine + orthopyroxene + clinopyroxene + liquid cotectics from MORB pyrolite in both projections from Di and plagioclase (Ab+An) and have similar major element contents to the equilibrium partial melts from MORB pyrolite. Similarly the two MgO-rich glass inclusions reported by Price et al. (1986) from the western Indian Ocean (Table 14, no.s 7, 8) plot in a similar position to a 18kbar olivine + orthopyroxene + clinopyroxene + liquid cotectic from MORB pyrolite, are similar in major element composition to the equilibrium partial melts from MORB pyrolite.

In summary amongst primitive glass inclusions from MORB are primary magmas from 8 to 18kbar based on a MORB pyrolite mantle source. The glass inclusions as well as the presence of calcic plagioclase and magnesian

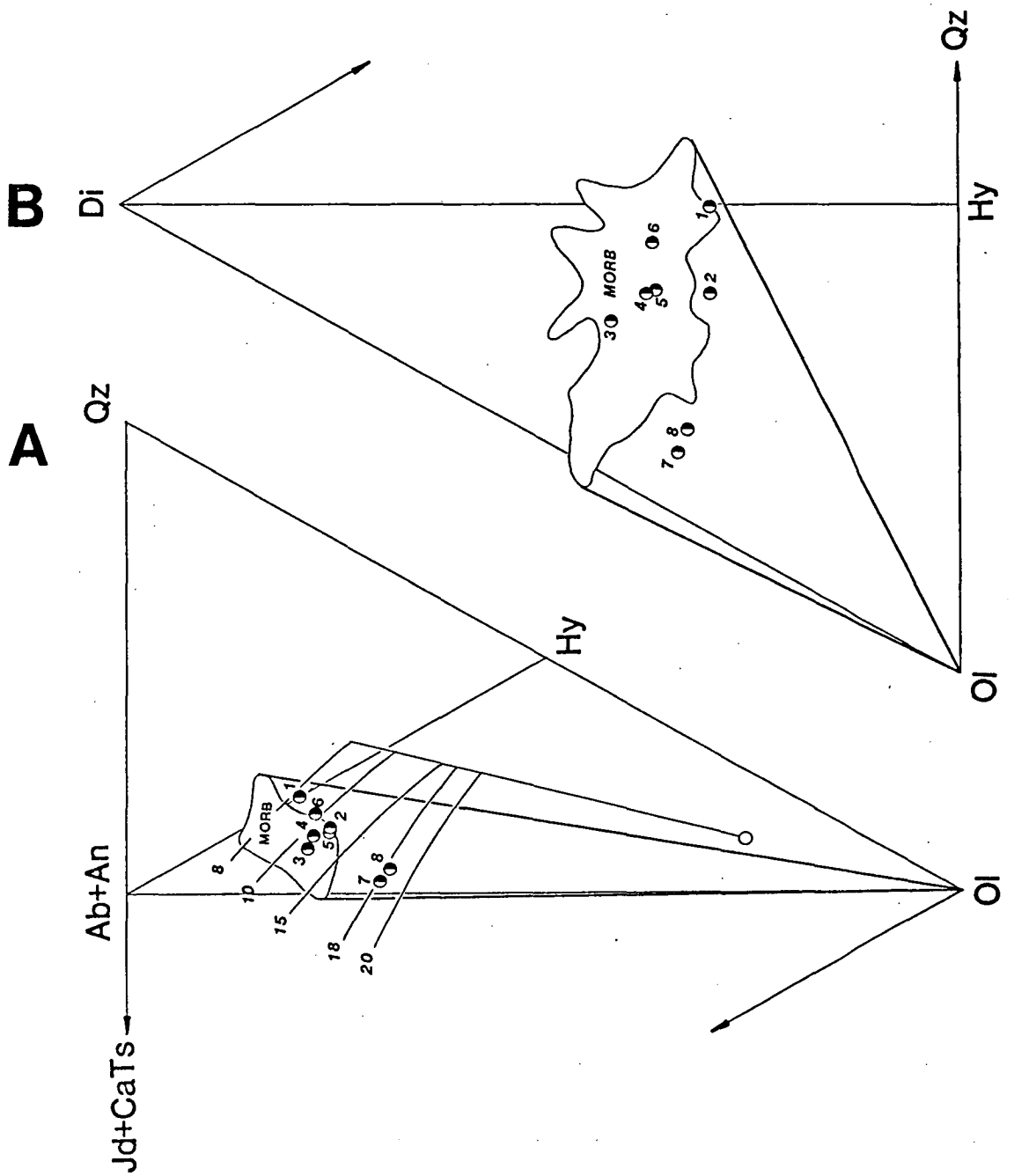

Figure 24.

The compositions of primitive MORB glass inclusions compared to equilibrium partial melt compositions from MORB pyrolite and primitive MORB glasses in the CIPW molecular normative basalt tetrahedron projected from diopside onto the base jadeite plus calcium tschermak's molecule (Jd + CaTs)-quartz (Qz)-olivine (Ol) in A, and from plagioclase (Ab + An) onto the face olivine (Ol)-diopside (Di)-quartz (Qz) in B. Lines and cotectics as for Fig.22.

(◑) numbered 1 to 8 are primitive MORB glass inclusions from Table 14.

(○) MORB pyrolite.

diopside megacrysts (Duncan & Green, 1980, 1987) provide evidence of primary melt compositions from more depleted mantle sources represented by Tinaquillo lherzolite. Such compositions are obscured amongst MORB glass compositions due to the processes of magma mixing. (Dungan & Rhodes, 1978; Donaldson & Brown, 1978; Thompson & Humphris, 1980).

2.7 PRIMARY MORB MAGMAS

The results of the melting study on MORB pyrolite and Tinaquillo lherzolite and the comparison of equilibrium melt compositions to the range in primitive MORB glasses, primitive trapped glass inclusions and MORB picrite compositions suggests that primary magmas parental to common MORB segregate from upwelling mantle peridotite at pressures of between approximately 8 to 25kbars, melt compositions ranging from alkali-rich slightly ne-normative picrites, to olivine-hypersthene picrites and to olivine and quartz normative tholeiite. The overwhelming majority of primitive MORB glasses are not primary magmas at 10kbar pressures (PART I) but are the result of olivine fractionation (11-25 wt%) from primary magma formed between the pressures of 15-25kbars. However amongst the range of primitive MORB glass compositions are compositions that are primary or near primary magmas at between 8 to 20kbars. The compositions of some primitive MORB glasses and glass inclusions requires that more depleted source compositions than MORB pyrolite are present.

2.8 DISCUSSION

The results of this study are in agreement with previous workers who have suggested that there exists a spectrum of primary MORB magma compositions (Francis, 1986; Bryan, 1983; Bryan et al., 1981; Grove & Bryan, 1983; Thompson, 1987; Klein & Langmuir, 1987; Christie & Sinton, 1986; Maaloe & Hansen, 1982). The results of this study are not in agreement with models which suggest that primary magmas are represented by the most primitive MORB glasses (Fujii & Scarfe, 1985; Fujii & Bougault, 1983; Presnall et al., 1979; Green & Ringwood, 1967). Three other studies have used larger data bases for the discussion of the petrogenesis of MORB and it is therefore important to compare the results of this study with these other studies. Klein & Langmuir (1987) have studied MORB major element systematics on a global basis, by correcting for crystal fractionation and comparing different MORB suites at an MgO content of 8wt%. Klein & Langmuir (1987) have demonstrated a strong negative correlation between FeO, Na_2O contents and CaO/Al_2O_3 ratios with axial

depth on a global scale. By applying the continuous melting model of McKenzie (1984) this global correlation can be explained by 'mean' melting intervals of between 5 to 15kbar. In the model of Klein & Langmuir (1987) picrite primary melts with >17 wt% MgO are not important in the generation of MORB, but primary magmas of between 10-17 wt% MgO are more dominant. Klein & Langmuir (1987) suggest that a temperature variation of over 200°C is required within upwelling oceanic mantle to account for the range in MORB compositions. This temperature interval agrees with the suggested range of temperatures of primary melts generated from a MORB pyrolite composition (1350°C-1550°C). The composition of primary melts generated during a continuous melting process will be substantially different from equilibrium batch partial melts present in this paper. It is clear however both from the major element composition of primitive MORB glasses and MORB compositions on a global scale (Klein & Langmuir, 1987) that they preserve a history of magma segregation from depths of a least 25kbars. If a continous melting process involving small melt fractions is involved then some mechanism is required to preserve picritic primary melt compositions from 20 to 25kbars, from being mixed into other melt fractions from shallower depths in the melting column. (see Thompson, 1987 for further discussion of this problem). Even if a continuous melting model is the most physically correct model, melt compositions would still be constrained to lie on olivine + orthopyroxene ± clinopyroxene + liquid cotectics and therefore still plot below primitive MORB glasses in the projection from plagioclase (Ab+An) in the basalt tetrahedron. Thus a range of olivine fractionation is still required to produce primitive MORB glasses. The calculations of such hybrid magma compositions is beyond the scope of this paper. However it is possible as the study by Klein & Langmuir (1987) suggests, that the equilibrium partial melts from MORB pyrolite approximate a 'mean' primary melt compositions, generated from the mixing of small melt fractions over a range of pressures.

Takahashi et al. (1987) have used a different approach for determining primary magma compositions to MORB. Using experimentally determined Kd's for CoO, MgO, FeO, NiO and MnO for olivine and liquid, they have incremently calculated the compositions of liquids in equilibrium with olivine until such stage as the calculated equilibrium olivine composition falls within the 'mantle array' for olivine in terms of NiO and MnO contents. This establishes the composition of the primary magma. Takahashi et al. (1987) suggest that primary magmas to MORB, range in MgO content from 11-16 wt%. Representative calculated primary melt compositions from Takahashi et al. (1987) are plotted in Fig.25a, b and are compared to

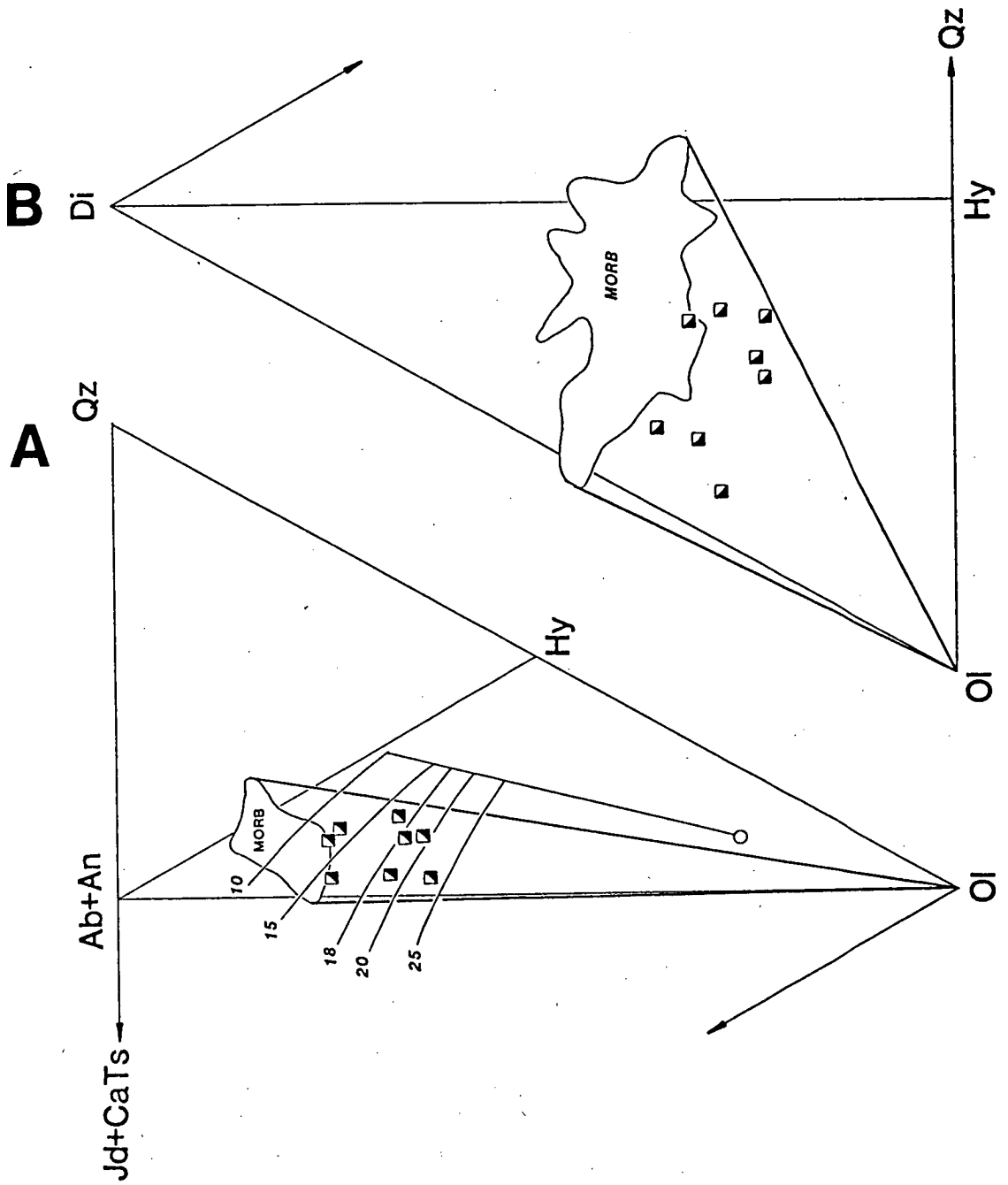

Figure 25.

Calculated primary MORB melt composition from Takahashi et al. (1987) compared with equilibrium partial melt compositions from MORB pyrolite and primitive MORB glasses in the CIPW molecular normative basalt tetrahedron projected from Di onto the base jadeite plus calcium tschermak's molecule (Jd + CaTs)-quartz (Qz)-olivine (Ol) in A, and from plagioclase (Ab + An) onto the face diopside (Di)-quartz (Qz)-olivine (Ol) in B. Lines and cotectics as for Fig.22.

(○) MORB pyrolite.

(◪) calculated primary MORB melt compositions from Takahashi et al. (1987).

primitive MORB glasses and equilibrium partial melts from MORB pyrolite. The calculated compositions mostly plot away from the primitive MORB glasses, however in the Di projection some plot close to the low Di end of the primitive MORB glasses. Compared to equilibrium partial melts from MORB pyrolite the calculated primary melts from Takahashi et al. (1987) represent magma segregation over pressures of 12 to 22kbars. The theoretical analysis of Takahashi et al. (1987) is in agreement with the experimental results from MORB pyrolite.

2.9 CASE STUDY IN MORB PETROGENESIS: FAMOUS-NARROWGATE-AMAR.

The FAMOUS-NARROWGATE-AMAR (FNA) area at 36° 47'N of the mid-Atlantic ridge is one of the most thoroughly documented areas of the mid-Atlantic ridge and has provided a large amount of data on the nature and composition of MORB (Bougault & Hekinian, 1974; Arcyana, 1977; Hekinian et al., 1976; Bryan & Moore, 1977; Langmuir et al., 1977; Bryan et al., 1979; Bryan, 1979a; Stakes et al., 1984; Le Roex et al., 1981; Nabelek & Langmuir, 1986; White & Bryan, 1977; Flower & Robinson, 1979; Bryan & Thompson, 1977). As most of the sampling was done by submersible dives there is good spatial and temporal control on the recovered lavas, not possible by dredging. Stakes et al. (1984) have demonstrated that the morphology of the rift valley area is dominated by either tectonic or volcanic processes, which are the result of the growth and solidification of ephemeral ridge-axis magma chambers (Stakes et al., 1984). The rift valley in the FAMOUS area is presently dominated by axial volcanic highs represented by Mt. Venus and Mt. Pluto, whereas the rift valley in the AMAR area is dominated by normal faulting. Of importance is the distinction between the younger pillowed units forming the central volcanic highs (Mt. Venus and Mt. Pluto), and the older sheet and massive lava flow units forming the valley floors and exposed in the rift valley walls. The younger pillowed units are of dominantly primitive compositions containing minor amounts of olivine as the main phenocryst phase, these basalts are also characterized by having relatively high Ni contents in olivine phenocrysts compared to the older series lavas (Nabelek & Langmuir, 1986; Le Roex et al., 1981). The older sheeted and massive flows, from the valley floors and walls, are characterized by more evolved compositions and include picritic basalts, plagioclase-pyroxene-olivine-phyric basalts, plagioclase-phyric basalts and aphyric basalts. These basalts belong to a low-Ni series due to low Ni in olivine phenocrysts relative to the younger pillowed lavas (Nabelek & Langmuir, 1986; Le Roex et al., 1981). Primitive glass compositions from these two distinctive series are plotted in the CIPW molecular normative

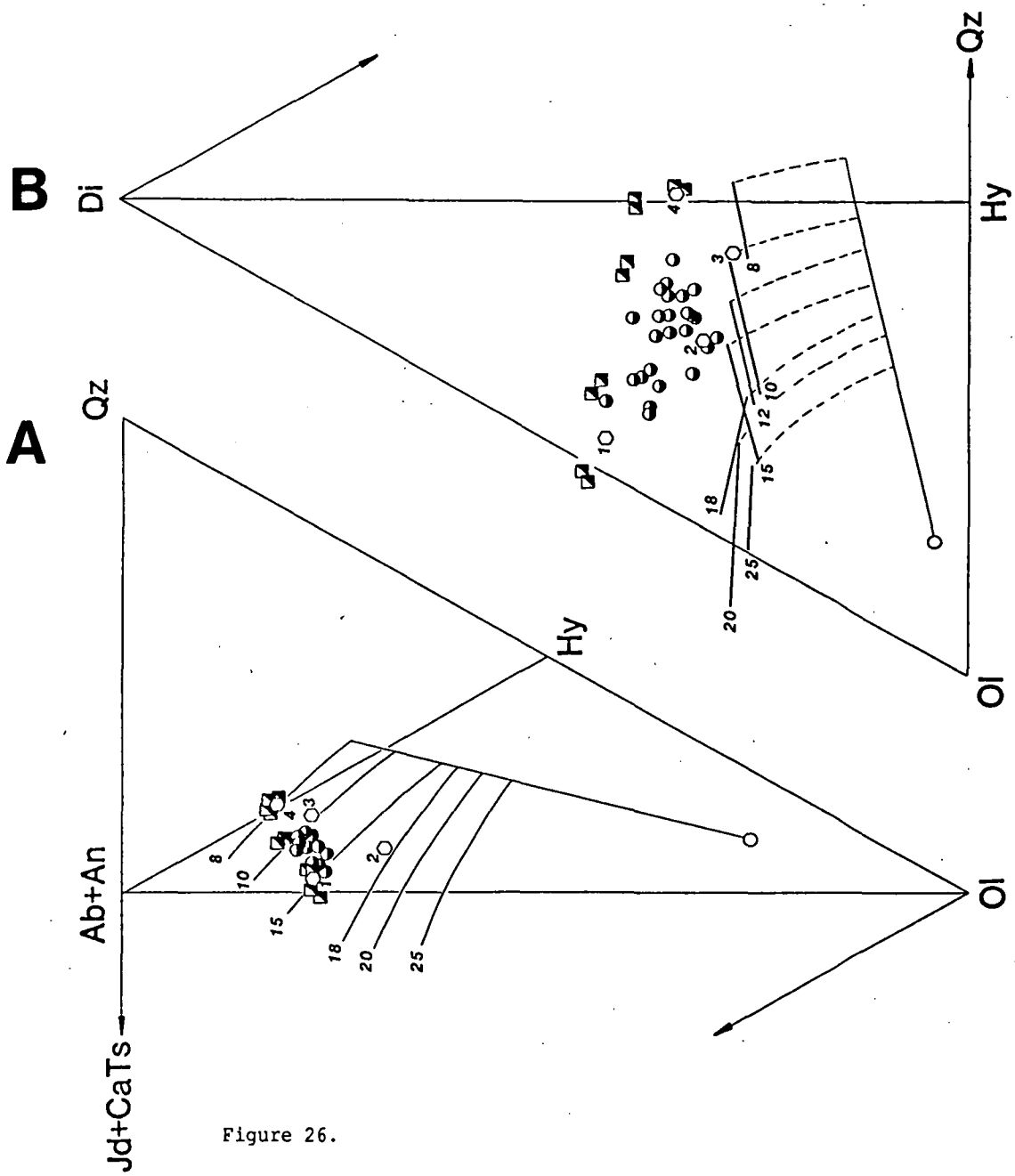

Figure 26.

Primitive glass compositions from the FAMOUS-NARROWGATE-AMAR area of the Mid-Atlantic ridge compared with equilibrium partial melt compositions from MORB pyrolite in the CIPW molecular normative basalt tetrahedron projected from Di onto the base jadeite plus calcium tschermak's molecule (Jd + CaTs)-quartz (Qz)-olivine (Ol) in A, and projected from plagioclase (Ab + An) onto the face diopside (Di)-quartz (Qz)-olivine (Ol) in B. In A lines are cotectics from MORB pyrolite as for Fig.22. In B cotectics as for Fig.18.

(◪) primitive glass compositions from the low-Ni series lavas (see Table 15 for data sources).

(◓) primitive MORB glass compositions from the high-Ni series lavas (see Table 15 for data sources).

(○) numbered 1 to 4 are as follows:

1 high-olivine parental composition (Bryan, 1979).

2 calculated parental magma composition to FAMOUS picrite basalts P_1 (Le Roex et al., 1981).

3 primitive olivine basalt composition P_2 (Le Roex et al., 1981).

4 low-olivine parental composition (Bryan, 1979a).

basalt tetrahedron in Fig.26. The range in major element composition of the two glass groups is summarized in Table 15. Primitive glass compositions from the low-Ni series are defined by glasses from picrite basalts, glasses from Fracture zone A (Bryan, 1979a), glasses from walls at the south and north valleys of the FAMOUS areas (Bryan, 1979a), and primitive glass compositions identified from the Narrowgate and AMAR valleys (Stakes et al., 1984). Also plotted are the high-olivine and low-olivine parental compositions from Bryan (1979a), and the parental magmas to picritic basalts and olivine basalts from Le Roex et al. (1981). Glasses from the high-Ni series are all from Bryan & Moore (1977). Primitive glasses from Fracture zone A (Bryan, 1979a) are distinctive in being slightly ne-normative. The low and high Ni series can be distinguished both in Fig.26a and 26b. The low Ni series is characterized by a large range in silica saturation and high CaO contents (Table 15). The high Ni series has lower CaO contents and a more restricted range in silica saturation. The high-olivine parental composition of Bryan (1979a) is a hybrid of glasses from low and high Ni series glasses as well as Fracture zone A glasses. The low-olivine parental composition of Bryan (1979a) is an average of primitive glasses from the low-Ni olivine series lavas.

Although two magma series have been identified in the FNA area, no single magma composition can be parental to an entire series as there is a large variation in TiO_2 contents and Na_2O/K_2O ratios at the high Mg#>0.68 end of the glass compositions from both series (Stakes et al., 1984). The range in silica saturation displayed by the FAMOUS glasses also argues against a single parental magma type but could be consistent with an array of primary magmas arriving at the base of sub-axial magma chambers. Amongst the glass compositions there is evidence for decoupling of minor elements (TiO_2, K_2O, P_2O_5) from major elements suggesting open-system magma chamber and magma mixing processes are taking place (O'Hara & Mathews, 1981).

The low CaO contents of the high-Ni series glasses indicates that they have undergone little olivine fractionation from primary olivine tholeiite magmas. The range in silica contents in the high-Ni series glasses indicates that primary liquids segregated from a MORB pyrolite source at between approximately 18-20kbar to 10kbars with little olivine fractionation (<10wt%). The primitive olivine tholeiite magma of Le Roex et al. (1981) is identical to 10kbar equilibrium liquids from MORB pyrolite (PART I) and represents a 10kbar primary olivine tholeiite liquid. However Le Roex et al. (1981) found that this composition was an unsuitable

Table 15

Famous-Narrowgate-Amar lava series

	Olivine Basalts High-Ni series	Picrite basalts low-Ni series	Fracture Zone
SiO_2	48.20 - 50.48	48.75 - 51.40	48.20
TiO_2	0.65 - 0.85	0.63 - 0.93	0.57
Al_2O_3	15.23 - 16.70	14.80 - 16.60	16.95
FeO	8.04 - 9.18	7.90 - 8.46	8.50
MgO	9.43 - 10.70	8.82 - 10.50	10.00
CaO	11.56 - 12.50	12.70 - 13.79	12.75
Na_2O	1.94 - 2.41	1.84 - 2.01	2.32
K_2O	0.04 - 0.16	0.05 - 0.14	0.04

Data sources: Bryan (1979), Stakes et al. (1984), Bryan & Moore (1977), Hekinian et al. (1976), Langmuir et al. (1977), Fujii & Bougault (1983), Bender et al. (1978), Le Roex et al. (1981).

composition to be parental to other more evolved olivine basalts in their study sample.

The low-Ni series glasses, including Fracture zone A glasses, are characterized by a large range of silica saturation indicating a larger range of partial melting (15-30 wt%) with both lherzolite and harzburgite residues. The high CaO contents indicate relatively high degrees of olivine fractionation. Based on the equilibrium liquids from MORB pyrolite depths of segregation of 20-25kbars are required to explain the low-Ni series glasses with between 20-25wt% olivine fractionation. Table 16 summarizes the results of this study concerning the nature of primary magmas in the FNA area with the volcanic cycle outlined by Stakes et al. (1984). It appears that during episodic periods of faster spreading, primary MORB magmas segregate from deeper depths and result from a larger range of partial melting and undergo greater amounts of olivine fractionation, than during periods of slower spreading. During periods of faster spreading primary picrite melts are trapped at the base of steady-state magma chambers where they undergo crystal fractionation.

The depths of magma segregation determined for the two magmas series at FNA agrees with the analysis of Klein & Langmuir (1987) and Nabelek & Langmuir (1986) concerning Ni-olivine relationships. Klein & Langmuir (1987) suggest that if MORB suites display differences in Ni, the suite with the lower Ni contents at a given MgO may be derived from parental magmas with higher MgO contents, derived from greater extents of melting at greater depth.

The parental magma for the picritic basalts (P_1) from Le Roex et al. (1981), in the projection from Di (Fig.26a) falls on or near an 18kbar cotectic from MORB pyrolite. However in the projection from plagioclase (Ab+An) the composition P_1 plots above the 18kbar cotectic suggesting it is not a primary magma and has undergone some degree of olivine fractionation, possibly from a more picritic parent lying on a 20 or 25kbar cotectic.

Table 16

Summary of the volcano-tectonic cycle of the FAMOUS-Narrowgate-AMAR area mid-Atlantic ridge and the composition of primary magmas based on Stakes et al. (1984)

Stage	Description	Primary magma compositions
0	Temporary period when no magma chamber exists beneath the rift valley. Melts expelled from the mantle rise directly to the surface through tensional fractures continually created by spreading.	Primary olivine tholeiite liquids from pressures of 10-18kbars, little (<10 wt%) or no olivine fractionation. Lherzolite residue, 20-25 wt% partial melting of a MORB pyrolite source.
1	Growth of a new magma chamber. Melts expelled from the mantle begin to collect in a new, inflating magma reservoir beneath the ridge axis. Some melt may bypass the small protochamber, leaking directly through to the surface.	
2	Steady state magma chamber. Replenishment balances crystallization and loss of melt to the surface.	Primary picrite liquids from pressures of 20-25kbars, lherzolite to harzburgite residue, large range of partial melting (17-30 wt%) of a MORB pyrolite source followed by, extensive (20-25 wt%) olivine fractionation.
3	Early stages of magma chamber solidification. Crystallization progressively gains ground on replenishment, and the chamber volume decreases.	
4	Advanced stage of magma chamber solidification. Replenishment ceases; crystallization plus or minus loss of melt to the surface causes chamber volume to rapidly diminish.	
5	Equals stage 0.	

PART III

DREDGED IGNEOUS ROCKS FROM THE NORTHERN TERMINATION OF THE TOFUA MAGMATIC ARC, TONGA AND ADJACENT LAU BASIN

3.1 INTRODUCTION

During the cruise of the 'Natsushima' to the North Tonga Ridge and Lau Basin in 1984, igneous rocks were recovered from seven dredge stations (Falloon, 1985). Six different morpho-tectonic elements of the intra-oceanic arc were sampled, while at one station backarc basin crust was sampled. In this PART, we present petrographic, wholerock major and trace element data and discuss the geochemical affinities of the dredged rocks. A more detailed treatment of the petrogenetic implications of some of this data will be presented in PART V.

Analysis of the petrogenesis of Tongan arc lavas has so far been limited to the study of axial chain volcanoes of the Tofua magmatic arc (Cole, 1982; Bryan & Ewart, 1971; Bryan, 1979b; Bryan et al., 1972; Ewart & Bryan, 1972; Ewart et al., 1973; Ewart, 1976; Ewart et al., 1977). These volcanoes are constructional features of relatively minor scale in terms of the volume of the Tongan arc. As passage of magmas from the mantle through arc crust to eruption provides ample opportunity for extensive fractionation and mixing of parental and evolved magmas, it is likely that the compositions of lavas erupted from the volcanoes will not be representative of the arc crust as a whole. This possibility emphasises the importance of the dredged samples. As they were are all dredged from water depths generally >2000 m, they offer an insight into the nature of arc magmatism away from axial chain volcanoes, a topic about which little information presently exists.

The igneous rocks recovered from each dredge station are geochemically distinct from the rocks of the Tonga Islands as well as from each other, indicating considerable geochemical complexity in the Tonga arc. Dredge stations on the North Tonga ridge and forearc were from a relatively restricted geographical area. Within this area, a range of mantle sources and possibly a range of partial melting conditions are

required to explain the geochemistry of the dredged rocks. Amongst the dredged rocks are highly magnesian lavas with affinities to both boninites and low-Ti ophiolitic basalts. The presence of these high-magnesian lavas has important implications for the petrogenesis of these distinctive rocks.

3.2 GEOLOGICAL AND TECTONIC SETTING

The Tonga ridge, trench and forearc together with the Lau backarc basin and remnant arc (the Lau-Colville ridge) form an intra-oceanic island arc system (Fig. 27). The Tonga ridge itself is morphologically complex, in its southern part consisting of two island chains separated by the 1800 m deep Tofua trough. The eastern chain of islands, the 'Vava'u-Eua' block, is covered by limestone and with the exception of Eua lacks exposed volcanic rock. The 'Vava'u-Eua' block represents an older Eocene to mid-Miocene forearc, formerly joined to the once active Lau-Colville ridge (Gill, 1976; Gill et al., 1984; Hawkins et al., 1984; Hawkins & Falvey, 1985; Duncan et al., 1985); it has since been separated by the opening of the Lau Basin. The western chain of islands is Plio-Pleistocene in age and comprises the presently active island arc, the 'Tofua magmatic arc' (TM-arc). This active chain of volcanic islands extends as far north as the islands of Tafahi and Nuiatoputapu; eruptive products range (in SiO_2 content) from basaltic andesite to dacite, with basaltic andesite being dominant (Ewart et al., 1973; Ewart et al., 1977; Bryan, 1979b). The most recent volcanic activity was the 1968 Metis Shoal eruption (Melson et al., 1970). The TM-arc north of the islands of the Tonga ridge is truncated by a graben subparallel to the bend of the Tonga Trench, where there is a transition from subduction to transform tectonics (Giardini & Woodhouse, 1986). The North Tonga ridge is morphologically distinct from the South Tonga ridge, as the 'Vava'u-Eua' block is no longer present; instead the North Tonga ridge has a deeply submerged, gently-dipping forearc.

3.3 DREDGE LOCATIONS

Dredge stations which recovered igneous material are shown in Fig. 28 and details are given in Table 17. Station 15, which sampled acoustic basement outcropping on the upper trench slope, yielded several kilograms of small fragments of volcanic and subvolcanic rocks present as clasts in a canyon-fill, debris-flow type deposit of Late Miocene to Early Pliocene age (Honza et al., 1985). The main clast type is a clinopyroxene + plagioclase-phyric basaltic andesite; dolerite and gabbro clasts with the same

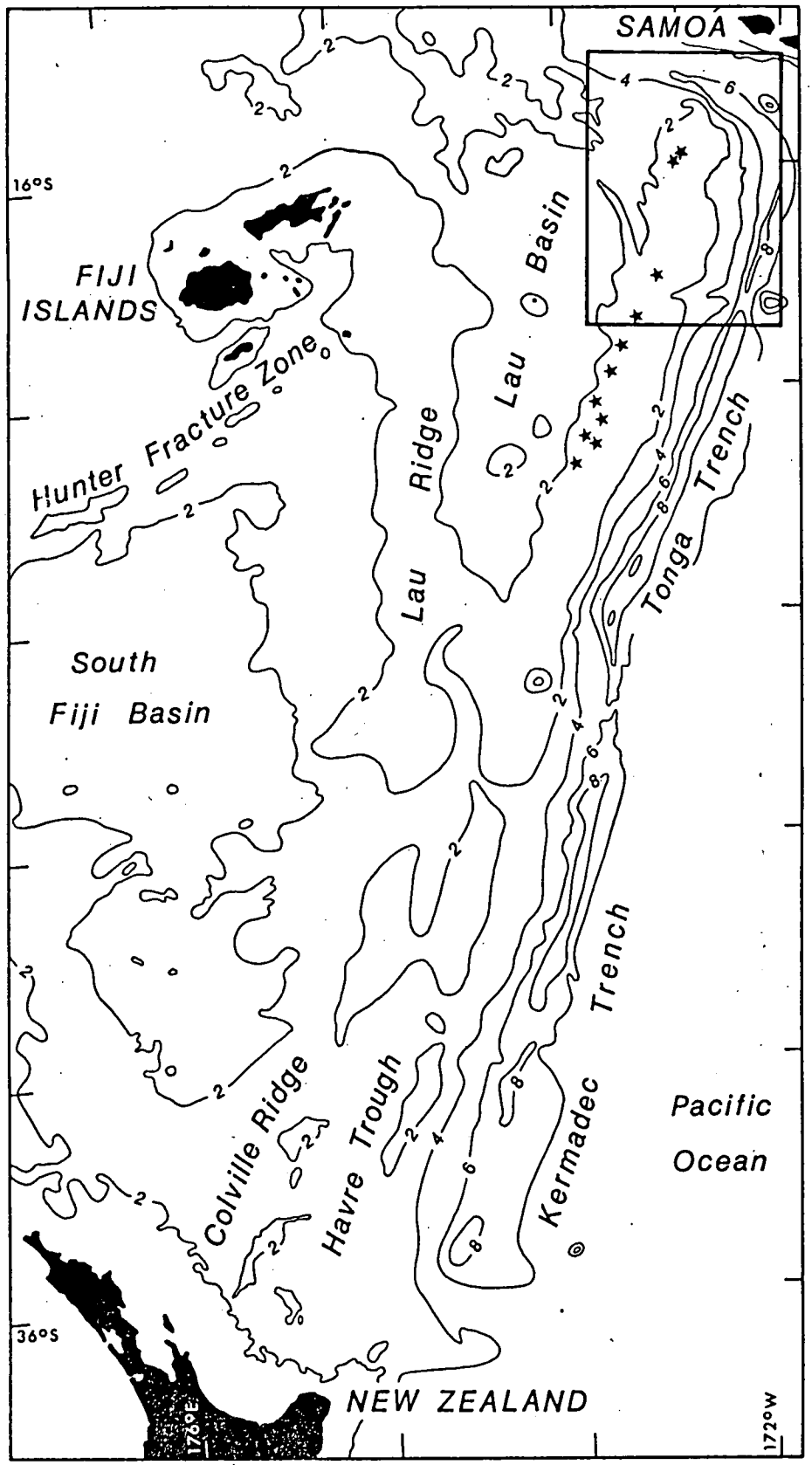

Figure 27.

Locality map southwest Pacific, showing the relationship of the Tonga ridge and trench to other elements of the SW Pacific region. (★) represents islands of the young Tofua magmatic arc. Square outline is the area covered by Fig.28. Water depth contoured in 1000's of metres.

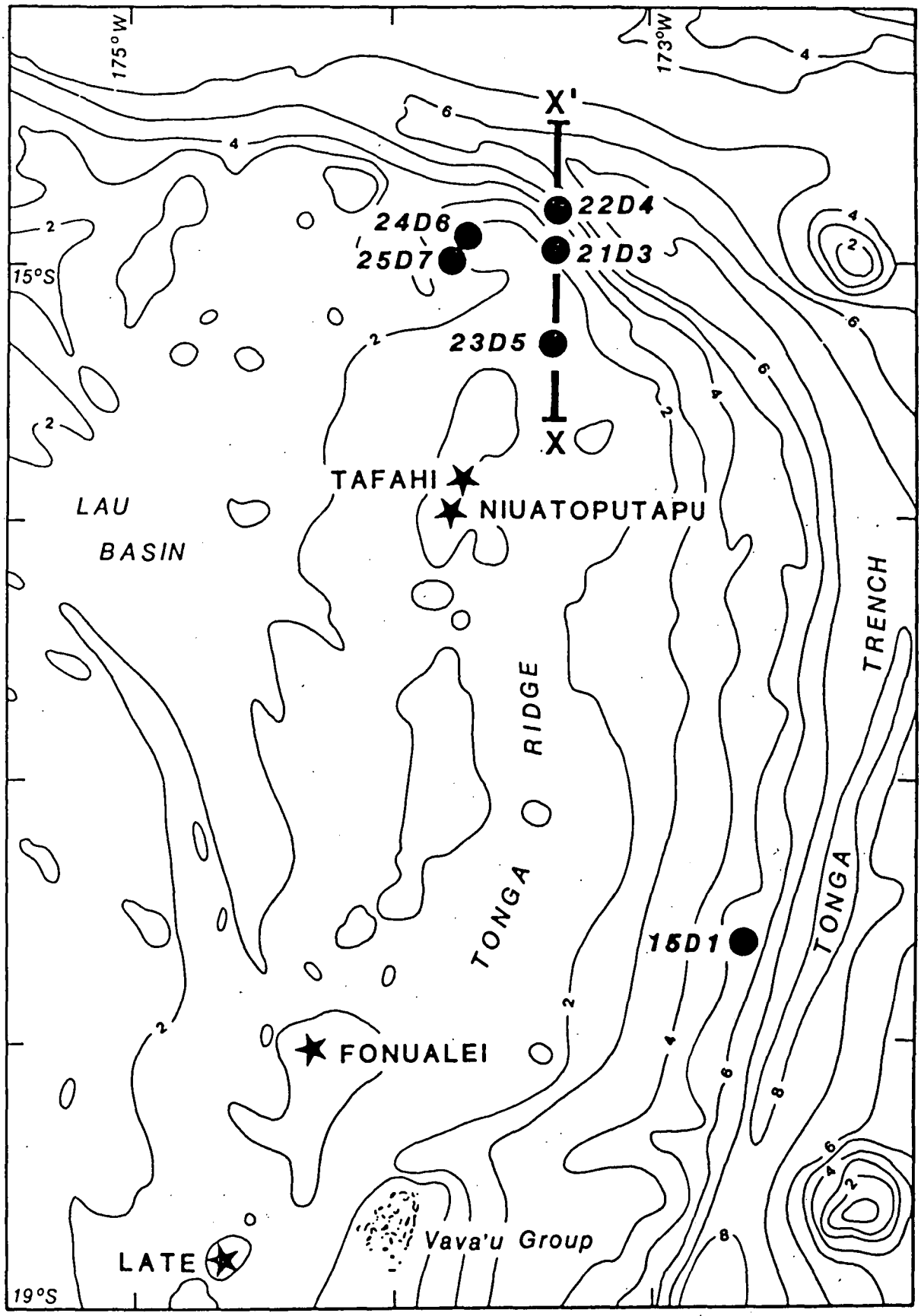

Figure 28.

Locality map of the north Tonga ridge showing the location of the dredge stations which recovered igneous rock. Station 31, not shown on this map, is located at the southeastern end of the Peggy Ridge in the adjacent Lau Basin. Line marked X to X′ is the line of the seismic profile shown in Fig.29.

Table 17

Summary of dredge locations, which recovered igneous material during the 1984 cruise of the 'Natsushima'

Dredge	Station	Latitude S	Longitude W	Water Depth (m)	Area	Recovery
1	15	17 37.7	172 41.5	4325-4860	Trench wall	Small basalt clasts, volcanogenic conglomerates, volcaniclastics.
3	21	14 57.9	173 23.4	1500-2000	Transform-Trench wall	Large haul of basaltic rock, volcaniclastics.
4	22	14 49.0	173 23.0	4400-4500	Transform-Trench wall	Metagabbros, plagiogranite, serpentinite, volcaniclastics.
5	23	15 19.6	173 23.9	1600-2250	Forearc	Blocks of vesicular basalts, volcaniclastics.
6	24	14 53.5	173 43.8	3090-3260	North Tonga ridge	Two large pieces of vesicular pillow basalt, volcaniclastics.
7	25	14 59.6	173 45.6	2728-2805	North Tonga ridge	Large haul fresh pillow lavas.
11	31	17 21.2	176 46.7	2220-2230	SE Peggy Ridge Lau Basin	Volcaniclastics, pumice, one small piece of pillow rind.

mineralogy as the basaltic andesite are also present. The igneous rocks represent an earlier volcanic episode than the young Tofua magmatic arc.

Stations 21 and 22 are on a large isolated block (Fig. 29), separated from the North Tonga ridge by a major graben. Station 21 provided a large amount of fresh porphyritic and aphyric basaltic andesite and andesite, while large blocks of fresh and altered plutonic rocks (metagabbro and plagiogranite), altered basalt and serpentinite were recovered from station 22.

Station 23, on the southern scarp of the graben (Fig. 29), yielded one large block and several smaller pieces of basaltic andesite and andesite, along with small clasts of highly vesicular olivine + orthopyroxene + clinopyroxene-phyric lava.

Stations 24 and 25 are on knolls aligned subparallel to the curved northern part of the Tonga Trench. Preliminary acoustic profiles show horsts and grabens with normal faults in this area (Honza et al., 1985). Large amounts of highly vesicular, fresh pillow basalt fragments with fresh glassy rinds were recovered from these stations.

Station 31, located at the southeastern end of the Peggy Ridge in the Lau Basin, in an area extensively sampled by previous dredging (Hawkins, 1976), gave rise to one small piece of pillow rind.

Stations 21, 22, 24 and 25 are in an area extensively sampled by the Russian vessel 'R/V Kallisto' (Sharaskin et al., 1983), which dredged mainly in deep water, recovering proportionately larger quantities of altered ultramafic and mafic plutonic material; 'boninite' was reported near stations 24 and 25. Stations 24 and 25 were chosen to confirm the Russian sampling.

3.4 ANALYTICAL TECHNIQUES

Major and trace element geochemistry, including REE, of representative samples from each dredge station are presented in Tables 19, 20 and 21. Major element geochemistry was determined by X-ray fluorescence spectrometry (XRF) using the method of Norrish & Hutton (1969). Ba, Rb, Sr, Zr, Nb, Y, Sc, Ni, Cr and V were determined on pressed powdered discs by XRF. REE's were also determined by XRF using the method of Robinson et al. (1986).

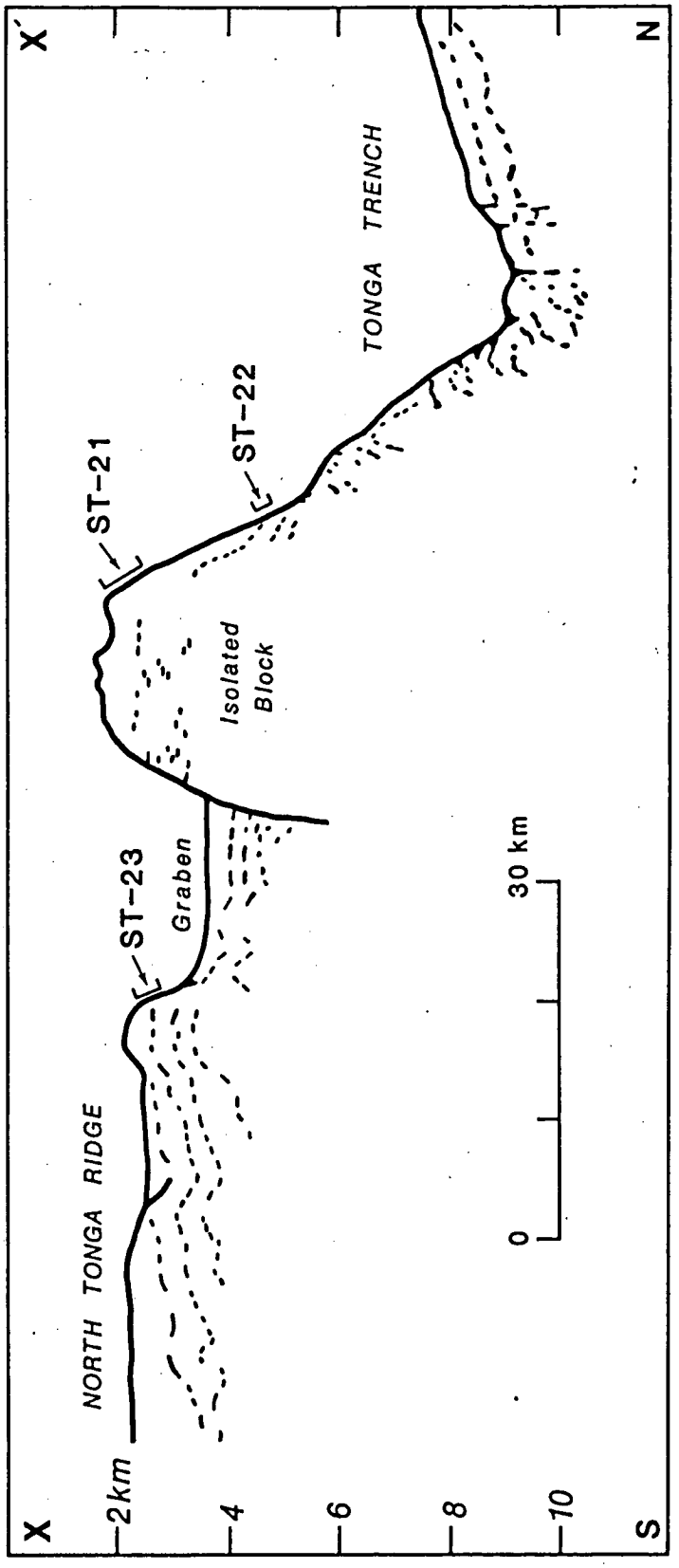

Figure 29.

Single channel seismic profile across the north Tonga ridge indicating the large graben and isolated block at the termination of the north Tonga ridge, and the positions of dredge stations 21, 22 and 23. Seismic profile is taken from Kitekei'aho et al. (1985).

Because each dredge station has its own distinctive petrographic and geochemical characteristics, the geochemical affinities of each dredge station will be presented separately. Before the dredge stations are discussed, it is worthwhile briefly outlining the known geochemistry of the TM-arc, because it will serve as a reference point in the discussion of the geochemical affinities of the dredged rocks.

3.5 TOFUA MAGMATIC ARC

The TM-arc, defined by the exposed Tongan volcanic islands, and dominated by basaltic andesites, with minor andesites and dacites (Ewart et al., 1973; Ewart et al., 1977; Bryan & Ewart, 1971; Bryan, 1979b), can be conveniently subdivided into two parts on geographic and geochemical criteria. The first part is defined by the volcanic islands of South Tonga which includes the basaltic andesites, andesites and dacites of Fonualei, Late, Hunga Ha'apai and Tofua. The basaltic andesites, which represent the least evolved compositions from the islands, have SiO_2 contents of between 53-55 wt% (Ewart et al., 1973) and form a well-defined tholeiitic Fe-enrichment trend on the FeOt/MgO vs SiO_2 diagram (Fig. 30). The basaltic andesites have high abundances of large ion lithophile (LIL) elements relative to the heavy Rare Earth elements (HREE); REE abundances are low, and chondrite-normalized REE patterns are flat to slightly light Rare Earth element (LREE)-depleted; a representative pattern from Late (sample L1) is shown in Fig. 31d. The second group is defined by the basaltic andesites from the Northern Tongan island of Tafahi and a single andesite from Niuatoputapu (Ewart, 1976). The basaltic andesites from Tafahi are distinctly different from those of the South Tonga islands, having slightly lower SiO_2 (51-54 wt%) and TiO_2 (0.36-0.41 wt% compared with 0.49-0.64 wt%) contents, and lower incompatible element abundances. The REE patterns are similar to basaltic andesites from the South Tonga islands, but REE abundances are lower (sample T-116 in Fig. 31d). One distinguishing characteristic of the Tafahi basaltic andesites is their low Zr content (8 ppm; Ewart, 1976), reflected in high Ti/Zr ratios compared with those from the South Tonga islands (269-307 compared with 119-144). Such high ratios are characteristic of very depleted (depleted in the abundance of silicate incompatible elements relative to a chondritic mantle model, Gast, 1968) sources (Sun & Nesbitt, 1978). The low REE and other incompatible abundances, and the lower TiO_2 contents compared with those of the South Tonga islands, are consistent with the basaltic andesites of the North Tonga islands having been derived from a mantle source more depleted in

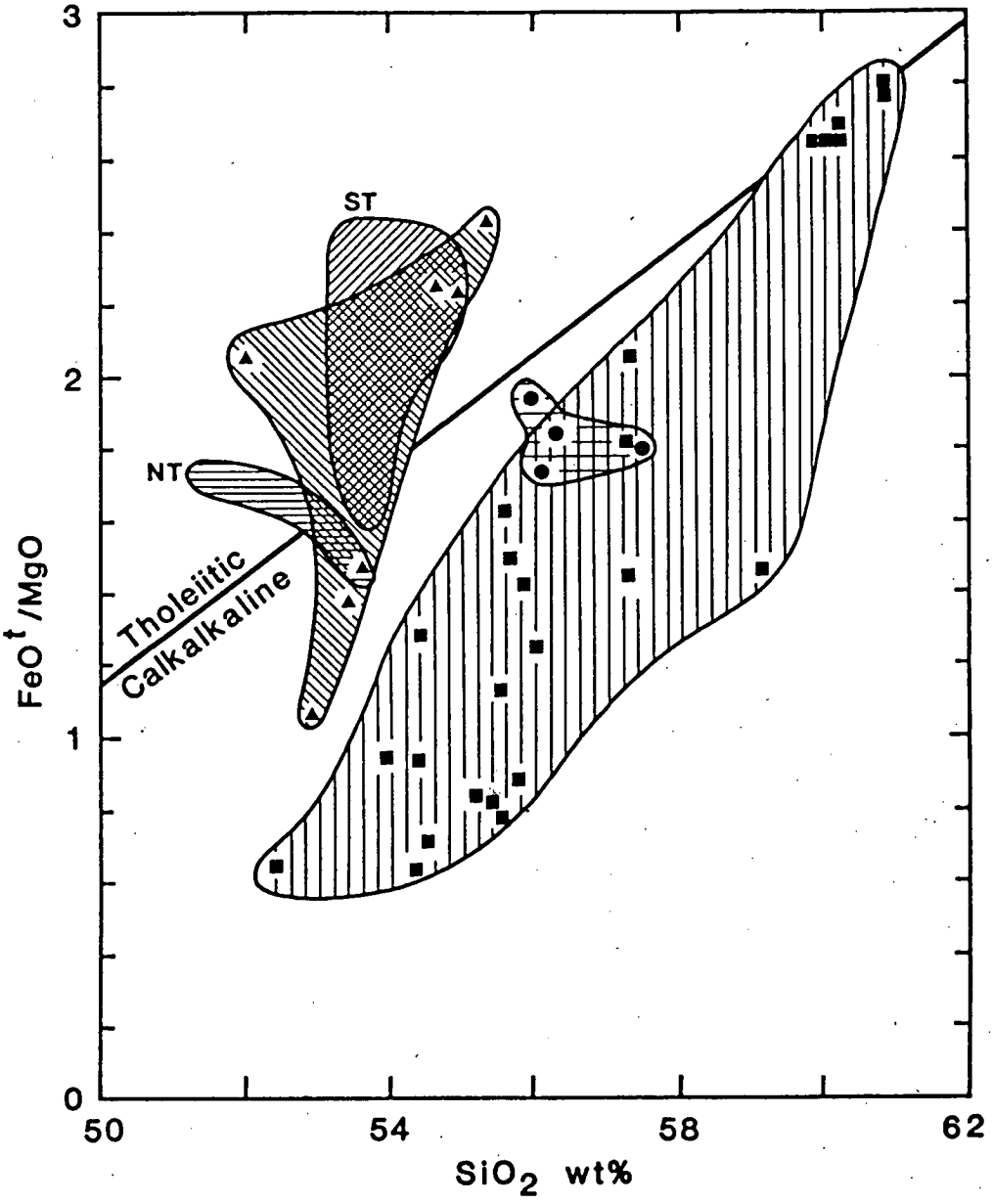

Figure 30.

FeO^t/MgO versus SiO_2 relationships of basaltic andesites and andesites from stations 15, 21 and 23 compared with those of the Tofua magmatic arc. The line is the dividing line between tholeiitic and calcalkaline suites of Miyashiro (1974). NT and ST are north and south Tonga respectively, the two main groups within the Tofua magmatic arc, as discussed in the text. Data for north Tonga and south Tonga taken from Ewart et al. (1973) and Ewart (1976).

(■) are station 21 basaltic andesities and andesites; data taken from Table 19 and Falloon unpubl. data.

(●) are station 23 basaltic andesites; data from Table 21.

(▲) are station 15 basaltic andesites; data from Table 19.

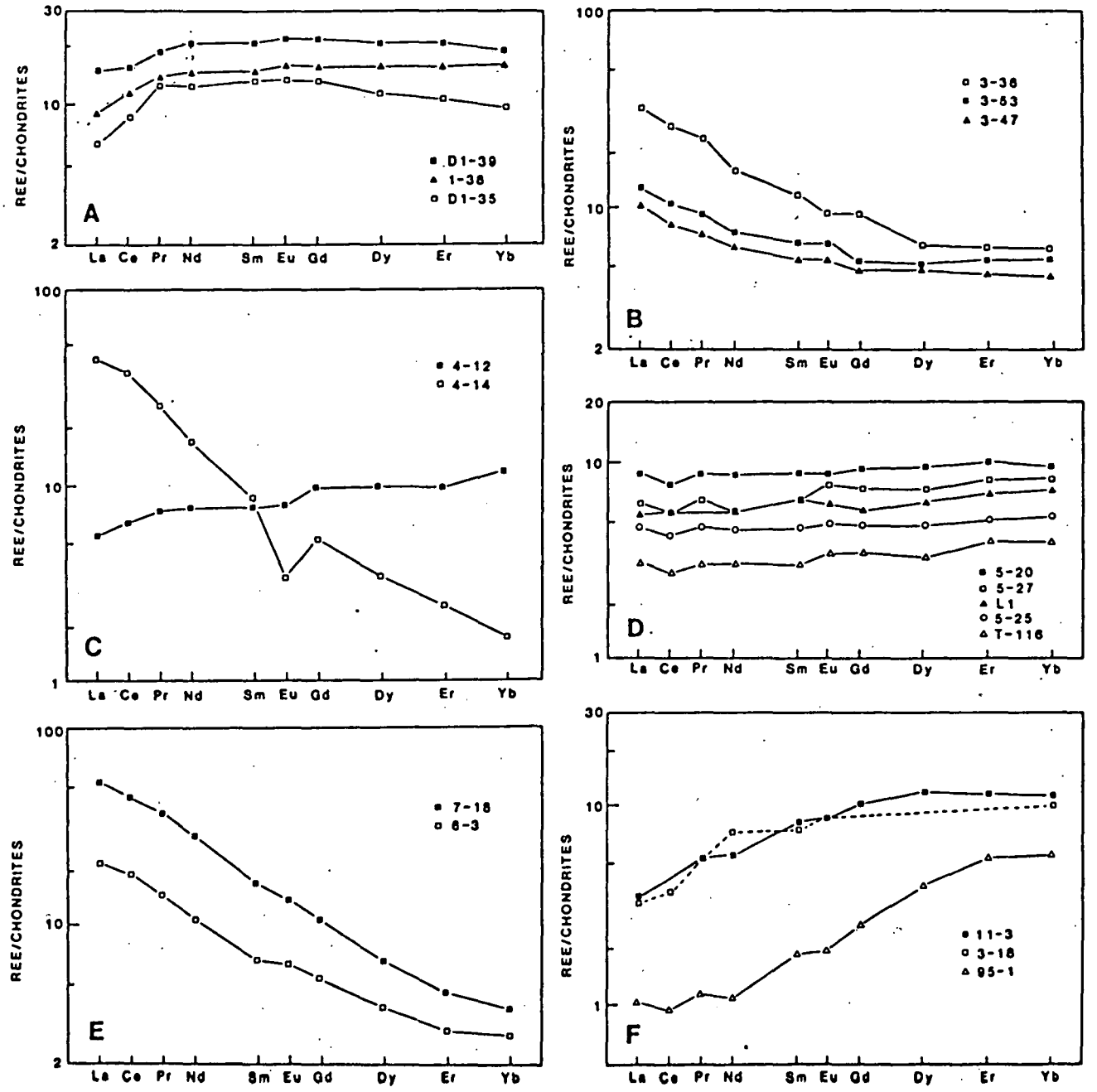

Figure 31.

REE patterns for dredged igneous rocks from the 1984 'Natsushima' cruise.

A. Station 15 basaltic andesites.

B. Station 21 basaltic andesites and one andesite (3-36).

C. Station 22, 4-12 ia a metagabbro, 4-14 a plagiogranite.

D. Station 23, as well as representative patterns from the Tofua magmatic arc; sample L1 is from south Tonga and sample T-116 from north Tonga (Ewart et al., 1977). Samples 5-20 and 5-27 are basaltic andesites, sample 5-25 is a Group B high-mg lava (Table 18).

E. High-mg lavas from sations 24 (6-3) and 25 (7-18).

F. REE pattern of glass rind 11-3 from station 31 compared with a primitive MORB glass DSDP3-18-7-1 (Frey et al., 1974) and a Lau Basin basalt 95-1 (Hawkins, 1976; Gill, 1976).

silicate incompatible elements than the basaltic andesites of the South Tonga islands.

In the following sections the petrography, geochemistry and geochemical affinities of the dredged samples is presented. Important petrographic features of the dredged lavas are summarized in Table 18.

3.6 STATION 15

3.6.1 Petrography

Lava clasts from station 15 are microphyric basaltic andesites containing plagioclase (~5%) and clinopyroxene (~1-2%) as single euhedral microphenocrysts as well as microglomerocrysts. The clasts display a range of groundmass textures reflecting a range of cooling rates. Some clasts come from the glassy selvages of pillows, where the groundmass consists mainly of brown devitrified glass with sparse plagioclase microlites. Others display more coarse-grained subophitic textures. Alteration in coarser-grained samples is confined to interstices where chlorite and yellow-green smectite replace original glass.

A single clast of metagabbro, too small for analysis, also from station 15, consists of approximately equal proportions of coarse-grained plagioclase and amphibole. The amphibole (actinolite + hornblende) replaces original clinopyroxene. Plagioclase shows signs of saussuritization. Minor anhedral titanomagnetite occurs between plagioclase and amphibole.

3.6.2 Geochemistry

Analysed clasts from station 15 (Table 19) are all basaltic andesites of relatively uniform compositions. SiO_2 contents vary from 52-55 wt%, while Mg#((Mg/(Mg+Fet), Fet total iron as FeO) varies from 0.59-0.45. In terms of the FeOt/MgO vs SiO_2 relationships, station 15 basaltic andesites show a tholeiitic trend, overlapping with and extending the TM-arc compositional trend (Fig. 30). However they differ from the TM-arc basaltic andesites being characterized by relatively high TiO_2 (>1.0 wt%) and Na_2O contents (>2.6 wt%), resulting in lower CaO/TiO_2, Al_2O_3/TiO_2 and CaO/Na_2O ratios, lower Ba (<29 ppm), Sr (130-158 ppm) and REE contents, and higher Zr (57-94 ppm) and Y (22-45 ppm) contents. REE patterns (Fig. 31a) are LREE-depleted with $(La/Yb)_N$ = 0.47-0.81; TM-arc basaltic andesites have flat to slightly depleted REE patterns (Ewart et al., 1973; Ewart et al., 1977).

Table 18

Petrographic summary of dredge lavas from North Tonga

Station no.	Group	Phenocrysts and microphenocrysts	Groundmass	Comments
15		Plag + Cpx	Glass (devitrified), plag + cpx microlites, timag, chlorite and smectite. Hyalopilitic to hyalo-ophitic.	Strong resorption in plag mph cores, patchy zoning in cpx mph. Some lavas show more coarse-grained subophitic textures.
21	I	Opx + Oliv + (Cpx) + (Cr-sp)	fresh glass, plag + cpx microlites, minor timg	Six types of glomerocrysts are observed in these lavas; (1) opx, (2) opx + cpx, (3) opx + oliv, (4) opx + cpx + oliv, (5) cpx + opx + plag, (6) plag, oliv, opx and plag have euhedral to strongly resorbed grain boundaries, lavas range from strongly vesicular to non-vesicular.
	II	Opx + Cpx + Oliv	coarse-grained sub-ophitic, minor chlorite + smectite	
		Opx + Cpx + (Oliv) + (Plag)	fresh glass, plag + cpx microlites, minor timg	
	III	Opx + Plag + Cpx + (Oliv)	as above	
		Opx + Plag + Cpx + Oliv + (Cr-sp) + (Timg)	fresh glass acicular pyx microlites	
	IV	Plag + Opx + Cpx	fresh glass plag + cpx microlites, minor timg	
	V	aphyric	as above	
23	BA	Plag + Opx + Cpx + (Oliv)	fresh glass plag + cpx microlites, minor timg	similar to station 21 lavas, oliv strongly resorbed.
	A	Opx + Oliv + (Cr-sp)	fresh glass, quench pyx, minor cr-sp euhedra	opx + oliv subhedral, euhedral to strongly resorbed, opx glomerocrysts common.
	B	Opx + Oliv + (Cr-sp) + (Cpx)	as above	
24		Oliv + Opx + Cr-sp	as above	many oliv mph have skeletal morhologies
25		Oliv + Cr-sp	as above	

phenocrysts and microphenocrysts are listed in order of modal abundances, brackets indicate trace abundances (<1%), Plag =plagioclase, Oliv =olivine, Opx =orthopyroxene, Cpx =clinopyroxene, Cr-sp =chromian spinel, Timg =titanomagnetite, mph =microphenocryst, BA =basaltic andesite, pyx =pyroxenes.

Table 19

Major, trace and REE geochemistry of basaltic andesites from station 15

	1-30	1-31	1-33	1-34	1-38	1-39	1-35	123 103-1	ANT 225-1
SiO_2	54.81	55.35	54.59	53.56	53.43	51.49	52.96	53.62	54.10
TiO_2	1.28	1.32	1.25	1.08	0.96	1.46	1.01	1.77	1.06
Al_2O_3	16.03	16.07	16.22	17.11	16.90	15.81	17.37	15.59	14.69
FeO^t	10.24	10.10	10.36	8.08	8.47	11.59	8.15	9.60	11.66
MnO	0.19	0.18	0.18	0.16	0.16	0.19	0.15	0.19	0.21
MgO	4.58	4.18	4.64	5.58	6.08	5.65	7.77	4.79	5.32
CaO	9.19	8.79	9.13	10.51	10.84	8.85	9.00	9.49	10.32
Na_2O	2.99	3.02	2.96	3.12	2.58	3.38	3.20	3.39	2.36
K_2O	0.61	0.87	0.58	0.68	0.48	0.49	0.29	0.51	0.11
P_2O_5	0.09	0.11	0.10	0.12	0.10	0.65	0.11	0.51	0.11
LOI	1.54	2.52	1.85	2.08	1.15	2.60	2.59	-	-
Mg#	0.44	0.42	0.44	0.55	0.56	0.46	0.63	0.47	0.45
Ba	28	29	24	26	29	16	29		
Rb	9	13	9	10	9	10	4		
Sr	130	131	133	158	132	156	136		
Zr	74	78	76	87	59	94	57		
Nb	<1	<1	1	1	1	<1	<1		
Y	30	31	30	32	29	45	22		
Sc	39	33	39	34	40	32	39		
V	349	357	349	244	259	267	257		
Ni	23	20	25	39	52	18	109		
Cr	46	33	43	131	204	27	234		
La					2.84	4.73	1.98		
Ce					9.23	12.41	7.22		
Pr					1.56	2.19	1.44		
Nd					8.40	12.24	7.34		
Sm					2.84	3.85	2.57		
Eu					1.11	1.53	0.96		
Gd					4.04	5.50	3.37		
Dy					5.03	6.68	3.71		
Er					3.28	4.58	2.25		
Yb					3.20	3.86	2.06		

Samples 123 103-1 and ANT 225-1 are examples of T-type LBB from Hawkins & Melchoir (1985). Major element geochemistry summed to 100% volatile free, FeO^t= total iron as FeO, LOI= loss on ignition. Major elements are in wt%, trace elements are in p.p.m.

3.6.3 Geochemical affinities

Basaltic andesites from station 15 are of particular significance because they come from the basement sequence underlying the TM-arc, as recognized on single channel seismic profiles (Honza et al., 1985). Sediment adherring to the clasts gives a preliminary age of mid-Miocene to Early Pliocene (10-3.5 Ma) based on microfossil content (Honza et al., 1985), providing a minimum age for the lavas. Using this age as a guide, there are four potential sources, of similar or older age, from which the basaltic andesites of station 15 could have been derived; these are discussed separately below:

3.6.3.1 'Eua-Vavau' block basement sequence

Volcanic rocks of the 'Eua-Vavau' basement sequence are exposed on the island of Eua (Ewart et al., 1977; Ewart & Bryan, 1972; Hawkins & Falvey, 1985; Duncan et al., 1985). Radiometric dating has identified three periods of volcanism (Duncan et al., 1985), namely Late to mid Eocene (40-41 Ma), Late Oligocene (31-33 Ma) and Early Miocene (17-19 Ma). The mid-Eocene phase of volcanism has been correlated with other Eocene basement sequences in the Southwest Pacific, all associated with the ancient 'Vitiaz' arc (Gill, 1984; Gill, 1976; Gill et al., 1984). The geochemical data on Eua are limited and lavas have been altered to varying degrees (Ewart & Bryan, 1972), making it difficult to characterize lava compositions. Despite these difficulties, there are significant geochemical differences between the Eocene phase of volcanism and basaltic andesites from station 15. Compared with the Eua lavas, those from station 15 have lower Ba, and higher contents of Zr, Y, Ni, Cr and TiO_2. The one published REE analysis from Eocene volcanics, sample E7 (Ewart & Bryan, 1972), is LREE depleted, similar to station 15 REE patterns. The character of Early Oligocene volcanics is poorly constrained but is similar to the older Eocene volcanics (Hawkins & Falvey, 1985). The Early Miocene phase of magmatism is represented by dikes, intruding the older volcanic sequence, which range in composition from basaltic andesite to andesite, and are also geochemically distinct from station 15 basaltic andesites.

3.6.3.2 Remnant arc, the Lau-Colville Ridge

The Lau-Colville ridge was part of the former volcanic arc before the opening and spreading of the Lau basin in latest Miocene or Early Pliocene

times. The oldest exposed rocks on the Lau-Colville ridge (Gill, 1976), the Lau Volcanics (6.4-9.0 Ma), are calc-alkaline, have a lower FeOt and no Fe-enrichment trend, and higher Ba, Sr, K, Rb and REE than station 15 lavas, (Gill, 1976); they are also LREE-enriched and have lower Ti/Zr ratios. It is highly unlikely that the station 15 tholeiites were formed during Lau-Colville Ridge volcanism.

3.6.3.3 Fiji

Basement rocks comprising the Wainimala and Savura Groups on Viti Levu are potential sources for the basaltic andesites of station 15, as Fiji would have been in the vicinity of the present day North Tonga ridge prior to the opening of the Lau Basin. The basement rocks of Fiji range in age from 33 to 10 Ma and are composed primarily of an island arc tholeiite suite ranging from basalt to rhyolite in composition, which has suffered metamorphism to zeolite or lower greenschist assemblages (Gill, 1984).

The Wainimala Group (Gill, 1970) displays a wide range in trace and minor element composition compared with the restricted range in composition present in the station 15 rocks. Important differences between the two suites are the higher abundances of Ba (50-124 ppm, compared with 16-29 ppm in station 15 lavas) and the presence of significant LREE enrichment in some of the Wainimala lavas [$(La/Yb)_N$ = 0.59-2.33]. All station 15 lavas analysed for REE are LREE-depleted. Similarly, the Savura Group differs from station 15 lavas in having higher Ba, Sr and lower Zr contents.

The Namosi Andesites, calc-alkaline lavas 6 Ma old, could be a potential source for station 15 clasts on the basis of age. They are excluded because of their calc-alkaline character, high Ba, Rb, Sr and K_2O contents, and low TiO_2 and LREE-enriched REE patterns (Gill, 1970), similar to those of the Lau volcanics.

3.6.3.4 Early Lau Basin Back-arc volcanism

A fourth possibility for the origin of the station 15 basaltic andesites, is that they were erupted during the early stages of development of the Lau back arc basin. The oldest fauna (3.1-3.4 Ma) found in the Lau Basin is in the base of DSDP hole 203. However the opening of the Lau basin probably began in the latest Miocene or Early Pliocene (Hawkins *et al.*, 1984), meaning that the Lau basin began to form before the onset of volcanism of the present TM-arc. The TM-arc therefore may have been

constructed on early-formed Lau basin backarc crust. Support for this hypothesis is found in the similarity in chondrite-normalized element abundance patterns between the Lau basin basalt from station 31 and station 15 basaltic andesites (Fig. 32a). The Lau basin sample 11-3 from station 31 and the station 15 basaltic andesites have similar abundances of incompatible elements and have LREE depleted REE patterns. In particular the station 15 basaltic andesites have low Ba/La (1.06-4.62) and Sr/Zr ratios (1.66-2.4), atypical of arc-related volcanics but similar to Lau basin basalts.

Despite these similarities in trace element signature, station 15 lavas are unlike typical Lau basin basalts, such as sample 11-3, because they are high in SiO_2 (51-55 wt%), whereas Lau Basin basalts have MORB-like major element chemistry with SiO_2 <50 wt%, and high Al_2O_3 and CaO contents (up to 14 wt%). The recognition of zonation in crustal composition of the Lau Basin by Hawkins & Melchior (1985) is therefore significant. Volcanics from the central part of the basin are N-MORB type basalts; these are flanked by belts of basalt similar to Mariana Trough basalts, designated normal(N)-type Lau Basin Basalt(LBB) and transistional(T)-type LBB respectively by Hawkins and Melchior (1985). The zonation is well-defined on the western side but is obscure in the eastern side because it is probably buried by the younger TM-arc. In terms of major element chemistry, station 15 basaltic andesites are similar to the T-type LBB from the western margin of the Lau Basin, which have similar SiO_2 (51-54 wt%), TiO_2 (1.06-1.77) and K_2O (0.17-1.02) contents (Table 19). It is suggested that the early stages of development of the Lau Basin involved shallower depths of melt segregation or higher contents of H_2O at higher pressure, producing more silica-saturated parental liquids than magmas parental to lavas currently supplied to the spreading zones. The trace element signature of the mantle source has remained constant despite variations in the conditions of partial melting (P-T-X_{H_2O}) during the evolution of the Lau Basin.

Station 15 basaltic andesites were probably erupted on the eastern side of the Lau Basin, early in its spreading history, and now form the basement to the TM-arc. Compared to conventional models of back-arc basin development (Crawford et al., 1981) it is unusual to find early Lau Basin crust outcropping on the forearc slope of the north Tonga trench. This implies either that a significant volume of pre-Lau Basin volcanic arc crust (of which the Lau-Colville Ridge is the remnant arc) has been subducted, despite its location on the over-riding plate, or that initial

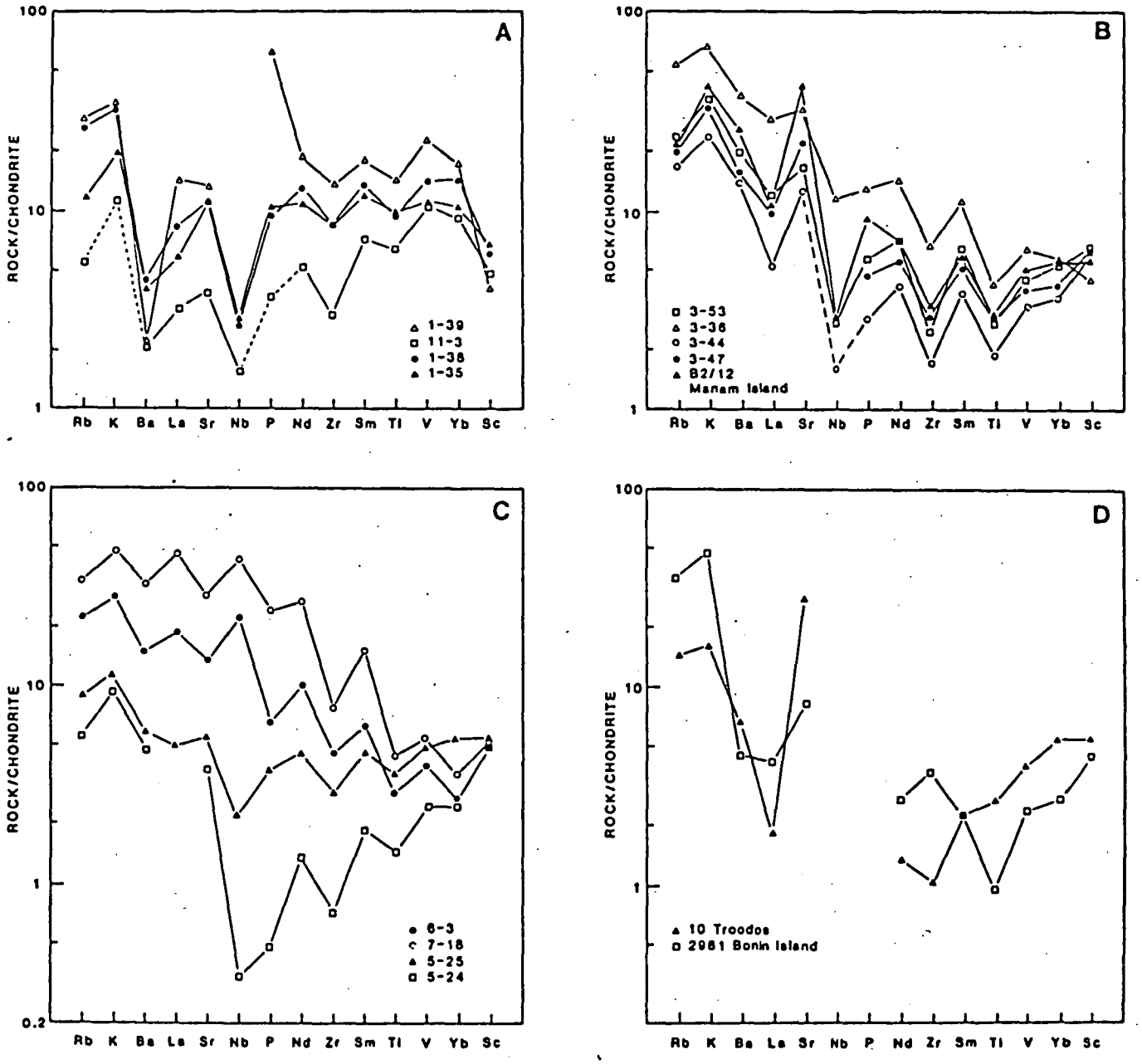

Figure 32.

Representative chondrite normalised abundance patterns for the dredge igneous rocks and othe related rocks. Normalising values are from Thompson et al. (1983), normalising value for Sc from Hickey & Frey (1982). The ordering of elements is taken from Hickey & Frey (1982), except the order of LIL elements (Rb, K, Ba, Sr) is based on experimental studies of Tatsumi et al. (1984).

A. Stations 15 and 31.

B. Station 21, (▲) is Manam Isalnd PNG (sample B2/12; Johnson et al., 1985).

C. High-mg lavas (Stations 23, 24 and 25).

D. Low-Ti ophiolitic basalt (sample 10, from the Troodos Upper Pillow Lavas, Cyprus; Cameron et al., 1983) and a boninite (sample 2981, Bonin Islands; Hickey & Frey, 1982).

Lau Basin rifting commenced in the forearc region of the Late Miocene arc. In the latter case, the Lau-Colville Ridge must represent the entire width of the Miocene arc axial ridge supporting the arc volcanoes. For the former case, the presence of in situ arc volcanics close to the Mariana Trench axis implies that blocks of Mariana forearc crust have been dragged into the subduction zone and subducted (Beccaluva et al., 1980). At this stage a forearc rifting model is favoured.

3.7 STATION 21

3.7.1 Petrography

Dredged rocks from station 21 are all fresh, porphyritic to aphyric, vesicular to non-vesicular lavas which can be subdivided into five petrographic groups based on the types and abundances of phenocryst phases (Table 18) and major element geochemistry; MgO contents tend to decrease from group I to V. The distinguishing characteristics of these lavas compared with TM-arc lavas are the dominance of orthopyroxene as a phenocryst phase, and the presence of significant amounts of olivine (up to 12 modal %) and Cr-spinel as microphenocrysts and inclusions in phenocryst phases. In contrast, the lavas of the Tonga islands are characterized by a two pyroxene-plagioclase assemblage, with plagioclase being the dominant phenocryst phase (Ewart et al., 1973). Olivine has only been reported as rare xenocrysts in basaltic andesites from the islands of Tofua and Kao, and in the Metis Shoal dacite (Bryan et al., 1972; Melson et al., 1970).

Olivine, orthopyroxene, clinopyroxene and plagioclase are all present as discrete phenocryst and microphenocryst phases and also as glomerophyric clusters, but plagioclase and olivine rarely coexist in the latter. Olivine and orthopyroxene phenocrysts are generally euhedral and vary from >4 mm in size to microphenocrysts. Some larger olivine and orthopyroxene phenocrysts have resorbed margins, the olivines being rimmed by orthopyroxene plus minor clinopyroxene. This evidence for disequilibrium and reaction between olivine and liquid contrasts with the presence of euhedral olivine microphenocrysts. Where olivine is present with orthopyroxene and clinopyroxene in glomerocrysts, it is present in the core of the glomerocryst, suggesting that pyroxene glomerocrysts may be the result of the complete reaction of a large olivine phenocryst with melt.

Plagioclase is most common as large glomeroporphyritic clusters, the glomerocrysts displaying either resorbed or euhedral grain boundaries. The

groundmass consists of generally fresh glass, plagioclase and clinopyroxene microlites. Textures range from hyalopilitic to more coarse-grained sub-ophitic textures. Titanomagnetite is present as minor anhedral to skeletal granules in the glass. Many samples have abundant feathery quench pyroxene in the groundmass.

3.7.2 Geochemistry

Representative analyses of station 21 lavas (Table 20) define a high MgO, low K (Gill, 1981), low Ti, tholeiitic suite. Because of their high SiO_2 content, station 21 compositions fall in the calc-alkaline field of Miyashiro (1974) but nevertheless show a distinct Fe-enrichment trend, emphasizing the inadequacy of this classification when dealing with high-Si, high-Mg lava suites. The low initial FeOt/MgO ratios are the result of relatively low FeOt contents (8.7-10.2 wt%), while MgO contents in station 21 lavas range from 15 to 3 wt% (Mg# ranges from 0.41 in evolved aphyric lavas to >0.70 for the more mafic compositions). At a given Mg#, station 21 lavas have lower TiO_2 (0.2-0.45 wt%) and higher SiO_2 contents (52-61 wt%) than TM-arc basaltic andesites (Fig. 33). They have relatively high Ni and Cr contents compared with most island arc basalts and basaltic andesites (Ni up to 265 ppm, Cr up to 1095 ppm), Cr/Ni ratios being high, and >5 in MgO rich samples, and when compared with TM-arc basaltic andesites, have high abundances of Ba, Rb, Sr and K_2O, but have lower abundances of Zr, Y and REE's. REE patterns are LREE-enriched (Fig. 31b); $(La/Yb)_N$ varies from 1.36-4.97, heavy REE are low, and have relatively flat patterns (Gd/Yb_N = 0.90-1.18, 1.52 in sample 3-36). Low Zr, Y and HREE abundances are similar to basaltic andesites from the island of Tafahi, but Tafahi samples differ in having higher REE abundances and LREE-depleted patterns (e.g. sample T116 has a $(La/Yb)_N$ ratio of 0.77; Ewart et al., 1977). Tafahi basaltic andesites also have lower abundances of Rb, Ba, Sr and K_2O, higher TiO_2 and lower SiO_2 for a given MgO content than lavas from station 21.

3.7.3 Geochemical affinities

Although station 21 lavas are distinctly different from those of the TM-arc suite, they show geochemical affinities with other low-Ti basaltic andesite suites, notably the Manam Island suite from Papua New Guinea (Johnson et al., 1985). Both the station 21 and the Manam suites have similar LREE-enriched REE patterns, low abundances of high field strength (HFS) elements (Y, Ti, Zr and P) relative to the REE's on chondrite normalized abundance patterns (Fig. 32b), and have high LIL elements (K,

Table 20

Major, trace and REE geochemistry of representative samples from station 21 and 22

	3-44	3-47	3-53	3-36	B2/12	4-11 G	4-12 G	4-15 G	4-14 P
SiO_2	54.35	55.18	57.51	60.17	52.64	58.27	54.59	53.38	73.23
TiO_2	0.20	0.31	0.29	0.42	0.30	0.59	0.44	0.33	0.11
Al_2O_3	10.67	10.94	13.18	15.21	14.93	16.42	15.04	14.65	14.38
FeO^t	9.41	10.00	9.22	8.90	8.30	7.60	8.42	10.69	1.79
MnO	0.19	0.19	0.18	0.15	0.17	0.16	0.17	0.19	0.03
MgO	14.99	12.14	8.14	3.35	9.12	5.52	8.65	8.42	0.60
CaO	8.66	9.24	9.53	7.68	11.43	6.50	10.67	10.21	7.45
Na_2O	1.14	1.48	1.35	2.96	2.40	4.63	1.85	1.91	2.30
K_2O	0.35	0.48	0.54	1.01	0.61	0.27	0.13	0.18	0.07
P_2O_5	0.03	0.05	0.06	0.14	0.10	0.04	0.03	0.03	0.04
LOI	0.05	0.98	-0.07	0.86	0.65	6.76	1.25	5.15	0.52
Mg#	0.76	0.71	0.64	0.43	0.66	0.56	0.65	0.58	0.37
Ba	106	113	140	271	180	26	29	37	60
Rb	6	7	8	19	8	5	1	3	--
Sr	151	172	202	385	514	82	74	69	550
Zr	12	20	17	44	22	51	45	57	48
Nb	<1	<1	<1	4	<1	1	2	2	16
Y	7	8	9	13	10	19	21	32	7
Sc	50	51	50	34	42	34	51	61	24
V	247	259	275	309	275	203	229	191	41
Ni	275	153	84	21	81	51	93	82	5
Cr	1095	762	365	17	288	108	189	187	9
La		3.25	3.94	9.49	3.33		1.73		13.34
Ce		6.53	7.95	20.85	7.92		5.24		30.60
Pr		0.82	0.94	2.57	nd		0.86		2.96
Nd		3.70	4.47	9.29	4.51		4.46		9.65
Sm		1.05	1.31	2.29	1.27		1.53		1.57
Eu		0.39	0.49	0.67	0.47		0.57		<0.24
Gd		1.29	1.34	2.38	nd		2.54		1.32
Dy		1.60	1.67	2.06	nd		3.20		1.07
Er		1.01	1.19	1.33	nd		2.04		0.52
Yb		0.95	1.19	1.26	1.21		2.31		0.37

Letters G and P signify metagabbro and plagiogranite respectively. Sample B2/12 from Manam Island, PNG (Johnson et al., 1985). Major element geochemistry summed to 100% volatile free, FeO^t = total iron as FeO, LOI = loss on ignition. Major elements are in wt%, trace elements are in p.p.m, nd not determined, (--) below detection limit.

Rb, Ba, Sr) abundances relative to the REE's and HFS elements. Overall, rocks from station 21 comprise a more primitive suite than Manam, having higher MgO, Ni and Cr abundances and lower incompatible element abundances.

The Manam and the station 21 suites share many petrogenetic similarities with boninite lavas from Western Pacific arcs (Hickey & Frey, 1982; Cameron et al., 1983; Johnson et al., 1985), such as evidence for a 'depleted' source peridotite metasomatized by two or more 'enriched' components, but their trace element signatures distinguish them from boninite sources. The most important distinguishing characteristic is the lack of a strong Zr-enrichment. Zircon enrichment in boninite suites is reflected by low Ti/Zr ratios (<70), and a Zr 'peak' relative to Sm on chondrite-normalized element abundance diagrams (Fig. 32b). The station 21 and Manam suites lack both of these features and have geochemical affinities with low-Ti ophiolitic basalts rather than with boninite.

3.8 STATION 22

3.8.1 Petrography

Metagabbros from station 22 possess primary pyroxene(s) which have been totally replaced by amphibole (hornblende and actinolite) and chlorite, fresh or slightly saussuritized plagioclase, and accessory titanomagnetite and secondary epidote. The plagiogranite is a fresh medium to fine grained holocrystalline rock with a microgranitic texture, and consists of equal amounts of quartz and plagioclase(An_{60}), plus ~5-10 modal % hornblende with accessory sphene and apatite. Small pieces of serpentinite recovered from station 22 consist of serpentine, except one sample which contains relict cores of olivine and orthopyroxene, suggesting a harzburgitic protolith.

3.8.2 Geochemistry and geochemical affinities

Metagabbros from station 22, characterized by high SiO_2 and low TiO_2 contents, have similar major element geochemistries to station 21 basaltic andesites. However the metagabbros have significantly lower abundances of Ba and Sr, higher abundances of Zr, and Y, and the least altered sample(4-12, Table 20) has a LREE-depleted REE pattern (Fig. 31c). These trace element abundances are not considered to have been significantly affected by alteration because of the consistency of element ratios between samples which have suffered varying degrees of alteration

(e.g. LOI which ranges from 1.25 to 6.76 wt%). For similar reasons, metagabbros from station 22 lack genetic relationships with TM-arc rocks. The metagabbros were dredged from depths comparable with those of basaltic andesites from station 15 (4500-4440 m compared with 4325-4860 m). They contain a trace element signature similar to that of the basaltic andesites, having low Ba and high Zr contents, and LREE depleted REE patterns. It is possible that the basement sequence exposed at station 15, characterized by high-Ti basaltic andesites, is continuous along the North Tonga ridge.

The plagiogranite from station 22 (Table 20) is characterized by high SiO_2, and low K_2O contents, consistent with the absence of K-feldspar. Unlike typical MORB-derived or ophiolitic plagiogranites which have flat HREE patterns (Coleman & Donato 1979), this specimen has a strongly HREE-depleted pattern [$(La/Yb)_N$ = 24, with a marked Eu anomaly (Fig.31c)]. The plagiogranite is high in Sr, and relatively low Ba and Rb, consistent with the absence of K-feldspar and is unusual in having a significance Nb (16 ppm) content compared with the low Nb contents of other Tongan rocks (mostly below detection limit). The HREE-depleted REE pattern suggests involvement of garnet as a residual or fractionating phase in the petrogenesis of this rock. It is possible that the plagiogranite is derived from a slab-derived (eclogitic residue) as opposed to a mantle-derived (peridotitic residue) parent magma.

3.9 STATION 23

Basaltic andesites and high-Mg lavas were recovered from station 23.

3.9.1 Basaltic andesites

3.9.1.1 Petrography

Petrographically, the basaltic andesites are similar to those from station 21, containing 6-14 modal % phenocrysts and microphenocrysts of orthopyroxene, clinopyroxene and plagioclase set in a hylopilitic groundmass of fresh glass, acicular plagioclase microlites and anhedral clinopyroxene grains. Olivine is present as rare resorbed phenocrysts surrounded by stubby orthopyroxene microphenocrysts, and contains Cr-spinel inclusions. Pyroxene-plagioclase glomerocrysts are common; larger orthopyroxene phenocrysts display blocky and patchy zoning and are frequently rimmed by clinopyroxene.

3.9.1.2 Geochemistry and Geochemical affinities

The basaltic andesites are relatively uniform in composition (Table 21) and compared with those of the TM-arc have on average higher SiO_2 contents (55-56 wt% compared with 53-55 wt% for TM-arc compositions), lower FeOt, higher MgO (reflected in lower FeOt/MgO ratios; Fig. 30) and higher Ni and Cr contents. Similarities with TM-arc basaltic andesites include TiO_2 contents (Fig.33b) and flat to slightly LREE depleted REE patterns (Fig. 5d); in these respects they contrast with the petrographically similar station 21 lavas. Incompatible element contents are lower than those of Tm-arc basaltic andesites, causing significant differences in trace element ratios such as Ba/La and Sr/La. The basaltic andesites from station 23 were derived from a mantle source different from, yet sharing many similar characteristics with, the mantle source of the TM-arc basaltic andesites.

3.9.2 High-Mg lavas

3.9.2.1 Petrography

Small highly vesicular, highly phyric pieces of high-Mg lavas, also recovered from station 23, can be subdivided into two groups on petrographic and geochemical criteria (Table 18). In both groups olivine occurs as large subhedral to euhedral phenocrysts, sometimes with resorbed margins. Orthopyroxene is present mainly in euhedral glomerophyric clusters, but also as discrete phenocrysts and microphenocrysts, sometimes showing resorption. Orthopyroxene is mostly unzoned, although some phenocrysts show an unusual blocky or patchy zoning and rims of clinopyroxene. Clinopyroxene in Group B lavas (Table 18) is present mainly as small subhedral to euhedral microphenocrysts, and rarely as, large resorbed clinopyroxene phenocrysts. The groundmass is hyalopilitic, consists of abundant acicular pyroxene microlites and fresh glass, and contains small euhedral olivine and Cr-spinel microphenocrysts; plagioclase is absent.

3.9.2.2 Geochemistry

Representative analyses of the high-Mg lavas are presented in Table 21. Samples 5-24 and 5-28 are from Group A and sample 5-25 is from Group B. Both groups are characterized by high MgO (16-21 wt%) at relatively high SiO_2 contents (52-53 wt%). Group A lavas are more 'primitive', containing

Table 21

Major, trace and REE geochemistry of basaltic andesites from station 23, high-Mg lavas from stations 23, 24 and 25, and pillow rind from station 31

	5-24	5-28	5-25	5-20	5-21	5-23	St-27	St-24 6-3	St-25 7-18	St-31 11-3
SiO_2	52.95	53.72	53.83	56.30	55.92	56.11	57.48	56.04	54.72	50.22
TiO_2	0.15	0.14	0.36	0.62	0.48	0.38	0.44	0.31	0.45	0.65
Al_2O_3	7.92	8.27	9.63	15.20	16.56	16.66	14.80	10.60	10.90	15.33
FeO^t	9.70	9.65	9.71	9.77	9.29	8.76	9.66	8.46	8.65	9.57
MnO	0.21	0.20	0.19	0.17	0.17	0.16	0.17	0.17	0.17	nd
MgO	20.89	19.65	16.30	5.33	4.75	5.07	5.36	13.61	12.97	8.87
CaO	7.18	7.54	8.50	10.20	10.80	11.03	10.11	9.17	9.65	13.40
Na_2O	0.85	0.69	1.27	2.08	1.80	1.58	1.67	1.14	1.52	1.96
K_2O	0.14	0.12	0.16	0.24	0.19	0.19	0.25	0.43	0.71	nd
P_2O_5	0.01	0.02	0.04	0.07	0.04	0.04	0.06	0.07	0.26	nd
LOI	0.13	-0.02	0.24	0.71	0.18	0.20	0.57	1.87	1.69	nd
Mg#	0.79	0.80	0.77	0.52	0.48	0.51	0.50	0.76	0.75	0.65
Ba	34	35	41	55	50	42	57	105	230	14
Rb	2	2	3	4	3	3	4	8	12	2
Sr	46	48	68	126	123	118	108	159	348	48
Zr	5	7	20	39	25	15	25	32	53	21
Nb	<1	<1	<1	<1	<1	<1	<1	8	16	<1
Y	5	6	10	17	14	11	13	8	11	22
Sc	44	43	44	44	46	44	49	43	44	51
V	191	200	225	298	270	231	270	214	223	299
Ni	501	433	341	37	27	29	40	189	199	133
Cr	2027	1767	1294	75	54	94	124	927	760	350
La			1.51	2.82			1.91	6.53	15.98	3.43
Ce			3.34	6.44			4.43	14.74	37.72	nd
Pr			0.55	1.01			0.76	1.73	4.48	5.52
Nd			2.72	5.17			3.56	6.36	17.29	5.83
Sm			0.89	1.72			1.24	1.30	3.23	8.17
Eu			0.36	0.62			0.59	0.45	1.02	8.61
Gd			1.27	2.37			1.90	1.35	2.68	10.58
Dy			1.62	3.10			2.46	1.27	1.84	11.57
Er			1.10	2.15			1.78	0.63	0.93	11.74
Yb			1.14	2.07			1.78	0.58	0.79	11.39

For sample St-31 11-3 major element geochemistry determined by electron microprobe; others summed to 100% volatile free. FeO^t = total iron as FeO, LOI = loss on ignition, nd = not determined. Major elements are in wt%, trace elements are in p.p.m.

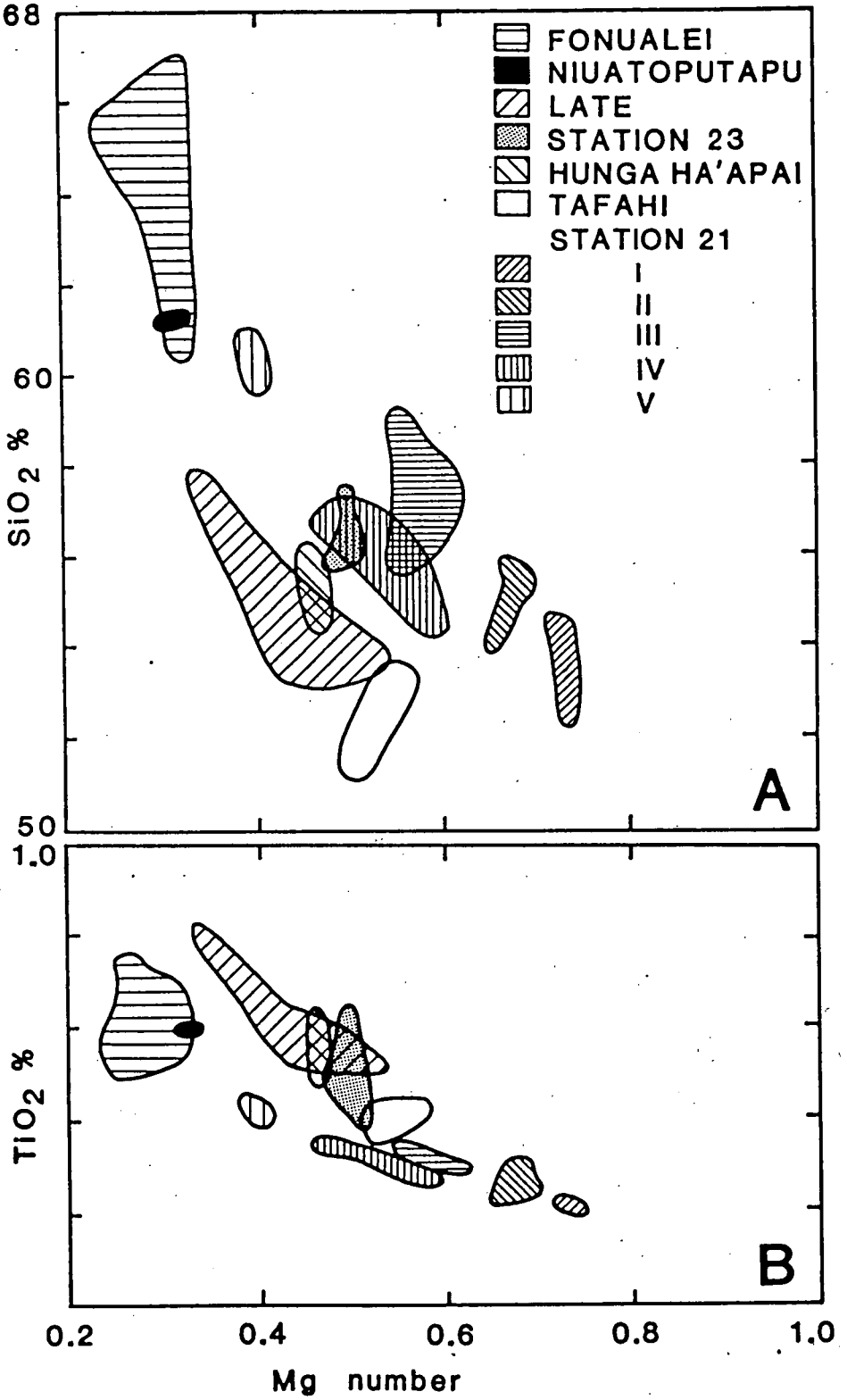

Figure 33.

A. SiO_2 versus Mg# (Mg/(Mg + Fe^t)) for dredged rocks from station 21 and the basaltic andesites from station 23 compared with rocks from the TM-arc. Roman numerals I-V refer to the petrographic groups from station 21 outlined in Table 18. Field for the station 23 basaltic andesites constructed from data taken from Table 21. Fields for station 21 lavas constructed from data taken from Table 20 and Falloon (unpubl. data). Fields for the islands of the TM-arc constructed from data taken from Ewart et al. (1973) and Ewart (1976).

B. TiO_2 versus Mg# for dredged rocks from station 21 and basaltic andesites from station 23 compared with rocks from the TM-arc. Key same as for Fig. 33.

higher MgO, Ni and Cr, lower TiO_2 and lower abundances of incompatible elements such as Ba, Sr, Zr and Y. Both groups have high Mg# (0.75-0.79) appropriate for them to be in equilibrium with mantle olivine (>Fo_{88}; Green, 1971). Although the high Mg# may also reflect the abundance of mafic phenocrysts in these lavas, so that whole rock compositions may not be representative of liquid compositions, the presence of euhedral olivine phenocrysts as magnesian as Fo_{94} strongly supports the claim that the lavas have near-primary compositions.

Group A lavas have low HREE abundances (<3X chondrites), such low abundances render the Group A samples unsuitable for the XRF-determined REE analytical technique of Robinson et al., (1986). Sample 5-25 from Group B has a flat REE abundance pattern (Fig. 31d) with $(La/Yb)_N$ = 0.87 and low REE abundances(5x chondrites). The REE pattern of sample 5-25 is similar to those of the basaltic andesites of station 23 and the TM-arc, suggesting that the high-Mg lavas could be parental to these andesites. This possibility is precluded by the high SiO_2 content >52 wt%, the parental magma of TM-arc basaltic andesites requiring <50 wt% SiO_2; and a low FeOt of 9.6-9.7 wt% for Group B lavas which produce low initial FeOt/MgO ratios and result in station 23 high-Mg lavas plotting away from the main TM-arc trend (Fig. 30).

The high-Mg lavas from station 23 could be the source of xenocrystal olivine (Fo_{93}), orthopyroxene and Cr-spinel in the Metis Shoal dacite (Melson et al., 1970), and could therefore be involved in magma mixing processes beneath the young TM-arc. The Group B high-Mg lavas are possibly co-magmatic with basaltic andesites from station 23, which have similar REE patterns. The geochemical affinities of high-Mg lavas from station 23 is discussed separately in conjunction with high-Mg lavas from stations 24 and 25.

3.10 STATIONS 24 AND 25

3.10.1 Petrography

The glass rind of pillow lavas from station 24 consists of abundant small euhedral olivine and orthopyroxene microphenocrysts, some with skeletal morphologies, minor small Cr-spinel euhedra and complexly intergrown quench clinopyroxene laths set in fresh glass. The glass rind of pillow lavas from station 25 are similar but contain no orthopyroxene microphenocrysts. Pillow interiors are characterized by interconnecting

elongate and spherulitic quench clinopyroxene laths, fresh glass, with abundant (~10 modal %) euhedral olivine microphenocrysts and phenocrysts. Station 24 pillow lava interiors also contain orthopyroxene microphenocrysts, however olivine is the more abundant phenocryst phase. Apart from the absence of large orthopyroxene phenocrysts, the petrography of station 24 and 25 pillow lavas is similar to that of the high-Mg lavas from station 23 in that the groundmass of both contain abundant olivine microphenocrysts, orthopyroxene and Cr-spinel euhedra. Lavas from stations 24 and 25 may have erupted at temperatures above the orthopyroxene liquidus, whereas those from station 23 quenched below the appearance temperature of orthopyroxene.

3.10.2 Geochemistry

Samples 6-3 and 7-18 (Table 21) are representative of the high-Mg lavas from stations 24 and 25 respectively. Compared with high-Mg lavas from station 23 they are higher in SiO_2 and TiO_2 (0.3-0.45 wt%), lower in MgO and are strongly enriched in incompatible elements Rb, Ba, Sr, Zr, Nb, Y and K. The REE patterns (Fig. 31e) are LREE-enriched (La/Yb_N = 7.46-13.4); those from station 25 are more enriched in incompatible elements than lavas from station 24. The geochemical affinities of the pillow lavas is discussed below.

3.11 STATION 31

3.11.1 Petrography, Geochemistry and Geochemical affinities

The pillow rind recovered from station 31 (sample 11-3, Table 21), consisting of minor euhedral plagioclase microlites, euhedral olivine microphenocrysts and fresh glass, has geochemical affinities with primitive MORB glasses (Langmuir et al., 1977; Bryan & Moore, 1977) but differs in its relatively higher FeOt, which produces a Mg# lower than primitive MORBs.

Sample 11-3 is geochemically and petrographically similar to other Lau Basin basalts (e.g. site 95, Hawkins, 1976, Hawkins & Melchoir, 1985). Although Hawkins & Melchoir (1985) emphasized their geochemical similarities with N-type MORB, there are significant differences, as illustrated by 11-3, which indicate a distinctive Lau Basin (back-arc basin) magma type. These characteristics include:

(1) Compared with primitive MORB glasses of similar Mg# or MgO content, sample 11-3 has significantly lower TiO_2 contents. The more magnesian sample 95-1 has only 0.35 wt% TiO_2 (Hawkins, 1976; Gill, 1976) whereas primitive MORB glasses have TiO_2 contents > 0.63 and mostly between 0.7-0.9 wt%.

(2) High CaO contents and high CaO/Al_2O_3 and CaO/Na_2O ratios. Combined with and other Lau Basin samples (e.g. 14.7 wt% CaO in sample 95-12; Hawkins & Melchoir, 1985) sample 11-3 has an exceptionally high CaO content even for relatively calcic MORB glasses.

(3) Lau Basin basalts have low abundances of incompatible elements, especially Sr (48 ppm in 11-3; 52-155 ppm in primitive MORB glasses), Zr (21 ppm in 11-3; 18-51 ppm in primitive MORB glasses) and Ba (14 ppm in 11-3; 11-50 ppm in primitive MORB glasses).

(4) Sample 11-3 has a strongly LREE-depleted REE pattern (Fig. 31f), with $(La/Yb)_N = 0.3$; sample 95-1 (Gill, 1976) has a more depleted pattern $(La/Yb)_N = 0.17$. Few primitive MORB glasses have such depleted patterns.

3.12 GEOCHEMICAL AFFINITIES OF THE HIGH-MG LAVAS

Samples from the flank area of the 'island arc' are remarkable for the consistency and dominance of 'primitive' highly magnesium lavas characterized by highly magnesian olivine and orthopyroxene phenocrysts and glass which has high Mg#. In contrast, there is a paucity of such rocks amongst the emergent volcanoes or indeed in the classical rocks comprising the island arc magma series (calc-alkaline, island arc tholeiite and shoshonitic volcanics; Gill, 1981). Thus it is significant that these high-Mg lavas, which contain both magnesian olivine and orthopyroxene, imply source compositions of peridotitic rather than eclogitic or pyroxenitic character.

A comparison of the high-Mg lavas from station 23, 24 and 25 with other primitive lavas indicates strong affinities with low-Ti ophiolitic basalts (Sun & Nesbitt, 1978), such as the Upper Pillow Lavas from the Arakapas Fault Belt region, Cyprus (Cameron, 1985). In terms of petrography alone the Tongan high-Mg lavas can be considered exact equivalents of Arakapas type pillow lavas. Arakapas lavas also contain orthopyroxene-dominated and olivine-dominated lavas, equivalent to rocks from station 23 and stations 24 and 25 respectively. Low-Ti ophiolitic basalts have

similar groundmass textures to boninites, leading to confusion in nomenclature (Cameron et al., 1979; Cameron et al., 1983). However the Tongan high-Mg lavas, together with low-Ti ophiolitic basalts, are distinguished from boninite by the following characteristics:

(1) Whereas Tongan lavas and low-Ti ophiolitic basalts have olivine as an important phenocryst and microphenocryst phase, olivine is rare or absent from boninites (Walker & Cameron, 1983; Jenner, 1981). The former rocks also lack clinoenstatite as a phenocryst phase.

(2) SiO_2 contents at a given MgO are lower in the Tongan and low-Ti ophiolitic lavas (Cameron et al., 1983).

(3) High CaO contents relative to boninites (Fig. 34) are reflected in high CaO/Al_2O_3 ratios. Pillow lavas from stations 23, 24 and 25 with CaO/Al_2O_3 ratios of between 0.7-0.9, are generally higher than primitive MORB glass compositions, and significantly higher than boninites which have characteristically low CaO/Al_2O_3 ratios (Cape Vogel boninites have CaO/Al_2O_3 ratios of 0.66-0.52) because of low CaO contents. In Fig. 34, the CaO content of Tongan high-Mg lavas overlaps with Troodos Upper Pillow Lava compositions and plots well away from clinoenstatite-bearing boninite. A clear separation appears to exist between boninite and Tongan lavas but two examples from the Bonin Islands plot with the Tongan lavas, while 'boninite' series rocks from site 458 (Meijer, 1980) seem to fall between the two fields (Fig. 34). The two examples from the Bonin Islands which plot with the Tongan lavas contain magnesian clinopyroxene instead of clinoenstatite and are unrelated to other typical boninite rocks on Chichijima (Unimo, 1986). These two rocks however are very similar to station 25 high-Mg lavas (PART V). Clinoenstatite is also absent from site 458 lavas. These 'intermediate' site 458 lavas could possibly be the result of mixing between a low CaO boninite-type liquid with a more calcic magma, such as a Troodos type liquid or even a calcic Lau Basin type liquid.

(4) Both the Tongan lavas and low-Ti ophiolitic basalts lack the characteristic enrichment of Zr over the middle REE element Sm on normalized abundance patterns present in boninites (see Fig. 32c for the Tongan high-Mg lavas and Fig. 32d where a representative boninite and Troodos pattern are compared). The chondrite-normalized element abundance patterns for the Tongan high-Mg lavas are variable, and different from the boninite and Troodos patterns in Fig. 32d. The differences between the Tongan high-Mg lavas and the Troodos Upper Pillow Lavas can be attributed

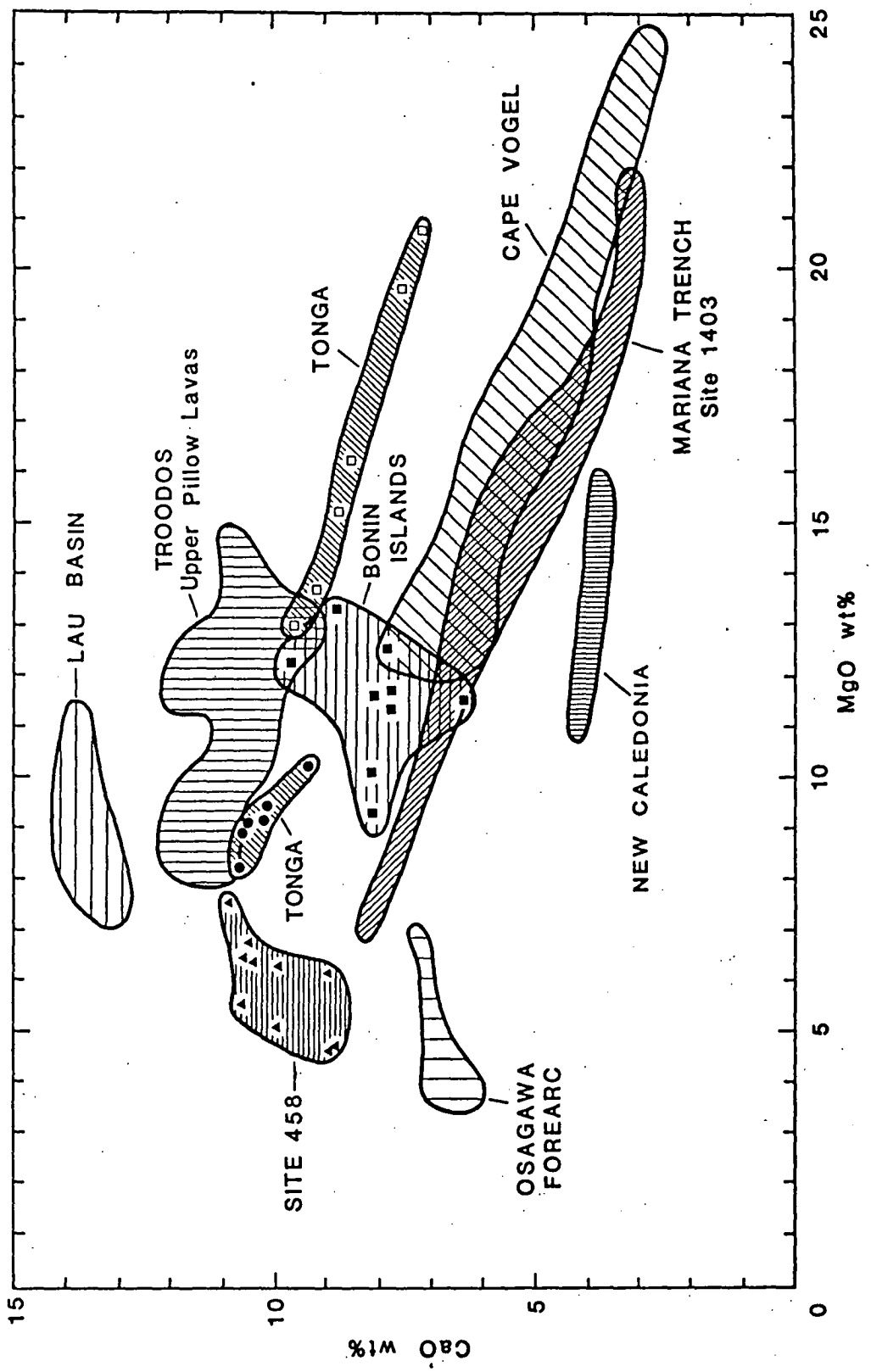

Figure 34.

CaO versus MgO wt% for high-Mg lavas from stations 23, 24 and 25. (□) are whole rock analyses from Table 21. (●) are the quenched groundmass compositions of the high-mg lavas (Falloon unpubl. data). Also shown are the fields for calcic Lau Basin back arc basin basalts (Hawkins, 1976) and boninites, data sources as follows:
DSDP site 458, Mariana forearc (Hickey & Frey, 1982; Meijer, 1980); individual data points represented by (▲).
Bonin Islands (Hickey & Frey, 1982; Cameron et al., 1983; Komatsu, 1980); individual data points represented by (■).
Cape Vogel, PNG (Jenner, 1981).
Mariana Trench, site 1403 (Sharaskin et al., 1980; Dietrich et al., 1978).
New Caledonia (Cameron et al., 1983).
Ogasawara forearc (Johnson, 1985).
Troodos Upper Pillow Lavas from Cameron (1985).

to a difference in the nature of an 'enriched' metasomatizing component, which invaded a depleted mantle source. The nature of the proposed 'enriched' component is presented in PART V.

3.13 SUMMARY

Apart from stations 15 and 31, dredging during the cruise of the 'Natsushima' in 1984 took place within a small area at the northern termination of the North Tonga ridge. Each dredge station yielded distinctive suites of rocks which are different both from one another and from the young volcanics of the Tofua magmatic arc, and which are primitive in having high Mg# compatibile with derivation from mantle peridotite sources. These characteristics require the existence of a range of mantle sources at the northern end of the Tonga ridge, as well as a probable range in partial melting conditions ($P\text{-}T\text{-}X_{H_2O}$). Possibly the unique tectonic setting of the dredged rocks, next to the intersection of a volcanic arc and a transform fault-oblique subduction system has allowed contributions from a variety of different sources (slab, mantle wedge, LVZ), through processes such as en echelon rifting, and minor spreading.

Basaltic andesites from station 23 display the closest affinities to those from the TM-arc; the higher SiO_2 contents at similar Mg# of station 23 lavas could be explained by a shallower depth of melt segregation or alternatively higher P_{H_2O} during partial melting (Green, 1976).

The high-Mg lavas have similarities with low-Ti ophiolitic basalts, and support an intraoceanic island arc setting for ophiolites with these distinctive types of lavas. They are primitive in character (high Mg#, Ni and Cr) and are possible mantle-derived primary melts in an island arc setting. Basaltic andesites from station 15, from the basement of the TM-arc, have strong geochemical affinities with early Lau Basin basalts. It is possible that the basement of the young TM-arc along the North Tonga ridge is old Lau Basin crust, as previously suggested by Hawkins et al. (1984), Hawkins & Falvey (1987), and Hawkins & Melchoir (1985). The dredged rocks demonstrate that arcs are geochemically complex, and that exposed volcanic islands may not be representative of the volcanism which constructed the arc.

PART IV

GLASS INCLUSIONS IN MAGNESIAN OLIVINE PHENOCRYSTS FROM TONGA: EVIDENCE FOR HIGHLY REFRACTORY PARENTAL MAGMAS IN THE TONGAN ARC.

4.1 INTRODUCTION

One of the important aims of petrological studies in island arcs is to determine the nature of 'parental' and 'primary' magmas for different magma series commonly observed (calc-alkaline, island arc tholeiite, boninite, etc.). However most volcanic rocks of these series are phenocryst-rich and lie on compositional trend lines in which effects of crystal fractionation, contamination, magma mixing and volatile loss can be reasonably proven or inferred. It is commonly not possible to identify parental or primary compositions in these magma series without somewhat arbitrary assumptions.

It is possible to avoid these complications by studying glass inclusions in early crystallizing phases of island arc magmas, such as Cr-spinels, olivines and orthopyroxenes. These trap small samples of their host magma, preserving them as inclusions (Anderson, 1974; Watson, 1976). The only problem with this approach is to see through the effects of post-entrapment interaction between the host mineral and glass inclusion.

We present here the compositions of trapped glass inclusions in very magnesian olivine (Fo_{94}) phenocrysts which occur in highly magnesian lavas dredged from the forearc of the north Tonga ridge during the 1984 cruise of the 'Natsushima' (Honza et al., 1985; PART III). The location of the dredged magnesian lavas is shown in Fig. 28 (PART III); details of the location, petrography and geochemistry of the dredged rocks are given in PART III. The particular samples reported here are 3-24 and 5-25 from stations 21 and 23 respectively.

4.2 PETROGRAPHY

The glass inclusions occur in large (<1-5mm) olivine phenocrysts, which have euhedral to resorbed grain boundaries and contain euhedral Cr-spinel inclusions. The olivines are very magnesian, with Fo_{94} in the cores, and rim compositions ranging from Fo_{85-88}; the latter are close to being in equilibrium with the quenched matrix of the host magma (Mg# = 0.706, Mg# = $Mg/(Mg + Fe^t)$); however the magnesian cores are significantly out of equilibrium. The glass inclusions range in size from <0.05 to 0.2mm (Fig. 35a). The glass in most of the inclusions has been effectively chilled, so that no quench crystals are visible under either optical or scanning electron microscopes. In some olivines, however, the glass inclusions display well developed quench pyroxenes (Fig. 35b) of ferro-augite composition. No amphiboles or any other hydrous phases have been detected in any of the inclusions. The glass inclusions also have a trapped volatile component, evidenced by a empty vapour bubble (Fig. 35c); we have not yet found examples of unbreached fluid inclusions.

4.3 COMPOSITION OF THE GLASS INCLUSIONS

The compositions of the glass inclusions were determined by a Jeol JXA-50A microprobe with an energy-dispersive analytical system. A composition range was observed with centres of large inclusions giving most magnesian compositions (6-8 wt% MgO) and rims of larger inclusions and cores and rims of small inclusions giving more Fe-rich compositions (2-5 wt% MgO, 4-5 wt% FeO) relative to MgO. This effect is attributed to growth of quench olivine on the walls of inclusions and thus the cores of large inclusions give the closest approach to the original entrapped liquid.

Compositions of some of the glass inclusions in the olivine phenocrysts are listed in Table 22. The glass totals from the electron microprobe are approximately 95 wt% indicating the possibility of H_2O dissolved in the glasses. This is currently being tested, using an infra-red microprobe technique. The glass compositions have all been modified by the host olivine, as evidenced by their low Mg# numbers (0.62-0.73), which are not in equilibrium with the host olivine core composition, assuming a Kd (equilibrium distribution coefficient for Fe and Mg between olivine and liquid) of 0.3 (Roedder & Emslie, 1970) and a $Fe^{2+}/(Fe^{2+} + Fe^{3+})$ ratio of 0.9. The olivine host becomes progressively more Fe-rich towards the glass inclusion; however it is difficult to establish the exact composition of

Figure 35a.

An example of a well quenched glass inclusion in a magnesian olivine phenocryst (Fo_{94}), sample 5-25, station 23, crossed nicols, magnification 16x.

Figure 35b.

Well developed quench pyroxenes in a glass inclusion in a olivine phenocryst, sample 3-24, station 21, crossed nicols, magnification 6.3x.

Figure 35c.

An example of a breached glass inclusion in a magnesian olivine phenocryst (Fo_{94}). Groundmass of the host lava consists of pyroxene and glass. A smaller glass inclusion occurs to the left of the breached inclusion. Sample 5-25, station 23, plane polarised light, magnification 6.3x.

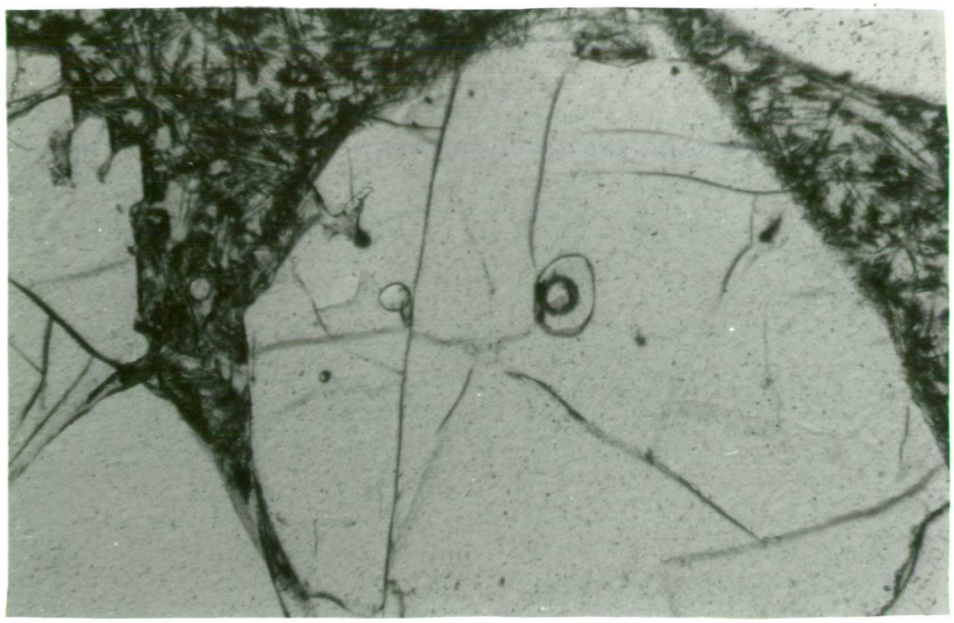

C

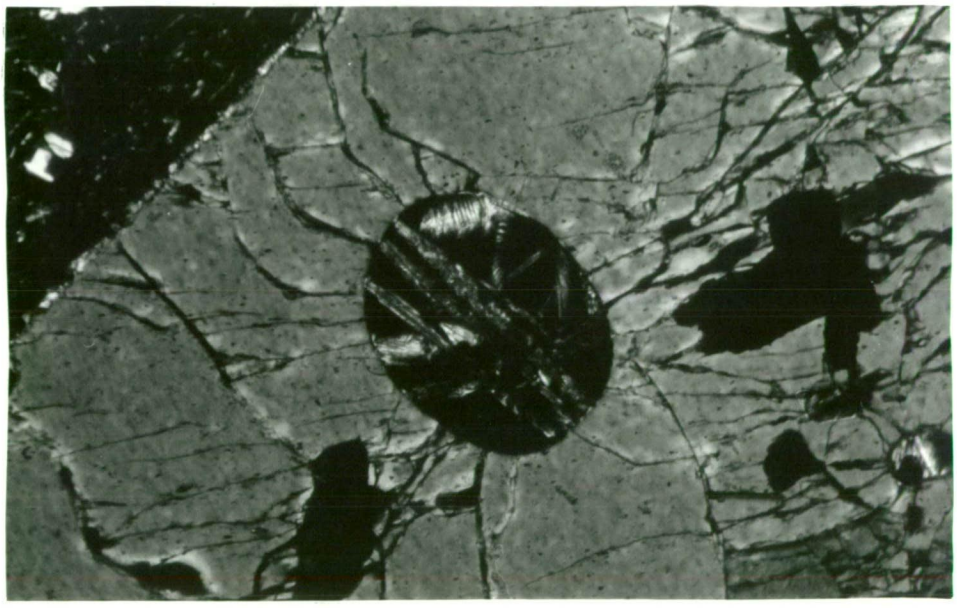

B

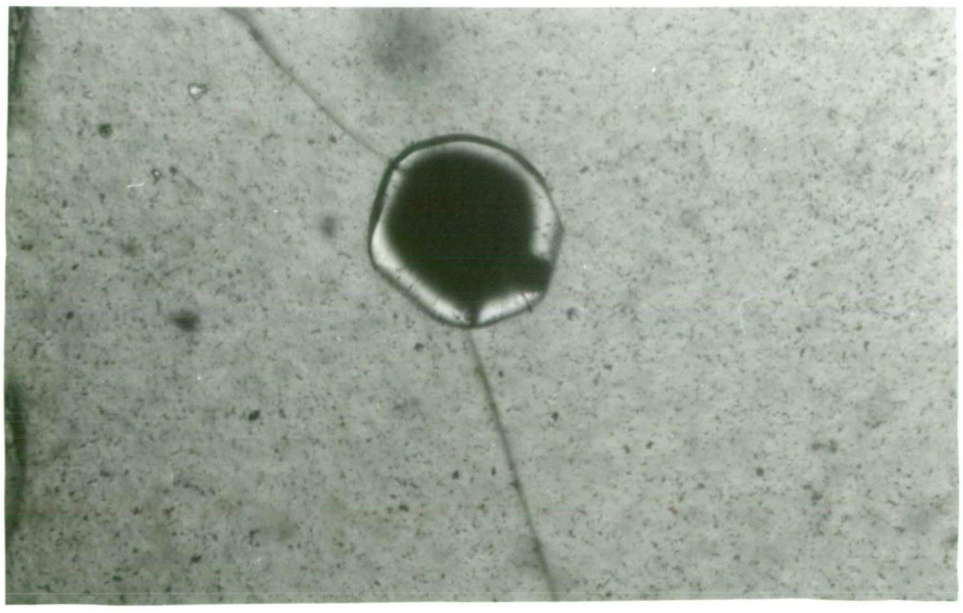

A

Table 22

Olivine glass inclusion microprobe analyses

	1	2	3	4	5	6	7	8
SiO_2	58.64	61.22	61.78	61.08	60.68	60.26	60.80	60.88
TiO_2	0.22	0.21	0.19	-	-	0.19	-	-
Al_2O_3	12.38	14.18	14.27	13.99	12.24	12.31	12.42	13.41
FeO	6.91	4.31	4.17	4.21	6.59	6.28	5.99	4.80
MgO	7.52	3.71	3.59	6.27	6.06	6.03	5.95	5.03
CaO	13.41	14.78	14.89	13.57	13.55	13.89	14.18	14.77
Na_2O	0.62	0.75	0.85	0.74	0.48	0.71	0.49	0.85
K_2O	0.19	0.16	0.16	0.15	0.30	0.20	0.17	0.18
Cl	0.10	0.08	0.10	-	0.11	0.12	-	0.07
Mg#	0.66	0.60	0.61	0.73	0.62	0.63	0.64	0.65

Remarks: no.s 1, 2, 6, 7, 8 are spot analyses, no.s 3, 4, 5 are broad area scan analyses. Glass totals normalised to 100%.

the olivine immediately adjacent to the glass, due to glass-olivine overlap. The glasses have high SiO_2 contents (58-62 wt%), low TiO_2 contents (0.19-0.22 wt%), and high CaO contents (13.9-14.9 wt%) relative to Al_2O_3 (12.4-14.27 wt%) and low Na_2O (0.48-0.85 wt%) contents. Because of the high CaO contents, the inclusions have high CaO/Al_2O_3 ratios (0.97-1.14) and exceptionally high CaO/Na_2O ratios (18-29).

Under the electron beam, especially during spot analysis, Na_2O may volatilize, resulting in anomalously low Na_2O contents. This problem was investigated by 1) comparing spot and broad area scans of the same inclusion and 2) by monitoring the counts on Na with time, for a spot analysis. Both approaches confirmed that Na-volatilization was not a problem, using the very low beam current (0.7 nanoamps) and spot and area scan techniques described above. The low Na_2O contents of these inclusions is definitely a primary feature.

4.4 CHEMICAL AFFINITIES OF THE CALCULATED PARENTAL MAGMA COMPOSITION

To establish the original magma chemistry sampled by a glass inclusion prior to post-entrapment processes it is necessary to incrementally add back olivine to the most magnesian glass compositions analysed. Two assumptions required are the $Fe^{2+}/(Fe^{3+} + Fe^{2+})$ ratio of the glass (0.9), and the Fe-Mg Kd between olivine and liquid (0.3). The relatively reduced $Fe^{2+}/(Fe^{3+} + Fe^{2+})$ ratio of 0.9 was chosen as the Cr-spinels which also occur as inclusions in the olivine phenocrysts, have very low Fe^{3+} contents ($Fe^{3+}/(Fe^{3+} + Al + Cr) \sim 0.06$) suggesting relatively low f_{O_2} in the original magma which crystallized the magnesian olivines. An example of a calculated magnesian magma composition, in equilibrium with Fo_{94} olivine, is given in Table 23 (analysis no. 4).

The calculated Tongan composition in terms of its high CaO, high CaO/Na_2O and CaO/Al_2O_3 ratios has geochemical affinities to proposed second-stage melts developed in oceanic tensional environments (Duncan & Green, 1980, 1987), such as the Upper Pillow Lavas from the Troodos ophiolite, Cyprus, and basalts from the Lau Basin (examples given in Table 23). Compared to stage-one melts, which are parental to typical MORB, second-stage melts have characteristically higher SiO_2 and CaO, and lower TiO_2 and Na_2O contents. A typical stage-one parental composition to MORB is given in Table 23, (analysis no. 1), it has a CaO/Na_2O ratio of 6.41 and a CaO/Al_2O_3 ratio of 0.79. The Tongan composition and other second-stage melts have CaO/Na_2O ratios $>\sim 14$ and CaO/Al_2O_3 ratios $>\sim 0.9$. Magmas of these

Table 23

Refractory melts developed in oceanic tensional settings

SiO_2	48.30	50.42	52.40	54.72	58.09	50.90
TiO_2	0.60	0.34	0.30	0.15	0.14	0.60
Al_2O_3	13.70	15.75	11.70	9.57	7.11	14.40
FeO	7.90	8.59	8.40	7.22	9.22	6.90
MnO	0.10	0.16	0.10	-	-	0.10
MgO	16.70	9.78	15.80	17.15	20.70	12.10
CaO	10.90	14.67	10.70	10.50	3.91	13.60
Na_2O	1.70	0.99	0.70	0.54	0.62	1.40
K_2O	0.10	0.01	0.10	0.15	0.21	0.10
Total	100.00	100.71	100.20	100.00	100.00	100.10
Mg#	0.79	0.67	0.77	0.81	0.80	0.76

(1) Primary MORB magma composition, olivine tholeiite DSDP3-18-7-1 (Frey et al., 1974) + 17 wt% Fo_{91} (Green et al., 1979).

(2) Lau Basin Basalt glass analysis 123 95-12 (Hawkins & Melchior, 1985).

(3) Inferred Upper Pillow Lava parental liquid (Duncan & Green, 1980).

(4) Calculated parental magma composition in equilibrium Fo_{94} olivine.

(5) Cape Vogel, parental magma composition (Walker & Cameron, 1983).

(6) Xenocryst melt inclusion (Donaldson & Brown, 1977).

(-) not determined.

characteristics have so far not been identified from major mid-ocean ridge tectonic environments, however several compositions have been identified which have a second stage melt 'fingerprint'. These are 1) xenocryst melt inclusions (e.g. Table 23, analysis no. 6), from the Mid-Atlantic ridge (Donaldson & Brown, 1977), 2) basaltic glass from DSDP site 236, Indian Ocean (Melson et al., 1977), 3) basaltic glass from the Costa Rica rift zone (Autio & Rhodes, 1984). All these samples have higher CaO/Na_2O and CaO/Al_2O_3 ratios than typical MORB. It is possible that more extreme compositions, such as those from Tonga, Troodos and the Lau Basin are involved in the production of ocean crust but are not directly observed due to processes such as magma mixing.

The Tonga composition shows the closest affinities to the inferred parental liquid to the Troodos ophiolite, Cyprus, but contains higher SiO_2 (54.7 compared to 52.4 wt%) and lower Na_2O contents (0.54 compared to 0.7 wt%) and TiO_2 contents (0.15 compared to 0.3 wt%). Such compositions may be a characteristic of forearc tensional environments. Boninites are another primitive magma composition which have been recovered from the forearc regions of W. Pacific island arcs. These are distinctly different from the Troodos, Tongan and Lau Basin compositions, in their characteristically high SiO_2 and very low CaO contents, which result in low CaO/Na_2O and characteristically low CaO/Al_2O_3 ratios (~<0.6). Although there are distinct major element differences between the primitive Tongan liquid identified and boninites, the Tongan composition does have geochemical affinities to boninites in terms of Cr-spinel compositions. Cr-spinels also occur as euhedral inclusions in the magnesian olivines containing the glass inclusions. They have very high Cr# >0.80, overlapping with Cr-spinels from boninites, and are distinctly more Cr-rich than spinels from Troodos (Cr# <0.80), (Fig. 36). The similarity in Cr-spinel compositions between the Tongan and boninite compositions indicates that they were derived from similar depleted mantle sources. There appears to be a spectrum of primitive magma compositions being supplied to the forearc and possibly back-arc regions of intra-oceanic island arcs.

The compositions in Table 23 are plotted in Fig. 37, for comparison with equilibrium partial melt compositions from a MORB pyrolite composition (PARTS I, II) and a more depleted peridotite composition, Tinaquillo lherzolite (Jaques & Green, 1980; Falloon et al., 1987). The stage-one melt S_1, is the MORB parental composition from Green et al. (1979) (DSDP3-18-7-1 + 17 wt% Fo_{91}), which is a primary melt at 20kb, segregating from a upper mantle peridotite (M, on Fig. 37) at 1420°C leaving a harzburgite residue

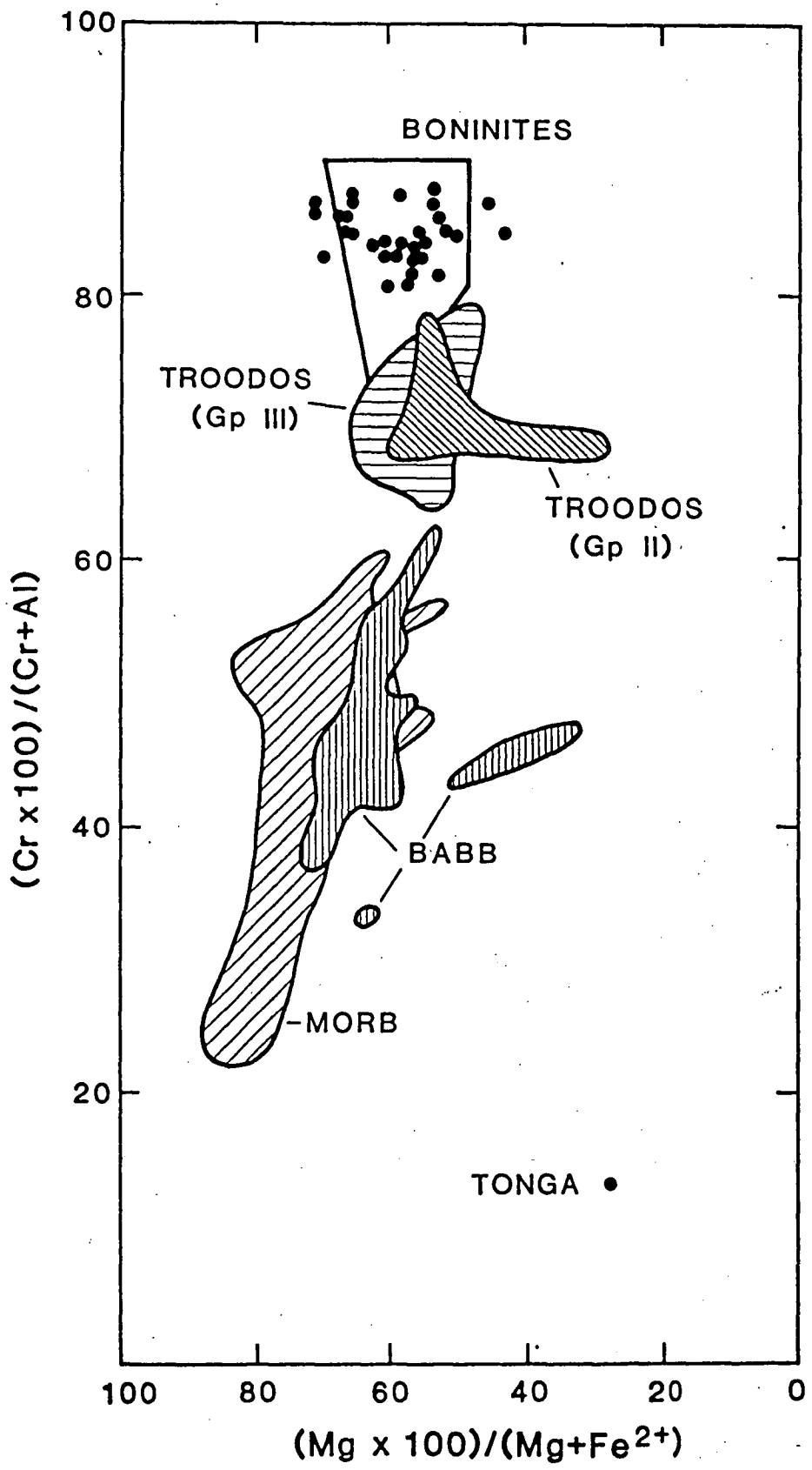

Figure 36.

Crx100/(Cr + Al) and Mgx100/(Mg + Fe) variations in spinel inclusions in magnesian olivine phenocrysts from north Tonga (Falloon unpubl. data) compared with spinels from Back-arc basin basalts (BABB), mid-ocean ridge basalts, boninites (Dick & Bullen, 1984), and Troodos Upper Pillow Lavas (Duncan & Green, 1987).

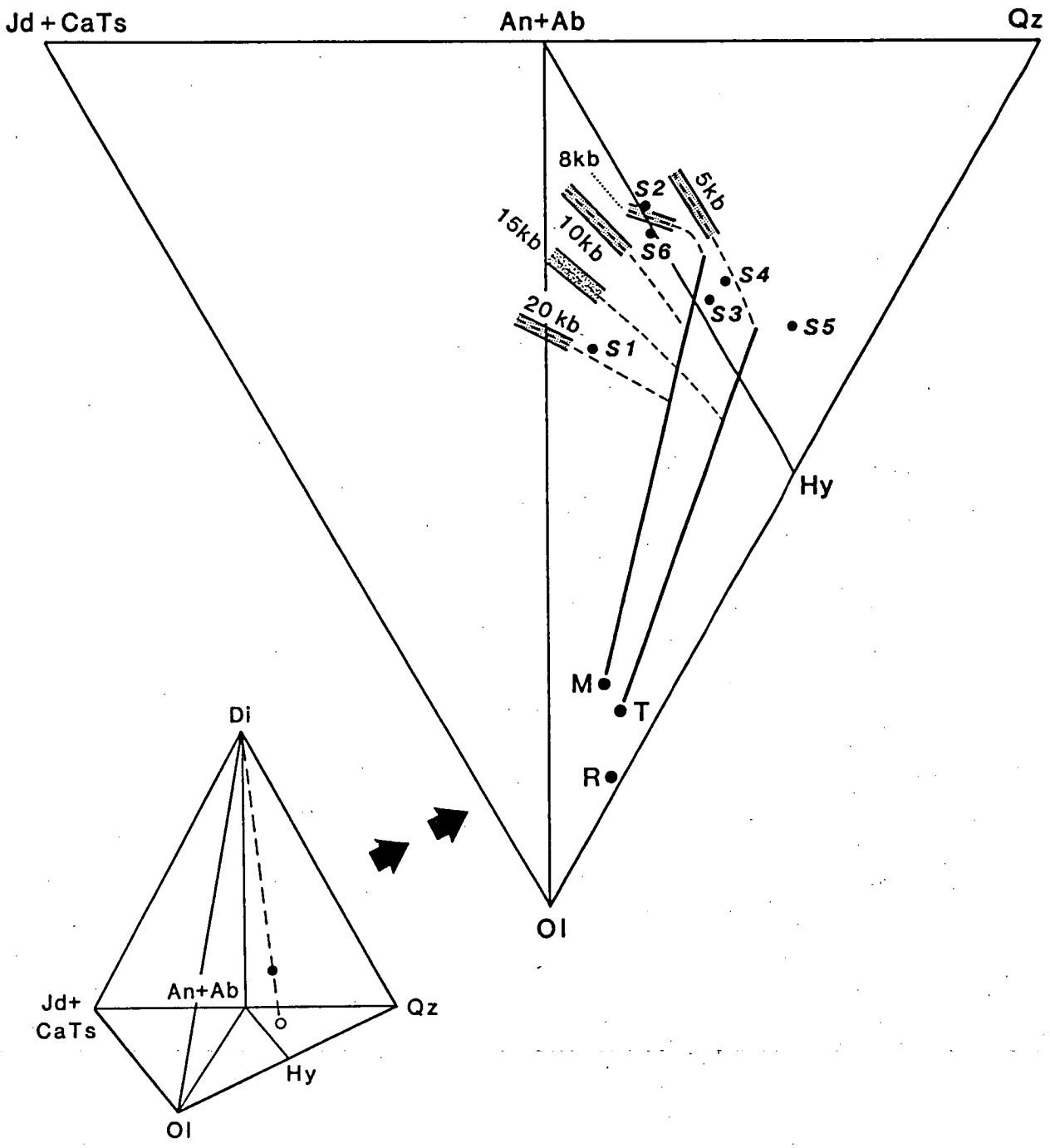

Figure 37.

CIPW molecular norm projection from Di onto the base of the basalt tetrahedron Jd + CaTs-Oliv-Qtz. M is a MORB pyrolite composition (PART I, II), T is Tinaquillo lherzolite (Jaques & Green, 1980) and R is the residual mantle composition after removal of stage-one melt composition S_1 (DSDP3-18-7-1 + wt% Fo_{91}, Green et al., 1979) from MORB pyrolite. Compositions S_1 to S_6 are taken from Table 23, ananlyses 1 to 6 respectively. Lines represent cotectics derived from the experimental melting of MORB pyrolite (PART I, II) and Tinaquillo lherzolite (Jaques & Green, 1980; Falloon et al., 1987).
Solid lines represent locus of liquids in equilibrium with olivine only.
Dashed lines represent locus of liquids in equilibrium with olivine and orthopyroxene only.
Dashed area represents locus of liquids in equilibrium with olivine and orthopyroxene and clinopyroxene.

(R, on Fig. 37). The residual diapir from this first stage melting event may continue to rise adiabatically and generate an additional melt fraction at some shallower depth. The range of second-stage melts (S_2, S_3, S_4, S_5, S_6) indicates a range of depleted residual mantle sources. Experimental studies on the Troodos parental composition (S_3), suggest it is a primary magma, having segregated from depleted upper mantle peridotite at about 25km, 1360°C leaving a harzburgite residue, with a water content of 0.5-1.0 wt% (Duncan & Green, 1987). The position of the Tongan primitive magma identified from the olivine glass inclusions (S_4), indicates a pressures of melt segregation of <5kb under anhydrous conditions in equilibrium with a harzburgite residue or at higher pressures (7-8kb), similar to the Troodos composition, at higher water pressures. The position of the boninite parental composition (S_5) requires it to have the most depleted of mantle sources. Experimental work by Jenner (1983) indicates that boninite compositions may derive from quite shallow levels (<5kb), provided water is present. The position of the Lau Basin glass (S_2) and the xenocryst melt inclusion (S_6) suggests that they are possible primary magmas at pressures of <8kb under anhydrous conditions, leaving a lherzolite residue from a mantle source similar to typical MORB but more depleted in Na_2O and TiO_2. Although this inference is compatible with the Jd + CaTs-Ol-Qz plot, it is not consistent with low pressure cotectic melts plotted in the Di-Ol-Qz plane of the basalt tetrahedron. The compositions (S_2, S_6) plot above the ol+opx+cpx+L cotectic, lying in the cpx phase volume in the Di-Ol_Qz projection from An + Ab. This suggests that S_2 and S_6 are fractionated compositions, having undergone fractionation from more picritic parents.

4.5 IMPLICATIONS FOR CALCIC PLAGIOCLASE IN ISLAND-ARC AND MID-OCEAN RIDGE BASALTS

The origin of extremely calcic plagioclase phenocrysts and megacrysts is a problem common to basalts both from island arcs and mid-ocean ridges (Donaldson & Brown, 1977; Gill, 1981; Arculus & Wills, 1980; Stakes et al., 1984). Plagioclase in dredged lavas from the north Tonga arc occurs as discrete phenocrysts and in large glomeroporphyritic clusters, either by itself or associated with clinopyroxene and orthopyroxene. Plagioclase can be either euhedral or subhedral, commonly displaying evidence of resorption. The plagioclase is extremely calcic, phenocryst core compositions range from An_{81} to An_{100}, and most plagioclase cores >An_{90}. These calcic plagioclase phenocrysts are not in equilibrium with the host rock in which they are found. This is demonstrated in Fig. 38 where the straight line shows the empirical relationship between the 100Ca/(Ca + Na)

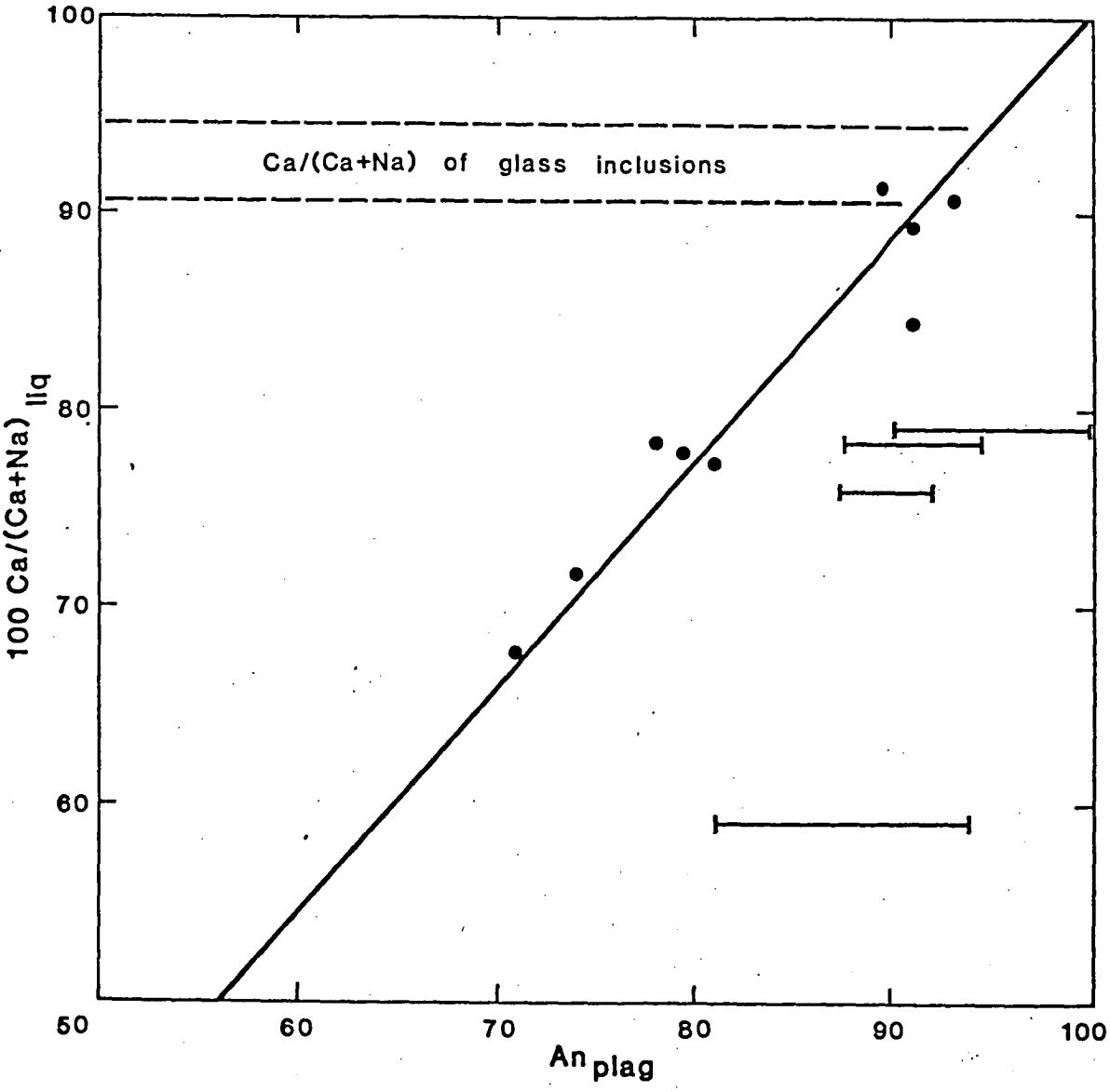

Figure 38.

The empirical relationship between the 100Ca/(Ca + Na) ratio of a bulk composition and the most anorthite-rich plagioclase capable of crystallizing under anhydrous conditions regardless of pressure and temperature (restricted to basaltic compositions of between 15-25 wt% normative Diopside). The line is based on the experimental studies (Duncan & Green, 1987; Green et al., 1979; Green et al., 1972; Bender et al., 1978; Fujii & Bougault, 1983; Dungan et al., 1978; Fukuyama & Hamuro, 1978). (●) are the data points taken from the above experiments. Bars indicate the range in plagioclase core compositions from dredged lavas from the north Tonga arc (Falloon, unpubl. data).

ratio of a bulk composition and the most anorthitic plagioclase which can crystallize from that composition under anhydrous conditions. The empirical relationships only holds for rocks of basaltic composition of between 15-25 % normative diopside, thus the relationship is applicable to MORB and the Tongan compositions. The line was constructed from the experimental studies listed in the caption of Fig. 38 and consisted of taking the most anorthitic plagioclase, regardless of pressure or temperature. Thus the relationship shown in Fig. 38 is a more general relationship than the Drake (1976) approach which requires some independent means of determining temperature before a plagioclase composition can be determined. The relationship in Fig. 38 emphasises the strong relationship between plagioclase composition and the 100Ca/(Ca + Na) ratio of the bulk rock composition. For anhydrous conditions, the plagioclase phenocryst cores in the Tongan lavas are out of equilibrium with their host rocks, i.e. they are hosted in rocks which have lower 100Ca/(Ca + Na) ratios than would be expected, similar results are found for MORB (see Fig. 16, in Stakes et al., 1984). An increase in P_{H_2O} is commonly cited in the literature, as an explanation of very anorthite-rich plagioclase in basaltic magma, based on experimental work in simple systems (Arculus & Wills, 1980). However this effect in complex systems has far not been demonstrated experimentally. Increasing P_{H_2O} will lower the plagioclase liquidus relative to clinopyroxene and orthopyroxene (Sekine et al.,1979), causing a less anorthite-rich plagioclase to crystallize, due to enhanced pyroxene fractionation. At the present time, P_{H_2O} can not be considered as having an important effect on the liquidus plagioclase composition, rather the bulk composition of the magma as reflected in its 100Ca/(Ca + Na) ratio, will have the determining role.

The relationship in Fig. 38 requires the existence of magmas with 100Ca/(Ca + Na) ratios of between 78 to 100 to account for the calcic plagioclase phenocrysts. The glass inclusions in the olivine phenocrysts from Tonga have 100Ca/(Ca + Na) ratios of between 91-94 (Fig. 38), and thus provide a ready solution to the problem of calcic plagioclase phenocrysts in the Tongan arc magmas. These calcic magmas may not be represented or seen in island arc and MORB lava piles due to the efficiency of processes such as magma mixing, which modify and mask primary compositional characteristics. This effect is illustrated in Fig. 39 where the CaO/Na_2O ratios of Tongan lavas are plotted against MgO contents. The inferred fractionation path of the primitive liquid composition, identified from glass inclusions, is also illustrated. The fractionation of mafic phases

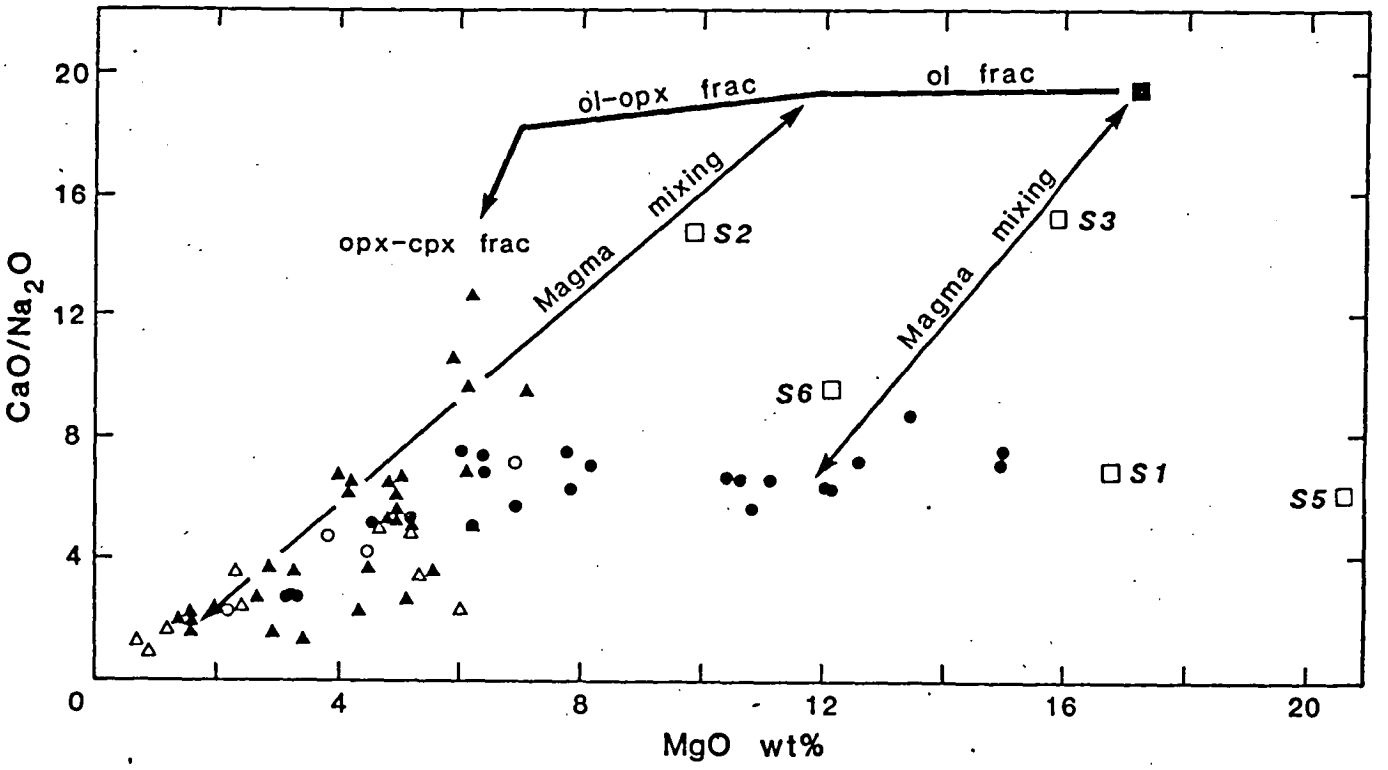

Figure 39.

CaO/Na_2O ratio versus MgO wt% for Tonga lavas from the Tonga islands (▲) (Ewart et al., 1973), and dredged lavas from the north Tongan arc (●) (PART III, Appendix 3). (■) is the primitive magma composition identified from glass inclusions in olivines. Compositions labelled S_1, S_2, S_3, S_4, S_5, S_6 are from Table 23.

(O) are groundmass compositions from dredged lavas from the north Tonga arc (Falloon unpubl. data).

(△) are calculated groundmass compositions for lavas from the Tongan islands (Ewart et al., 1973).

Thick solid line is the inferred fractionation path for the primitive magma composition identified from melt inclusions.

such as olivine will have little effect on the CaO/Na_2O ratio whereas the pyroxenes will have a slight (orthopyroxene) to major (clinopyroxene) effect on the CaO/Na_2O ratio. The primitive Tongan composition will fractionate mafic phases until plagioclase saturation is reached and the plagioclase composition which crystallizes will be very calcic. These partially crystallized liquids, containing plagioclase and other phenocrysts can then be mixed with magmas of lower CaO/Na_2O ratios. Thus the bulk rock compositions from dredged and emergent island samples, (Fig. 39) may represent the mixing of at least two liquids, one of which is defined by the melt inclusions, and other by the quenched glasses and aphyric groundmass compositions of the host rocks; this suggests similar ol + opx control but with lower CaO/Na_2O ratios. Some of the groundmass compositions of the Tongan lavas have significantly lower CaO/Na_2O ratios than some of the Whole rock compositions. This could be explained by contributions from magmas of high CaO/Na_2O ratios being mixed into the more common low CaO/Na_2O ratio magmas. On Fig. 39 several different mixing lines are shown to illustrate this point. Mixing may occur at any point along the fractionation trend of the primitive Tonga composition, accounting for the scatter in data points seen in this diagram.

PART V

PETROGENESIS OF HIGH-MG LAVAS AND ASSOCIATED ISLAND ARC THOLEIITES FROM NORTH TONGA

5.1 INTRODUCTION

The nature of primary magmas in island arc settings is presently a subject of controversy both with respect to the nature of the melted source rock (peridotitic versus eclogitic) and to the origin of the distinctive trace element and isotopic enrichments observed (wedge, subducted oceanic lithosphere, subducted sediment, hydrous fluid or mantle metasomatism). The scarcity of primary or near-primary magmas in arcs adds further to this problem. Distinctive high-SiO_2, high-mg lavas dredged from the north Tonga arc (Fig.28) during the 1984 cruise of the research vessel 'Natsushima' are characterised by highly magnesian olivine (upto Fo_{94}) and orthopyroxene (upto Mg# 90) and glass which has high Mg# (>0.66). They are, therefore, important to this debate as they have the appropriate characteristics to be primary or near-primary liquids from the partial melting of a upper mantle peridotitic source (PART III, PART IV). These lavas are also very fresh, so that their trace element and isotopic characteristics can be confidently used in evaluating potential source components.

Details about the dredge locations, major and trace element geochemistry and affinities of the dredged north Tongan lavas are given in PART III. PART IV presented evidence from the chemistry of glass inclusions in magnesian olivine phenocrysts for the existence of extremely refractory parental magmas in the Tonga arc. In this study we present detailed petrographic and mineral chemical data on the high-mg lavas, with the aim of demonstrating that magma mixing has occurred. We also present new Sr and Nd isotopic data on the dredged lavas and discuss the petrogenesis of the high-mg lavas in light of models currently proposed for the origin of island-arc magmas.

5.2 PETROGRAPHY AND MINERAL CHEMISTRY

Table 24 summarizes the mineral chemical and petrographic features of representative samples of the dredged lavas. The mineral chemistry of pyroxene, plagioclase and Cr-spinel is summarized in Figs. 40, 41 and 42 and 43, representative analyses are given in Tables 25, 26, and 29. The compositions of glass inclusions trapped in magnesian olivine phenocrysts are given in Table 28 and wholerock, groundmass and glass rind compositions of the representative samples are given in Table 27.

The petrography and mineral chemistry of the lavas indicates disequilibrium between assemblages of phenocryst-phenocryst and phenocryst-liquid. This disequilibrium can be explained by magma mixing. This conclusion is supported by compositions of glass inclusions trapped in magnesian olivine phenocrysts. The discussion below concentrates mainly on those features of the mineral chemistry indicating disequilibrium and implied magma mixing.

The petrography and mineral chemistry define four groups of high-mg lavas from north Tonga (Table 24), basaltic andesites were recovered with high-mg lavas from station-23 and are included in this discussion.

5.2.1 Groundmass pyroxenes

Groundmasses of all four groups of high-mg lavas consist of fresh glass, abundant laths of pyroxene and small Cr-spinel euhedra. The groundmass of the station 23 basaltic andesites contains plagioclase, pyroxene and fresh glass; Cr-spinel is absent.
Representative compositions of groundmass pyroxenes are presented in Table 25 and summarized in Fig. 40a, b and d.

Quench pyroxene compositions in station 25 high-mg lavas are augitic and are distinguished from other pyroxene compositions by low Mg#, low SiO_2, and high Al_2O_3 contents (Table 25, no.s 3 and 4). Also present in the groundmass of the station 25 high-mg lavas are small euhedra of magnesian endiopside (Table 25, no.1). Random microprobe analyses produced a continuous range of compositions from magnesian pigeonite to magnesian endiopside. SEM back-scattered electron images, however, reveal the presence of distinct pigeonite cores to the endiopside euhedra (Fig. 41). Similar magnesian pigeonite cores to diopside microphenocrysts are present

Table 24

Summary of the petrography and mineral chemistry of the dredged lavas from North Tonga.

Station no.	Group	Phenocrysts and microphenocrysts	Groundmass Phases
23	Group A high-Mg lavas (sample no. 5-24, 28)	1) Olivine (15%), Mg# 85.0-91.8, euhedral to resorbed Cr-spinel inclusions (Cr# 83.8-87.5), glass inclusions 2) Orthopyroxene (18%), Mg# 83.6-89.7, zoning (R, N, U), euhedral to resorbed, glomeroporphyritic clusters common, Cr-spinel inclusions (Cr# 75.2-82.5). 3) Clinopyroxene (X), Mg# 84.8, strongly resorbed. 4) Cr-spinel (<1%), Cr# 82.1-83.3.	Fresh glass and spherulitic quench pyroxene (augite zoned to subcalcic augite [Mg# 84.8-72.3]), small orthopyroxene (Mg# 86.4) and Cr-spinel (Cr# 76.7-87.4) euhedra, strongly vesicular (40%).
23	Group B high-Mg lavas (sample no. 5-25)	1) Olivine (16%), Mg# 84.6-94.0, euhedral to resorbed Cr-spinel inclusions (Cr# 80.2-87.1), glass inclusions. 2) Orthopyroxene (8%), Mg# 86.5-81.1, zoning (N, R), resorbed to euhedral, glomeroporphyritic clusters common, Cr-spinel inclusions (Cr# 71.9-84.1). 3) Clinopyroxene (2%), Mg# 90.2-82.9, zoning (N, R), euhedral to resorbed, Cr-spinel inclusions (Cr# 67.5). 4) Cr-spinel (<1%), Cr# 76.6-86.5.	Fresh glass and quench pyroxene microlites (pigeonite zoned to augite [Mg# 85.3-81.6]) Cr-spinel euhedra (Cr# 82.4-85.9), strongly vesicular (50%).
23	Basaltic andesites (sample no. 5-20,21 23, 27)	1) Plagioclase (3-14%), An 83-96, zoning (R,O), strongly resorbed to euhedral, glomeroporphyritic clusters with pyroxene common, both having mutually subhedral grain contacts. 2) Clinopyroxene (1-2%), Mg# 83.9-76.5, zoning (N, R, U), euhedral to resorbed. 3) Orthopyroxene (1-4%), Mg# 82.7-77.3, zoning (N, R, U), euhedral to resorbed. 4) Olivine (X), strongly resorbed, Mg# 80.4, Cr-spinel inclusion (90.7).	Fresh hyalopilitic texture, plagioclase microlites (An 64-81), quench pyroxene laths (pigeonite zoned to augite [Mg# 75.1-61.4] or augite zoned to subcalcic augite [Mg# 81.6-56.4]), vesicules (0-40%).
24	high-Mg lavas (sample no. 6-2, 3)	1) Olivine (14%), Mg# 88.5-91.7, euhedral to skeletal, Cr-spinel inclusions (Cr# 80.5-85.9), glass inclusions. 2) Orthopyroxene (4%), Mg# 89.3, euhedral. 3) Orthopyroxene (X), Mg# 86.3-89.8, Clinopyroxene (X), Mg# 87.4, both resorbed.	Fresh glass and spherulitic quench pyroxene (augite zoned to subcalcic augite [Mg# 84-60.8]), Cr-spinel euhedra (Cr# 82.6-85.4), vesicular (30%).
25	high-Mg lavas (sample no. 7-14, 15, 16, 18)	1) Olivine (10%), Mg# 87.4-92.1, euhedral to skeletal, Cr-spinel inclusions (Cr# 81.5-84.1).	Fresh glass, spherulitic quench pyroxene (augite [Mg# 75.3-69.2]), Small endiopside euhedra (Mg# 88.7) with pigeonite cores (Mg# 86.0, 3.4-4.0 wt% CaO), Cr-spinel euhedra (Cr# 76.8-84.5), vesicules (30%).

modal percentages for phenocryst phases based on point counting of >1000 points, and have been resummed on the basis of 0% vesicles, R, N, O, and U stand for reversely, normally , oscillatory and unzoned respectively. X stands for rare <<1% xenocryst.

Table 25

Representative electron microprobe analyses of groundmass pyroxenes from north Tonga lavas

	1	2	3	4	5	6	7	8	9	10	11	12	13	14	15	16	17	18	19	20
SiO_2	52.83	56.70	49.65	48.42	56.86	52.06	47.37	56.81	53.70	48.65	55.66	53.05	54.16	52.18	51.70	49.44	53.94	50.78	53.74	50.54
TiO_2	0.25	-	0.61	0.81	-	0.32	0.42	-	-	0.26	-	-	-	0.32	0.18	0.63	-	0.41	0.17	0.45
Al_2O_3	1.76	0.63	6.07	6.92	0.81	3.12	9.66	0.60	1.62	7.72	0.60	1.51	1.57	1.98	2.91	3.86	1.70	4.69	0.79	3.03
Cr_2O_3	1.27	0.22	-	-	0.69	-	-	0.32	0.35	-	0.30	0.28	-	-	0.29	-	-	-	-	-
FeO	5.05	8.79	8.66	11.13	7.05	6.67	14.78	8.86	5.93	11.50	10.39	7.93	15.70	16.75	8.89	18.40	15.65	14.96	17.35	16.38
MnO	-	-	-	-	-	-	-	-	-	-	-	-	-	0.25	-	0.33	0.32	0.37	-	0.26
MgO	18.71	30.24	13.88	12.91	32.94	16.75	12.88	31.51	18.27	14.85	30.00	17.41	25.68	18.06	17.49	12.93	23.76	17.23	23.19	14.17
CaO	20.13	3.42	21.13	19.81	1.65	21.08	14.88	1.90	20.13	17.02	3.05	19.82	2.95	10.46	18.54	14.40	4.63	11.55	4.46	15.17
Total	99.97	100.00	100.00	100.00	100.00	100.00	99.99	100.00	100.00	100.00	100.00	100.00	100.06	100.00	100.00	99.99	100.00	99.99	99.70	100.00
Mg#	0.87	0.86	0.74	0.67	0.89	0.82	0.61	0.86	0.85	0.70	0.84	0.80	0.74	0.66	0.78	0.56	0.73	0.67	0.70	0.61
$Mg\#^1$	0.89	0.86	0.75	0.69	0.89	0.84	0.61	0.86	0.85	0.72	0.85	0.82	0.75	0.66	0.82	0.56	0.73	0.67	0.71	0.61
Wo	38.40	6.60	40.50	37.30	3.20	40.50	24.00	3.60	38.90	29.80	6.00	38.40	6.00	22.00	35.00	27.00	9.50	25.90	9.00	29.00
En	54.60	80.30	44.80	43.40	86.50	50.00	46.20	83.20	51.80	50.80	80.20	50.20	70.60	51.30	53.00	41.20	66.10	49.80	64.40	43.60
Fs	6.90	13.10	14.70	19.30	10.40	9.50	29.80	13.10	9.30	19.40	13.80	11.30	23.40	26.70	12.00	31.90	24.40	24.30	26.60	27.40

(-) indicates below detection limit, $Mg\#^1 = Mg/(Mg + Fe^{2+})$ with Fe^{3+} calculated by stoichiometry, all analyses normalised to 100% volatile free. Analyses are as follows: (1) clinopyroxene microphenocryst 7-16, (2) pigeonite core to clinopyroxene microphenocryst 7-16, (3) quench clinopyroxene, (4) quench clinopyroxene 7-18, (5) orthopyroxene microphenocryst 6-2, (6) quench clinopyroxene 6-2, (7) quench clinopyroxene 6-2, (8) orthopyroxene microphenocryst 5-28, (9,10) quench clinopyroxene 5-28, (11) quench pigeonite 5-25, (12) quench clinopyroxene 5-25, (13) quench pigeonite 5-27, (14) quench clinopyroxene 5-27, (15,16) quench clinopyroxene 5-20, (17) quench pigeonite 5-23, (18) quench clinopyroxene 5-23, (19) quench pigeonite 5-21, (20) quench clinopyroxene 5-21.

Figure 40.

Representative compositions of pyroxenes from north Tonga lavas. Pyroxene endmember solid solutions as follows, Di diopside, Hd hedenbergite, En enstatite, Fs ferrosalite. Classification of pyroxene compositions from Deer et al. (1966), D diopside, S salite, ED endiopside, A augite, SA subcalcic augite, MP magnesian pigeonite.

A) Pyroxene compositions from station 24 high-mg lavas (samples 6-2, 6-3), (■) orthopyroxene cores to small groundmass pyroxene euhedra, enclosing field encloses range of orthopyroxene microphenocrysts, (●) random microprobe spot analyses of groundmass pyroxenes indicating overlap between orthopyroxene cores and quench pyroxene rims, field of quench clinopyroxene is indicated, (□) xenocrystal endiopside.

B) Representative compositions from station 25 (samples 7-14, 7-15, 7-16, 7-18) high-mg lavas, (■) pigeonite core to endiopside microphenocrysts (see also Fig. 3a, b), (□) endiopside microphenocrysts, (●) random microprobe analyses of groundmass pyroxenes, resulting in overlap between pigeonite cores to endiopside microphenocrysts and endiopside and quench augite compositions. Field encloses range of quench clinopyroxene compositions.

C) Orthopyroxene and clinopyroxene phenocrysts in the north Tonga lavas compared with the range observed in Tofua magmatic arc lavas (Ewart et al., 1973). A corresponds to Group A high-mg lavas from station 23 (samples 5-24, 5-28), B corresponds to Group B high-mg lava from station 23 (sample 5-25), stippled field corresponds to station 23 basaltic andesites (samples 5-27, 5-20, 5-21, 5-23), cross-hatched field corresponds to Tofua magmatic arc pyroxenes.

D) Groundmass pyroxene trends in dredged lavas from station 23, north Tonga. Arrows indicate the change in pyroxene compositions from core to rim.

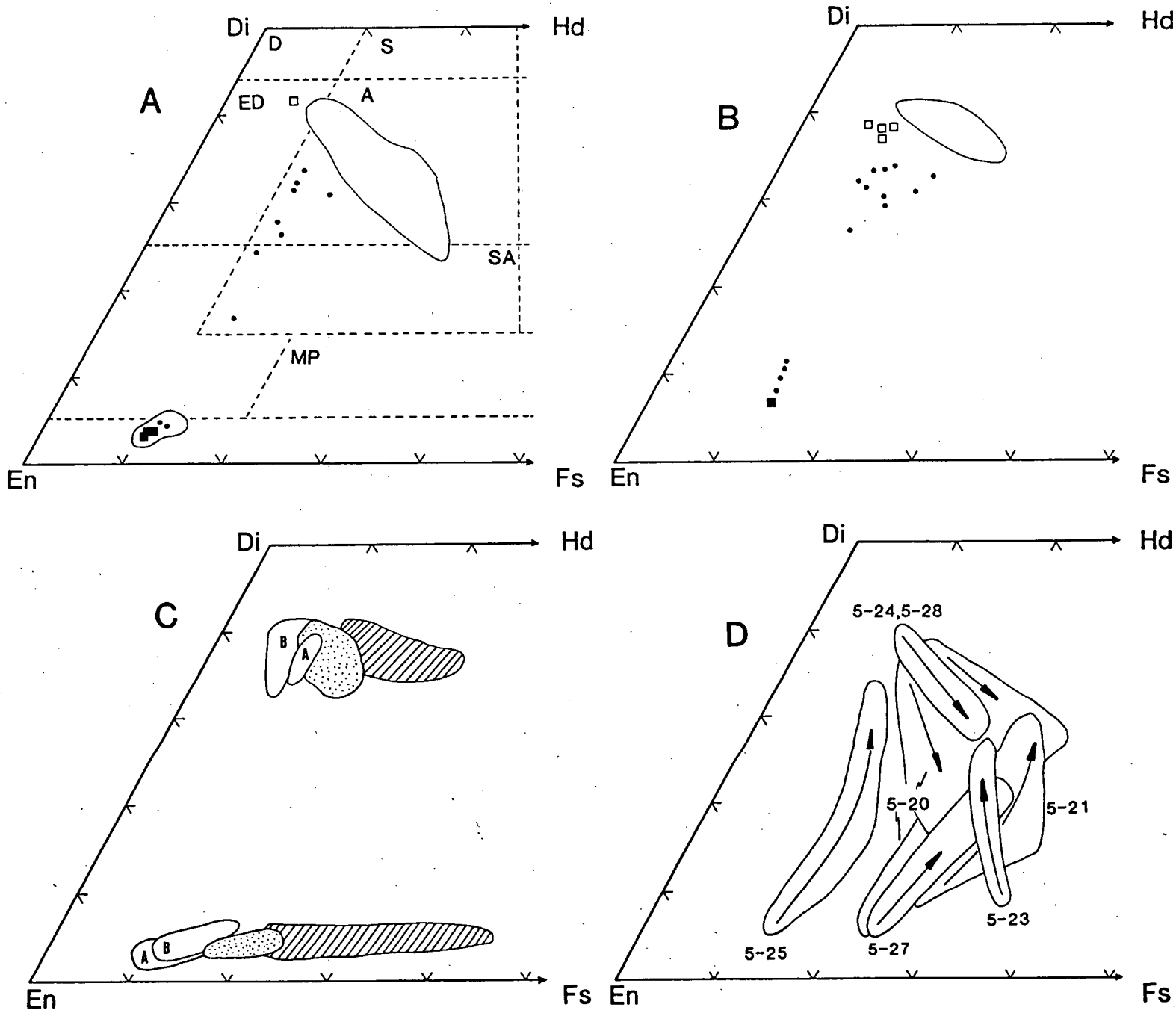
A
Di
Hd
En
Fs
D
S
ED
A
SA
MP
B
Di
Hd
En
Fs
C
Di
Hd
En
Fs
B
A
A
B
D
Di
Hd
En
Fs
5-24,5-28
5-20
5-21
5-23
5-25
5-27

Figure 41a.

SEM backscattered electron image of small endiopside microphenocrysts within the groundmass of sample 7-16 (station 25, high-mg lava). Dark areas correspond to magnesian pigeonite cores (Table 25, no.2) scale black and white bands correspond to 100 μm.

Figure 41b.

same as in A scale bars correspond to 10 μm.

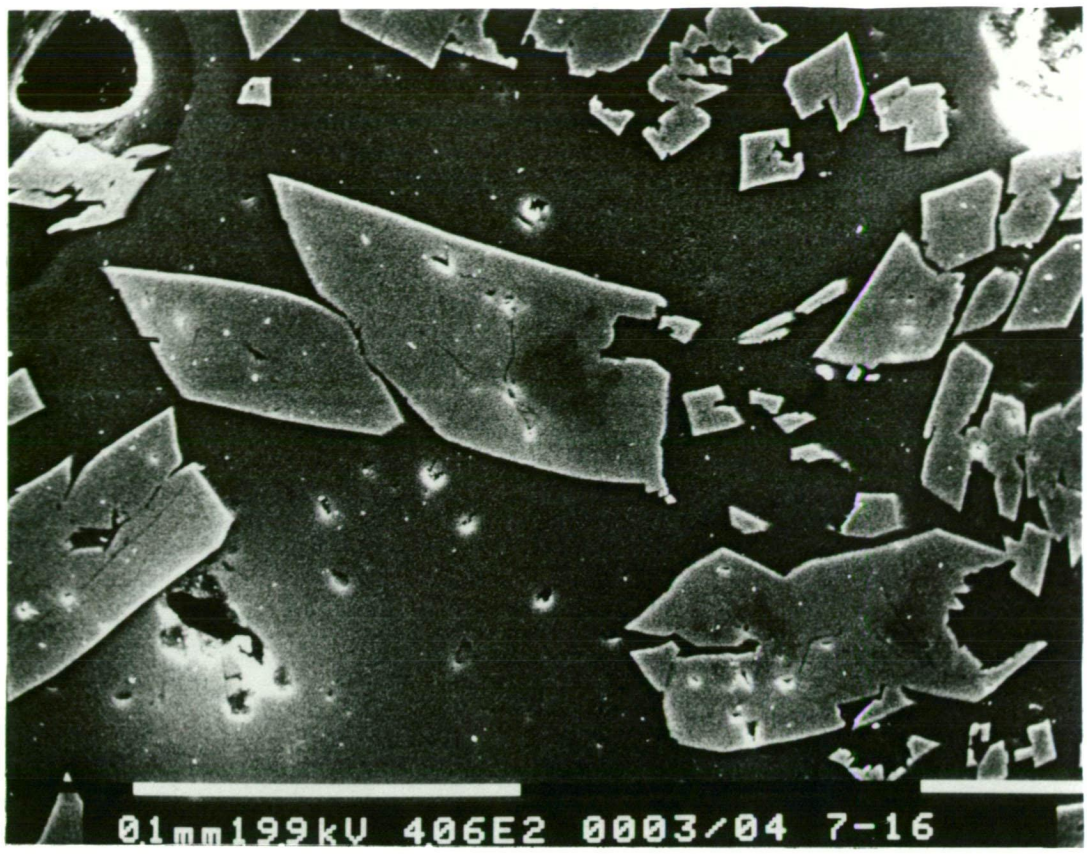
01mm199kV 406E2 0003/04 7-16

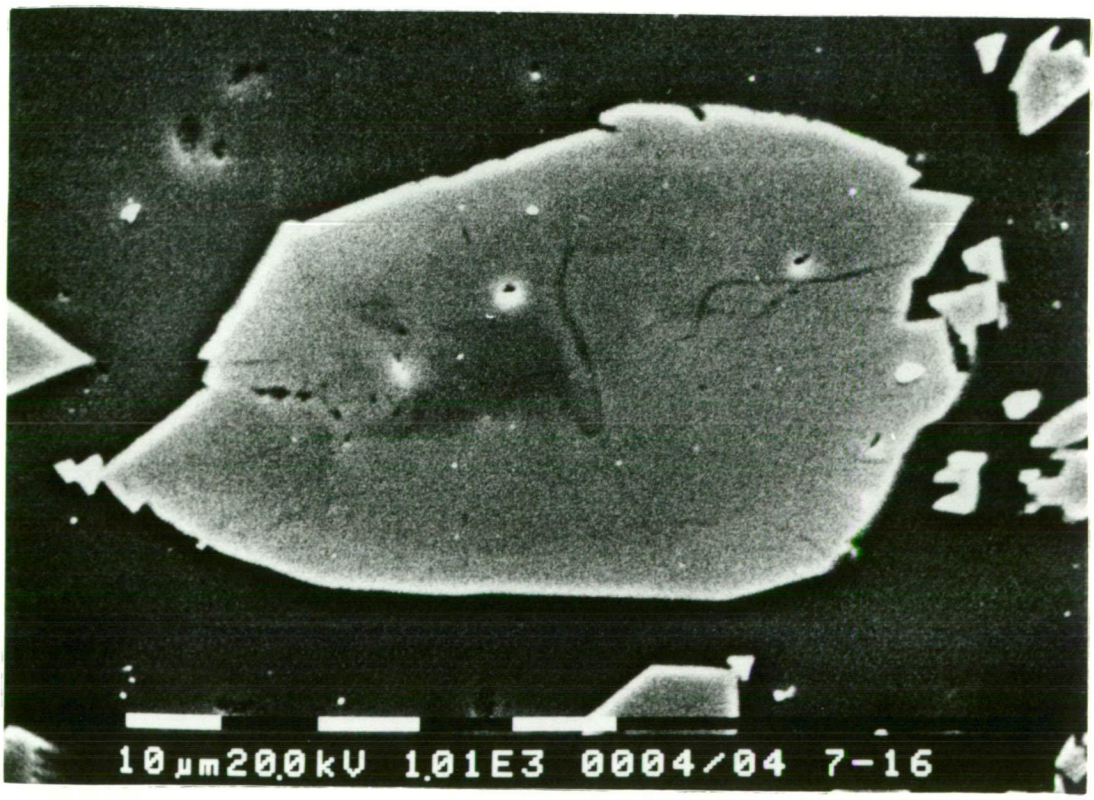
10µm20.0kV 1.01E3 0004/04 7-16

in sample 61358 from the Troodos upper pillow lavas (Duncan & Green, 1987). Experimental studies (Duncan & Green, 1987) on a reconstructed Troodos parental magma composition (compositionally very similar to station 25 high-mg lavas) demonstrated that these magnesian pigeonite cores started to crystallize close to 5kbar, and were overgrown by clinopyroxene enroute to the surface before eruption; during eruption, the quench augite compositions crystallized. Similar groundmass magnesian pigeonites have been reported by Umino (1986) in type IV boninite lavas from Chichijima, Bonin Islands which have similar major element compositions to the station 24 and 25 high-mg lavas. Umino (1986) found that the type IV boninite was unrelated to the other clinoenstatite-bearing boninites on Chichijima.

Quench pyroxenes in Group A high-mg lavas from station 23 and station-24 high-mg lavas range in compositions from augite to subcalcic augite (Table 25, nos. 6, 7, 9 and 10). A range of core composition was also noted by random microprobe analyses; core compositions zoned continuously from a magnesian orthopyroxene (Table 25, no.5) to less magnesian quench pyroxene. SEM back-scattered electron images revealed the presence of small compositionaly uniform orthopyroxene microphenocrysts with quench overgrowths. Quench pyroxenes in Group B high-mg lava sample 5-25 are zoned from pigeonite cores to augite rims. Groundmass pyroxenes in station 23 basaltic andesites are also zoned from pigeonite cores to augite rims; sample 5-20 is distinct in having two quench pyroxene trends (Fig. 40d), one extending from pigeonite cores to augite rims, the other extending from augite cores to subcalcic augite rims (Fig. 40d).

5.2.2 Pyroxene phenocrysts

Representative pyroxene phenocryst compositions are presented in Table 26 and shown in Fig. 40c. The pyroxenes in the dredged north Tongan lavas are in general more magnesian than pyroxenes reported from Tofua magmatic arc volcanics (Ewart et al., 1973). Pyroxene phenocrysts exhibit a range of zoning with respect to Mg#, from relatively unzoned, to normal- and reverse zoned. They also show a significant range in Mg# within one individual host rock; e.g. in sample 5-25 pyroxene phenocryst range in Mg# from 0.81 to 0.90. Based on experimentally-determined pyroxene-liquid Kd's for Mg-Fe partitioning (Grove et al., 1982; Grove & Bryan, 1983) many of the less magnesian pyroxene compositions are not in equilibrium with their host groundmass compositions (Table 27). Pyroxene compositions in station 23 basaltic andesites are less magnesian than pyroxenes in the high-mg

Table 26

Representative electron microprobe analyses of pyroxene phenocrysts and microphenocrysts in north Tonga lavas

	1		2	3	4	5		6		7		8		9		10	11		12	
	C	R	C	C	C	C	R	C	R	C	R	C	R	C	R	C	C	R	C	R
SiO_2	52.60	53.80	52.92	53.70	53.15	53.38	53.70	52.25	51.02	54.93	55.43	56.83	57.38	56.14	55.97	57.38	54.83	56.03	55.48	54.55
TiO_2	-	-	-	-	-	-	-	-	0.33	-	-	-	-	-	-	-	-	-	-	-
Al_2O_3	1.92	0.93	1.53	1.62	1.76	1.70	1.36	2.16	3.42	0.98	1.09	0.55	0.55	0.93	1.02	0.46	1.06	0.79	1.06	1.21
Cr_2O_3	0.29	0.56	0.79	0.35	-	0.42	0.65	0.61	-	0.20	-	0.51	0.35	-	0.57	0.38	0.39	0.27	-	-
FeO	7.25	6.59	5.47	5.93	5.99	7.13	6.35	8.07	10.40	13.21	10.95	8.01	7.07	9.09	8.36	6.77	13.22	11.32	11.76	13.93
MnO	-	-	-	-	-	-	-	-	-	-	-	-	-	-	-	-	0.21	-	0.27	0.30
MgO	17.52	20.52	18.62	18.27	17.75	17.27	17.84	17.99	15.91	28.74	30.46	32.55	33.39	31.75	32.32	33.31	28.21	29.66	29.55	28.09
CaO	20.42	17.60	20.67	20.13	21.35	20.10	20.10	18.92	18.92	1.94	2.07	1.55	1.26	2.09	1.76	1.70	2.08	1.93	1.87	1.92
Total	100.0	100.0	100.0	100.0	100.0	100.0	100.0	100.0	100.0	100.0	100.0	100.0	100.0	100.0	100.0	100.0	100.0	100.0	100.0	100.0
Mg#	0.81	0.85	0.86	0.85	0.84	0.81	0.83	0.80	0.73	0.80	0.83	0.88	0.89	0.86	0.87	0.90	0.80	0.82	0.82	0.78
$Mg\#^1$	0.85	0.87	0.90	0.85	0.87	0.81	0.83	0.84	0.76	0.81	0.85	0.88	0.89	0.88	0.89	0.90	0.80	0.82	0.83	0.80
Wo	39.30	33.10	39.30	38.90	41.20	39.10	39.00	36.00	36.00	3.90	4.10	3.00	2.40	4.10	3.50	3.20	4.20	3.80	3.70	3.90
En	51.60	58.60	54.70	51.80	51.40	49.50	50.90	53.70	49.00	77.90	81.80	85.30	87.20	84.20	86.00	86.90	76.90	79.30	79.70	77.00
Fs	9.10	8.40	5.90	9.30	7.40	11.50	10.20	10.30	15.00	18.20	14.00	11.70	10.40	11.70	10.50	9.90	19.00	17.00	16.60	19.10

(-) indicates below detection limit, C = core, R = rim, $Mg\#^1$ = $Mg/(Mg + Fe^{2+})$ with Fe^{3+} calculated by stoichiometry, all analyses normalised to 100% volatile free. Analyses are as follows: (1) reversally zoned clinopyroxene phenocryst 5-25, (2) clinopyroxene phenocryst 5-25, (3) resorbed xenocrystal clinopyroxene 5-28, (4) resorbed xenocrystal clinopyroxene 6-3, (5) reversally zoned clinopyroxene phenocryst 5-27, (6) normally zoned clinopyroxene phenocryst 5-20, (7) reversally zoned orthopyroxene phenocryst 5-25, (8, 9) reversally zoned orthopyroxene microphenocrysts 5-24, (10) resorbed orthopyroxene core in olivine host (Fo_{90}) 6-2, (11) reversally zoned orthopyroxene phenocryst 5-27, (12) normally zoned orthopyroxene phenocryst 5-21.

lavas, and overlap with Tofua magmatic arc pyroxene compositions (Fig. 40). Reverse zoning is also present in these pyroxenes.

5.2.3 Plagioclase

Plagioclase occurs only in the station 23 basaltic andesites. Plagioclase compositions are shown in Fig. 42 and summarized in Table 24. The plagioclase is extremely calcic, a characteristic of Tonga arc lavas (Ewart et al., 1973; PART IV). The plagioclase phenocryst compositions however are significantly out of equilibrium with their host whole rock and groundmass compositions (Table 27) based on the empirical relationship presented in PART IV relating bulk rock Ca/(Ca + Na) ratio to expected plagioclase composition under anhydrous conditions. The plagioclase phenocrysts are hosted in rocks with CaO/Na_2O ratios which are too low to have crystallized such calcic plagioclase. PART IV argued that P_{H_2O} would not have a significant effect on plagioclase composition in complex systems. Experimental work (Baker & Eggler, 1987) on high-alumina basalt compositions produced no change in plagioclase compositions with varying water contents, confirming the conclusion of PART IV.

5.2.4 Olivine and olivine-glass inclusions

Olivine is an abundant phenocryst phase in all high-mg lavas from north Tonga (10-16 modal %, Table 24). Compositions of small groundmass olivine euhedra and rims of microphenocrysts and phenocrysts are in equilibrium with host groundmass compositions; however core compositions of microphenocrysts and phenocrysts are significantly out of equilibrium based on a $K_d^{Mg-Fe}_{Ol-Liq}$ of 0.3 (e.g. sample 5-25 contains olivine phenocryst core compositions of both Fo_{94} and Fo_{90}).

Compositions of olivine-hosted glass inclusions can be used to calculate the original parental liquid compositions which crystallized the olivine compositions (PART IV; Anderson, 1974; Watson, 1976). In Table 28 compositions of trapped glass inclusions and calculated compositions in equilibrium with the host olivine (using the method outlined in PART IV) are presented. The glass inclusion compositions indicate that olivine compositions found in sample 5-25 (Table 28, no. 3 and 4) crystallized from distinctly different liquid compositions, not related by crystal fractionation. Glass inclusions in olivine phenocrysts from station-24 (Table 28, no. 1 and 2) do not indicate distinctly different parental compositions but preserve evidence of a more primitive magma composition,

Table 27

Wholerock and groundmass major element chemistry of high-mg lavas and basaltic andesites from north Tonga

	5-25		5-24		5-28		6-2		6-3		7-14		7-15		7-16		7-18		5-27		5-20	
	WR	GDM	WR	GDM	WR	GDM	WR	GL	WR	GL	WR	GL	WR	GL	WR	GL	WR	GL	WR	GDM	WR	GDM
SiO_2	53.83	57.29	52.95	56.52	53.72	56.36	55.55	58.44	56.04	58.40	54.70	57.78	54.96	57.94	55.01	57.81	54.72	56.83	57.48	59.42	56.30	56.89
TiO_2	0.36	0.31	0.15	0.21	0.14	0.22	0.30	0.33	0.31	0.29	0.43	0.47	0.44	0.44	0.42	0.46	0.45	0.49	0.44	0.43	0.62	0.49
Al_2O_3	9.63	13.00	7.92	13.07	8.72	13.17	10.10	12.53	10.60	11.92	10.77	12.82	10.89	12.81	10.95	12.83	10.90	12.02	14.80	15.20	15.20	16.30
FeO	9.71	8.90	9.70	9.22	9.65	9.13	8.37	7.79	8.46	7.94	8.68	7.88	8.47	7.99	8.51	8.01	8.65	8.21	9.66	9.35	9.77	8.40
MnO	0.19	-	0.21	-	0.20	-	0.16	-	0.17	-	0.17	-	0.15	-	0.16	-	0.17	-	0.17	-	0.17	-
MgO	16.30	8.80	20.89	9.18	19.65	9.08	15.29	8.27	13.61	9.44	13.28	7.43	13.08	7.39	12.94	7.30	12.97	8.98	5.36	3.95	5.33	4.74
CaO	8.50	9.90	7.18	10.28	7.54	10.56	8.79	10.64	9.17	10.13	9.50	10.74	9.64	10.78	9.70	10.69	9.65	10.58	10.11	9.67	10.20	10.20
Na_2O	1.27	1.50	0.85	1.13	0.69	1.13	0.96	1.35	1.14	1.26	1.57	1.70	1.49	1.78	1.43	1.73	1.52	1.67	1.67	1.65	2.08	2.30
K_2O	0.16	0.20	0.14	0.26	0.12	0.24	0.40	0.50	0.43	0.50	0.62	0.73	0.60	0.71	0.60	0.71	0.71	0.77	0.25	0.23	0.24	0.39
P_2O_5	0.04	-	0.01	-	0.02	-	0.06	-	0.07	-	0.28	0.30	0.28	-	0.28	0.29	0.26	0.28	0.06	-	0.07	-
Cl	-	0.10	-	0.13	-	0.11	-	0.15	-	0.13	-	0.15	-	0.16	-	0.17	-	0.17	-	0.10	-	0.29
LOI	0.24	-	0.13	-	-0.02	-	1.78	-	1.87	-	1.75	-	1.45	-	1.58	-	1.69	-	0.57	-	0.71	-
Mg#	0.77	0.66	0.79	0.66	0.80	0.66	0.78	0.68	0.76	0.70	0.75	0.65	0.75	0.65	0.75	0.64	0.75	0.66	0.50	0.45	0.52	0.53

WR = Whole rock, GDM = groundmass as determined by electron microprobe broad beam area scans, GL = quench glass rind analysis as determined by electron microprob broad beam area scans, LOI = loss on ignition, major elements are in wt%.

Whole rock data determined by X.R.F (PART III), all analyses are resummed to 100% volatile free.

Mg# determined on the basis of $Fe^{2+}/(Fe^{2+}+ Fe^{3+})$ = 0.9, (-) not determined.

Table 28

Microprobe analyses of olivine glass inclusions and calculated parental magma compositions

	1		2		3		4
	a	b	a	b	a	b	
SiO_2	58.58	55.77	59.06	57.67	57.07	52.80	54.72
TiO_2	0.35	0.29	0.39	0.36	0.39	0.29	0.15
Al_2O_3	12.42	10.39	12.36	11.46	12.71	9.53	9.57
FeO	8.25	9.04	8.05	8.49	9.80	10.88	7.22
MgO	6.25	12.89	6.68	9.53	5.65	15.71	17.15
CaO	12.36	10.34	11.79	10.93	12.75	9.56	10.50
Na_2O	1.07	0.89	1.19	1.10	1.39	1.04	0.54
K_2O	0.35	0.29	0.39	0.36	0.14	0.10	0.15
Cl	0.12	0.10	0.10	0.09	0.12	0.09	-
Total	99.99	100.00	100.01	99.99	100.02	100.00	100.00
Mg#	0.60	0.74	0.62	0.69	0.53	0.74	0.82
CaO/Na_2O		11.55		9.90		9.15	19.40
CaO/Al_2O_3		0.99		0.95		1.00	1.09
CaO/TiO_2		35.31		30.23		32.69	70.00
Al_2O_3/TiO_2		35.48		31.69		32.59	64.00

(-) not determined, Mg# calculated on the basis of $Fe^{2+}/(Fe^{2+} + Fe^{3+}) = 0.9$, (1 a) broad area scan analysis of glass inclusion in Fo_{90} olivine, sample 6-2, (1 b) calculated parental composition in equilibrium with Fo_{90} olivine, (2 a) broad area scan of glass inclusion in Fo_{88} olivine, sample 6-2, (2 b) calculated parental composition in equilibrium with Fo_{88} olivine, sample 6-2, (3 a) broad area scan analysis of glass inclusion in Fo_{90} olivine, sample 5-25, (3 b) calculated parental composition in equilibrium with Fo_{90} olivine, (4) calculated parental composition in equilibrium with Fo_{94} olivine, sample 5-25 (PART IV).

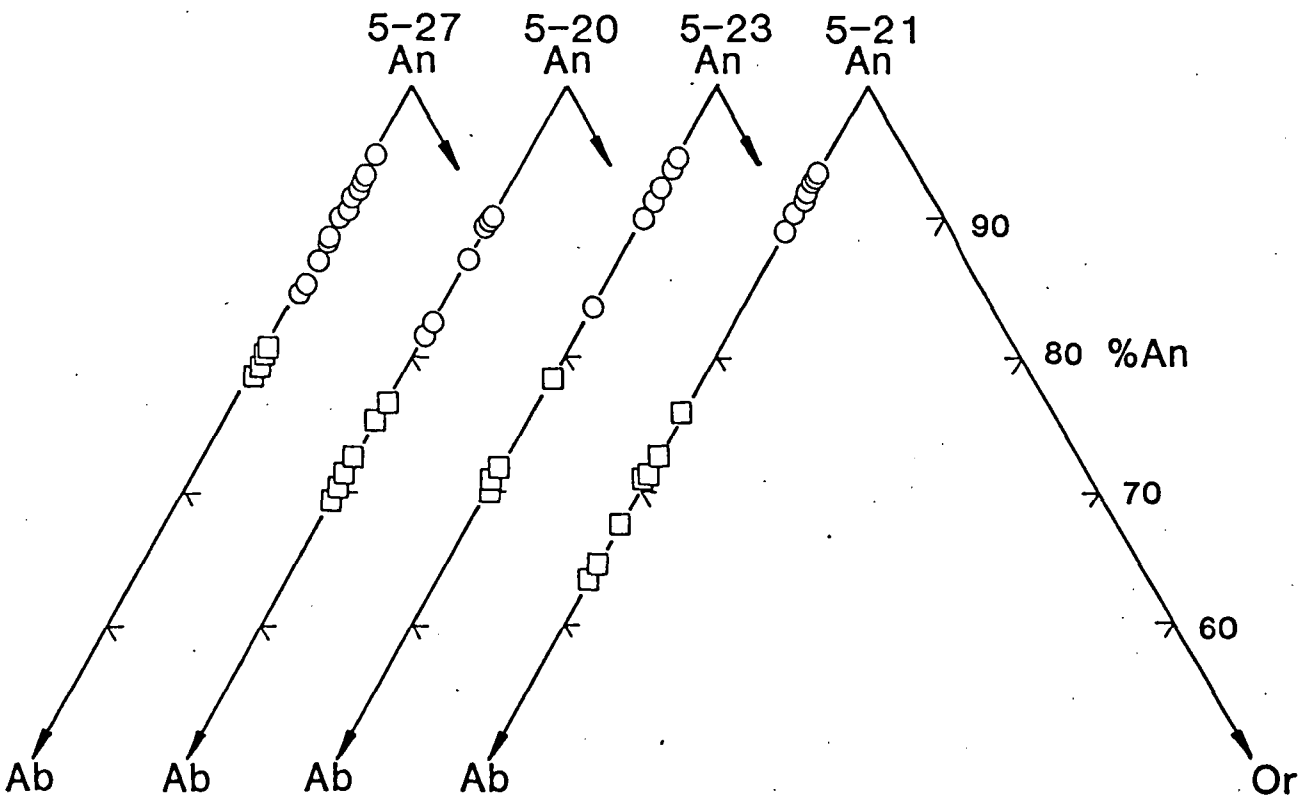

Figure 42.

Plagioclase phenocryst and groundmass compositions in basaltic andesites from station-23, north Tonga, (O) cores and rims of phenocrysts and microphenocrysts, (□) cores and rims of groundmass plagioclase.

which can be related to the glass rind compositions by olivine and orthopyroxene fractionation.

5.2.5 Cr-spinel

Cr-spinel is a ubiquitous accessory phase in the high-mg lavas from north Tonga, occurring as small groundmass euhedra, as microphenocrysts and as inclusions in all phenocryst phases. Representative Cr-spinel compositions are shown in Table 29 and summarized in Fig. 43a, b and c. The Cr# versus Mg# relationships of Cr-spinel compositions from dredged north Tonga lavas have been previously reported by PART IV (see Fig. 36). The Cr# ratio of the Cr-spinels are very high overlapping with Cr-spinels from boninites, and are distinctly more Cr-rich than Cr-spinels from the Troodos upper pillow lavas and MORB (PART IV).

As the composition of Cr-spinel is extremely sensitive to the bulk composition of the host liquid from which it crystallizes, the composition of Cr-spinel preserves the history of magmatic differentiation in a suite of related lavas (Dick & Bullen, 1984). Cr-spinel compositions in high-mg lavas from station 23 provide evidence that mixing of relatively evolved and primitive magmas has occurred in a sub-arc magma chamber.

In Fig. 43a the variation in trivalent cation ratios Y(Cr) $[Cr^{3+}/(Cr^{3+}+ Al^{3+}+ Fe^{3+})]$, Y(Al) $[Al^{3+}/(Cr^{3+}+ Al^{3+}+ Fe^{3+})]$ and $Y(Fe^{3+})$ $[Fe^{3+}/(Cr^{3+}+ Al^{3+}+ Fe^{3+})]$ of Cr-spinels in the high-mg lavas is shown. The trivalent ratios show good correlations with each other, indicating that the dominant substitution is $2Cr^{3+} \Leftrightarrow Al^{3+}Fe^{3+}$ (Fig. 43a). The coherent trends in Fig. 43a also indicate that the Cr-spinels can be related to a single magmatic trend. Cr-spinel inclusions in xenocrystal olivine in basaltic andesite 5-27 (Table 29, no.11) plot at higher Y(Cr) and lower Y(Al) at a given $Y(Fe^{3+})$ than the Cr-spinels hosted in the high-mg lavas, and therefore belong to a separate magmatic differentiation trend than Cr-spinels in the high-mg lavas. In Fig. 43b Cr# versus Mg# of Cr-spinels are plotted according to individual host rocks. Cr-spinels in high-mg lavas from station 23 display a significant range in composition (e.g. in sample 5-25 their Cr# varies from 0.67 to 0.86) suggesting mixing of relatively evolved and primitive magmas.

Fig. 43c shows the relationship between the Cr-spinel Mg# versus the Mg# of their host phase (olivine, orthopyroxene). The good linear trend suggests that the Mg# of the Cr-spinels is in equilibrium with their

Table 29

Representative electron microprobe analyses of chromites from north Tonga lavas

	1		2			3	4	5	6	7	8	9	10	11
	C	R	C	R_1	R_2									
TiO_2	0.84	0.35	-	-	-	1.61	0.42	0.30	0.20	0.30	0.32	0.23	-	-
Al_2O_3	8.54	7.19	6.79	6.81	6.75	10.62	10.72	5.95	8.37	11.46	6.69	7.90	7.04	4.22
Cr_2O_3	41.74	53.36	64.00	62.82	64.18	32.89	52.48	61.23	59.62	51.35	60.79	57.44	61.23	61.38
FeO	38.61	28.40	13.18	17.76	13.60	46.83	24.78	22.00	17.05	25.01	18.05	22.73	18.61	27.25
MgO	10.27	10.49	16.03	12.61	15.46	7.65	11.47	10.52	14.76	11.89	14.15	11.51	13.13	7.16
Total	100.00	99.79	100.00	100.00	99.99	99.60	99.87	100.00	100.00	100.01	100.00	99.81	100.01	100.01
Y(Al)	0.165	0.141	0.128	0.132	0.128	0.208	0.205	0.117	0.158	0.218	0.128	0.153	0.136	0.086
Y(Cr)	0.542	0.701	0.812	0.816	0.817	0.432	0.675	0.809	0.757	0.655	0.780	0.748	0.791	0.837
$Y(Fe^{3+})$	0.272	0.150	0.060	0.053	0.054	0.320	0.110	0.066	0.080	0.120	0.084	0.093	0.074	0.077
Mg#	0.493	0.515	0.766	0.617	0.742	0.364	0.550	0.520	0.703	0.570	0.680	0.562	0.640	0.370
Cr#	0.766	0.833	0.863	0.861	0.864	0.675	0.770	0.873	0.827	0.750	0.859	0.829	0.854	0.907
Fe#	0.512	0.379	0.339	0.216	0.297	0.492	0.326	0.214	0.349	0.355	0.342	0.297	0.291	0.196

(-) indicates below detection limit, trivalent and divalent cation ratios calculated on the basis of stoichiometry, all analyses normalised to 100%, C = core, R = rim.

(1) microphenocryst 5-25, (2) microphenocryst attached to olivine (Fo_{94}), R_1 rim next to glass, R_2 rim next to olivine 5-25, (3) inclusion in clinopyroxene (Mg# 0.84) 5-25, (4) groundmass 5-28, (5) groundmass 5-24, (6) inclusion in olivine (Fo_{91}) 5-24, (7) inclusion in orthopyroxene (Mg# 0.87) 5-24, (8) inclusion in olivine (Fo_{91}) 6-3, (9) groundmass 6-2, (10) groundmass 6-2, (11) inclusion in resorbed olivine (Fo_{80}) 5-27.

Figure 43.

Compositional relationships in Cr-spinels from north Tonga.

A. The variation of trivalent cation ratios Y(Cr), Y(Al) with $Y(Fe^{3+})$ and Y(Cr) versus Y(Al), (★) Cr-spinel inclusions in xenocrystal olivine (sample 5-27).

B. Cr# versus Mg# of Cr-spinels in north Tonga lavas, (○) Cr-spinel inclusions in olivine phenocrysts, (□) Cr-spinels inclusions in orthopyroxene phenocrysts, (◪) Cr-spinel inclusions in clinopyroxene phenocrysts, (◑) Cr-spinel euhedra in groundmass, (⬡) Cr-spinel microphenocrysts. R_1 and R_2 refer to rim compositions in Table 29 (no.2, also see text). Cr-spinel compositions enclosed in box are from resorbed xenocrystal olivine in 5-27, (○) Cr-spinel inclusions in resorbed olivine xenocryst, (□) Cr-spinel inclusions in surrounding orthopyroxene microphenocrysts.

C. Mg# of Cr-spinel inclusions versus the Mg# of olivine (○) or orthopyroxene (□) host.

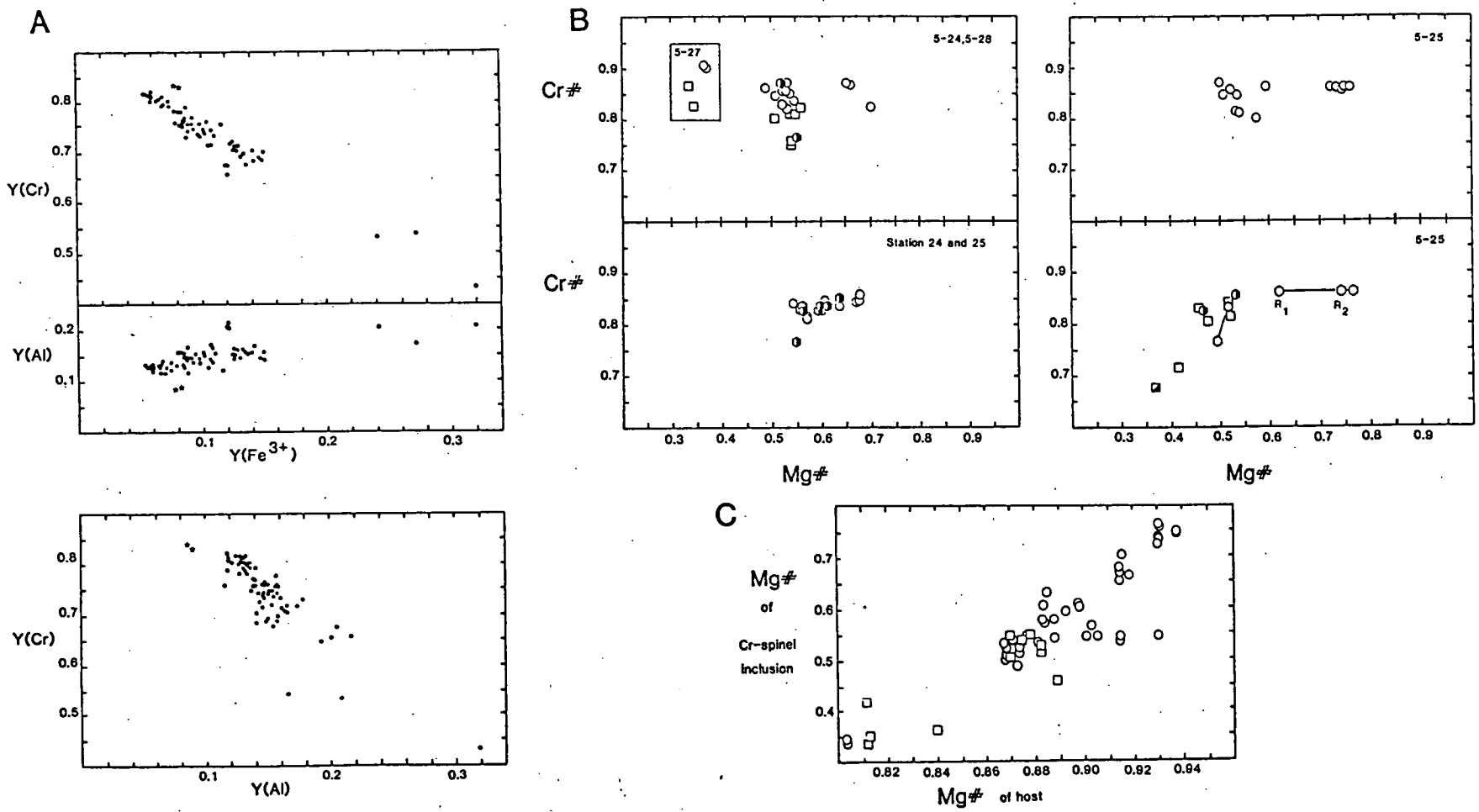
A
Y(Cr)
Y(Al)
Y(Fe3+)
Y(Cr)
Y(Al)
B
5-27
5-24,5-26
5-25
Station 24 and 25
5-25
Cr#
Cr#
Mg#
Mg#
R1
R2
C
Mg# of Cr-spinel inclusion
Mg# of host

respective hosts. However a number of Cr-spinels included in olivine have significantly lower Mg# than expected given the Mg# of their hosts. This can be explained by subsolidus re-equilibration of the Cr-spinel, as the Mg# of Cr-spinel is sensitive to temperature (Dick & Bullen, 1984). However due to the size of the olivine host, little change is observed in the Mg# of olivine. An example of subsolidus re-equilibration is given in Table 29, no.2 and Fig. 43b. Here, a Cr-spinel is attached to a magnesian olivine phenocryst (Fo_{94}, the olivine host is significantly out of equilibrium with the host groundmass) such that one half is enclosed by the olivine, the other half is enclosed by the groundmass. The rim of the Cr-spinel next to the olivine has a much higher Mg# than the rim enclosed by the groundmass, yet the Cr# is identical. This can be explained by subsolidus re-equilibration of the Cr-spinel Mg# when in contact with the lower temperature groundmass host. The overall trend of the Cr-spinel compositions, taking into account the effects of subsolidus reequilibration is consistent with fractionation of olivine and pyroxene depleting residual liquids in Cr and Mg.

The low $Y(Fe^{3+})$ contents of the Cr-spinels (generally <0.085 as inclusions in olivine hosts and as a groundmass phase) suggests crystallization under fO_2 significantly lower than FMQ (Barnes, 1986; Murck & Campbell, 1986).

5.3 DISCUSSION

Evidence from mineral chemistry of olivines, pyroxenes and Cr-spinels and olivine glass inclusions demonstrate that station 23 high-mg lavas are the result of magma mixing of relatively evolved and primitive magmas. Compositions of olivine-hosted glass inclusions further suggest that the primitive magmas involved are distinct from each other and cannot be related to each other by crystal fractionation. The Group B high-mg lava sample 5-25 requires at least three different liquid compositions. These three liquids are as follows;

1) liquid 1, which crystallized Fo_{94} olivine phenocrysts.

2) liquid 2, which crystallized Fo_{90} olivine phenocrysts.

3) liquid 3, which crystallized less magnesian orthopyroxene and clinopyroxene (see Table 24).

The groundmass composition of sample 5-25 (Table 27) is a result of some combination of these three liquids. The wholerock composition is the result of the combination of these three liquids plus their entrained phenocryst populations.

The evidence for such dramatic magma mixing places doubts on using whole rock compositions alone to establish primary magma compositions in the island-arc setting. Although the groundmass composition of sample 5-25 may be considered a parental liquid composition due to its high Mg# (0.66), it cannot be used as a constraint on the nature of primary island arc magmas. Trapped olivine-hosted glass inclusions, however, offer one possible solution (PART IV).

High-mg lavas from station 24 and 25 appear to be relatively free from the effects of magma mixing although the presence of resorbed xenocrystal pyroxenes (Table 26, Fig. 40) suggests they have had some minor contribution from another magma source.

Plagioclase phenocryst compositions of station 23 basaltic andesites also suggest that magma mixing has occurred since such compositions could only have crystallized from liquids with much higher CaO/Na_2O ratios than observed in their respective host rocks (Table 27). The CaO/Na_2O ratios of trapped olivine-hosted glass inclusions are appropriately high, and provide a ready solution to the presence of calcic plagioclase.

Due to the lower density of plagioclase relative to magnesian olivines and pyroxenes, plagioclase phenocrysts may float to the top of a subarc magma chamber after crystallizing from a primitive high CaO/Na_2O magma at the base of a magma chamber. The plagioclase crystals are then incorporated into a more evolved magma composition before eruption. The complexity of magma chamber dynamics allows more complex models to be proposed (O'Hara & Matthews, 1981; Sparks et al., 1977; Sparks et al., 1980; Huppert & Sparks, 1980), however the possible processes involved are beyond the scope of this paper.

5.4 GEOCHEMISTRY

Major, trace and REE geochemistry of representative samples from north Tonga are presented in Table 30. The Sr and Nd isotopic compositions for the representative lavas from north Tonga are presented in Table 31. Included in Table 30 and 31 are representative samples from stations 15, 21

Table 30

Representative major, trace and REE geochemistry of dredged lavas from north Tonga and Lau Basin

	1-38	3-44	3-24	5-20	5-24	5-25	6-3	7-18	11-3
SiO_2	53.43	54.35	59.19	56.30	52.95	53.83	56.04	54.72	49.13
TiO_2	0.96	0.20	0.25	0.62	0.15	0.36	0.31	0.45	0.71
Al_2O_3	16.90	10.67	10.96	15.20	7.92	9.63	10.60	10.90	15.07
FeO	8.47	9.41	8.83	9.77	9.70	9.71	8.46	8.65	9.70
MnO	0.16	0.19	0.18	0.17	0.21	0.19	0.17	0.17	0.18
MgO	6.08	14.99	10.80	5.33	20.89	16.30	13.61	12.97	9.18
CaO	10.84	8.66	7.78	10.20	7.18	8.50	9.17	9.65	13.13
Na_2O	2.58	1.14	1.37	2.08	0.85	1.27	1.14	1.52	2.85
K_2O	0.48	0.35	0.56	0.24	0.14	0.16	0.43	0.71	0.02
P_2O_5	0.10	0.03	0.07	0.07	0.01	0.04	0.07	0.26	0.03
LOI	1.15	0.05	0.01	0.71	0.13	0.24	1.87	1.69	-0.72
Mg#	0.56	0.76	0.71	0.52	0.80	0.77	0.76	0.75	0.65
Ba	29	106	140	55	34	41	105	230	14
Rb	9	6	10	4	2	3	8	12	2
Sr	132	151	175	126	46	68	159	348	48
Zr	59	12	19	39	5	20	32	53	21
Nb	1	<1	2	<1	<1	<1	8	16	<1
Y	29	7	7	17	5	10	8	11	22
Sc	40	50	43	44	44	44	43	44	51
V	259	247	251	298	191	225	214	223	299
Ni	52	275	117	37	501	341	189	199	133
Cr	204	1095	605	75	2027	1294	927	760	350
La	2.84	1.74	4.0	2.82	-	1.59	6.53	15.98	3.43
Ce	9.23	4.10	8.44	6.44	-	3.34	14.74	37.72	-
Pr	1.56	-	1.06	1.01	-	0.55	1.73	4.48	5.52
Nd	8.40	2.85	4.51	5.17	0.90	2.72	6.36	17.29	5.83
Sm	2.84	0.82	1.32	1.72	0.28	0.89	1.30	3.23	8.17
Eu	1.11	-	0.50	0.62	-	0.36	0.45	1.01	8.61
Gd	4.04	1.27	1.38	2.37	0.59	1.27	1.35	2.68	10.58
Dy	5.03	1.16	1.65	3.10	0.77	1.62	1.27	1.84	11.57
Er	3.28	0.80	1.20	2.15	0.46	1.10	0.63	0.93	11.74
Yb	3.20	0.86	1.14	2.07	0.66	1.14	0.58	0.79	11.39

LOI = loss on ignition, all iron as FeO, (-) not determined, all analyses resummed to 100% volatile free, major elements in wt%, trace elements are in parts per million, Mg# determined on the basis of a $Fe^{2+}/(Fe^{2+} + Fe^{3+}) = 0.9$.

Table 31

Sr and Nd isotopes of representative dredged lavas from north Tonga and Lau Basin

Sample no.	Rb	Sr	Sm	Nd	Rb/Sr	Sm/Nd	$^{87}Sr/^{86}Sr$	$2\sigma \times 10^{-4}$	$^{143}Nd/^{144}Nd$	$2\sigma \times 10^{-4}$	εNd	2σ
1-38	9	132	2.84	8.40	0.0682	0.338	0.702937	0.13	0.512958	0.01	5.91	0.19
3-24	10	175	1.32	4.51	0.0571	0.293	0.704384	0.13	0.512785	0.06	2.54	0.12
3-44 unl							0.704537	0.01	0.512787	0.09	2.57	0.17
3-44	6	151	0.82	2.85	0.0397	0.288	0.704528	0.35				
5-20 unl							0.703861	0.15				
5-20	4	126	1.72	5.17	0.0317	0.333	0.703844	0.13	0.512961	0.13	5.97	0.25
5-24	2	46	0.28	0.90	0.0435	0.311	0.704422	0.11	0.512770	0.06	2.24	0.12
5-25	3	68	0.89	2.72	0.0441	0.327	0.704047	0.25	0.512961	0.09	5.97	0.17
6-3	8	159	1.30	6.36	0.0503	0.204	0.704515	0.27	0.512708	0.08	1.03	0.17
7-18	12	348	3.23	17.29	0.0345	0.187	0.704175	0.13	0.512730	0.01	1.46	0.19
11-3	2	48	1.57	3.48	0.0417	0.451	0.703364	0.01	0.512963	0.01	6.00	0.20

unl= unleached, all other samples leached in 6N HCl overnight, $\varepsilon Nd(0) = 0.512655$, $^{143}Nd/^{144}Nd$ ratio normalised to a $^{146}Nd/^{144}Nd$ ratio of 0.7219.

and 31 (PART III). The silicate incompatible element geochemistry is summarized on a series of normalized abundance patterns (NAP) (Fig. 44). Included in Fig. 44 are representative NAP from the south Tonga and north Tonga islands (L1 and T116, Fig. 44a respectively).

The geochemistry and geochemical affinities of the dredged lavas is presented in PART III. Briefly the north Tongan high-mg lavas, and basaltic andesites belong to a low-Ti, low-K, island arc tholeiite series, on the basis of their low TiO_2 and K_2O contents, the lack of phenocrystal amphibole, the presence of extremely calcic plagioclase and low abundances of incompatible elements. However the north Tonga lavas (except for station 15 basaltic andesites) fall in the calc-alkaline field of Miyashiro (1974) when plotted on a FeO^t/MgO versus SiO_2 diagram (Fig. 30, PART III), due to their relatively high MgO contents compared to most other island arc tholeiite suites when compared at similar SiO_2 contents. Station 23 basaltic andesites show strong affinities to Tofua magmatic arc (TM-arc) volcanics on the basis of similar REE patterns and NAP (Fig. 44a,c), (PART III). The high-mg lavas recovered from station 23, 24 and 25 show strong affinities to low-Ti ophiolitic basalts, such as Troodos Group II and III upper pillow lavas (Cameron, 1985) and are distinctly different from clinoenstatite bearing boninite (PART III). In the following section the petrogenesis of the dredged north Tonga lavas is discussed in the light of the new Sr and Nd isotopic data.

5.5 PETROGENESIS

There is no doubt that the petrogenesis of island arc lavas requires the mixing of two or more source components (Arculus & Powell, 1986; Morris & Hart, 1984; Hickey & Frey, 1982; Cameron et al., 1983; Von Drach et al., 1986; Wheller et al., 1987). However there is controversy over the ultimate origin and nature of these source components. Arculus & Powell (1986) have summarized and evaluated three of the main models proposed for island arc petrogenesis, which are;

1) wedge (peridotitic upper mantle) only (Arculus, 1981; Stern, 1981; Morris & Hart, 1983),

2) wedge plus arc crust (Arculus & Johnson, 1981; Coulon & Thorpe, 1981; Leeman, 1983),

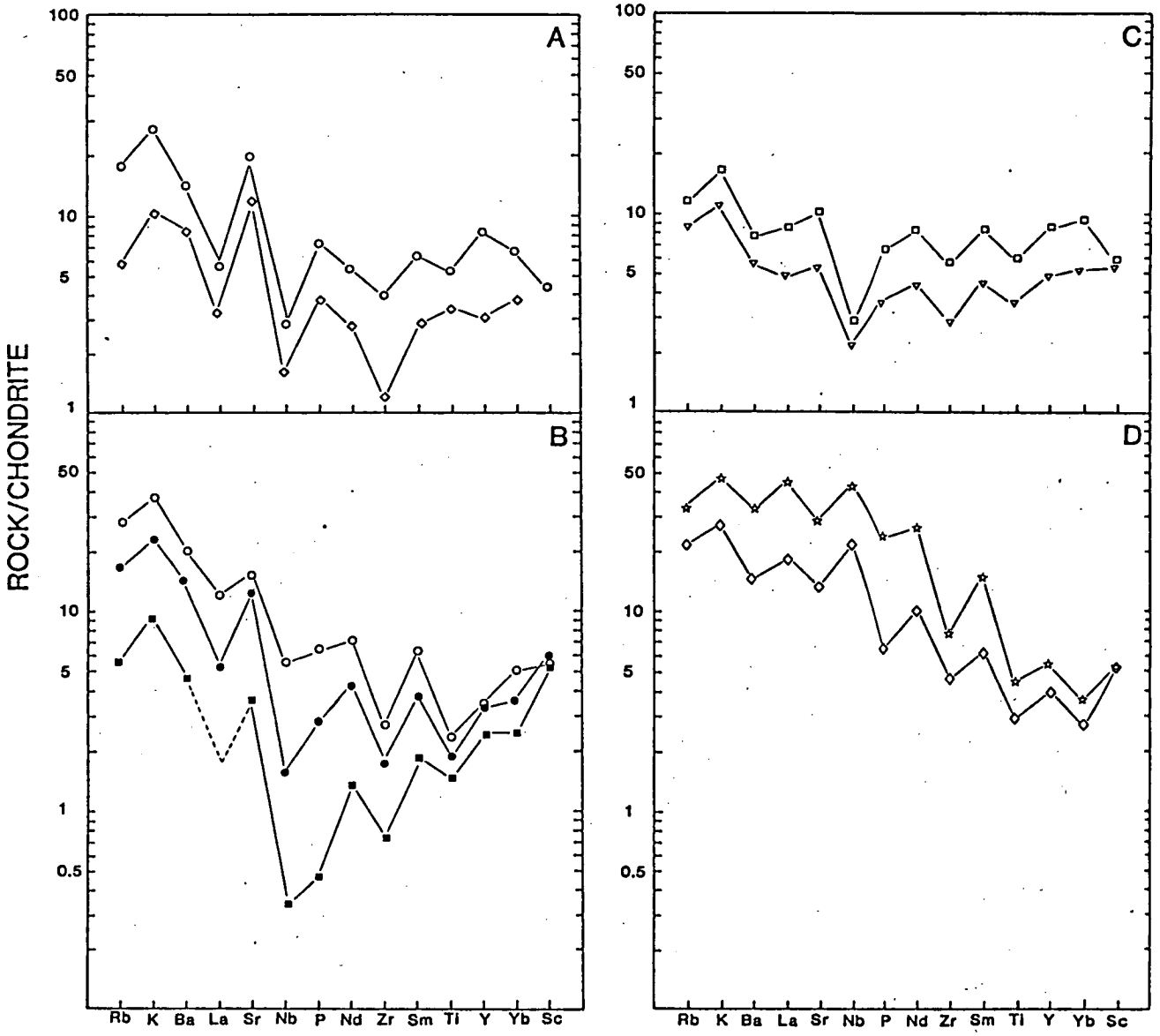

Figure 44.

Representative chondrite normalised abundance patterns for dredged north Tonga lavas. Normalising values are from Thompson et al. (1983), normalising value for Sc from Hickey & Frey (1982). The ordering of elements is taken from Hickey & Frey (1982), except the order of LIL elements (Rb, K, Ba, Sr) is based on experimental studies of Tatsumi et al. (1984).

A. Representative patterns of Tofua Magmatic arc basaltic andesites (Ewart et al., 1973), (○) L1, from the island of Late, south Tonga, (◇) T116, from the island of Tafahi, north Tonga.

B. Representative patterns of station 21 lavas and Group A high-mg lava from station 23, (○) 3-24, station 21, (●) 3-44, station 21, (■) 5-24, station 23, La is estimated.

C. Representative patterns of station 23 basaltic andesites and Group B high-mg lava, (□) 5-20 basaltic andesite, (▽) 5-25 high-mg lava (Group B).

D. Representative patterns of high-mg lavas from station 24 and 25, (◇) 6-3, station 24, (☆) 7-18, station 25.

3) wedge plus slab (Kay, 1980; Sun, 1980; Mc Culloch & Perfit, 1981; Gill, 1981; White & Patchett, 1984),

to this list can be added the following two models;

4) slab only (Marsh, 1979, 1982; Brophy & Marsh, 1986; Johnston, 1986; Brophy, 1986; Myers et al., 1986a,b). In this model high-alumina basalts are primary arc magmas generated by partial melting of subducted oceanic crust plus intercalated sediments. More magnesian lavas, such as Tonga high-mg lavas result from contact melting between high temperature diapirs from the subducted lithosphere and peridotitic wedge. This model is evaluated by Crawford et al., (1987),

5) Wedge plus enriched mantle components (Varne, 1985; Varne & Foden, 1985; Wheller et al., 1987; Hickey & Frey, 1982). In this model a peridotitic mantle source is 'enriched' in silicate incompatible elements by a mantle metasomatic melt phase, with no or little involvement from the subducted slab.

The petrogenesis of the north Tonga lavas is best explained by model 5 above. The source mantle which was partially melted to produce the Tonga lavas was the result of the mixing of at least three components. One component is identified as depleted mantle peridotite (more depleted than N-MORB and OIB sources) which had been enriched by at least 2 'enriched' components. One 'enriched' component was a mantle component with similarities to enrichments seen in oceanic island basalts of the Cook-Austral-Samoa islands (part of the Dupal mantle anomaly, Palacz & Saunders, 1986) and in Group II ultrapotassic rocks of Foley et al., (1987). A second 'enriching' component is either a hydrous fluid phase from the subducted oceanic slab or alternatively a mantle-derived fluid phase.

The discussion below outlines in more detail the evidence for these three components. The approach is essentially empirical and qualitative, no quantitative numerical model is presented as such modelling at this stage would be unconstrained and essentially ad hoc.

5.5.1 Depleted source component

In Fig. 45 the CIPW molecular normative chemistry of the wholerock, groundmass/glass and olivine-hosted glass inclusion compositions of the north Tonga lavas are presented in the projection from Diopside onto the

Figure 45.

CIPW molecular normative projection from Di onto the base of the basalt tetrahedron jadeite plus calcium tschermaks molecule (Jd + CaTs)-olivine (Ol)-quartz (Qz) after Green (1970). Hy hypersthene, Ab albite, An anorthite.

Field enclosing MORB are primitive MORB glasses (Appendix 2).

TMa Tofua Magmatic arc, field encloses range in whole rock compositions (Ewart et al., 1973).

CV Cape Vogel, Papua New Guinea, field encloses wholerock compositions of boninites (Jenner, 1981).

Tr Troodos, field encloses range in wholerock compositions of Group II and III Upper Pillow Lavas (Cameron, 1985).

ST21 station 21, field encloses range in wholerock compositions of station 21 lavas (PART III, Appendix 3).

ST15 station 15, field encloses range in wholerock compositions of station 15 basaltic andesites (PART III).

Lau Basin field encloses range in quenched glass compositions (Hawkins & Melchoir, 1985).

(○) M is a MORB pyrolite composition (PART I, II).

(□) T is Tinaquillo lherzolite (Jaques & Green, 1980).

(●) R is the residual mantle composition after removal of a stage one MORB picrite composition (Green et al., 1979).

(★) is the boninite parental magma composition calculated by Walker & Cameron (1983).

(☆) is the calculated parental magma composition to Troodos Group II and III upper pillow lavas (Duncan & Green, 1987).

(⧅) groundmass compositions of station 23 basaltic andesites (Table 27).

(⬡) groundmass and glass compositions compositions of north Tonga high-mg lavas (Table 27).

(◑) calculated parental magma compositions in equilibrium with magnesian olivine phenocrysts from north Tonga (Table 28).

(□) whole rock compositions of station 23 basaltic andesites (Table 27).

(△) whole rock compositions of station 24 and 25 high-mg lavas (Table 27).

(○) whole rock compositions of station 23 high-mg lavas (Table 27).

———— locus of liquids in equilibrium with olivine + orthopyroxene ± clinopyroxene at 10, 15, 20 and 30kbars from MORB pyrolite (PART I, II).

– – – – – – locus of liquids in equilibrium with olivine + orthopyroxene ± clinopyroxene at 5kbars from Tinaquillo lherzolite (Falloon et al., 1987).

—·—·—·— locus of liquids in equilibrium with olivine only.

——→ denotes change in residue compositions with progressive

– – –→ equilibrium batch partial melting, solid arrow indicates lherzolite residues, dashed arrow indicates harzburgite residues, dunitic residues plot at the Ol apex.

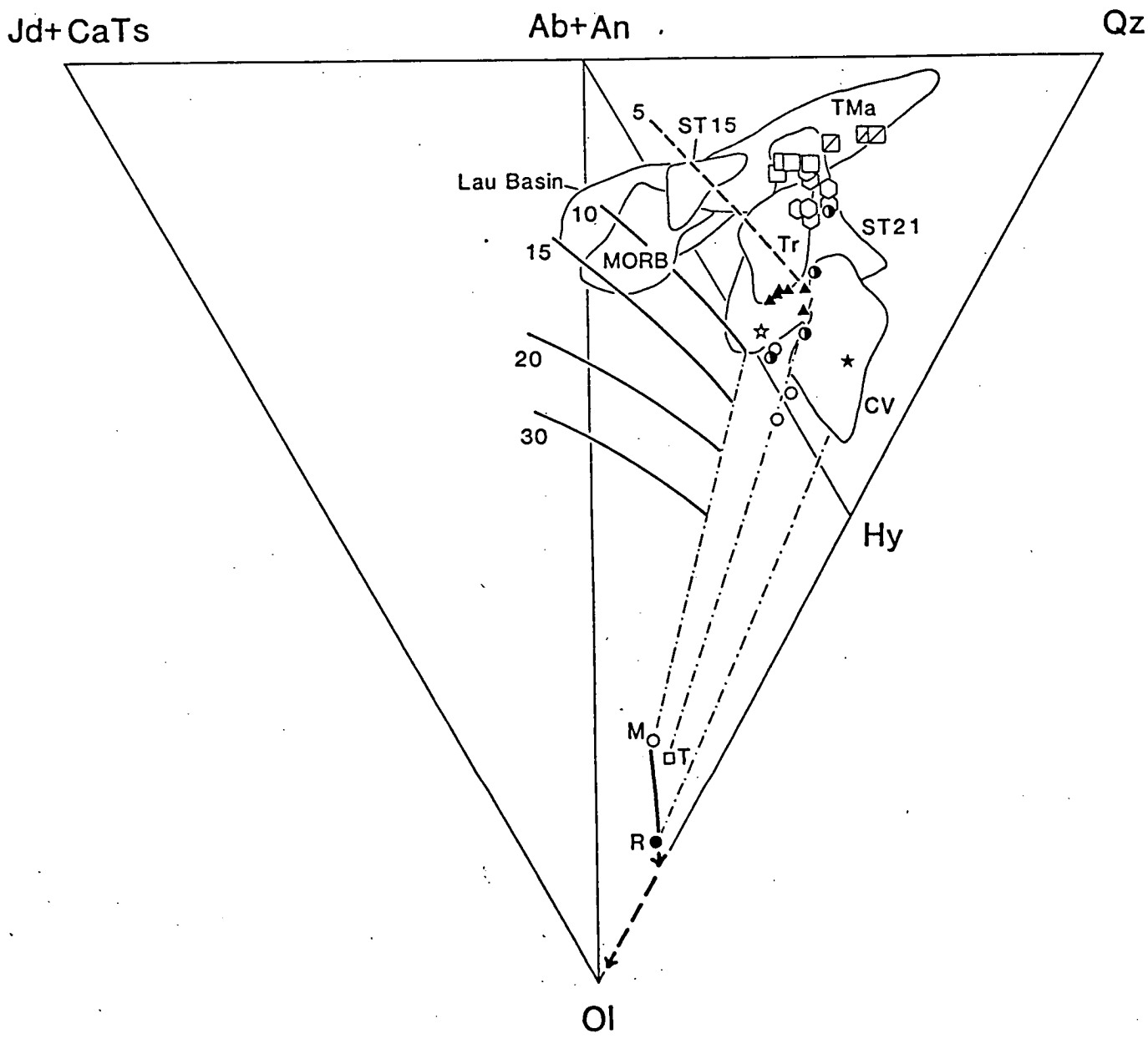
Jd+CaTs
Ab+An
Qz
5
ST15
TMa
Lau Basin
10
ST21
15
MORB
Tr
20
CV
30
Hy
M
T
R
Ol

base of the basalt tetrahedron jadeite plus calcium tschermaks molecule (JdTs + CaTs)-quartz (Qz)-olivine (Ol). This diagram is helpful in evaluating the roles of differing source compositions, degrees of partial melting and depths of magma segregation on lava compositions (Green et al., 1987). The Tonga compositions are also compared with the compositional fields of Cape Vogel boninites (Jenner, 1981), Troodos upper pillow lavas (Cameron, 1985; Duncan & Green, 1987), Tofua arc volcanics (Ewart et al.,1973), Lau Basin back-arc basalts (Hawkins, 1976; Hawkins & Melchoir, 1985) and primitive MORB glasses (Appendix 2).

Also shown in Fig. 45 are olivine + orthopyroxene ± clinopyroxene + liquid cotectics defined by partial melting experiments on a MORB pyrolite composition at 10, 15, 20 and 30kbars (PART I, PART II) and Tinaquillo lherzolite at 5kbar (Jaques & Green, 1980; Falloon et al., 1987). An important constraint on the range of liquid compositions able to be produced from any specific source composition is an olivine control line drawn from the Olivine apex through the bulk composition (Green et al., 1987). Liquid compositions can only be produced to the left-hand side of this control line in the projection from Diopside during equilibrium batch partial melting. For example primitive MORB glasses plot well to the left of the olivine control line through the MORB pyrolite composition, confirming that MORB pyrolite and possibly more refractory sources are capable of producing primitive MORB glasses. However as all the primitive north Tonga compositions plot to the right of the olivine control line through MORB pyrolite, a MORB-type source cannot produce the high-mg lavas from north Tonga by partial melting; a more refractory source is required. More refractory compositions such as Tinaquillo lherzolite or the residue composition (point R, Fig. 45) after extraction of a stage-one (melting stages after Duncan & Green, 1980, 1987; Green et al., 1979) MORB picrite composition from a MORB pyrolite starting composition, are capable of producing primitive north Tonga high-mg lavas by partial melting. The composition labelled T in Fig. 45 is the parental composition for the Troodos upper pillow lavas studied experimentally by Duncan & Green (1987). The Troodos parental composition is compositionally very similar to the Tongan high-mg lavas. The Troodos composition was found to be multiply saturated in olivine and orthopyroxene at 1360^{o}C, 8kbar and thus may be a primary melt leaving a harzburgite residue (Duncan & Green, 1987). Water contents in the Troodos magma batches were estimated to have been <1.0 wt% by Duncan & Green (1987). The results of the experimental study of Duncan & Green (1987) combined with the information gained from Fig. 45, suggests that the high-mg lavas from station 24 and 25 as well as the refractory

magma compositions identified from olivine-hosted glass inclusions are the result of partial melting of a refractory mantle peridotite at pressures <10 kbars, leaving a harzburgite residue. Water contents were probably <1 wt%, similar to the Troodos Upper Pillow Lavas.

Boninites from Cape Vogel, Papua New Guinea (Jenner, 1981; Dallwitz et al., 1968) plot further to the right towards Hy (Fig. 45), than the north Tonga lavas and as such require an even more refractory mantle source. Composition Star (Fig. 45) is the parental Cape Vogel boninite composition of Walker & Cameron (1983). Experimental work by Jenner (1983) suggests boninite primary magmas are the result of partial melting at low pressures <5kb with water present.

In summary, the CIPW molecular normative chemistry of the high-mg lavas from north Tonga suggests that the mantle source was more refractory than the sources to MORB but not as refractory as boninite sources.

The CaO/Al_2O_3 ratios of the north Tonga high-mg lavas provide a further constraint on the nature of the mantle source. In Fig. 46 the change in CaO/Al_2O_3 ratio of the residue during equilibrium partial melting of MORB pyrolite is illustrated. The CaO/Al_2O_3 ratio of the residue increases with partial melting until clinopyroxene is exhausted, then falls sharply until orthopyroxene is exhausted. This results in a large variation in CaO/Al_2O_3 ratio with little change in bulk rock Mg#, as observed in refractory harzburgites from Papuan ophiolites (Fig. 46). The CaO/Al_2O_3 ratios of primitive north Tonga high-mg lavas and calculated refractory magma compositions (Table 28) range from 0.95 to 1.10, higher than CaO/Al_2O_3 ratios of primitive MORB glasses (0.67-0.88) and significantly higher than CaO/Al_2O_3 ratios of clinoenstatite-bearing boninites from Cape Vogel (<0.66). This is consistent with the source for north Tonga high-mg lavas and calculated refractory magma compositions (Table 28) being more refractory than MORB sources but still containing some clinopyroxene. The clinopyroxene would be eliminanted during partial melting, leaving a harzburgite residuum; however the original presence of clinopyroxene is required to explain the high CaO/Al_2O_3 ratios in the Tonga lavas and olivine-hosted glass inclusions. The CaO/Al_2O_3 ratios of boninites from Cape Vogel, however, can be explained by partial melting of a more refractory harzburgite source containing no clinopyroxene.

The high CaO/Na_2O ratios of the north Tonga lavas and olivine-hosted glass inclusions (>10) also indicate a more refractory source than MORB

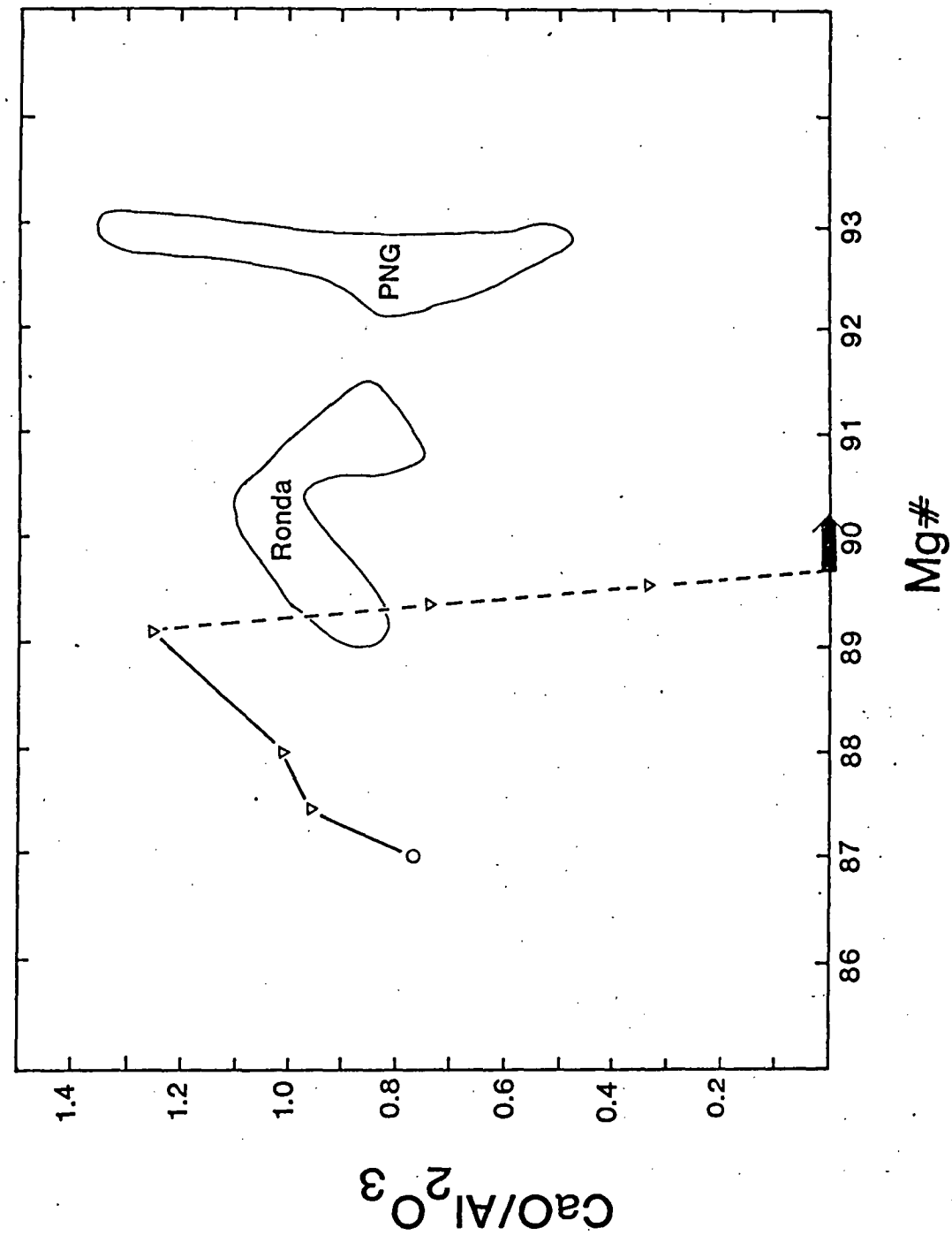

Figure 46.

CaO/Al_2O_3 ratio of residue compositions from equilibrium batch partial melting of a MORB pyrolite composition at 10kbar (PART I) versus Mg# (x100) of the residue. RONDA encloses the field of peridotite compositions from the Ronda high temperature peridotite intrusion (Frey et al., 1985), PNG encloses the field of harzburgite from the Papua New Guinea ultramafic belt (Jaques & Chappell, 1980), (O) MORB pyrolite starting composition, (▽) calculated residue compositions (Falloon unpubl. data),

——— lherzolite residues.

- - - - - - - - harzburgite residues.

▬▬▶ dunitic residues.

(CaO/Na_2O ratios <9.5). As boninite sources require the most refractory of mantle sources, the CaO/Na_2O ratio in boninites would be expected to be high; however boninites have anomalously low CaO/Na_2O ratios. This can be explained if Na_2O was part of an enriching component which had modified the depleted source before partial melting (Hickey & Frey, 1982; Cameron et al., 1983).

Many of the trace element characteristics of the north Tonga lavas also suggest a refractory mantle source, taking into account the effect of subsequent enriching components. They have low Ti/V and Ti/Sc ratios compared to MORB and overlap with Bonin Islands and Cape Vogel boninites (Fig. 47). Low Ti/V and Ti/Sc can be explained by melting of a depleted mantle source (Hickey & Frey, 1982; Nelson et al., 1984). The low abundances of TiO_2, Y and HREE's in the Tonga high-mg lavas compared to N-type and depleted MORB mantle (Fig. 44 and 49a) is consistent with a mantle source more depleted in these elements than MORB source mantle. The relatively high Al_2O_3/TiO_2 and CaO/TiO_2 ratios of the north Tonga lavas compared to MORB are also consistent with a depleted mantle source (Sun & Nesbitt, 1978; Sun et al., 1979).

Many of the petrographic and mineral chemical features of the north Tonga lavas also suggest a refractory mantle source. The presence of very magnesian olivine phenocrysts (up to Fo_{94}) and very Cr-rich spinels (up to Cr# 0.87), which are significantly more magnesian and Cr rich respectively than observed in MORB (olivine generally $<Fo_{92}$, Cr-spinel Cr#<0.60).

5.5.2 Enriched source components

Figure 48 shows the εNd and $^{87}Sr/^{86}Sr$ ratios of the north Tonga lavas. Compared to Pacific MORB the north Tonga lavas have lower εNd and higher $^{87}Sr/^{86}Sr$. On the basis of εNd, the analysed north Tonga lavas (Table 31) define two broad groups.

One group is defined by basaltic andesites from station 15 and 23 along with the Group B high-mg lava 5-25 and the Lau Basin back-arc basin basalt 11-3 which all have εNd of +6.0 despite their showing significantly different $^{87}Sr/^{86}Sr$ ratios. A similar range of $^{87}Sr/^{86}Sr$ ratios was observed at constant εNd by Von Drach et al. (1986) in Aleutian island arc magmas; these authors attributed this to be a result of efficient localised mantle mixing producing a homogeneous source in terms of εNd, which was subsequently invaded by a component with a high Sr/Nd ratio. The isotopic

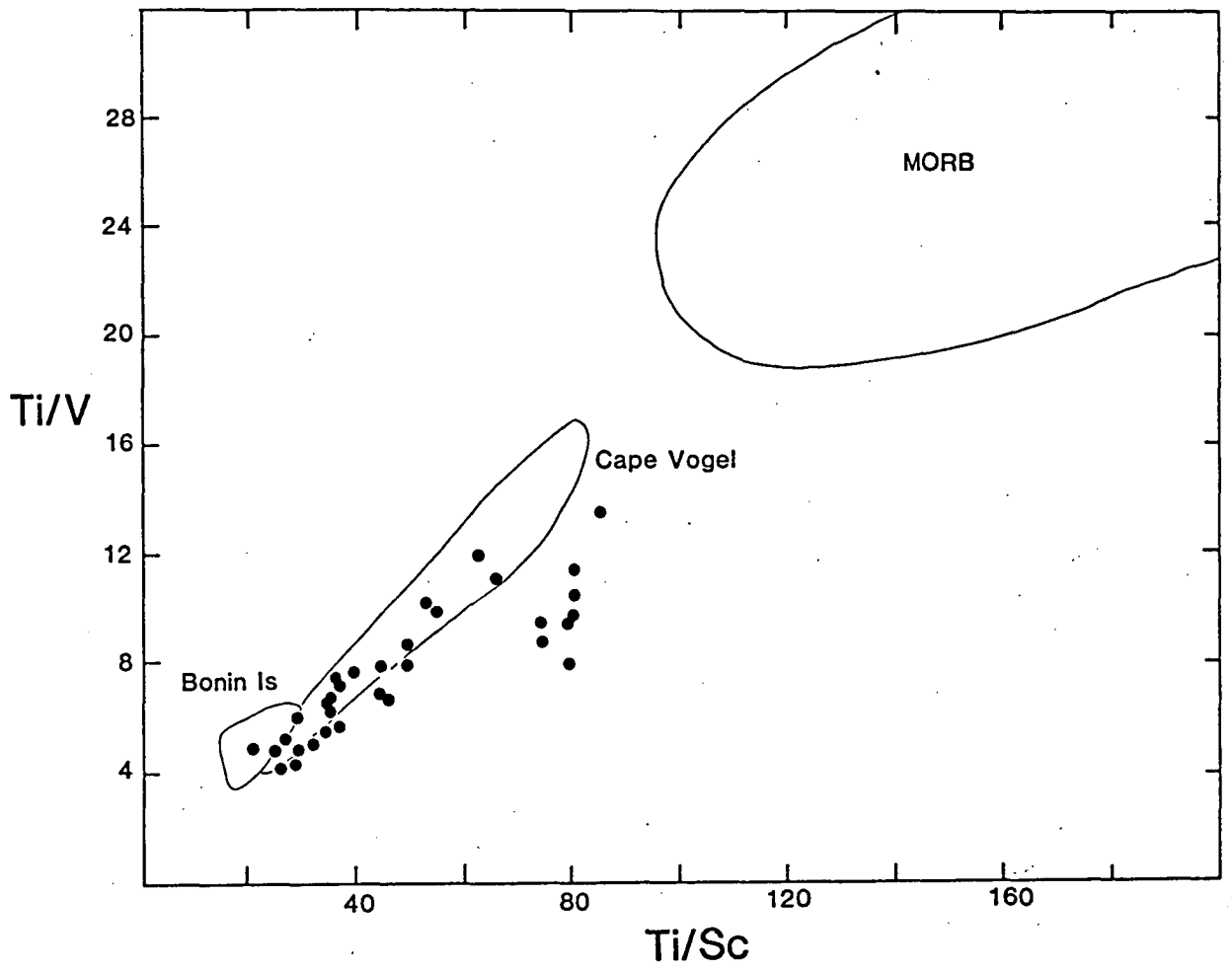

Figure 47.

Ti/V versus Ti/Sc ratio of dredged north Tonga lavas (this study, PART III, Appendix 1). Fields for Cape Vogel, Papua New Guinea and Bonin Islands, Japan, boninites compiled from Jenner (1981), Hickey & Frey (1982) and Cameron et al. (1983). MORB field from Hickey & Frey (1982).

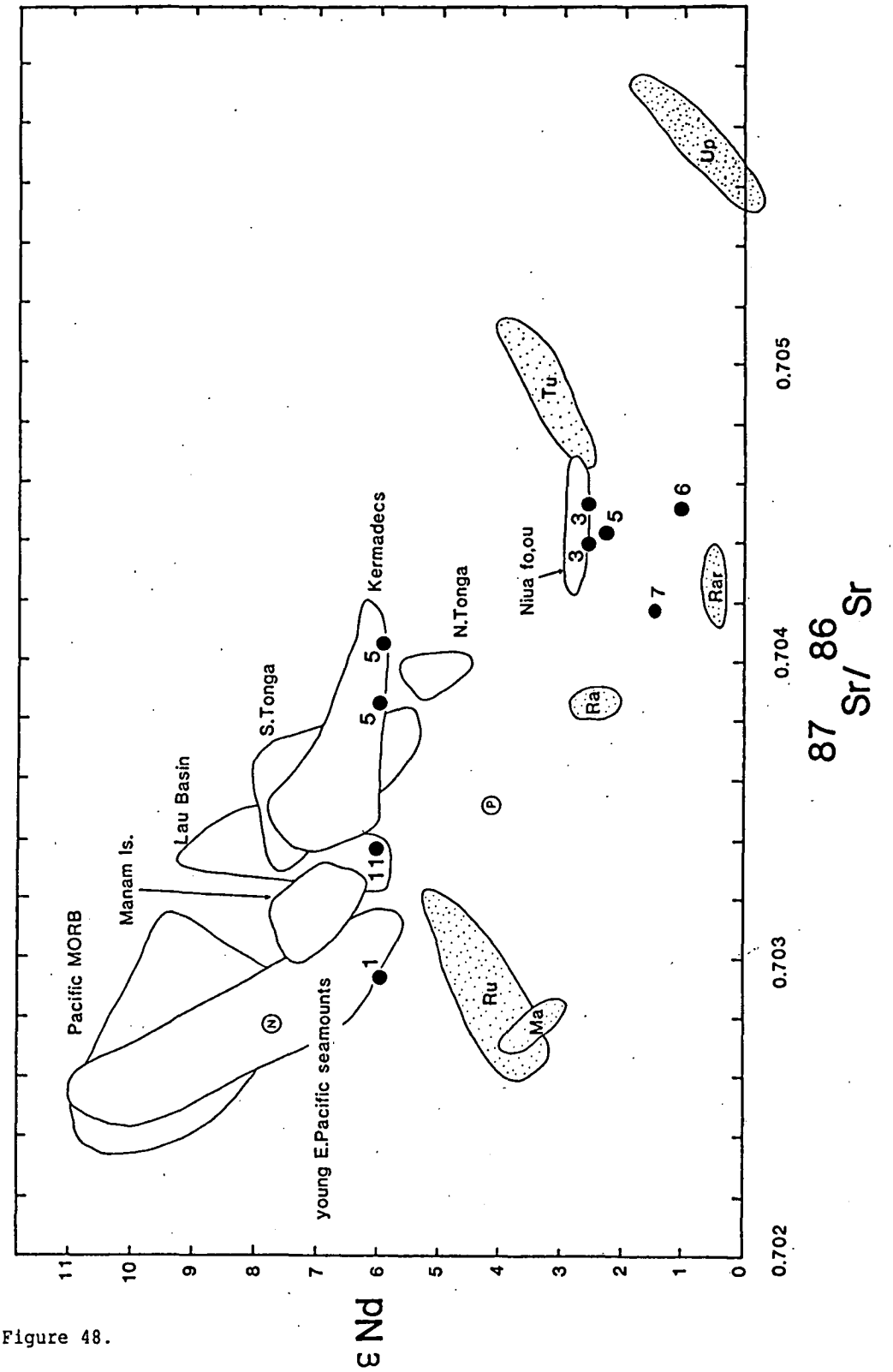

Figure 48.

Nd versus Sr isotopic composition of dredged north Tonga lavas, (●) north Tonga dredged lavas, data from Table 31, numbers refer to dredge stations. Data for south Tonga, north Tonga, Kermadecs and Niua fo'ou from Ewart & Hawkesworth (1987). Data for Lau Basin back-arc basalts from Sinton et al. (1987) and Carlson et al. (1978). Data for Manam Island from Johnson et al. (1985). Data for young east Pacific seamounts from Zindler et al. (1984). Data for Pacific MORB from Mac Dougall & Lugmair (1985), Newsom et al. (1986), Allegre et al. (1980), Ito et al. (1980) and White & Hofmann (1982). N and P refer to N-type and P-type MORB respectively (Le Roex et al., 1985). Stippled fields are data from ocean islands of the Samoa-Cook-Austral chain (Palacz & Saunders, 1986), Ru Rurutu, Ma Mangaia, Ra Rapa, Rar Rarotonga, Tu Tutuila, Up Upolu.

compositions are similar to analysed subaerial lavas from the Kermadecs and Tonga islands (Ewart & Hawkesworth, 1987) and to rocks from the Lau Basin and young Pacific rise seamounts (Fig. 48). Sample 1-38 from station 15 is distinctive in having significantly lower $^{87}Sr/^{86}Sr$ than other analysed Tonga lavas confirming the conclusion of PART III that the basaltic andesites from station 15 were unrelated to the currently active Tofua magmatic arc, but showed strong affinities to Lau Basin back-arc crust. The isotopic composition of basaltic andesites from station 23 confirms their strong chemical affinities to Tofua magmatic arc volcanics (PART III; Ewart et al., 1973; Ewart & Hawkesworth, 1987).

The second group of rocks have lower εNd values from +1.0 to +2.5, and include high-mg lavas from stations 24, 25 and 23 (Group A) and lavas from station 21. The analysed Group A high-mg lava 5-24 has similar εNd and $^{87}Sr/^{86}Sr$ ratios to station 21 island arc tholeiites, as well as similar NAP pattern (Fig. 49b), suggesting that station 23 Group A high-mg lavas may be parental magmas to station 21 lavas. The lower εNd and higher $^{87}Sr/^{86}Sr$ compared to the other group of north Tonga lavas is consistent with the presence of LREE-enriched patterns compared to the flat to depleted LREE patterns present in the first group. The second group of lavas have similar isotopic compositions to lavas from Niua fo'ou (Ewart & Hawkesworth, 1987) and hotspot associated volcanics from the Cook-Austral-Samoa islands (Fig. 48) (Palacz & Saunders, 1986).

The NAP of the north Tonga lavas (Fig. 44) show significant enrichments in large ion lithophile elements (LILE) relative to the REE and high field strength elements (HFSE), in common with other island arc lavas (Arculus & Powell, 1986); this is inconsistent with a depleted mantle source. Station 24 and 25 lavas also show significant enrichment in not only the LILE but also in LREE and HFSE , especially Nb and Zr. Compared to other north Tonga lavas and Tofua magmatic arc lavas, station 24 and 25 lavas have significantly lower La/Nb and Ti/Zr ratios and high $(La/Yb)_N$ ratios.

5.5.3 A two component mixing model

The evidence for a depleted mantle source with superimposed enriched components is similar to that seen in boninites; Hickey & Frey (1982) and Cameron et al. (1983) haved proposed two component mixing models to explain the trace element and isotopic characteristics of boninites. Hickey & Frey (1982) defined two different end members on the basis of trace element and

isotopic correlations with Nd. Cameron et al. (1983) calculated the amount of an 'enriched' component on the basis of a two component mixing model involving the REE's. Cameron et al. (1983) found significant trace element and isotopic correlations with the calculated amount of added enriched component. Both Hickey & Frey (1982) and Cameron et al. (1983) demonstrated that a two component mixing model is successful in explaining the trace element and isotopic characteristics of boninite rocks.

The REE element variation of the north Tonga lavas can also be explained successfully by a two-component mixing model, as significant correlations exist between trace element contents, ratios and isotopes with the REE ratios Sm/Nd, La/Nd or calculated amount of enriching component (based on the method of Cameron et al., 1983). However poor correlations exist between LILE/REE ratios and $^{87}Sr/^{86}Sr$ ratios (e.g. Sr/La has a relatively constant value of 45 for samples 1-38, 11-3, 5-20, 5-25 and 3-24 despite the $^{87}Sr/^{86}Sr$ isotope ratio varying from 0.7029-0.7041). Although a two component mixing model can explain most of the trace element and isotopic characteristics, it is not a full or complete explanation.

With regards to the HFSE in a two component mixing model, the low Nb and other HFSE in the Tofua magmatic arc and north Tonga lavas is due to the nature of the depleted source component. The NAP pattern of a depleted Costa Rica MORB from site 504B (Hole et al., 1984) shows a significant Nb depletion relative to the other HFSE (Fig. 49a). There is no need to invoke any residual titanate phase to explain the high La/Nb ratios in the Tonga lavas. The relatively high Nb in the station 24 and 25 lavas is due to the nature of the enriching component, as demonstrated by the good correlation of Nb with calculated % enriched component, using the method of Cameron et al. (1983) (Fig.50).

5.5.4 Origin of the enriched component in the two component mixing model

The two most likely 'enriched' components which are capable of producing the trace element enrichments and range in Nd and Sr isotopes observed in the north Tonga lavas are either subducted oceanic sediment (dominantly pelagic) or a mantle-derived phase (fluid or melt).

In Fig. 49b, c NAP of possible 'enriched' components are presented. Included are two examples of pelagic sediment (Hole et al., 1984; Jenner et al., 1987, Fig. 49b) and two examples of enrichments seen in mantle derived

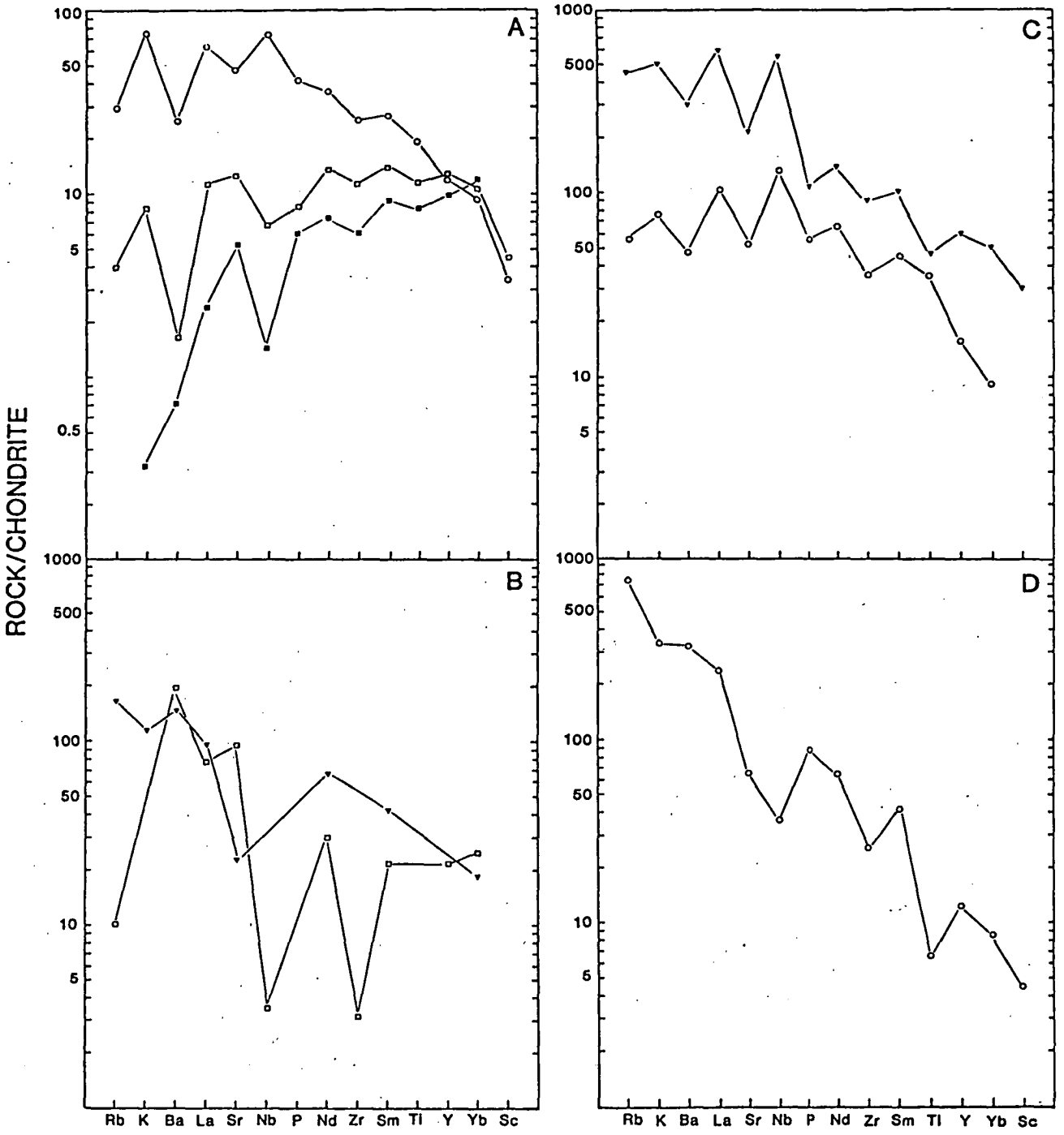

Figure 49.

Chondrite normalised abundance patterns of possible depleted and enriched endmember components.

A. (■) depleted MORB basalt from site 504B (Hole et al., 1984), (□) N-type MORB V27-19 (Le Roex et al., 1985), (O) P-type MORB V33-66 (Le Roex et al., 1985).

B. (□) Pacific authigenic mean weighted sediment (Hole et al., 1984), (▼) Tonga sediment (Jenner et al., 1987).

C. (▼) Toro Ankole mafic mafurite C4802 (Foley, 1986), (O) alkali basalt R198, Rapa Island (Palacz & Saunders, 1986).

D. (O) Batu Tara sample B4155, Indonesia (Stolz et al., 1987).

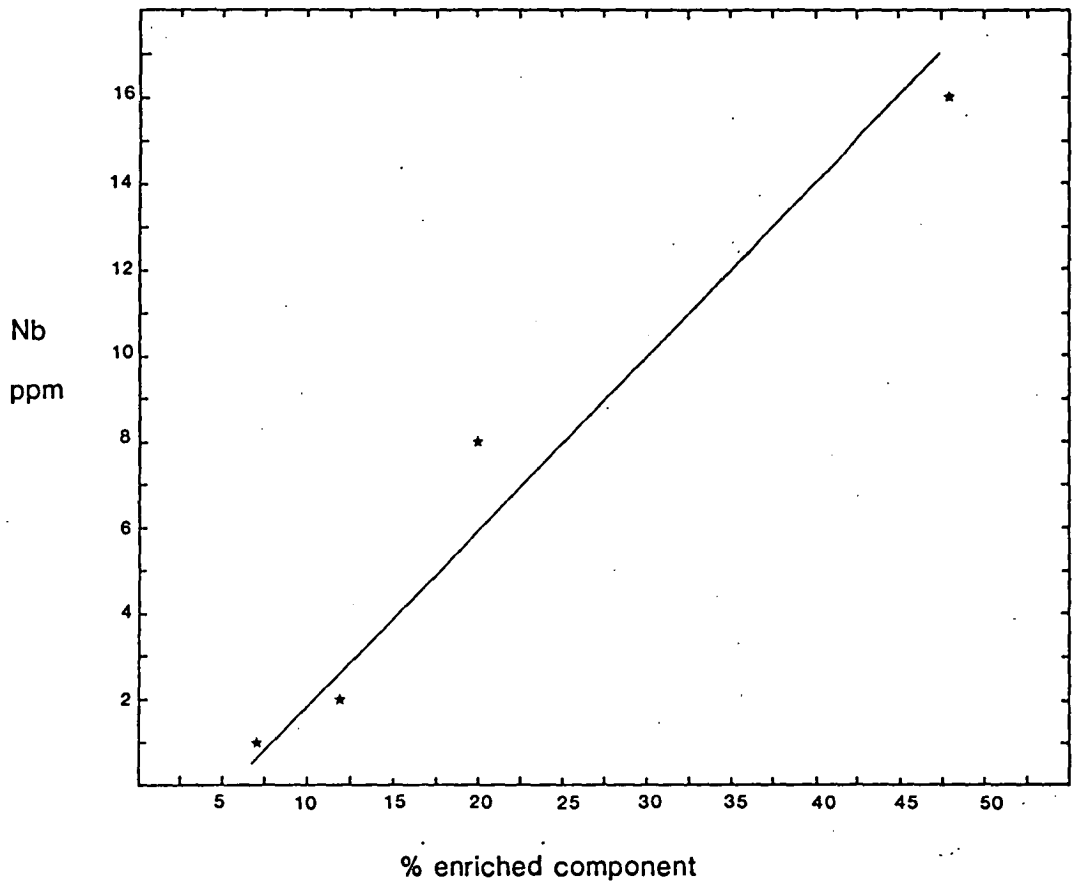

Figure 50.

Nb ppm versus % enriched component (calculated by method of Cameron et al., 1983) for the dredged north Tonga lavas.

rocks from Samoa (Rapa) and the east African rift (Toro Ankole) (Fig. 49c) (references see caption to Fig. 49).

Based on a two component mixing model, the station 24 and 25 high-mg lavas both have the highest calculated amounts of enriched components (see Fig.50) and are more likely to reflect the trace element signature of the enriched component. As can be seen from comparing Fig. 44d and 49c there is a marked similarity between the NAP from Rapa and Toro Ankole with station 24 and 25 high-mg lavas. There is a marked dissimilarity between the NAP of the sediment components, especially with regards to Nb and La when compared to station 24 and 25 high-mg lavas (Fig. 49b). The similarity in NAP between station 24 and 25 lavas and hot-spot and rift related within plate lavas is taken as strong evidence that the enriched component is a mantle-derived phase and not subducted oceanic sediment. The suggestion that subducted sediment is unlikely to be responsible for the 'enriched' trace element and isotopic signature of the Tonga lavas relative to MORB is supported by the Pb isotopic data from Ewart & Hawkesworth (1987) which show no evidence for sediment involvement (Fig. 51). Pb isotopes from the Tofua magmatic arc volcanics lie entirely within the mantle array falling along the NHRL in a ^{208}Pb-^{206}Pb plot and plotting slightly above the NHRL in a ^{207}Pb-^{206}Pb plot in a similar position to oceanic islands of the Dupal anomaly. There is no well defined trend towards subducted oceanic sediment (Fig. 51).

The enrichments seen in the north Tonga station 24 and 25 lavas, although of mantle derivation, is unlike mantle-derived enrichments seen in other island arc volcanics such as from the Indonesian arc (Wheller et al., 1986; Varne, 1985; Varne & Foden, 1986; Stolz et al., 1987) or that seen in boninites (Hickey & Frey, 1982; Cameron et al., 1983). Varne (1985) proposed that the characteristic enrichment in K-group elements seen in the Indonesian volcanics is due to a component from enriched subcontinental lithosphere. The NAP from Batu Tara (Fig. 49d), an example of the enrichment present in the Indonesian arc volcanics, is unlike NAP's from station 24 and 25; it has a Nb-anomaly relative to La and is much more enriched in K-group elements (Rb, Ba, K, Sr). The Nb anomaly is interpreted to result from equilibrium with a residual titanate phase (Varne, 1985; Foley & Wheller, 1987). No residual titanate phase is required in the case of the enrichment seen in station 24 and 25 high-mg lavas. The Tonga high-mg lavas lack the distinctive Zr enrichment relative to Sm seen in NAP (Fig. 44d) (Hickey & Frey, 1982; Sun & Nesbitt, 1978; PART III).

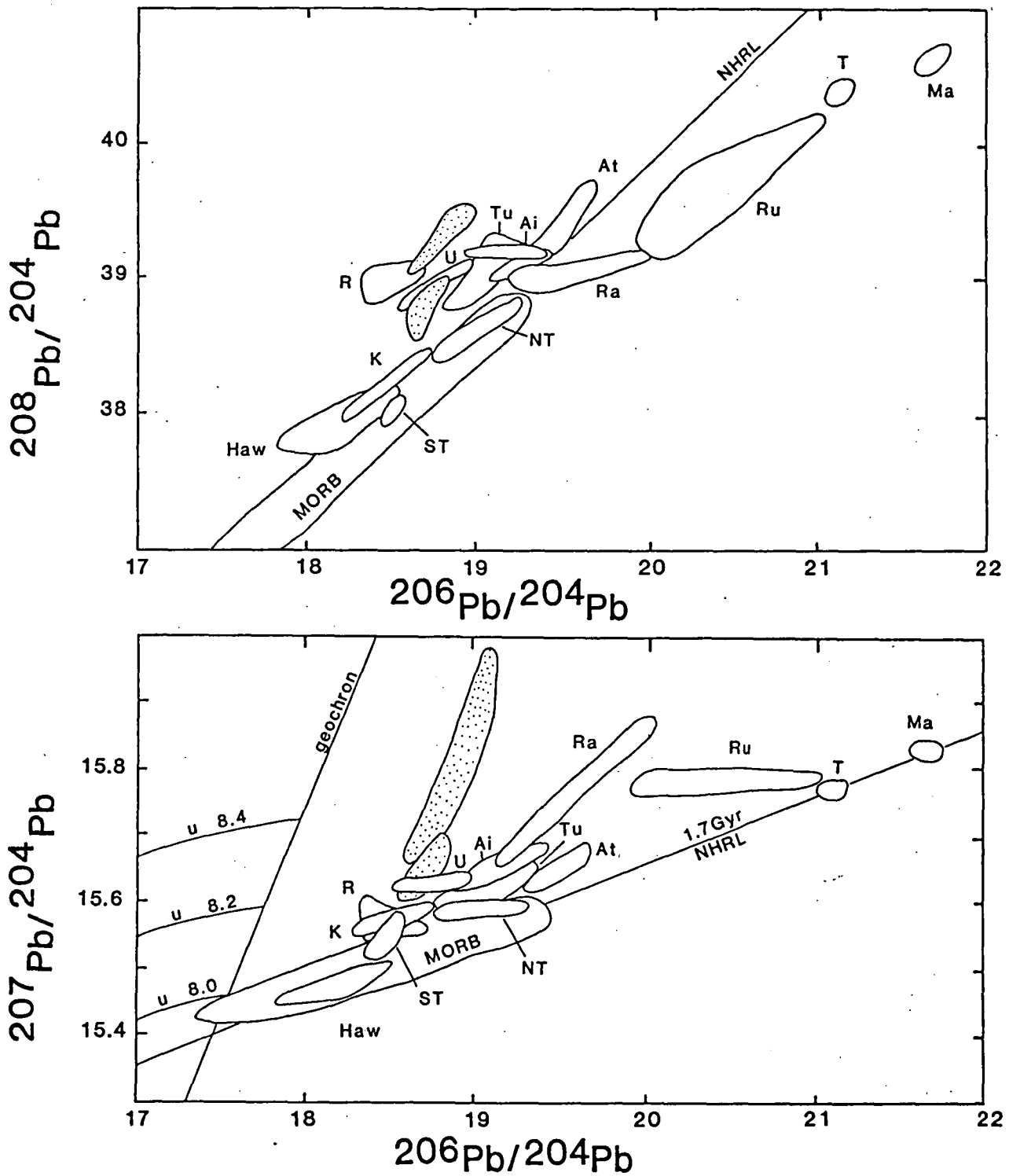

Figure 51.

Pb isotopic composition of Tofua Magmatic arc volcanics compared to ocean islands of the Cook-Austral-Samoa chains (Palacz & Saunders, 1986). NT north Tonga, ST south Tonga, K Kermadecs (Ewart & Hawkesworth, 1987). Stippled field Pacific pelagic sediment from Hole et al. (1984). HAW Hawaii (Sun, 1980; Stille et al., 1983). MORB data from Sun (1980) and Allegre et al. (1980). R Rarotonga, U Upolu, Ai Aitutaki, At Atiu, Tu Tutuila, T Tubuai, Ma Mangaia, Ru Rurutu, Ra Rapa. NHRL northern hemisphere reference line (Hart, 1984). u values refer to single stage evolution models.

5.5.5 Evidence for a second enriched component

Although a two component mixing model can explain most of the trace element and isotopic compositions of the north Tonga lavas, an additional component with high LILE/LREE ratios is also required. In Fig.52 the Sr/La and Ba/La ratios of the north Tonga lavas are compared with ratios in likely depleted and enriched source components. Enrichments produced by mantle components fall in a broad array from a high Sr/La, low Ba/La end-member equivalent to depleted MORB mantle to enriched end-members similar to Group I (Foley et al., 1987) continental ultrapotassic lavas. The north Tonga lavas define a trend towards a component with high Sr/La and Ba/La. This component is difficult to identify due to the lack of any correlation between Sr/La and $^{87}Sr/^{86}Sr$ isotopic ratios. However potential sources are a hydrous fluid from subducted oceanic crust or a mantle derived fluid component. Green et al. (1987) suggest an important role for reduced fluid volatiles and associated mantle degassing in the generation of basalt magma. In particular they suggest that transform-trench intersections (north Tonga) are favourable sites for deep earth degassing of reduced volatiles (dominantly CH_4). The interaction of reduced (C-H-O) fluids with oxidised subducted lithosphere produces a H_2O-rich fluid at low fO_2 (~ MW). The presence of H_2O promotes melting of refractory peridotite in the mantle wedge. The presence of a reduced volatile phase explains well the very low $Y(Fe^{3+})$ contents of the north Tonga Cr-spinels, which suggest very low fO_2 conditions (Murck & Campbell, 1986; Barnes, 1986). The LIL elements (K, Ba, Rb, Sr) would be carried from the subducted lithosphere via the hydrous fluid phase. The predicted high Sr/Nd of this fluid phase could produce a range in $^{87}Sr/^{86}Sr$ ratios at relatively constant εNd.

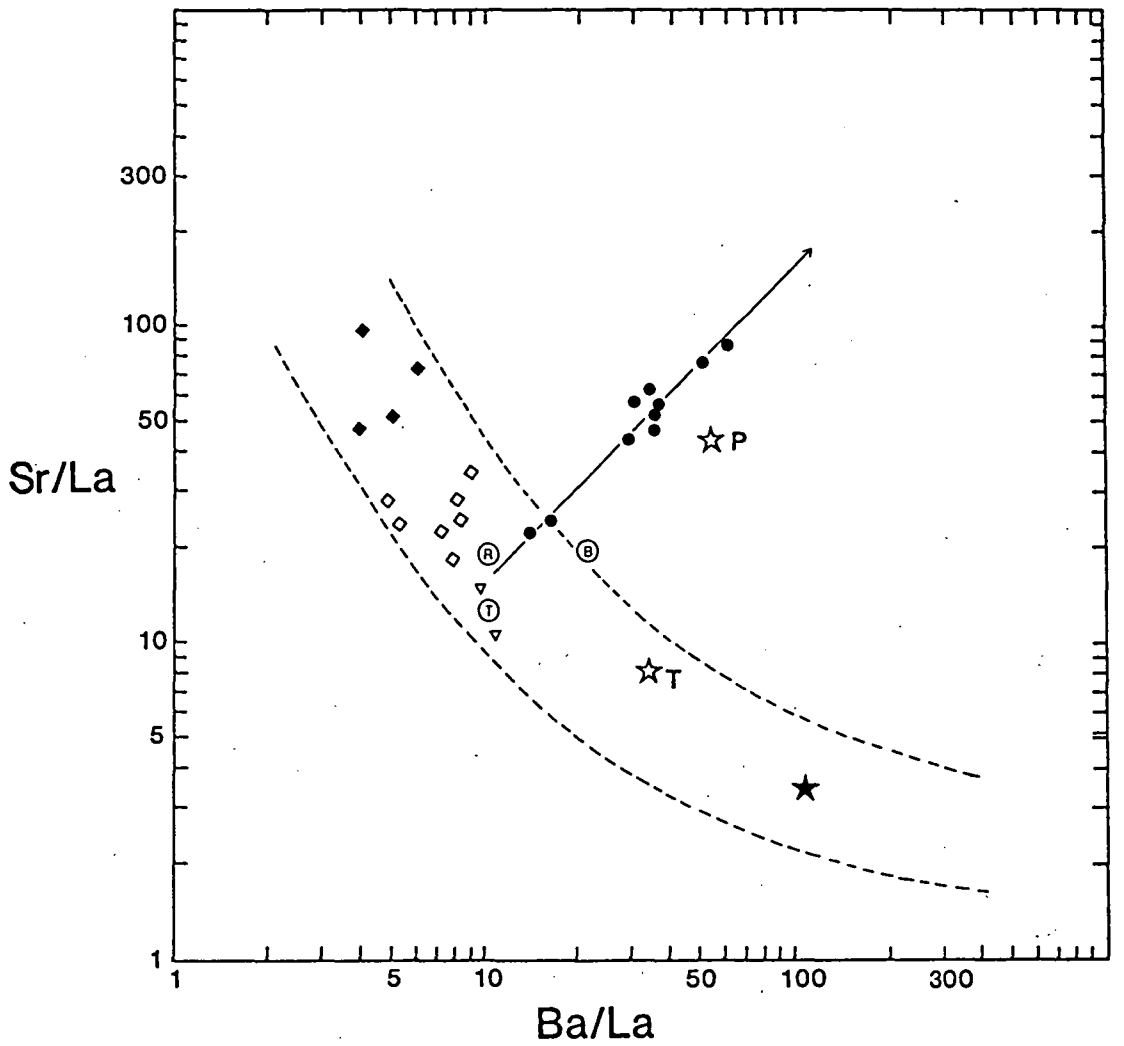

Figure 52.

Sr/La versus Ba/La ratios of north Tonga lavas. (◆) N-type MORB (Langmuir et al., 1977; Frey et al., 1974), (◇) E-type MORB (Sun, 1980; Le Roex et al., 1985), (Ⓡ) R198 Rapa Island (see also Fig. 49), (Ⓣ) Toro Ankole C4802 (see also Fig. 49), (Ⓑ) Batu Tara B4155 (see also Fig. 49), (▽) ocean island basalts (Sun, 1980), (☆) T, P Tonga and Pacific authigenic mean weighted sediment respectively (see also Fig. 49), (★) continental ultrapotassic lava EL7WAK17 (Jaques et al., 1984). Arrow points in direction of high Sr, Ba/La component.

APPENDIX 1

REPRESENTATIVE RESIDUAL PHASE COMPOSITIONS FROM SANDWICH EXPERIMENTS ON MORB PYROLITE, HAWAIIAN PYROLITE AND TINAQUILLO LHERZOLITE

all analyses are normalised to 100%, OL =olivine, OPX= orthopyroxene, CPX =clinopyroxene, SP =spinel, PLG =plagioclase, GA =garnet

Run no.	Phase	SiO_2	TiO_2	Al_2O_3	FeO	MgO	CaO	Na_2O	Cr_2O_3	NiO	Mg#
T-1511	OL	40.31			12.15	47.54					0.875
	OPX	53.52	0.30	6.31	7.35	29.01	2.66		1.05		0.876
	CPX	51.61	0.35	6.28	4.67	18.79	17.09	0.39	0.82		0.878
	SP			55.76	10.19	20.59			13.46		0.783
T-1472	Ol	40.74		0.22	11.22	47.60	0.24				0.883
	OPX	53.53		5.61	6.80	30.33	2.82		0.91		0.888
	SP		0.50	54.50	9.50	17.00			18.50		0.761
T-2123	OL	40.51			11.51	47.76	0.21				0.881
	OPX	53.56	0.19	5.45	6.93	30.12	2.92		0.82		0.886
	CPX	51.03	0.31	7.04	4.92	19.95	16.69	0.32			0.874
T-1493	OL	40.26			11.47	47.85	0.22		0.20		0.881
	OPX	53.47		5.52	7.00	30.29	2.85		0.88		0.885
	CPX	51.07	0.36	7.52	4.93	19.11	16.69	0.32			0.874
T-1478	OL	40.40			10.81	48.20	0.29		0.30		0.888
	OPX	54.38		3.80	6.84	31.05	2.79		1.14		0.89
	CPX	52.26	0.24	5.86	5.44	21.67	13.28	0.24	1.00		0.876
T-2140	OL	40.79			10.68	48.02	0.28		0.23		0.889
	OPX	54.24		4.89	6.49	30.38	2.64		1.36		0.893
	CPX	52.14	0.21	5.96	4.82	20.67	14.58		1.62		0.884
	SP		0.22	36.12	11.10	18.58			33.99		0.749
T-1461	OL	40.59			10.39	48.57	0.21		0.24		0.893
	OPX	54.64		4.14	6.49	31.18	2.51		1.03		0.895

T-1480	OL	40.52			10.32	48.68	0.21		0.27	0.894
	OPX	55.03		2.98	6.67	31.82	2.35		1.15	0.895
T-1464	OL	40.44			10.19	48.97	0.20		0.20	0.895
	OPX	55.51		2.98	6.53	32.13	2.17		0.86	0.90
T-2113	OL	40.73			9.82	48.84	0.40		0.22	0.899
	OPX	54.89		4.02	5.58	31.41	2.73		1.36	0.909
	CPX	51.96	0.19	5.83	4.57	20.84	15.03		1.59	0.891
T-2117	OL	40.22			12.84	46.67	0.27			0.866
	OPX	54.53	0.59	4.12	7.22	29.87	2.53		1.15	0.881
	CPX	51.13	1.40	5.92	5.64	19.46	14.57	0.37	1.57	0.86
T-2133	OL	40.84			10.08	48.65	0.21		0.22	0.896
	OPX	54.06	0.22	7.26	6.33	29.19	2.51		0.43	0.892
	CPX	51.29	0.30	7.00	4.05	19.18	16.81	0.24	1.14	0.885
	SP			48.39	9.46	20.58			21.57	0.795
T-2121	OL	40.21			12.37	47.22	0.21			0.872
	OPX	52.82		7.57	6.11	30.27	2.25		0.98	0.898
	CPX	51.03	0.65	7.08	4.78	18.57	16.44	0.44	1.00	0.874
	SP	0.67	0.34	44.19	11.39	19.49			23.92	0.753
	PLG	52.21		30.61	0.19		13.60	3.39		
T-2078	OL	40.63			10.44	48.66	0.27			0.891
	OPX	54.01	0.23	5.88	6.16	30.14	2.93		0.66	0.897
	CPX	51.68	0.25	6.45	4.22	19.80	16.05	0.35	1.19	0.873
	SP	0.89	0.19	54.00	8.67	21.36	0.15		14.75	0.815
T-2138	OL	41.18			10.03	48.53	0.27			0.896
	OPX	53.99		6.63	5.92	29.97	2.60		0.88	0.90
	CPX	51.76	0.27	6.68	4.59	21.23	13.71		1.51	0.892
	SP	2.00	0.34	43.47	9.75	19.59	0.34		24.51	0.782
T-2136	OL	40.96			9.22	49.59	0.24			0.906
	OPX	53.77		3.74	5.48	33.54	2.22		1.24	0.916
	CPX	51.52	0.26	6.65	3.92	20.06	15.64	0.31	1.63	0.901
	SP		0.18	43.29	9.20	20.39			26.94	0.798
T-1516	OL	40.23			10.78	48.51	0.24		0.24	0.889

	OPX	54.23		4.01	6.76	30.91	2.96		1.13		0.89
	CPX	51.42	0.29	5.66	4.33	19.36	17.05	0.24	1.64		0.888
T-1512	OL	40.68			10.11	48.70	0.19		0.32		0.896
	OPX	55.00		3.42	6.66	31.40	2.30		1.22		0.894
T-1479	OL	40.79			10.12	48.88	0.32		0.19		0.902
	OPX	53.91		4.07	6.45	31.89	2.66		1.02		0.898
T-1994	OL	41.24			9.43	48.82	0.32		0.19		0.902
	OPX	53.87		5.74	5.42	30.81	2.46		1.69		0.91
	CPX	52.81	0.19	6.16	4.92	23.70	10.69		1.54		0.896
T-2189	OL	41.31			8.94	49.29	0.25		0.21		0.908
	OPX	53.45		3.96	5.70	33.38	2.13		1.38		0.913
T-1989	OL	41.72			10.31	44.83			0.34		0.886
	OPX	53.10	0.24	7.31	6.35	29.70	2.63		0.68		0.893
	CPX	51.05	0.42	9.10	4.61	18.17	16.10	0.55			0.875
	SP		0.38	57.57	9.86	23.70			8.47		0.811
T-1999	OL	41.10			9.18	48.75	0.27		0.24	0.45	0.904
	OPX	53.16	0.20	6.65	5.39	30.15	2.68		1.77		0.909
	CPX	52.65	0.17	6.94	5.22	23.39	10.05	0.44	1.14		0.889
T-2192	OL	41.36			8.53	49.94	0.17				0.913
	OPX	54.89		5.07	5.05	31.32	2.44		1.23		0.917
T-2056	OL	41.41			7.54	50.73	0.32				0.923
	OPX	55.05		4.26	4.77	31.79	2.72				0.922
T-2029	OL	40.93			11.35	47.49	0.14				0.882
	OPX	53.25		8.17	5.95	29.36	2.48		0.79		0.898
	CPX	51.78	0.32	8.36	5.50	22.16	10.75	0.40	0.73		0.878
T-2031	OL	41.01			9.24	48.83	0.23		0.26	0.43	0.904
	OPX	54.11		6.22	5.06	30.75	2.61		1.25		0.915
	CPX	52.13		7.66	4.27	21.66	12.67		1.61		0.90
	SP		0.22	52.37	8.14	21.37			17.41		0.824
T-2069	OL	41.29			8.16	50.07	0.20		0.29		0.916

	OPX	54.78		4.13	5.28	32.18	2.63		1.00	0.916
T-1515	OL	40.12			11.60	48.10	0.18			0.881
	OPX	53.90		5.23	6.24	30.86	2.79		0.99	0.898
	CPX	51.97		6.94	5.13	21.18	13.22	0.63	0.94	0.88
	SP			58.04	9.52	21.50			10.93	0.801
T-1501	OL	40.21			10.88	48.34	0.24		0.20	0.888
	OPX	53.98		5.64	5.90	31.38	2.35		0.75	0.904
	CPX	53.91		4.88	5.82	25.39	8.93	0.40	0.67	0.886
T-1513	OL	40.39			10.76	48.39	0.27			0.889
	OPX	53.97		5.63	5.96	31.01	2.40		1.03	0.903
	CPX	53.91		4.88	5.82	25.39	8.93	0.40	0.67	0.886
T-1499	OL	40.80			10.19	48.60	0.20		0.22	0.895
	OPX	53.84		6.33	5.99	30.40	2.68		0.77	0.90
T-2207	OL	41.02			9.25	49.30	0.20		0.23	0.905
	OPX	54.83		5.00	5.89	31.03	2.07		1.17	0.904
T-2086	OL	41.48			7.71	50.61	0.20			0.921
	OPX	54.00		6.03	4.82	31.71	2.49		0.95	0.921
	CPX	52.80		7.52	4.03	24.40	9.80	0.34	1.10	0.915
T-2065	OL	41.51			7.49	50.60	0.19		0.21	0.923
	OPX	54.86		5.77	4.31	31.71	2.37		0.97	0.929
	CPX	53.25		6.85	4.07	25.34	8.73	0.53	1.24	0.917
T-2075	OL	41.35			7.08	51.13	0.20		0.23	0.928
	OPX	55.65		4.65	4.23	32.60	2.15		0.72	0.932
T-2087	OL	41.35			7.97	50.47	0.21			0.919
	OPX	55.82		4.76	4.60	32.03	2.14		0.64	0.925
	CPX	53.82	0.23	6.47	4.21	24.22	9.47	0.99	0.59	0.911
	GA	42.23	0.47	22.95	5.88	22.06	5.12		1.29	0.87

APPENDIX 2

PRIMITIVE MORB GLASS DATA BASE

Sample no.	Ref no.	SiO_2	TiO_2	Al_2O_3	FeO	MgO	CaO	Na_2O	K_2O	P_2O_5	MnO	Cr_2O_3	Total	Mg#
504B 35-1, 15	1	49.32	0.82	17.22	8.67	9.36	12.97	2.16	0.01	0.08			100.60	0.68
504B 35-1, 81	1	48.87	0.83	16.98	8.43	9.21	12.97	2.12	0.02	0.07			99.50	0.68
504B 35-1, 108	1	49.33	0.81	16.99	8.60	9.31	12.86	2.13	0.05	0.06			100.14	0.68
SD-7ED 4980	2	49.15	0.96	17.58	8.01	9.58	12.14	2.38	0.04	0.10			99.94	0.70
DS-3-3A 3864	2	49.31	0.98	17.60	7.95	9.06	12.37	2.44	0.04	0.09			99.84	0.69
DS-3-3B 3865	2	49.10	0.98	17.48	7.98	9.17	12.32	2.42	0.04	0.08			99.57	0.69
I607 3-14	3	49.97	0.73	17.26	8.39	9.51	12.92	1.99	0.01	0.05			100.81	0.69
I608 3-14	3	50.02	0.81	17.62	8.35	9.24	12.88	2.02	0.01	0.05			101.00	0.69
3-14	4	49.99	0.77	17.44	8.37	9.37	12.90	2.00	0.01	0.04			100.89	0.69
3-14	5	50.00	0.79	18.20	8.21	9.99	12.80	1.99	0.03				102.01	0.71
3-14-10-1, 40	6	50.00	0.79	17.40	8.22	9.81	12.90	2.28	0.02		0.13		101.55	0.70
3-18-7-1, 10	6	50.30	0.73	16.60	7.99	10.20	13.20	2.00	0.01		0.12		101.15	0.72
3-18-7-1	7	49.70	0.72	16.40	7.90	10.10	13.10	2.00	0.01		0.12	0.07	100.12	0.72
3-18	5	49.90	0.70	17.40	7.78	10.40	12.80	1.89	0.01		0.12		101.00	0.73
72-17-44	8	49.68	0.86	16.75	7.67	9.19	12.23	2.31	0.05	0.10	0.13		98.97	0.70
72-17-31	8	49.77	1.12	16.77	8.51	9.31	12.06	2.63	0.14	0.08	0.14		100.53	0.68
T3-71D 159-10C1	9	47.28	0.97	14.48	10.98	12.52	10.78	2.38	0.04	0.09	0.19		99.71	0.71
T3-71D 159-10C4	9	48.61	1.00	14.65	10.28	10.83	10.78	2.35	0.04	0.07	0.17		98.78	0.70
A36.80 N1	10	49.54	0.74	16.62	8.74	9.43	12.84	2.08	0.09	0.08			100.16	0.68
A36.81 N1	10	49.00	0.86	16.37	8.88	9.55	12.38	1.96	0.10	0.09			99.19	0.68
A36.81 N1	10	49.52	0.85	16.04	8.96	9.86	12.39	2.07	0.17	0.09			99.95	0.69
335-6-6 22-24	11	49.30	1.20	15.50	9.40	10.10	11.70	2.50	0.20		0.10		100.00	0.68
332B 36-3	12	49.56	0.67	15.90	8.29	9.19	13.57	2.15	0.07		0.17		99.57	0.69
ARP73 10-3	13	48.75	0.64	16.59	8.00	10.17	13.22	1.98	0.14				99.49	0.72
ARP73 10-3	14	48.80	0.63	16.60	7.90	10.50	13.40	1.98	0.07		0.14	0.03	100.05	0.72
519-2-1	15	49.24	0.78	16.53	8.77	9.69	12.07	2.15	0.07		0.17	0.10	99.57	0.69
519-2-3	15	48.48	0.75	16.39	8.86	9.81	12.37	2.14	0.09		0.16	0.03	99.08	0.69
519-4-1	15	49.07	0.74	16.44	8.86	10.15	11.65	2.13	0.07		0.16	0.03	99.30	0.69
519-4-1	16	49.10	0.78	16.60	8.04	9.51	12.47	2.08	0.08		0.14	0.06	98.86	0.70
519-4-2	15	48.81	0.73	16.34	8.92	9.91	11.99	2.16	0.08		0.16	0.04	98.86	0.70
520-2-1B	15	49.64	0.78	16.34	8.72	9.82	11.76	2.25	0.09		0.15	0.06	100.03	0.69
522-2-1	15	49.65	0.87	16.05	8.72	9.82	11.76	2.25	0.09		0.15	0.06	99.42	0.69
525-5-2	14	48.90	0.84	16.10	8.74	10.50	11.80	2.41	0.09		0.15	0.09	99.62	0.70
525-5-2	15	48.95	0.84	16.14	8.75	10.49	11.84	2.41	0.09		0.15	0.09	99.73	0.70
525-5-2	16	48.80	0.83	16.00	8.51	9.94	12.00	1.98	0.13		0.15	0.04	98.38	0.70
528-4-1	15	49.93	0.72	15.82	8.37	9.78	12.67	1.96	0.05		0.15	0.08	99.53	0.70
528-4-1	16	49.00	0.75	16.60	7.68	9.73	12.38	2.07	0.06		0.16	0.06	98.49	0.71
525-5-3	15	48.96	0.82	15.75	8.52	9.79	11.92	1.97	0.11		0.13	0.08	97.55	0.69

527-1-1	15	48.82	0.66	16.54	8.77	9.74	12.45	2.23	0.06		0.18	0.13	99.58	0.69
527-1-1	17	48.20	0.73	16.30	8.92	10.70	12.00	1.95	0.09		0.25	0.05	99.19	0.70
527-1-1	16	48.30	0.65	16.70	8.70	9.65	12.50	2.04	0.08		0.15	0.04	98.81	0.69
527-1-2	15	49.50	0.66	16.51	8.76	9.86	12.68	2.08	0.04		0.17	0.11	100.37	0.69
525-5-1	15	49.19	0.85	16.12	8.74	10.41	11.91	2.35	0.09		0.14	0.08	99.93	0.70
528-1-1	15	48.83	0.84	16.17	9.00	9.76	12.43	2.35	0.09		0.16	0.09	99.72	0.68
528-2-1	15	49.44	0.81	15.92	9.18	10.03	12.28	2.08	0.09		0.13		99.96	0.68
528-3-2	15	49.75	0.84	15.92	8.67	9.43	12.45	2.07	0.07		0.17	0.09	99.46	0.68
ARP74-10-16	18	50.00	0.86	15.50	8.05	10.50	12.20	2.10	0.13	0.14	0.17		99.65	0.72
ARP74-10-16	18	49.47	0.82	15.23	8.15	10.66	12.21	1.94	0.16	0.10	0.14		98.88	0.72
530-3-1	15	49.98	0.77	15.24	8.60	10.11	12.45	2.23	0.07		0.13		99.58	0.70
534-2-1	15	50.30	0.84	15.99	8.70	9.91	12.33	2.16	0.09		0.13	0.08	100.53	0.69
534-2-1C	15	50.33	0.84	15.89	8.72	9.70	12.49	2.13	0.09		0.09	0.10	100.29	0.69
534-2-2A	15	50.37	0.84	15.86	8.57	9.82	12.33	2.18	0.09		0.16	0.09	100.31	0.69
ARP74-14-31	14	48.20	0.51	17.00	8.51	10.10	12.70	2.30	0.04		0.16		99.56	0.70
ARP74-14-33	14	48.20	0.50	16.90	8.50	9.91	12.80	2.30	0.04		0.15	0.01	99.31	0.70
CYP31-35	18	49.57	0.85	15.26	8.15	10.63	12.11	2.11	0.19	0.11	0.14		99.12	0.71
CHAIN 43-23	19	49.50	0.81	15.70	7.45	10.00	13.00	1.95	0.17	0.08	0.15	0.14	98.95	0.73
AII 32 II-37	20	50.73	0.92	15.61	7.97	9.34	13.29	1.94	0.24	0.10			100.14	0.70
AII 32 II-90	20	50.41	0.92	15.64	7.95	9.09	13.35	2.05	0.28	0.11			99.80	0.69
CHAIN 21 D20-29	19	48.26	0.89	16.80	9.32	10.48	11.23	2.40	0.03	0.06	0.17		99.64	0.69
483B 32-2, 141	21	51.00	1.30	15.60	7.30	8.10	13.20	2.50	0.10	0.10	0.10		99.3	0.69
3-18-7-1, 30-35	6	50.40	0.79	17.10	7.97	9.88	12.90	1.62	0.02				100.68	0.71
3-18	22	50.40	0.79	17.09	7.97	9.88	12.93	1.62	0.02	0.08			100.78	0.71
3-18	3	50.14	0.74	16.81	8.25	9.59	13.01	1.71	0.04				100.29	0.70
3-18	3	50.73	0.73	16.88	8.22	9.84	13.33	1.68	0.04	0.05			101.50	0.70
3-18	3	49.95	0.69	17.29	7.91	9.14	13.23	1.76	0.04				100.01	0.70
3-18	4	49.86	0.71	16.93	8.12	9.49	13.23	1.76	0.02	0.04			100.04	0.70
A36.82 N1	10	49.82	0.85	16.11	8.48	9.11	13.00	1.85	0.13	0.10			98.95	0.68
A36.82 N1	10	51.14	0.95	16.28	8.29	9.40	12.26	2.06	0.16	0.12			100.40	0.68
A36.83 N1	10	50.89	0.89	16.21	8.29	9.40	12.26	2.06	0.16	0.12			100.28	0.69
529-3-2	15	50.82	0.92	15.92	7.91	9.38	12.07	2.30	0.16		0.13	0.06	99.67	0.70
822-8	23	49.99	0.82	16.25	8.42	8.97	13.34	2.01	0.10	0.09			99.99	0.68
826-1	23	50.10	0.78	16.42	8.23	8.82	13.38	1.84	0.07	0.06			99.70	0.68
826-2	23	49.69	0.71	16.48	8.26	8.98	13.79	1.88	0.05	0.10			99.94	0.68
828-1	23	49.20	0.74	16.05	8.46	9.12	13.48	1.83	0.05	0.07			99.00	0.68
E203	3	50.41	0.92	15.64	7.95	9.09	13.35	2.05	0.28	0.11			99.80	0.69
E202	3	50.73	0.92	15.61	7.97	9.34	13.29	1.94	0.24	0.10			100.14	0.70
	4	50.57	0.92	15.62	7.96	9.21	13.32	1.99	0.26	0.10			99.95	0.70
TR-154 140-1	24	51.36	1.29	16.48	7.64	8.39	12.02	2.49	0.25	0.09	0.06		100.07	0.68
TR-138 10-2	24	51.15	1.15	16.14	7.74	8.37	12.23	2.71	0.22		0.16		99.87	0.68

212	3	51.33	0.61	15.60	7.86	8.97	13.48	1.42	0.05	0.03			99.35	0.69
526-1-1B	15	51.36	0.78	15.03	7.86	9.01	12.38	2.04	0.10		0.10	0.11	98.77	0.69
AII 77 37-1	14	51.40	0.95	14.80	8.48	9.30	12.70	1.84	0.11		0.18	0.05	99.81	0.68
AII 77 76-61	14	51.20	0.84	15.00	7.98	9.02	13.30	1.89	0.08		0.16	0.08	99.55	0.69
AII 77 76-71	14	51.40	0.83	15.00	8.05	9.15	13.20	1.97	0.09		0.16	0.07	99.92	0.69
KN42 129-16	14	51.00	0.99	15.30	8.31	8.96	12.00	2.00	0.32		0.13		99.01	0.68
TR 154 13D-1	24	51.64	1.10	15.61	7.16	8.51	12.55	2.33	0.13	0.05	0.08		99.16	0.68

Ref no.	Reference
1	Natland et al. (1984)
2	Natland & Melson (1980)
3	Melson et al. (1977)
4	Melson et al. (1976)
5	Frey et al. (1973)
6	Frey et al. (1974)
7	Green et al. (1979)
8	O'Donnell & Presnall (1980)
9	Keays & Scott (1976)
10	Melson & O'Hearn (1979)
11	Scarfe & Smith (1977)
12	Shipboard. S. P. (1977)
13	Hekinian et al. (1976)
14	Bryan (1979)
15	Bryan & Moore (1977)
16	Langmuir et al. (1977)
17	Bender et al. (1978)
18	Fujii & Bougault (1983)
19	Basaltic volcanism study project (1981)
20	Shibata et al. (1979)
21	Barker et al. (1983)
22	Melson (1973)
23	Stakes et al. (1984)
24	Sigurdsson (1981)

APPENDIX 3

GEOCHEMICAL ANALYSES OF DREDGED IGNEOUS ROCKS FROM THE 1984 CRUISE OF THE 'NATSUSHIMA'

A3.1 Major element geochemistry

major elements in wt%, LOI =loss on ignition, total iron as Fe_2O_3

no.	SiO_2	TiO_2	Al_2O_3	Fe_2O_3	MnO	MgO	CaO	Na_2O	K_2O	P_2O_5	LOI	Total
1-30	53.22	1.24	15.56	11.05	0.18	4.45	8.92	2.90	0.59	0.09	1.54	99.74
1-31	53.27	1.27	15.47	10.80	0.17	4.02	8.46	2.91	0.84	0.11	2.52	99.84
1-33	52.76	1.21	15.68	11.13	0.17	4.48	8.82	2.86	0.56	0.10	1.85	99.62
1-34	51.64	1.04	16.50	8.66	0.15	5.38	10.13	3.01	0.66	0.12	2.08	99.37
1-38	52.22	0.94	16.52	9.20	0.16	5.94	10.59	2.52	0.47	0.10	1.15	99.81
1-39	49.91	1.40	15.19	12.38	0.18	5.43	8.50	3.25	0.47	0.62	2.60	99.93
1-35	50.87	0.97	16.68	8.70	0.14	7.46	8.64	3.07	0.28	0.11	2.59	99.51
3-21	53.05	0.22	12.57	10.72	0.16	10.34	9.63	1.52	0.43	0.04	1.07	99.75
3-49	51.20	0.21	10.86	10.36	0.18	14.53	9.76	1.38	0.20	0.05	1.46	100.19
3-51	52.67	0.22	12.57	10.64	0.16	10.15	10.25	1.56	0.44	0.03	1.33	100.02
3-44	53.66	0.20	10.53	10.32	0.19	14.80	8.55	1.13	0.35	0.03	0.05	99.81
3-39	53.46	0.22	11.21	10.13	0.18	13.08	9.34	1.07	0.33	0.03	0.36	99.41
3-45	54.37	0.28	10.65	10.77	0.18	11.83	9.19	1.45	0.47	0.05	0.59	99.83
3-47	54.18	0.30	10.74	10.91	0.19	11.92	9.07	1.45	0.47	0.05	0.98	100.26

3-22	55.32	0.29	13.71	10.65	0.19	7.68	9.86	1.61	0.46	0.06	-0.15	99.68
3-24	58.36	0.25	10.81	9.67	0.18	10.65	7.67	1.35	0.55	0.07	0.01	99.57
3-25	54.69	0.29	11.22	10.75	0.18	10.86	9.11	1.39	0.57	0.05	1.08	100.19
3-34	58.34	0.34	13.13	10.03	0.18	6.18	9.02	1.76	0.63	0.09	-0.04	99.66
3-41	55.07	0.33	14.27	10.78	0.19	6.83	9.84	1.72	0.60	0.07	0.50	100.20
3-46	54.71	0.24	10.41	10.90	0.19	12.34	9.33	1.01	0.35	0.04	0.28	99.80
3-26	54.71	0.29	15.05	10.50	0.17	6.28	10.39	1.43	0.46	0.06	0.45	99.79
3-28	53.86	0.27	14.66	11.03	0.17	7.74	10.58	1.37	0.40	0.04	0.04	100.16
3-31	56.13	0.33	15.08	10.17	0.17	5.05	9.53	1.82	0.66	0.08	0.13	99.15
3-40	56.14	0.34	16.01	10.31	0.15	4.50	9.85	1.96	0.63	0.09	0.04	100.02
3-52	56.52	0.30	14.53	10.31	0.18	6.39	10.30	1.51	0.46	0.09	0.03	100.62
3-53	56.85	0.29	13.03	10.13	0.18	8.05	9.42	1.33	0.53	0.06	-0.07	99.80
3-27	54.66	0.30	15.25	10.73	0.17	5.91	10.53	1.39	0.42	0.04	0.30	99.70
3-29	58.52	0.41	14.78	9.66	0.14	3.24	7.46	2.71	1.14	0.14	1.73	99.93
3-30	58.87	0.42	14.48	9.38	0.15	3.01	7.24	2.77	1.31	0.14	2.23	100.00
3-36	58.89	0.41	14.96	9.82	0.15	3.22	7.53	2.78	0.98	0.15	0.86	99.75
3-36b	58.81	0.41	14.87	9.67	0.15	3.27	7.51	2.89	0.99	0.14	0.83	99.54
3-36c	58.08	0.40	14.72	9.53	0.15	3.27	7.39	2.76	1.20	0.14	2.25	99.89
3-32	58.34	0.40	14.89	9.59	0.15	3.26	7.43	2.77	1.21	0.14	2.02	100.20
3-42	59.83	0.42	15.04	9.53	0.14	3.09	7.34	2.95	0.98	0.15	-0.03	99.44
4-11	53.97	0.55	15.21	7.82	0.15	5.11	6.02	4.29	0.25	0.04	6.76	100.17

4-12	53.19	0.43	14.65	9.12	0.17	8.43	10.40	1.80	0.13	0.03	1.25	99.60
4-15	49.73	0.31	13.65	11.07	0.18	7.84	9.51	1.78	0.17	0.03	5.15	99.42
4-14	72.69	0.11	14.27	1.97	0.03	0.60	7.40	2.28	0.07	0.04	0.52	99.98
5-24	52.39	0.15	7.84	10.67	0.21	20.67	7.10	0.84	0.14	0.01	0.13	100.15
5-25	52.91	0.35	9.47	10.61	0.19	16.02	8.36	1.25	0.16	0.04	0.24	99.60
5-28	53.07	0.14	8.17	10.60	0.20	19.41	7.45	0.68	0.12	0.02	-0.02	99.84
5-20	55.36	0.61	14.95	10.68	0.17	5.24	10.03	2.05	0.24	0.07	0.71	100.11
5-21	55.00	0.47	16.29	10.16	0.17	4.67	10.62	1.77	0.19	0.04	0.18	99.56
5-23	55.53	0.38	16.49	9.64	0.16	5.02	10.92	1.56	0.19	0.04	0.20	100.13
5-27	56.19	0.43	14.47	10.50	0.17	5.24	9.88	1.63	0.24	0.06	0.57	99.38
6-2	54.16	0.29	9.85	9.07	0.16	14.91	8.57	0.94	0.39	0.06	1.78	100.18
6-3	54.66	0.30	10.34	9.17	0.17	13.28	8.94	1.11	0.42	0.07	1.87	100.33
7-9	53.53	0.42	10.59	9.32	0.15	12.91	9.45	1.38	0.59	0.27	1.45	100.06
7-11	53.12	0.44	10.59	9.36	0.16	12.89	9.32	1.41	0.66	0.24	1.64	99.83
7-12	53.39	0.44	10.68	9.24	0.16	12.93	9.40	1.42	0.58	0.26	1.33	100.03
7-14	53.30	0.42	10.49	9.40	0.17	12.94	9.26	1.53	0.60	0.27	1.75	100.13
7-15	53.35	0.43	10.61	9.17	0.15	12.74	9.39	1.45	0.58	0.27	1.45	99.77
7-16	53.50	0.41	10.65	9.20	0.16	12.58	9.43	1.39	0.58	0.27	1.58	99.75
7-18	52.97	0.44	10.55	9.31	0.16	12.56	9.34	1.47	0.69	0.25	1.69	99.43
11-3	48.95	0.71	15.01	10.73	0.18	9.15	13.09	2.84	0.02	0.03	-0.72	100.00

A3.2 **Trace element geochemistry**

Trace elements in ppm

no.	Ba	Rb	Sr	Zr	Nb	Y	Sc	V	Ni	Cr
1-30	28	9	130	74		30	39	349	23	46
1-31	29	13	131	78		31	33	357	20	33
1-33	24	9	133	76	1	30	39	349	25	43
1-34	26	10	158	87	1	32	34	244	39	131
1-38	29	9	132	59	1	29	40	259	52	204
1-39	16	10	156	94		45	32	267	18	27
1-35	29	4	136	57		22	39	257	109	234
3-21	112	4	172	10		5	48	326	122	435
3-49	98	2	264	9		8	45	253	233	935
3-51	104	5	175	9		6	53	343	123	445
3-44	106	6	151	12		7	50	247	275	1095
3-39	86	7	161	11	2	7	51	261	215	814
3-45	108	7	177	18	1	9	48	247	150	729
3-47	113	7	172	20		8	51	259	153	762
3-22	131	7	236	14	1	10	49	281	78	281
3-24	140	10	175	19	2	7	43	251	117	605
3-25	117	9	190	18	1	10	46	252	132	607
3-34	163	10	223	19		11	47	275	47	196
3-41	161	12	271	18	1	9	47	292	67	196
3-46	93	5	156	11		8	53	256	143	774
3-26	123	8	212	16	2	10	50	345	64	159
3-28	107	3	118	15	1	11	51	323	99	287
3-31	170	12	260	23	2	11	45	333	43	94
3-40	180	9	319	20	1	11	42	288	40	88
3-52	116	10	206	14	2	8	52	338	63	180
3-53	140	8	202	17	1	9	50	275	84	365
3-23	268	20	387	40	4	12	33	305	19	14
3-27	104	7	196	16	2	9	52	330	150	78
3-29	270	21	389	43	5	12	32	310	19	13
3-30	278	21	379	41	4	12	32	274	16	17
3-36	274	19	399	41	2	12	32	311	17	13
3-36b	271	19	385	44	4	13	34	309	21	17
3-36c	267	21	376	39	3	12	33	300	19	14

3-32	267	20	384	40	3	13	32	307	17	13
3-42	274	13	396	41	3	14	32	247	18	16
4-11	26	5	82	51	1	19	34	203	51	108
4-12	29	1	74	45	2	21	51	229	93	189
4-15	37	3	69	57	2	32	61	191	82	187
4-14	60		550	48	16	7	24	41	5	9
5-24	34	2	46	5		5	44	191	501	2027
5-25	41	3	68	20		10	44	252	132	607
5-28	35	2	48	7		6	43	200	433	1767
5-20	55	4	126	39	1	17	44	298	37	75
5-21	50	3	123	25		14	46	270	27	54
5-23	42	3	118	15		11	44	231	29	94
5-27	57	4	108	25		13	49	270	40	124
6-2	104	8	146	32	7	7	39	202	239	952
6-3	105	8	159	159	8	8	43	214	189	927
7-9	222	13	348	49	17	8	43	213	204	782
7-11	229	23	345	50	16	7	42	229	215	805
7-12	221	12	353	49	18	10	41	227	212	802
7-14	211	12	347	50	18	10	43	221	224	810
7-15		11	355	50	18	12		221	200	770
7-16	228	11	351	50	18	11	40	218	189	743
7-18	230	12	348	53	16	11	44	223	199	760
11-3	14	2	48	21		22	51	299	133	350

A3.3 **REE geochemistry**

REE in ppm

no.	La	Ce	Pr	Nd	Sm	Eu	Gd	Dy	Er	Yb
1-35	1.98	7.22	1.44	7.34	2.57	0.96	3.37	3.71	2.25	2.06
1-38	2.84	9.23	1.56	8.40	2.84	1.11	4.04	5.03	3.28	3.20
1-39	4.73	12.41	2.19	12.24	3.85	1.53	5.50	6.68	4.35	3.86
3-44	1.77	4.1		2.85	0.82		1.27	1.16	0.80	0.86
3-49	3.11	5.63	0.72	3.35	0.88	0.32	1.18	1.26	0.85	0.90
3-47	3.25	6.53	0.82	3.70	1.05	0.39	1.29	1.60	1.01	0.95
3-51	2.20	4.45	0.63	2.46	0.57	0.19	0.76	0.97	0.63	0.67
3-27	3.12	6.00	0.72	3.68	0.94	0.36	1.20	1.45	0.90	0.95
3-24	4.00	8.44	1.06	4.51	1.32	0.50	1.38	1.65	1.20	1.14
3-53	3.94	7.95	0.94	4.47	1.31	0.49	1.34	1.67	1.19	1.19
3-36	9.49	20.85	2.57	9.29	2.29	0.67	2.38	2.06	1.33	1.26
4-14	13.34	30.60	2.96	9.65	1.57	<0.24	1.32	1.07	0.52	0.37
4-12	1.73	5.24	0.86	4.46	1.53	0.57	2.54	3.20	2.04	2.31
5-25	1.51	3.34	0.55	2.72	0.89	0.36	1.27	1.62	1.10	1.14
5-27	1.91	4.43	0.76	3.56	1.24	0.59	1.90	2.46	1.78	1.78
5-20	2.82	6.44	1.01	5.17	1.72	0.62	2.37	3.10	2.15	2.07
5-24				0.90	0.28		0.59	0.77	0.46	0.66
6-3	6.53	14.74	1.73	6.36	1.30	0.45	1.35	1.27	0.63	0.58
7-18	15.98	37.72	4.48	17.29	3.23	1.02	2.68	1.84	0.93	0.79
11-3	1.08		0.64	3.48	1.57	0.62	2.74	3.76	2.50	2.37

REFERENCES

Allegre, C. J., Brevart, O., Dupre, B., & Minster, J. F., 1980. Isotope and chemical effects produced in a continuously differentiating convecting Earth Mantle. *Philos. Trans. R. Soc. Lond, Ser. A*, **297**, 447-477.

Allegre, C. J., Treuil, M., Minster, J., Minster, B., & Albarede, F., 1977. Systematic use of trace elements in igneous process. Part 1: Fractional crystallization processes in volcanic suites. *Contr. Miner. Petrol.* **60**, 57-65.

Anderson, A. T., 1974. Evidence for a picritic, volatile-rich magma beneath Mt. Shasta, California. *J. Petrol.* **15**, 243-267.

Arculus, R. J., 1981. Island arc magmatism in relation to the evolution of the crust and mantle. *Tectonophysics*, **75**, 113-133.

Arculus, R. J., & Wills, K. J. A., 1980. The petrology of plutonic blocks and inclusions from the Lesser Antilles island arc. *J. Petrol.* **21**, 743-799.

Arculus, R. J., & Johnson, R. W., 1981. Island-arc magma sources: a geochemical assessment of the roles of slab-derived components and crustal contamination. *Geochemical. Journ.* **15**, 109-133.

Arculus, R. J., & Powell, R., 1986. Source component mixing in the regions of arc magma generation. *J. Geophys. Res.* **91**, 5913-5926.

Arcyana, 1977. Rocks collected by bathyscaph and diving saucer in the FAMOUS area of the mid-Atlantic rift valley: petrological diversity and structural setting. *Deep-Sea Research*, **24**, 565-589.

Arndt, N. T., 1977. Partitioning between olivine and ultrabasic and basic komatiite liquids. Carnegie Inst. Wash. Yearb. **76**, 553-557.

Autio, L. K., & Rhodes, J. M., 1984. Costa Rica rift zone basalts: geochemical and experimental data from a possible example of multistage melting. In: Cann, J. R., Langseth, M. G., Honnorez, J., Von Herzen, R. P., & White, S. M.(ed.) *Initial Reports of the Deep Sea Drilling Project*, **69**, Washington (U.S. Government Printing Office), 729-745.

Baker, D. R., & Eggler, D. H., 1987. Compositions of anhydrous and hydrous melts coexisting with plagioclase, augite, and olivine or low-Ca pyroxene from 1atm to 8kbar: application to the Aleutian volcanic center of Atka. *Am. Mineral.* **72**, 12-28.

Barker, S. E., Kudo, A. M., & Keil, K., 1983. Mineral chemistry of basalts from Holes 483 and 483B. In: Lewis, B. T. R., Robinson, P., et al.(ed) *Initial Reports of the Deep Sea Drilling Project*, **65**, Washington (U.S. Government Printing Office), 635-642.

Barnes, S.J., 1986. The distribution of chromium among orthopyroxene, spinel and silicate liquid at atmospheric pressure. *Geochim. cosmochim. Acta*, **50**, 1889-1909.

Basaltic Volcanism Study Project, 1981. *Basaltic Volcanism on the Terrestrial Planets*. Pergamon Press.

Beccaluva, L., Maciotta, G., Savelli, C., Serri, G., & Zeda, O., 1980. Geochemistry and K/Ar ages of volcanics dredged in the Philippine Sea (Mariana, Yap, Palau Trenches and Parece Vela Basin).In: Hayes, D. E., (ed.) The Tectonic and Geologic Evolution of Southeast Asian Seas and Islands. *American Geophysical Union, Geophysical Monogram Series* **23**, 247-260.

Beets, D. J., Klaver, G. Th., Beunk, F. F., Kieft, C., & Maaskant, P., 1982. Picrites as parental magma of MORB-type tholeiites. *Nature*, **296**, 341-343.

Bence, A. E., Baylis, D. M., Bender, J. F., & Grove, T. L., 1979. Controls on the major and minor element chemistry of mid-ocean ridge basalts and glasses. In: Talwani, M., Harrison, C. G., & Hayes, D. E. (ed) *Deep Drilling Results in the Atlantic Ocean: Oceanic Crust*. Am. Geophys. Union, 331-341.

Bender, J.F., Hodges, F. N., & Bence, A. E., 1978. Petrogenesis of basalts from the project FAMOUS area: experimental study from 0-15 kbars. *Earth planet. Sci. Lett.* **41**, 277-302.

Bickle, M. J., Ford, C. E., & Nisbet, E. G., 1977. The petrogenesis of peridotitic komatiites: evidence from high-pressure melting experiments. *Earth planet. Sci. Lett.* **37**, 97-106.

Bougault, H., & Hekinian, R., 1974. Rift valley in the Atlantic ocean near $36^{\circ}50'$N: Petrology and geochemistry of basaltic rocks. *Earth planet. Sci. Lett.* **24**, 249-261.

Boyd, F. R., England, J. L., & Davis, B. T. C., 1964. Effects of pressure on the melting and polymorphism of enstatite, $MgSiO_3$. *J. Geophys. Res.* **69**, 2101-2109.

Brophy, J. G., 1986. The Cold Bay volcanic center, Aleutian volcanic arc, I. implications for the origin of high-alumina arc basalts. *Contrib. Mineral. Petrol.* **93**, 368-380.

Brophy, J. G., & Marsh, B. D., 1986. On the origin of high-alumina arc basalt and the mechanics of melt extraction. *J. Petrol.* **27**, 763-789.

Bryan, W. B., 1979a. Regional variation and petrogenesis of basalt glasses from the FAMOUS area, mid-Atlantic ridge. *J. Petrol.* **20**, 293-325.

Bryan, W. B., 1979b. Low-K_2O dacite from the Tona-Kermadec island arc: Petrography, chemistry and petrogenesis. In: Barker, F. (ed.) *Trondhjemites, Dacites, and related rocks*, 581-600.

Bryan, W. B., 1983. Systematics of modal phenocryst assemblages in submarine basalts: petrologic implications. *Contrib. Min. Petrol.* **83**, 62-74.

Bryan, W. B., & Ewart, A., 1971. Petrology and geochemistry of volcanic rocks from Tonga. *Carnegie Inst. washington Year Book*, **69**, 249-258.

Bryan, W. B., & Moore, J. G., 1977. Compositional variations of young basalts in the mid-Atlantic ridge rift valley near lat 36°49′ N. *Geol. Soc. Am. Bull.* **88**, 556-570.

Bryan, W. B., & Dick, H. J. B., 1982. Contrasted abyssal basalt liquidus trends: evidence for mantle major element heterogeneity. *Earth Planet Sci.* Lett, **58**, 15-26.

Bryan, W. B., & Thompson, G., 1977. Basalts from DSDP Leg 37 and the FAMOUS area: compositional and petrogenetic comparisons. *Can. J. Earth Sci.* **14**, 875-885.

Bryan, W. B., Stice, G. D., & Ewart, A., 1972. Geology, petrology and geochemistry of the volcanic islands of Tonga. *Journal of Geophysical Research* **77**, 1566-1585.

Bryan, W. B., Thompson, G., & Micheal, P. J., 1979. Compositional variation in a steady-state zoned magma chamber: mid-Atlantic ridge at 36°50′N. *Tectonophysics*, **55**, 63-85.

Bryan, W. B., Thompson, G., & Ludden, J. N., 1981. Compositional variation in Normal MORB from 22°-25°N: mid-Atlantic ridge and Kane Fracture Zone. *J. Geophysical Research*, **86**, 11,815-11,836.

Bryan, W. B., Thompson, G., Frey, F. A., & Dickey, J. S., 1976. Inferred geologic settings and differentiation in basalts from the Deep Sea Drilling Project. *J. Geophys. Res.* **81**, 4285-4304.

Budahn, J. R., 1986. Evidence for equilibrium conditions during the partitioning of nickel between olivine and komatiite liquids. *Am. Miner.* **71**, 1337-1342.

Cameron, W. E., 1985. Petrology and origin of primitive lavas from the Troodos ophiolite, Cyprus. *Contri. Miner. Petrol.* **89**, 239-255.

Cameron, W. E., Nisbet, E. G., & Dietrich, V. J., 1979. Boninites, komatiites and ophiolitic basalts. *Nature* **280**, 550-553.

Cameron, W. E., Mc Culloch, M. T., & Walker, D. A., 1983. Boninite petrogenesis: chemical and Nd-Sr isotopic constraints. *Earth and Planetary Science Letters* **65**, 75-89.

Carlson, R. W., Mac Dougal, J. D., & Lugmair, G. W., 1978. Differential Nd and Sm evolution in oceanic basalts. *Geophysical Research Letters*, **5**, 229-232.

Christie, D. M., & Sinton, J. M., 1986. Major element constraints on melting, differentiation and mixing of magmas from the Galapagos 95.5°W propagating rift system. *Contri. Miner. Petrol.* 94, 274-288.

Christie, D. M., Carmichael, I. S. E., & Langmuir, C. H., 1986. Oxidation states of mid-ocean ridge basalt glasses. *Earth planet. Sci. Lett.* 79, 397-411.

Clarke, D. B., & O'Hara, M. J., 1979. Nickel and the existence of high-MgO liquids in nature. *Earth planet. Sci. Lett.* 44, 153-158.

Cole, J. W., 1982. Tonga-Kermadec-New Zealnad. In: Thorpe, R. S., (ed.) *Andesites: Orogenic andesites and related rocks.* John Wiley & Sons, 245-257.

Coleman, R. G., & Donato, M. M., 1979. Oceanic plagiogranite revisited. *In* Barker F. ed. *Trondhjemites and related rocks*, pp. 78-93. Elsevier, Amsterdam.

Coulon, C., & Thorpe, R. S., 1981. Role of continental crust in petrogenesis of orogenic volcanic associations. *Tectonophysics*, 77, 79-93.

Crawford, A.J., Becculuva, L., & Serri, G., 1981. Tectono-magmatic evolution of the West Philippine-Mariana region and the origin of boninites. *Earth and Planetary Science Letters*, 54, 346-356.

Crawford, A. J., Falloon, T. J., & Eggins, S. E., 1987. The origin of island arc high-alumina basalts. *Contrib. Mineral. Petrol.* (in press)

Dallwitz, W. B., 1968. Chemical composition and genesis of clinoenstatite-bearing volcanic rocks from Cape Vogel, Papua: a discussion. *XXIII International Geological Congress*, 2, 229-242.

Deer, W. A., Howie, R. A., & Zussman, J., 1966. *An introduction to the rock forming minerals*. Longman, London, 528p.

Dick, H. J. B., & Bullen, T., 1984. Cr-spinel as a petrogenetic indicator in oceanic environments. *Contrib. Mineral. Petrol.* 86, 54-76.

Dick, H. J. B., & Fisher, R. L., 1984. Mineralogic studies of the residues of mantle melting: abyssal and alpine type-peridotites. In: Kornprobst, J.(ed.) *Kimberlites II. The mantle and crust-mantle relationships*. Amsterdam: Elsevier, 295-308.

Dietrich, V., Emmermann, R., Oberhanski, R., & Puchelt, H., 1978. Geochemistry of basaltic and gabbroic rocks from the West Mariana Basin and the Mariana Trench. *Earth and Planetary Science Letters* 39, 127-144.

Donaldson, C. H., & Brown, R. W., 1977. Refractory megacrysts and magnesium-rich melt inclusions within spinel in oceanic tholeiites: indicators of magma mixing and parental magma composition. *Earth planet. Sci. lett.* 37, 81-89.

Drake, M. J., 1976. Plagioclase-melt equilibria. *Geochim. cosmochim. acta*. **40**, 457-465.

Duncan, R. A., & Green, D. H., 1980. Role of multistage melting in the formation of oceanic crust. *Geology*, **8**, 22-26.

Duncan, R. A., & Green, D. H., 1987. The genesis of refractory melts in the formation of oceanic crust. *Contri. Miner. Petrol.* (in press).

Duncan, R. A., Pickthorn, L. G., & Vallier, T. L., 1985. Volcanic episodes at Eua, Tonga Islands. In: Vallier, T. L., & Scholl, D. W., (eds.). Geology and offshore resources of Pacific island arcs -Tonga region. *Circum-Pacific Council for Energy and Mineral Resources, Earth Science Series*, **2**, 236-245.

Dungan, M. A., & Rhodes, J. M., 1978. Residual glasses and melt inclusions in basalts from DSDP Legs 45 and 46: evidence for magma mixing. *Contrib. Mineral. Petrol.* **67**, 417-431.

Dungan, M. A., Long, P. E., & Rhodes, J. M., 1978. The petrography, mineral chemistry and one-atmosphere phase relations of basalts from site 395. In: Melson, W. G., Rabinowitz et al., (ed.) *Initial reports of the Deep Sea Drilling Project*, **45**, Washington (US Government Printing Office), 461-477.

Eissen, J. P., Bideau, D., & Juteau, T., 1981. Presence de basaltes porphyriques dans les zones de fracture de la dorsale Est Pacifique. *C. R. Acad. Sci. Paris* **293**, 61-66.

Elthon, D., 1983. Isomolar and isostructural pseudo-liquidus phase diagrams for oceanic basalts. *Am. Miner.* **68**, 506-511.

Elthon, D., 1986. Comments on "Composition and depth of origin of primary mid-ocean ridge basalts" by D. C. Presnall and J.D. Hoover. *Contr. Miner. Petrol.* **94**, 253-256.

Elthon, D., & Ridley, W. I., 1979. Comments on: 'The partitioning of Ni between olivine and silicate melt' by S. R. Hart & K. E. Davis. Earth planet. Sci. Lett. **44**, 162-164.

Elthon, D., & Scarfe, C. M., 1980. High pressure equilibria of a high-mg basalt: implications for the origin of MORB. *Carnegie Institute of Washington Yearbook*, **79**, 277-281.

Elthon, D., & Scarfe, C. M., 1984. High-pressure phase equilibria of a high-magnesia basalt and the genesis of primary oceanic basalts. *Am. Miner.* **69**, 1-15.

Elthon, D., & Casey, J. F., 1985. The very depleted nature of certain primary mid-ocean ridge basalts. *Geochim. cosmochim. Acta*, **49**, 289-298.

Elthon, D., Casey, J. F., & Komor, S., 1982. Mineral chemistry of ultramafic cumulates from the North Arm Mountain Massif of the Bay of

Islands ophiolite: evidence for high pressure crystal fractionation of oceanic basalts. *J. Geophy. Res.* **87**, 8717-8734.

Ewart, A., 1976. A petrological study of the younger Tongan andesites and dacites, and the olivine tholeiites of Niua Fo'ou Island, s.w. Pacific. *Contributions to Mineralogy and Petrology* **58**, 1-21.

Ewart, A., & Bryan, W. B., 1972. Petrography and geochemistry of the igneous rocks from Eua, Tongan Islands. *Geological Society of America Bulletin* **83**, 3281-3298.

Ewart, A., & Hawkesworth, C. J., 1987. The Pleistocene-Recent Tonga-Kermadec arc lavas. Interpretation of new isotopic and rare earth data in terms of a depleted mantle source model. *J. Petrol.* **28**, 495-530.

Ewart, A., Bryan, W. B., & Gill, J. B., 1973. Mineralogy and geochemistry of the younger volcanic islands of Tonga, s.w. Pacific. *Journal of Petrology* **14**, 429-465.

Ewart, A., Brothers, R. N., & Mateen, A., 1977. An outline of the geology and geochemistry, and the possible petrogenetic evolution of the volcanic rocks of the Tonga-Kermadec-New Zealand island arc. *Journal Volcanology and Geothermal Research* **2**, 205-250.

Falloon, T. J., 1985. Preliminary petrography and geochemistry of igneous rocks from the northern Tonga ridge and adjacent Lau Basin. In: Honza E., Lewis K.B. & Shipboard Party. A Marine Geological and Geophysical Survey of the Northern Tonga Ridge and Adjacent Lau Basin. *Natural Resources of Tonga Field Report* **1**, 63-71.

Falloon, T. J., Green, D. H., Hatton, C. J., & Harris, K. L., 1987. The anhydrous partial melting of a fertile and depleted peridotite from 2-30kbar. *J. Petrol.* (submitted).

Fisk, M. K., 1984. Depths and temperature of mid-ocean ridge magma chambers and the composition of their source magmas. In: Gass, I. G., Lippard, S.J., & Shelton, A.W.(ed.) *Ophiolites and oceanic lithosphere*. Oxford: Blackwell Scientific Publications, 17-23.

Foley, S. F., 1986. The origin of ultrapotassic rocks. Ph.D thesis, University of Tasmania, Hobart.

Foley, S. F., & Wheller, G. E., 1987. Titanium-rich phase saturation at high pressures and the origin of the geochemical signatures of island-arc volcanics and mantle enrichment events. (unpubl. manuscript).

Foley, S. F., Venturelli, G., Green, D. H., & Toscani, L., 1987. The ultrapotassic rocks: characteristics, classification and constraints for petrogenetic models. *Earth Sci, Reviews*, **24**, 81-134.

Flower, M. F. J., & Robinson, P. T., 1979. Evolution of the FAMOUS ocean ridge segment: evidence from submersible and deep-sea drilling investigations. In: Talwani, M., Harrison, G. C., & Hayes, D. E.,

Francis, D., 1985. The Baffin Bay lavas and the value of picrites as analogues of primary magmas. *Contrib. Miner. Petrol.* **89**, 144-154.

Francis, D., 1986. The pyroxene paradox in MORB glasses- a signature of picritic parental magmas? *Nature*, **319**, 586-588.

Frey, F. A., & Green, D. H., 1974. The mineralogy, geochemistry and origin of lherzolite inclusions in Victorian basanites. *Geochim. Cosmochim. Acta*, **38**, 1023-1059.

Frey, F. A., Bryan, W. B., & Thompson, G., 1974. Atlantic Ocean Floor: Geochemistry and Petrology of basalts from Legs 2 and 3 of the DSDP. *J. Geophys. Res.* **79**, 5507-5527.

Frey, F. A., Suen, C. J., & Stockman, H. W., 1985. The Ronda high temperature peridotite: Geochemistry and petrogenesis. *Geochim. cosmochim. Acta*, **49**, 2469-2491.

Frey, F. A., Bryan, W.B., Thompson, G., & Roy, S., 1973. Petrological and Geochemical results for basalts from DSDP Legs 2 and 3. *EOS Trans. AGU*, **54**, 1004-1006.

Fujii, T., & Fujioka, K., 1978. Petrology of dolerites, hole 395A. In: Melson, W. G., Rabinowitz, P. D., et al., (ed) *Initial Reports of the Deep Sea Drilling Project*, **45**, Washington (U. S. Government printing office), 519-528.

Fujii, T., & Bougault, H., 1983. Melting relations of a magnesian abyssal tholeiite and the origin of MORBs. *Earth planet. Sci. Lett.* **62**, 283-295.

Fujii, T., & Kushiro, I., 1977. Melting relations and viscosity of an abyssal tholeiite. *Yb. Carnegie Instn. Wash.* **76**, 461-465.

Fujii, T., & Scarfe, C. M., 1985. Composition of liquids coexisting with spinel lherzolite at 10kbar and the genesis of MORBs. *Earth planet. Sci. Lett.* **90**, 18-28.

Fujii, T., Kushiro, I., & Hamuro, K., 1978. Melting relations and viscosity of an abyssal olivine tholeiite. In: Melson, W. G., Rabinowitz, P. D., et al. (ed) *Initial Reports of the Deep Sea Drilling Project*, **45**, Washington (U.S. Government Printing Office), 513-517.

Fukuyama, H., & Hamuro, K., 1978. Melting relations of Leg 46 basalts at atmospheric pressure. In: Dmitiriev, L., Heirtzler, J., et al., (ed.) *Initial reports of the Deep Sea Drilling Project*, **46**, Washington (US Government Printing Office), 215-226.

Gast, P. W., 1968. Trace element fractionation and the origin of tholeiitic and alkaline magma types. *Geochimica et Cosmochimica Acta* **32**, 1057-1086.

Giardini, D., & Woodhouse, J. H., 1986. Horizontal shear flow in the mantle beneath the Tonga arc. *Nature* **319**, 551-555

Gill, J. B., 1970. Geochemistry of Viti Levu, Fiji, and its evolution as an island arc. *Contributions to Mineralogy and Petrology* **27**, 179-203.

Gill, J. B., 1976. Composition and age of Lau Basin and Ridge volcanic rocks: Implications for evolution of an interarc basin and remnant arc. *Geological Society of America Bulletin* **87**, 1384-1395.

Gill, J. B., 1981. *Orogenic andesites and plate tectonics*. Springer-Verlag, New York, 385 pp.

Gill, J. B., 1984. Sr-Pb-Nd isotopic evidence that both MORB and OIB sources contribute to oceanic island arc magmas in Fiji. *Earth and Planetary Science Letters* **68**, 443-458.

Gill, J. B., Stork, A. L., & Whelan, P. M., 1984. Volcanism accompanying back-arc basin development in the southwest Pacific. *Tectonophysics* **102**, 207-224.

Green, D. H., 1970. The origin of basaltic and nephelinitic magmas. *Trans. Leicester lit. phil. society*, **64**, 28-54.

Green, D. H., 1971. Composition of basaltic magmas as indicators of conditions of origin: application to oceanic volcanism. *Phil. Trans. Roy. Soc. Lond.* **268**, 707-725.

Green, D.H., 1973. Experimental melting studies on a model upper mantle composition at high pressure under water-saturated and water-undersaturated conditions. *Earth planet. Sci. Lett.* **19**, 37-53.

Green, D. H., 1976. Experimental testing of "equilibrium" partial melting of peridotite under water-saturated, high-pressure conditions. *Canadian Mineralogists*, **14**, 255-268.

Green, D. H., & Ringwood, A. E., 1967. The genesis of basaltic magmas. *Contri. Miner. Petrol.* **15**, 103-190.

Green, D. H., Hibberson, W.O., & Jaques, A. L., 1979: Petrogenesis of mid-ocean ridge basalts. In: Mc Elhinney, M. W. (ed.) *The Earth: Its origin structure and evolution*. London: Academic Press, 265-299.

Green, D. H., Falloon., & Taylor, W. R., 1987. Mantle derived magmas-role of variable source peridotite and variable C-H-O fluid compositions. In: Mysen, B. O.(ed.) *Magmatic Processes: Physiochemical Principles. The Geochemical Society Spec. Publ.* **1**, 139-154.

Green, D. H., Ringwood, A. E., Ware, N. G., & Hibberson, W. O., 1972. Experimental petrology and petrogenesis of Apollo 14 basalts. *Proceedings third lunar sci. conf.* **1**, 197-206.

Griffin, B. J., & Varne, R., 1980. The Macquarie Island ophiolite complex: mid-tertiary oceanic lithosphere from a major ocean basin. *Chem. Geol.* **30**, 285-308.

Grove, T. L., & Bryan, W. B., 1983. Fractionation of pyroxene-phyric MORB at low pressure: An experimental study. *Contri. Miner. Petrol.* **84**, 293-309.

Grove, T. L., & Kinzler, R. J., 1986: Petrogenesis of andesites. *Ann. Rev. Earth Planet. Sci.* **14**, 417-454.

Grove, T. L., Gerlach, D. C., & Sando, T. W., 1982. Origin of Calc-Alkaline Series Lavas at Medicine Lake Volcano by fractionation, assimilation and mixing. *Contri. Miner. Petrol.* **80**, 160-182.

Hart, S. R., 1984. A large scale isotope anomaly in the southern hemisphere mantle. *Nature*, **309**, 753-757.

Hart, S. R., & Davis, K. E., 1978. Nickel partitioning between olivine and silicate melt. *Earth planet. Sci. Lett.* **40**, 203-219.

Hawkins, J. W., 1976. Petrology and geochemistry of basaltic rocks of the Lau Basin. *Earth and Planetary Science Letters* **28**, 283-297.

Hawkins, J. W., & Melchior, J. T., 1985. Petrology of Mariana Trough and Lau Basin Basalts. *J. Geophys. Res.* **90**, 11,431-11,468.

Hawkins, J. W., & Falvey, D. A., 1985. Petrology of andesitic dikes and flows from Eua, Tonga. In Vallier, T. L., & Scholl, D. W., (eds.) Geology and offshore resources of Pacific island arcs -Tonga region. *Circum-Pacific Council for Energy and Mineral Resources, Earth Science Series*, 2, 269-279.

Hawkins, J. W., Bloomer, S. H., Evans, C. A., & Melchior, J. T., 1984. Evolution of intra-oceanic arc-trench systems. *Tectonophysics* **102**, 175-205.

Hekinian, R., Moore, J. G., & Bryan, W. B., 1976. Volcanic rocks and processes of the mid-Atlantic ridge rift valley near 36°49′ N. *Contri. Miner. Petrol.* **58**, 83-110.

Hickey, R. L., & Frey, F. A., 1982. Geochemical characteristics of boninite series volcanics: implications for their source. *Geochimica et cosmochimica acta* **46**, 2099-2115.

Hole, M. J., Saunders, A. D., Marriner, G. F., & Tarney, J., 1984. Subduction of pelagic sediments: implications for the origin of Ce-anomalous basalts from the Mariana Islands. *J. Geol Soc. Lond.* **141**, 453-472.

Honza, E., Lewis, K. B., & Shipboard Party, 1985. A Marine Geological and Geophysical Survey of the Northern Tonga Ridge and adjacent Lau Basin. *Natural Resources of Tonga, Field Report* **1**.

Huppert, H. E., & Sparks, R. S. J., 1980. The fluid dynamics of a basaltic magma chamber replenished by influx of hot, dense ultrabasic magma. *Contrib. Mineral. Petrol.* **75**, 279-289.

Ito, E., White, W. M., Drach, V., Hofmann, A. W., & James, D. E., 1981. Isotopic studies of ocean ridge basalts. *C. I. W. Yb.* 80, 465-471.

Jagoutz, E., Palme, H., Baddenhausen, H., Blum, K., Cendales, M., Dreibus, G., Spettel, B., Lorenz, V., & Wanke, H., 1979. The abundance of major, minor and trace elements in the earth's mantle as derived from primitive ultramafic nodules. *Proc. lunar planet. Sci. Conf. 10th, Geochim. Cosmochim. Acta, Supplement* 11, 2031-2050.

Jaques, A. L., 1980. Petrologic and experimental studies on the petrogenesis of Papua New Guinea ophiolites. Ph.D Thesis, University of Tasmania, Hobart, Tasmania.

Jaques, A. L., & Green, D. H., 1979. Determination of liquid compositions in high-pressure melting of peridotite. *Am. Miner.* 64, 1312-1321.

Jaques, A. L., & Chappell, B. W., 1980. Petrology and trace element geochemistry of the Papuan ultramafic belt. *Contrib. Mineral. Petrol.* 75, 55-70.

Jaques, A. L., & Green, D. H., 1980:.Anhydrous melting of peridotite at 0-15kbar pressure and the Genesis of Tholeiitic basalts. *Contri. Miner. Petrol.* 73, 287-310.

Jaques, A. L., Lewis, J. D., Smith, C. B., Gregory, G. P., Ferguson, J., Chappell, B. W., & Mc Culloch, M. T., 1984. The diamond bearing ultrapotassic (lamproitic) rocks of the west Kimberley region, western Australia. In: Kornprobst, J., (ed) *Kimberlites I: Kimberlites and related rocks*, 225-254.

Jenner, G., 1981. Geochemistry of high-Mg andesites from Cape Vogel Papua New Guinea. *Chemical Geology* 33, 307-332.

Jenner, G. A., 1983. Petrogenesis of high-mg andesites: an experimental and geochemical study with emphasis on high-mg andesites from Cape Vogel, PNG. Ph.D thesis, University of Tasmania, Hobart.

Jenner, G. A., Cawood, P. A., Rautenschlein, M., & White, W. M., 1987. Composition of back-arc volcanics, Valu Fa ridge, Lau Basin: evidence for a slab-derived component in their mantle source. *Geochim Cosmochim. Acta*, (in press).

Johnston, A. D., 1986. Anhydrous P-T phase relations of near-primary high alumina basalt from the South Sandwich Islands. implications for the origin of island arcs and tonalite-trondhjemite series rocks. *Contrib. Mineral. Petrol.* 92, 368-382.

Johnson, K. T. M., 1985. Major, trace and rare earth element abundances in boninitic lavas from the Ogasawara forearc. *Journal faculty of science Hokkaido University* 21, 453-463.

Johnson, R. W., Jaques, A. L., Hickey, R. L., McKee, C. O., & Chappell B. W., 1985. Manam Island, Papua New Guinea: petrology and geochemistry

of a low-TiO_2 basaltic island arc volcano. *Journal of Petrology* **26**, 283-323.

Kay, R. W., 1980. Volcanic arc magmas: implications of a melting-mixing model for element recycling in the crust-upper mantle system. *J. Geol.* **88**, 497-522.

Keays, R. R., & Scott, R. B., 1976. Precious metals in ocean ridge basalts: implications for basalts as source rocks for Gold mineralization. *Econ. Geol.* **71**, 705-720.

Kitekei'aho, T., Tappin, D., Honza, E., Okuda, Y., Miyazaki, T., Yokokura, T., & Lewis, K. B., 1985. Seismic profiles from Northern Tonga. In Honza, E., Lewis, K. B., & Shipboard Party. A Marine Geological and Geophysical Survey of the Northern Tonga Ridge and Adjacent Lau Basin. *Natural Resources of Tonga Field Report* **1**, 31-35.

Klein, E. M., & Langmuir, C. H., 1987. Ocean ridge basalt chemistry, axial depth, crustal thickness and temperature variations in the mantle. *J. Geophysical Research* (in press).

Komatsu, M., 1980. Clinoenstatite in volcanic rocks from the Bonin Islands. *Contributions to Mineralogy and Petrology* **74**, 329-338.

Kushiro, I., 1973. Origin of some magmas in oceanic and circum-oceanic regions. *Tectonophysics*, **17**, 211-222.

Kushiro, I., 1975. On the nature of silicate melt and its significance in magma genesis: regularities in the shift of the liquidus boundaries involving olivine, pyroxene and silica minerals. *Am. J. Sci.* **275**, 411-431.

Kushiro, I., & Thompson, R. N., 1972. Origin of some abyssal tholeiites from the mid-Atlantic ridge. *Carnegie Inst. Washington Yearb.* **71**, 403-406.

Langmuir, C. H., & Hanson, G. N., 1980. An evaluation of major element heterogeneity in the mantle sources of basalts. *Phil. Trans. R. Soc. Lond.* **297**, 383-407.

Langmuir, C. H., Bender, J. F., Bence, A. E., & Hanson, G. N., 1977. Petrogenesis of basalts from the FAMOUS area: Mid-Atlantic ridge. *Earth planet. Sci. lett.* **36**, 133-156.

Leeman, W. P., 1983. The influence of crustal structure on compositions of subduction-related magmas. *J. Volcanol. Geotherm. Res.* **18**, 561-588.

Leitch, E. C., 1984. Island arc elements and arc-related ophiolites. *Tectonophysics*, **106**, 177-203.

Le Roex, A. P., Erlank, A. J., & Needham, H. D., 1981. Geochemical and Mineralogical evidence for the occurrence of at least three distinct magma types in the FAMOUS region. *Contrib. Miner. Petrol.* **77**, 24-37.

Le Roex, A. P., Dick, H. J. B., Reid, A. M., Frey, F. A., Erlank, A. J., & Hart, S. R., 1985. Petrology and geochemistry of basalts from the American-Antarctic Ridge, Southern Ocean: implications for the westward influence of the Bouvet mantle plume. *Contrib. Mineral. Petrol.* **90**, 367-380.

Maaloe, S., & Hansen, B., 1982. Olivine phenocrysts of Hawaiian olivine tholeiite and oceanite. *Contrib. Miner. Petrol.* **81**, 203-211.

Maaloe, S., & Aoki, K., 1977. The major element composition of the upper mantle estimated from the compositon of lherzolites. *Contri. Miner. Petrol.* **63**, 161-173.

Mac Dougall, J. D., & Lugmair, G. W., 1985. Extreme isotopic homogeneity among basalts from the southern east Pacific rise. mantle or mixing effect. *Nature*, **313**, 209-211.

Marsh, B. D., 1979. Island arc development: some observations, experiments and speculations. *J. Geol.* **87**, 687-713.

Marsh, B. D., 1982. The Aleutians. In: Thorpe, R. S., (ed) *Andesites*, New York, Wiley, 99-114.

Mao, H. K., & Bell, P. M., 1971. Behaviour of thermocouples in the single-stage piston-cylinder apparatus. *Carnegie Inst. Wash. Year Book*, **69**, 207-216.

Mao, H. K., Bell, P. M., & England, J. L., 1971. Tensional errors and drift of thermocouple electromotive force in the single-stage piston-cylinder apparatus. *Carnegie Inst. Wash. Year Book*, **70**, 281-287.

Mc Culloch, M. T., & Perfit, M. R., 1981. $^{143}Nd/^{144}Nd$, $^{87}Sr/^{86}Sr$ and trace element constraints on the petrogenesis of Aleutian Island arc magmas. *Earth Planet. Sci. Lett.* **56**, 167-179.

Mc Kenzie, D., 1984. The generation and compaction of partially molten rock. *J. Petrology*, **25**, 713-765.

Meijer, A., 1980. Primitive arc volcanism and a Boninite Series: examples from Western Pacific island arcs. In Hayes D. ed. The Tectonic and Geologic Evolution of Southeast Asian Seas and Islands. *AGU Geopysical Monogram* **23**, 269.

Melson, W. G., 1973. Basaltic glasses from the Deep Sea Drilling Project: Chemical characteristics, compositions of alteration products, and fission track 'ages', *EOS*, **54**, 1011.

Melson, W. G., & O'Hearn, T., 1979. Basaltic glass erupted along the mid-Atlantic ridge between 0-37°N: Relationships between composition and latitude. In: Talwani, M., Hay, W., Ryan, W. B. F. (ed) *Deep Sea Drilling Results in the Atlantic Ocean: Ocean Crust*. Am. Geophys. Union, Maurice Ewing ser. 2, 273-284.

Melson, W. G., Jarosewich, E., & Lundquist, C. A., 1970. Volcanic eruption at Metis Shoal, Tonga, 1967-68: description and petrology. *Smithsonian Contributions to the Earth Sciences* **4**, 1-17.

Melson, W. G., Vallier, T., Wright, T. L., Byerly, G., & Nelen, J., 1976. Chemical diversity of abyssal volcanic glass erupted along Pacific, Atlantic, and Indian Ocean sea-floor spreading centers. *AGU Geophys. Mon.* **19**, 351-368.

Melson, W. G., Byerly, G. R., Nelen, J. A., O'Hearn, T., Wright, T. L., & Vallier, T., 1977. A catalog of the major element chemistry of abyssal volcanic glasses. *Smithsonian Contri. Earth Sci.* **19**, 31-60.

Merrill, R. B., & Wyllie, P. J., 1973. Absorption of iron by platinum capsules in high pressure rock melting experiments. *Am. Miner.* **58**, 16-20.

Miyashiro, A., 1974. Volcanic rock series in island arcs and active continental margins. *American Journal of Science* **274**, 321-355.

Morris, J. D., & Hart, S. R., 1983. Isotopic and incompatible element constraints on the genesis of island arc volcanics from Cold Bay and Amak Island, Aleutians, and implications for mantle structure. *Geochim. Cosmochim. Acta*, **47**, 2015-2030.

Morrison, M. A., & Thompson, R. N., 1983. Alteration of basalt: Deep sea drilling project Legs 64 and 65. In: Lewis, B. T., et al. (ed.), *Initial Reports of the Deep Sea Drilling Project*, **65**, U. S. Government Printing Office, Washington, D. C., 643-6600.

Murck, B. W., & Campbell, I. H., 1986. The effects of temperature, oxygen fugacity and melt composition on the behaviour of chromium in basic and ultrabasic melts. *Geochim. cosmochim. Acta*, **50**, 1871-1887.

Myers, J. D., Marsh, B. D., & Sinha, A. K., 1986a. Geochemical and strontium isotopic characteristics of parental Aleutian arc magmas: evidence from the basaltic lavas of Atka. *Contrib. Mineral. Petrol.* **94**, 1-11.

Myers, J. D., Frost, C. D., & Angevine, C. L., 1986b. A test of a quartz eclogite source for parental Aleutian magmas: a mass balance approach. *J. Geol.* **94**, 811-828.

Nabelek, P. I., & Langmuir, C. H., 1986. The significance of unusual zoning in olivines from FAMOUS area basalt 527-1-1. *Contrib. Miner. Petrol.* **93**, 1-8.

Natland, J. H., Adamson, A. C., Laverne, C., Melson, W.G., & O'Hearn, T., 1984.A compositionally nearly steady-state magma chamber at the Costa Rica Rift: Evidence from basalt glass and mineral data, deep sea drilling project sites 501, 504 and 505. In: Cann, J. R., Langseth, M. G., Honnorez, J., Von Herzen, R. P., & White, S. M., et al.(ed.)

Natland, J.H., & Melson, W. G., 1980. Compositions of basaltic glasses from the East Pacific Rise and Siqueiros fracture zone, near 9°N. In: Rosendahl, B. R., Hekinian, R., et al. (ed) I.R.O.S.O.P., 54, 705-723.

Initial Reports of the Deep Sea Drilling Project, **69**, Washington (U.S. Government Printing Office), 811-858.

Nehru, C. E., & Wyllie, P. J., 1975. Compositions of glasses from St. Pauls peridotite partially melted at 20kbar. *J. Geol.* **83**, 455-471.

Nelson, D. R., Crawford, A. J., & Mc Culloch, M. T., 1984. Nd-Sr isotopic and geochemical systematics in Cambrian boninites and tholeiites from Victoria, Australia. *Contrib. Mineral. Petrol.* **88**, 164-172.

Newsom, H. E., White, W. M., Jochum, K. P., & Hofmann, A. W., 1986. Siderophile and chalcophile element abundances in oceanic basalts, Pb isotope evolution and growth of the Earth's core. *Earth planet. Sci. Lett.* **80**, 299-313.

Nickel, K. G., & Green, D. H., 1984: The nature of the upper-most mantle beneath Victoria, Australia as deduced from ultramafic xenoliths. In: Kornprobst, J. (ed.) *Kimberlites II. The mantle and crust-mantle relationships*. Amsterdam: Elsevier, 161-178.

Norrish, K., & Hutton, J. T., 1969. An accurate X-ray spectrographic method for the analysis of a wide range of geologic samples. *Geochimica et cosmochimica acta* **33**, 431-451.

O'Donnell, T. H., & Presnall, D. C., 1980. Chemical variations of the glass and mineral phases in basalts dredged from 25°-30°N along the mid-Atlantic ridge. *Am. J. Sci.* **280**, 845-868.

O'Hara, M. J., 1965. Primary magmas and the origin of basalts. *Scot. J. Geol.* **1**, 19-40.

O'Hara, M. J., 1968. Are ocean floor basalts primary magma? *Nature*, **220**, 683-686.

O'Hara, M. J., & Humphreys, D. J., 1977. Problems of iron gain and loss during experimentation on natural rocks: The experimental crystallization of five lunar basalts at low pressure. *Phil. Trans. R. Soc. Lond.* **286**, 313-330.

O'Hara, M. J., & Mathews, R. E., 1981. Geochemical evolution in an advancing, periodically replenished, periodically tapped, continuously fractionated magma chamber. *J. Geol. Soc. Lond.* **138**, 237-277.

Palacz, Z. A., & Saunders, A. D., 1986. Coupled trace element and isotope enrichment in the Cook-Austral-Samoa islands, southwest Pacific. *Earth Planet. Sci. Lett.* **79**, 270-280.

Presnall, D. C., & Hoover, J. D., 1984. Composition and depth of origin of primary mid-ocean ridge basalts. *Contri. Miner. Petrol.* **87**, 170-178.

Presnall, D. C., & Hoover, J. D., 1986. Composition and depth of origin of primary mid-ocean ridge basalts-reply to D. Elthon. *Contri. Miner. Petrol.* **94**, 257-261.

Presnall, D. C., Brenner, N. L., & O'Donnell, T. H., 1973. Drift of $Pt/Pt_{90}Rh_{10}$ and $W_3Re_{97}/W_{25}Re_{75}$ thermocouples in single stage piston-cylinder apparatus. *Am. Miner.* **58**, 771-77.

Presnall, D. C., Dixon, J. R., O'Donnell, T. H., & Dixon, S. A., 1979. Generation of mid-ocean ridge tholeiites. *J. Petrol.* 20, 3-35.

Price, R. C., Kennedy, A. K., Riggs-Sneeringer, M., & Frey, F. A., 1986. Geochemistry of basalts from the Indian Ocean triple junction: implications for the generation and evolution of Indian Ocean ridge basalts. *Earth planet. Sci. Lett.* **78**, 379-396.

Ramsay, W. R. H., Crawford, A. J., Foden, J. D., 1984. Field setting, mineralogy, chemistry and genesis of arc picrites, New Georgia, Solomon Islands. *Contrib. Miner. Petrol.* **88**, 386-402.

Robinson, P., Higgins, N. C., & Jenner, G. A., 1986. Determination of rare-earth elements, Yttrium and Scandium in rocks by an ion exchange x-ray fluorescence technique. *Chemical Geology* **55**, 121-137.

Roeder, P. L., & Emslie, R. F., 1970. Olivine-liquid equilibrium. *Contri. Miner. Petrol.* **29**, 275-289.

Sato, H., 1977. Nickel content of basaltic magmas: identification of primary magmas and a measure of the degree of olivine fractionation. *Lithos*, **10**, 113-120.

Scarfe, C. M., & Smith, D. G. W., 1977. Secondary minerals in some basaltic rocks from DSDP Leg 37. *Can. J. Earth Sci.* **14**, 903-910.

Schilling, J. -G., Zajac, M., Evans, R., Johnston, T., White, W., Devine, J. D., & Kingsley, R., 1983. Petrologic and geochemical variations along the mid-Atlantic ridge form $29^{\circ}N$ to $73^{\circ}N$. *Am. J. Sci.* **283**, 510-586.

Schrader, E. L., Rosendahl, B. R., & Furbish, W. R., 1979. Picrites from the east Pacific rise. *Oceanologica Acta*, **2**, 339-347.

Sekine, T., Katsura, T., & Aramaki, S., 1979. Water saturated phase relations of some andesites with application to the estimation of the initial temperature and water pressure at the time of eruption. *Geochim cosmochim. act.* **43**, 1367-1376.

Sen, G., 1982. Composition of basaltic liquids generated from a partially depleted lherzolite at 9kbar pressure. *Nature*, **299**, 336-338.

Sharaskin, A. Y., Dobretsov N. L., & Sobolev, N. V., 1980. Marianities: the clinoenstatite bearing pillow-lavas associated with the ophiolite assemblage of Mariana Trench. In Panayiotou, A., (ed.) *Ophiolites, Proceedings International Ophiolite Symposium Cyprus 1980*, pp.473. Ministry of Agricultural and Natural Resources, Nicosia.

Sharaskin, A. Y., Putchin, I. K., Zlobin, S. K., & Kolesov, G. M., 1983. Two ophiolite sequences from the basement of the Northern Tonga Arc. *Ofioliti* 8, 411-438.

Shibata, T., & Thompson, G., 1986. Peridotites from the mid-Atlantic ridge at 43°N and their petrogenetic relation to abyssal tholeiites. *Contri. Miner. Petrol.* 93, 144-159.

Shibata, T., DeLong, S. E., & Walker, D., 1979. Abyssal tholeiites from the oceanographer fracture zone. I. Petrology and fractionation. *Contri. Miner. Petrol.* 70, 89-102.

Shipboard Scientific Party, 1977. *Initial Reports of the Deep Sea Drilling Project*, 37, Washington (U.S. Government Printing Office), 15-326.

Sigurdsson, H., 1981. First-order major element variation in basalt glasses from the mid-Atlantic ridge 29°N to 73°N. *J. Geophys. Res.* 86, 9483-9502.

Sinton, J. M., Price, R. C., Johnson, K. T. M., Staudigel, H., & Zindler, A., 1987. Petrology and geochemistry of submarine lavas from the Lau and north Fiji back-arc basins. *Circum-Pacific Council for Energy and Mineral Resources, Earth Science Series*, (in press).

Sparks, R. S. J., Sigurdsson, H., & Wilson, L., 1977. Magma mixing: a mechanism for triggering acid explosive eruptions. *Nature*, 267, 315-318.

Sparks, R. S. J., Meyer, P., & Sigurdsson, H., 1980. Density variation amongst mid-ocean ridge basalts: implications for magma mixing and the scarcity of primitive lavas. *Earth planet. Sci. Lett.* 46, 419-430.

Stakes, D. S., Shervais, J. W., & Hopson, C. A., 1984. The volcanic-tectonic cycle of the FAMOUS and AMAR valleys, mid-Atlantic Ridge (36°47'N): Evidence from basalt glass and phenocryst compositional variations for a steady state magma chamber beneath the valley midsections, AMAR 3. *J. Geophys. Res.* 89, 6995-7028.

Staudigel, H., & Bryan, W. B., 1981. Contrasted glass-whole rock compositions and phenocryst re-distribution, IPOD sites 417 and 418. *Contrib. Mineral. Petrol.* 78, 255-262.

Stern, R. J., 1981. A common mantle source for western Pacific island arc and 'Hot-spot' magmas-implications for layering in the upper mantle. *C. I. W. Yb.* 80, 455-462.

Stern, C. R., & Wyllie, P. J., 1975. Effect of iron absorption by noble-metal capsules on phase boundaries in rock melting experiments at 30kbar. *Am. Mineral.* 60, 681-689.

Stille, P., Unruh, D. M., & Tatsumoto, M., 1983. Pb, Sr, Nd, and Hf isotopic evidence of multiple sources for Oahu, Hawaii basalts. *Nature*, 304, 25-29.

Stolper, E., 1980. A phase diagram for mid-ocean ridge basalts: preliminary results and implications for petrogenesis. *Contri. Miner. Petrol.* **74**, 13-27.

Stolper, E., Walker, D., 1980. Melt density and the average composition of basalt. *Contrib. Mineral. Petrol.* **74**, 7-12.

Stolz, A. J., Varne, R., Wheller, G. E., Foden, J. D., & Abbott, M. J., 1987. The geochemistry and petrogenesis of K-rich alkaline volcanics from the Batu Tara Volcano, eastern Sunda arc. *Contrib. Mineral. Petrol.* (submitted).

Sun, S. -S., 1980. Lead isotopic study of young volcanic rocks from mid-ocean ridges, ocean islands and island arcs. *Phil. Trans. R. Soc. London. Ser. A*, **297**, 409-445.

Sun, S. -S., & Nesbitt, R. W., 1978. Geochemical regularities and genetic significance of ophiolite basalts. *Geology*, **6**, 689-693.

Sun, S. -S., Nesbitt, R. W., & Sharaskin, A. Ya., 1979. Geochemical characteristics of mid-ocean ridge basalts. *Earth planet. Sci. Lett.* **44**, 119-138.

Takahashi, E., 1980. Olivine/liquid nickel partitioning at high pressures: experiments with an olivine capsule. *EOS*, **61**, 397.

Takahashi, E., 1986. Melting of a dry peridotite KLB-1 up to 14 Gpa: Implications on the origin of peridotitic upper mantle. *J. Geophys. Res.* **91**, 9367-9382.

Takahashi, E., & Kushiro, I., 1983. Melting of a dry peridotite at high pressures and basalt magma genesis. *Am. Min.* **68**, 859-879.

Takahashi, E., Uto, K., & Schilling, J.-G., 1987. Primary magma compositions and Mg/Fe ratios of their mantle residue along Mid Atlantic Ridge 29°N to 73°N. *Nature* (submitted).

Tatsumi, Y., Hamilton, D. L., & Nesbitt, R. W., 1984. Transport of incompatible elements associated with the dehydration of serpentine in a down-going slab. *National Energy and Research Council*, **25**, 6-12.

Taylor, W. R., 1985. The role of C-O-H fluids in upper mantle processes-a theoretical, experimental and spectrographic study. Unpubl. Ph.D. Thesis, University of Tasmania, Hobart, Tasmania, 358.

Taylor, W. R., & Green, D. H., 1987. The role of reduced C-O-H fluids in mantle partial melting. *Proc. 4th Int. Kimberlite Conf., Geol. Soc. Aust. Special Publ.* **1** (in press).

Thompson, R. N., 1980. Major-element chemistry of basaltic glasses in hole 418A lavas and a dyke: deep sea drilling project Legs 52 and 53. In: Donnelly, T., et al. (ed) *Initial Reports of the Deep Sea Drilling Project*, **51**, Washington (U. S. Government printing office), 973-976.

Thompson, R. N., 1984. Dispatches from the basalt front. I. Experiments. *Proc. Geol. Assoc.*, **95**, 249-262.

Thompson, R. N., Morrison, M. A., Dickin A. P., & Hendry, G. L., 1983. Continental flood basalts...arachnids rule oK?. In Hawkesworth, C. J. & Norry, M. J. (ed.) *Continental Basalts and Mantle Xenoliths*, pp. 158-185, Shiva Geology Series, Cheshire.

Thompson, R. N., 1987. Phase-equilibria constraints on the genesis and magmatic evolution of oceanic basalts. *Earth Science Reviews* (in press).

Thompson, R. N., & Humphris, S. E., 1980. Silicate mineralogy of basalts from the East Pacific Rise, OCP Ridge and Siqueiros fracture zone: Deep Sea Drilling Project Leg 54. In: Rosendahl, B. R., et al. (ed.), Initial Reports of the Deep Sea Drilling Project, **54**, *U.S. Government Printing Office, Washington, D. C.*, 651-669.

Thompson, R. N., Morrison, M. A., Hendry, G. L., & Parry, S. J., 1984. An assesment of the relative roles of crust and mantle in magma genesis: an elemental approach. *Phil. Trans. R. Soc. Lond.*, **A310**, 549-590.

Umino, S., 1986. Magma mixing in boninite sequence of Chichijima, Bonin islands. *J. Volc. Geotherm. Res.* **29**, 125-157.

Varne, R., 1985. Ancient subcontinental mantle: a source for K-rich orogenic volcanics. *Geology*, **13**, 405-408.

Varne, R., & Foden, J. D., 1985. Geochemical and isotopic systematics of eastern sunda arc volcanics: implications for mantle sources and mantle mixing processes. In: Wezel, F. -C., (ed) *The origin of arcs*, Elsevier, 159-189.

Von Drach, V., Marsh, B. D., & Wasserburg, G. J., 1986. Nd and Sr isotopes in the Aleutians: multicomponent parenthood of island-arc magmas. *Contrib. Mineral. Petrol.* **92**, 13-34.

Walker, D., Shibata, T., & DeLong, S. E., 1979. Abyssal tholeiites from the oceanographer fracture zone. II. Phase equilbria and mixing. *Contri. Miner. Petrol.* **70**, 111-125.

Walker, D. A., & Cameron, W. E., 1983. Boninite primary magmas: evidence from the Cape Vogel peninsula, PNG. *Contributions to Mineralogy and Petrology* **83**, 150-158.

Watson, B. E., 1976. Glass inclusions as samples of early magmatic liquid: determinative method and application to a south Atlantic basalts. *J. Volc. Geoth. Res.* **1**, 73-84.

Wheller, G. E., Varne, R., Foden, J. D., & Abbott, M. J., 1987. Geochemistry of Quaternary volcanism in the Sunda-Banda arc, Indonesia, and three component genesis of island arc basaltic magmas. *J. Volc. Geotherm. Res.* **31**, (in press).

White, W. M., & Hofmann, A. W., 1982. Sr and Nd isotope geochemistry of oceanic basalts and mantle evolution. *Nature*, **296**, 821-825.

White, W. M., & Patchett, J., 1984. Hf-Nd-Sr isotopes and incompatible element abundances in island arcs: implications for origins and crust-mantle evolution. *Earth Planet. Sci. Lett.* **67**, 167-185.

White, W. M., & Bryan, W. B., 1977. Sr-isotope, K, Rb, Cs, Sr, Ba, and rare-earth geochemistry of basalts from the FAMOUS area. *Geol. Soc. Amer. Bull.* **88**, 571-576.

Wilkinson, J. F. G., 1982. The genesis of mid-ocean ridge basalts. *Earth Science reviews*, **18**, 1-57.

Wilkinson, J. F. G., 1985. Undepleted mantle composition beneath Hawaii. *Earth planet. Sci. Lett.* **75**, 129-138.

Wyllie, P. J., Donaldson, C. H., Irving, A. H., Kesson, S. E., Merrill, R. B., Presnall, D. C., Stolper, E. M., Usselman, T. M., & Walker, D., 1981. Experimental petrology of basalts and their source rocks, chapter 3. In: *Basaltic volcanism study project*, National Aerospace Administration, Houston, 493-630.

Yoder, H. S. Jr., & Tilley, C. E., 1962. Origin of basalt magmas: an experimental study of natural and synthetic rock systems. *J. Petrol.* **3**, 342-532.

Zindler, A., Staudigel, H., & Batiza, R., 1984. Isotope and trace element geochemistry of young Pacific seamounts: implications for the scale of upper mantle heterogeneity. *Earth planet. Sci. Lett.* **70**, 175-195.